



University of
Salford
MANCHESTER

**Investigating the Effect of Perforation Diameter and CO₂ Bubble Size
Distribution on Heavy Oil Recovery**

Akpovi Godstime Okudolor

PhD Thesis

2018



University of
Salford
MANCHESTER

**Investigating the Effect of Perforation Diameter and CO₂ Bubble Size Distribution on
Heavy Oil Recovery**

Akpovi Godstime Okudolor

School of Computing, Science and Engineering
Petroleum Technology and Spray Research Group
University of Salford, Manchester,
The United Kingdom

A Thesis Submitted in Partial Fulfilment of the Requirements for the
Degree of Doctor of Philosophy

March 2018

Contents

Contents	i
List of Figures	vi
List of Tables	ix
Acknowledgement	x
Declaration.....	xi
Confidentiality Notice.....	xii
List of Publications and Conferences	xiii
Conversion Table	xiv
Nomenclature	xv
Abstract	xvii
Chapter 1	1
Introduction.....	1
1.1 Problem Statement	1
1.2 Research Contributions	2
1.3 Aims.....	3
1.4 Objectives	3
1.5 Thesis Outline	4
Chapter 2.....	5
Background Details and Literature Survey.....	5
2.1 Introduction.....	5
2.2 Petroleum Resources and World Energy Mix	5
2.3 Heavy Oil	9
2.4 Origin of Heavy Oil	10
2.5 Properties of Heavy Oil	10
2.5.1 Physical Properties of Heavy Oil.....	10
2.5.1.1 Sampling of Heavy Oil	11
2.5.1.2 Elemental Analysis	11
2.5.1.3 Specific Gravity and Density	12
2.5.1.4 Viscosity of Heavy Oil.....	13
2.5.1.5 Metal Content.....	13
2.5.1.6 Solubility.....	14
2.5.2 Thermal Properties.....	16
2.5.2.1 Carbon Residue	16

2.5.2.2 Specific Heat	16
2.5.2.3 Heat of Combustion	17
2.5.2.4 Volatility	17
2.6 Types of Oil Recovery	17
2.7 Principles of Heavy Oil Recovery	18
2.8 Heavy Oil Recovery Methods.....	20
2.8.1 Chemical flooding Methods.....	20
2.8.1.1 Polymer Flooding.....	20
2.8.1.2 Surfactant Flooding.....	21
2.8.1.3 Alkaline Flooding	21
2.8.1.4 Limitation of Chemical Flooding Methods.....	21
2.8.2 Thermal Methods	22
2.8.2.1 Cyclic Steam Stimulation (CSS).....	22
2.8.2.2 Steam Drive	23
2.8.2.3 In-Situ Combustion.....	23
2.8.2.4 Limitation of Thermal Recovery Methods	23
2.8.3 Carbon-Dioxide (CO ₂) Flooding.....	24
2.8.3.1 Mechanism of Carbon-dioxide Immiscible Flooding.....	24
2.8.4 Laboratory Reports of Immiscible CO ₂ Flooding.....	25
2.8.5 Field Reports of Immiscible CO ₂ Flooding	26
2.8.6 Challenges Facing Immiscible CO ₂ Flooding Process	27
2.9 Perforation diameter and CO ₂ Bubbles.....	28
2.9.1 Perforation.....	28
2.9.2 Bubble Formation	29
2.10: Literature Survey	30
2.10.1 Review of Literatures on CO ₂ Bubbles in Micro-channels	31
2.10.2 Review of Literatures on Heavy Oil Viscosity	32
2.10.3 Review of literatures on CO ₂ Bubbles and Oil Recovery.....	33
2.11 Research Gaps.....	34
2.12 Chapter Summary	34
Chapter 3.....	35
Methodology	35
3.1 Introduction.....	35
3.2 Phase I: Rig Validation	37
3.2.1 Apparatus	37

3.2.1.1 Rig Setup.....	37
3.2.1.2 Imaging Setup	39
3.2.2 Materials	39
3.2.3 Procedures.....	40
3.2.3.1 Pressure Testing	40
3.2.3.2 Particle Imaging	40
3.2.4 Errors and Accuracy	41
3.3 Phase II: Particle Characterisation and Viscosity Measurement	42
3.3.1 Apparatus	42
3.3.1.1 Rig Setup.....	42
3.3.1.2 Viscometer	43
3.3.1.3 Dantec Dynamic Studio Software 5.0.....	44
3.3.2 Materials	46
3.3.3 Procedures for Particle Characterisation and Viscosity Measurement	46
3.3.4 Error and Accuracy	47
3.4 Phase III: Reservoir Petrophysics and Core Flooding	48
3.4.1 Apparatus	48
3.4.1.1 Core Flooding Experimental Setup.....	48
3.4.1.2 Reservoir Saturation System.....	49
3.4.1.3 Mud Balance	50
3.4.1.4 PORG -200 Porosimeter	51
3.4.1.5 PERG -200 Permeameter	55
3.4.1.6 PERL-200 Permeameter	58
3.4.1.7 Pheonix V Tome x S Scanner	62
3.4.2 Materials	67
3.4.3 Procedures.....	68
3.4.4 Errors and Accuracy	69
3.4.5 Chapter Summary:	70
Chapter 4.....	71
Results and Discussion	71
4.1 Overview	71
4.2 Results of Preliminary Experiment (Phase I).....	72
4.2.1 Pressure Testing of Experimental Rig	72
4.2.2 Particle Imaging: Choice of Led Light Source	72
4.3 Result of Particle Characterisation Experiment (Phase II)	74

4.3.1 Effect of Perforation Diameter on CO ₂ bubble Size distribution	74
4.3.1.1 Comparative Analysis of the Effect of Perforation Diameter on CO ₂ Bubble Size Distribution	76
4.3.2 Effect of Perforation Diameter on Heavy Oil Viscosity	76
4.3.2.1 Comparative Analysis of Viscosity Reduction Methods	78
4.4 Results of Reservoir Petrophysics and Core flooding (Phase III)	80
4.4.1 Reservoir Petrophysics.....	80
4.4.1.1 Dimension and Weight of Core Samples.....	80
4.4.1.2 Porosity Measurement	81
4.4.1.2 Gas Permeability Measurement	83
4.4.1.3 Liquid Permeability Measurement.....	84
4.4.1.4 Computer Tomography (CT) Scan	85
4.5 Result of Core Flooding Tests (Phase III)	88
4.5.1 Effect of Perforation Diameter on Heavy Oil Recovery in Homogeneous Reservoirs ..	88
4.5.2 Effect of Perforation Diameter on heavy oil Recovery in Heterogeneous Reservoirs ..	90
4.5.3 Comparative Analysis of Heavy Oil Recovery Process and CO ₂ Utilisation.....	92
4.6 Economic Analysis	94
4.6.1 Analysis Framework	94
4.6.2 Reservoir Performance Model.....	95
4.6.3 Revenue Model.....	95
4.6.4 Cost Model.....	96
4.6.5: Analysis Scenario and Evaluation Metrics	97
4.6.5.1 Price Scenario	97
4.6.5.2 Net Present value	97
4.6.6 Methodology for Economic Analysis	97
4.6.6.1. Reservoir Description and simulation parameters	97
4.6.6.2 Reservoir Production and performance Data.....	98
4.6.6.3 Project Cost and Revenue.....	100
4.6.6.4 Net Present Value	101
4.6.6.5 Payback Period.....	104
4.7 Chapter Summary	105
Chapter 5	106
Conclusions and Recommendations	106
5.1 Conclusions.....	106
5.2 Recommendations.....	108

References.....	109
Appendix A : Bibliography of Literature Review	119
Appendix B: Rig Design Specifications	123
Appendix C: Camera Specification	125
Appendix D: Particle Characterisation and Viscosity Data.....	126
Appendix E: Image Processing Process.....	147
Appendix F: Core Flooding Test Heterogeneous Model.....	158
Appendix G: Core Flooding Test-Homogeneous Model.....	205
Appendix H: Figure 4.4 (b) –(f).....	254
Appendix I: Figure 4.10 (b)-(f).....	257
Appendix J : Figure 4.12 (b) –(f).....	260

List of Figures

Figure 2.1: International energy outlook	5
Figure 2.2: World energy mix.....	6
Figure 2.3: History and forecast of world conventional oil discoveries	7
Figure 2.4: Illustrates the regional distribution of proven and recoverable reserves of unconventional oils.	8
Figure 2.5: Representation of the variation of the solubility parameter of petroleum fractions with the H/C ratio of benzene and polynuclear aromatic systems	14
Figure 2.6: Variation of the solubility parameter of the asphaltene fraction and the oil with reaction progress	15
Figure 2.7: Order of deposition of asphaltene constituents during thermal alterations	16
Figure 2.8: A chart showing the different stages and terminology of the oil recovery process	18
Figure 2.9: Principles of chemical flooding. Water is used as the supporting fluid to drive the polymer into the reservoir pay zone to affect mobility control.	20
Figure 2.10: Thermal recovery method.	22
Figure 2.11: Carbon-dioxide EOR process	24
Figure 2.12: Effect of nitrogen content on oil recovery.....	26
Figure 2.13: Performance evaluation of Forest and Oropouche Field Projects.....	26
Figure 2.14: Performance evaluation of non-thermal methods for heavy oil recovery	27
Figure 2.15: Geometric parameters of a completed perforation	28
Figure 2.16: Gas bubbles in a liquid	29
 Figure 3.1 Sequence of experimental investigation	 36
Figure 3.2 Schematic of the experimental rig	37
Figure 3.3 Snapshot of the experimental rig	38
Figure 3.4: Setup for image acquisition	39

Figure 3.5 Schematic of a section of the rig showing how the various instruments are connected.	42
Figure 3.6 Viscolite VL 700HP Portable Viscometer.....	43
Figure 3.7 Process flow chart for the interferometric particle imaging.....	45
Figure 3.8 Core flooding rig schematics.....	48
Figure 3.9 Snapshot of the core holder, the perforated seal and section A.....	49
Figure 3.10 Schematics for reservoir saturation system	49
Figure 3.11 Snapshot of reservoir saturation system	50
Figure 3.12 Mud balance	50
Figure 3.13: PORG-200 Porosimeter and core holder.....	51
Figure 3.14 Front Panel of PORG-200 Porosimeter	53
Figure 3.15 PERG-200 Permeameter connected to a core holder	55
Figure 3.16 Front Panel of PERG-200 Permeameter.....	57
Figure 3.17 PERL-200 permeameter	58
Figure 3.18 Front panel of PERL-200 Permeameter:	60
Figure 3.19 Phoenix V Tome x S Scanner	63
Figure 3.20 3D Computer Tomography with Flat Panel Detector.....	65
Figure 3.21 Influence factors in Computer Tomography	66
Figure 3.22 Boise (a) and Castlegate sample (b)	67
Figure 4.1 Original and filtered image from water jet bubbles	73
Figure 4.2 Original and processed image of air bubbles in water.....	73
Figure 4.3 (a) Original image (b) Processed image	74
Figure 4.4: (a) Variation of CO ₂ bubbles size with perforation diameter at 1.2bar.....	75
Figure 4.5 Variation of dynamic viscosity of sunflower oil at different injection pressure ..	77
Figure 4.6 A comparative chart showing the results of other researchers and this work	78

Figure 4.7 Calibration graph showing the disk volume versus the pressure ratio	82
Figure 4.8 CT scan of Boise core sample.	86
Figure 4.9 CT scan of Castlegate core sample.....	87
Figure 4.10: (a) Oil recovery at 0.5mm perforation diameter	89
Figure 4.11 Heavy oil recovery at different perforation diameter for the homogeneous model.	90
Figure 4.12 :(a) Oil recovery at 0.5mm perforation diameter	91
Figure 4.13 Heavy oil recovery obtained in this study at different perforation diameter.....	92
Figure 4.14 A chart comparing the results of this study to other researchers.....	93
Figure 4.15 Analysis framework used in this study	94
Figure 4.16 Payback period for project case A and B.	104

List of Tables

Table 2.1: Regional distribution of heavy oil and bitumen reserves	8
Table 2.2: Crude oil classification (Brazilian National Petroleum Agency)	10
Table 4.1: Weight and Dimension of the Experimental Core Samples.....	80
Table 4.2 Calibration table and sample input data	81
Table 4.3 Coefficient table	82
Table 4.4 Testing Table.....	82
Table 4.5 Core Sample Petro-physical Properties.....	83
Table 4.6 Measured and Factory Gas Permeabilities.....	84
Table 4.7 Measured and factory Liquid Permeability	85
Table 4.8 Revenue model parameters and formulas	95
Table 4.9 Cost model parameters and equations	96
Table 4.10 Reservoir Model Parameters	98
Table 4.11 Results of Eclipse EOR simulation for Field X	99
Table 4.12 Field and Operational input for Field X.....	99
Table 4.13 Revenue and Expenditure of the EOR project	100
Table 4.14 Project A: NPV at 5% discount rate.....	102
Table 4.15 Project A: NPV at 10% discount rate.....	102
Table 4.16 Project B: NPV at 5% discount rate	103
Table 4.17 Project B: NPV at 10% discount rate	103

Acknowledgement

I would like to pay special thankfulness, warmth and appreciation to the persons below who made my research successful and assisted me at every point to cherish my goal:

My Supervisor, Dr Abubakar Abbas for his vital support and assistance. His encouragement made it possible to achieve the goal.

My Assistant Supervisor, Professor Ghasem Nasr, whose insightful suggestions and guidance at every point during my research helped me to work in time.

Dr Godspower Enyi, whose instruction pointed me in the right direction for my research.

The laboratory technician, Mr Allan Mappin for his understanding and support in my research laboratory work.

All the faculty, staff members of the Petroleum Technology and Spray Research Group, whose services turned my research a success.

My friends and research colleagues: Abdul, Aminu, Dapo, Egena, Peace, Aminu, Kabiru, Sunday, and Umaru, for their support and encouragement.

My brothers and sisters, Isaac, Lucky, Vincent, Theresa, Evelyn, Patience for their moral support.

My wife and son, for their love, care and support.

My Guardian, Chief Benson Ogwu for his moral, emotional and financial support

Finally to God Almighty, for His love, protection and guidance; without which this achievement would not have been possible.

Declaration

I, Akpovi Godstime Okudolor, declare that this thesis is my original work, and has not been submitted elsewhere for any award. Any section, part or phrasing used or copied from other literature or documents has been referenced at the point of use as well as in the reference section of the thesis work.

Signature /Date: -----

Akpovi Godstime Okudolor

Signature /Date: -----

Dr Abubakar Abbas

(Supervisor)

Signature /Date: -----

Prof G.G Nasr

(Co-Supervisor)

Confidentiality Notice

This document and the information contained herein are proprietary and confidential and is provided in strict confidence for the sole purpose of the thesis. Journal publications written from this document are awaiting publication. It is not to be disclosed to any third party or used for any other purpose without the written consent of the author.

List of Publications and Conferences

1. Okudolor, A.G., Abbas, A., and Nasr, G.G, (2017) Investigating the Effect of Perforation Diameter and CO₂ Bubble Size Distribution on Heavy Oil Recovery. *Salford Postgraduate Research Conference (SPARC 2017)*
2. Okudolor, A.G., Abbas, A.J, Enyi, G.C., and Nasr, G.G, (2017) The Effect of CO₂ Bubble Size Distribution on Heavy oil viscosity. *Journal of Engineering Technology (JOET)* (Submitted)
3. Okudolor, A.G., Abbas, A.J, and Nasr, G.G, (2017) Experimental Investigation of the Impact of Perforation Diameter and CO₂ Bubble Size Distribution on Heavy Oil Recovery Process. *Journal of Petroleum Science and Engineering (Elsevier)*(Submitted)

Conversion Table

Parameter	SI Units	Other Conversion factors
Length	1m	1000mm 1000000μm 3.2808333 ft. 39.37in 1.09361 yd
Area	m ²	10.76387 ft ²
Volume	m ³	1000 Litres 6.28983
Viscosity	1Ns/m ²	1000 cP
Pressure	101.325KPa	1atm 1.01325 bar 0.101325 MPa 101325 Pa 14.7 psi
Temperature	0°C	32 °F 273.1 5K 492 R
Mass	1kg	1000 g
Time	1s	1/60 min 1/3600 hr

Nomenclature

API	American petroleum Institute
BOPD	Barrels of oil per day
OOIP	Original oil in place
GOR	Gas oil ratio
EOR	Enhanced oil recovery
PV, V_p	Pore volume
CO ₂	Carbon dioxide
H/C	Hydrogen carbon ratio
N/C	Nitrogen carbon ratio
O/C	Oxygen-carbon ratio
S/C	Sulphur carbon ratio
C	Specific heat
D	Specific gravity
Q	Heat of combustion
k	permeability
Dp	Differential pressure
Dx	Unit distance
M	Mobility ratio
μ , η	Viscosity
Λ	Fluid Mobility
Ca	Capillary number
T	Temperature
V	Flow velocity
γ	Interfacial tension
U	Darcy's superficial velocity
P	Pressure
G	Gravity
H	Depth
A	Cross-sectional area
P ₁	Upstream pressure
P ₂	Downstream pressure
P ₁	Initial absolute pressure
P ₂	Expanded absolute pressure
v_1	Initial volume
v_2	Expanded volume
T ₁	Initial absolute temperature
T ₂	Expanded absolute volume
V _g	Grain Volume
V _c	Sample chamber volume
V _r	Reference chamber volume
V _v	Valve displacement volume
δP	Pressure drop across sample
δL	

P	Density
Ks	Permeability at infinite mean pressure
Pm	Mean Pressure
B	Klinkenberg factor
T	Time
L	Length of flow
E	Energy
<i>H</i>	Plank constant
C	Speed of light
Vg	Grain volume
Vb	Bulk volume
M\$	Million dollars

Abstract

Global demand for energy is rising steeply because of escalating energy consumption coupled with depleting conventional petroleum reserves. To address this challenge, heavy oil has been considered as a strategic petroleum resource that can be produced intensively to supplement the global supply of conventional hydrocarbons. In recent years, thermal-based techniques, such as cyclic steam stimulation (CSS) and steam assisted gravity drainage (SAGD), have traditionally been used to enhance heavy oil recovery. However, due to shallow pay zones in heavy oil reserves, wellbore heat losses can become excessive, making the process ineffective and uneconomical. For in-situ combustion, high-temperature oxidation reaction model is very challenging to maintain; which inevitably leads to low-temperature oxidation and consequently poor oil recovery. Another method considered for the heavy oil-Enhanced Oil Recovery (EOR) process is chemical flooding. However, the formation of brine with high salinity and divalent ions leads to process inefficiencies.

In this study, experimental techniques have been developed to examine the effect of perforation diameter and CO₂ bubble size distribution on the viscosity and recovery of heavy oil during Enhanced Oil Recovery process. To conduct the investigation, an experimental rig was constructed to simulate the flow of CO₂ in heavy oil. The oil viscosity, CO₂ bubble sizes were measured at different pipe perforation diameters and constant CO₂ injection pressure. Also, core flooding experiments were conducted on two reservoir models using a core holder modified to incorporate different perforated seals for the CO₂ flooding experiment

Findings from the first experiment showed a 28 % reduction in the dynamic viscosity of the heavy oil when CO₂ was injected at a 2.2 bar gauge pressure through a perforation of 0.5 mm in diameter. However, when the seal was replaced with 3 mm centrally perforated seal, the percentage reduction in the dynamic viscosity obtained at 2.2 bar was 5%. In all cases of perforation diameter investigated, the results indicate a direct variation between the perforation diameter and the dynamic viscosity of the heavy oil. In addition, it was observed that the concentration of the CO₂ microbubbles in the range of 1-100 μm varied directly with the perforation diameter but inversely with the oil viscosity. In the core flooding experiments, oil recovery improved by 24.5 % by changing the perforation diameter to 0.5 from 3.0 mm in the homogeneous model. For the heterogeneous model, the improvement was 16 %. The amount of CO₂ utilised in both models also dropped as the perforation diameter was reduced.

An economic analysis of a heavy oil recovery process was conducted using the perforation reduction method typified in this study. The analysis aimed to ascertain the economic viability of the proposed method. Parameters from a heavy oil field were used for the simulation of a model to generate a five-year production data. Two projects were used for the analysis: A and B. Project A represents the heavy oil recovery process without any reduction of the well casing perforation diameter, while project B denotes the recovery process with the reduction of perforation diameter by a factor of six as demonstrated in this study. In both cases, the net present value at a discount rate of 5% and 10% were computed to ascertain their viability. In addition, the payback period for the both viable projects were determined.

Findings from the economic analysis indicated that projects A and B were viable at 5% discount rate with A generating a net present value of 0.1million US dollars as against B that made 4 million US dollars in five years. At 10% discount rate, only project B was viable, recording a net present value of 3.2 US million dollars. The discounted payback period for project A and B were 2 years, 5 months and 1 year, 2 months respectively. The implication of the different period is that heavy oil production using the reduced perforation diameter (project B) would recover its initial investment in half the time it would take project A.

Finally, the results from both the experimental study and economic analyses show that heavy oil recovery process in sandstone reservoirs can be significantly improved by the application of well completion with smaller perforation diameter.

Chapter 1

Introduction

The oil and gas sector is often described as an industry whose sole interest is to drill for new oil and gas wells. This view is supported by the fact that most oil companies focus on the business of exploration . Nevertheless, there are many others whose focus is to extend the life of difficult reservoirs that can no longer produce oil with its natural energy. To deal with the enormous challenges posed by these problematic reservoirs, these producing companies often require a more extensive set of engineering skills. However, irrespective of these additional skills, experience has shown that getting more oil from these reservoirs results in the higher cost of production per barrel of oil. Consequently, most companies opt for the explorative path that has the advantage of providing lesser challenges during production and more financial reward for the companies and their stakeholders[1] . This shift to the exploration by these companies was also the case even when there is the prospect of long-term production from the depleted reservoirs [2].

Recently, the trend is changing. The global energy demand is rising against declining oil production [3]. Proven global reserves of conventional oil amount to 1.3 trillion barrels – enough for up to 40 years supply at the current rate of production. However, as predicted by the Peak Oil Scenario, conventional oil and gas exploration targets are becoming increasingly rare. Indeed, as production from conventional acreage declines at a rate of about 5% per year, global demand is rising steadily. Growth is projected to be around 1% per year for the next 20 years, driven mainly by China, India and Brazil [4]. Therefore, the option available now is to employ new techniques to enable the production of oil in unconventional sources such as heavy oil reservoirs. A viable method of achieving this is by the application of carbon dioxide enhanced oil recovery processes [5].

1.1 Problem Statement

For the first 10 years of field operation, Carbon dioxide (CO₂) purchases are the single most enormous expense in carbon dioxide enhanced oil recovery (CO₂-EOR) floods, representing as much as 68% of total costs [6]. As such, optimal use of CO₂ resources is required to assure profitability. For field scale miscible CO₂-EOR floods, projected incremental recoveries range from 7 to 23% of the original oil in place (OOIP). Plus, the net amount of CO₂ required is estimated to be between 2.5 to 11 MCF/STB of incremental recovery with an average value of

6 to 7 MCF/STB [7]. However, from the data available on immiscible floods, actual incremental oil recovery has been on the order of 9 to 19% of the original oil in place with net CO₂ requirements of 5 to 12 MCF/ STB [8]. Because of the inherently higher utilisation efficiency of CO₂ in miscible systems, practically all worldwide CO₂-EOR projects are miscible. In the U.S., enhanced oil production from miscible CO₂ floods is reported to be on the order of 245,000 BOPD, while enhanced oil production from immiscible floods is reported to be on the order of 2,700 BOPD [9].

For heavy oil recovery operations, there is the added challenge of poor displacement efficiency due to the large viscosity contrast between the injected CO₂ and the heavy oil [10].

With rising energy demand and declining production from conventional reservoirs, production of unconventional sources like heavy oil reservoir is no longer an option but a necessity. The option now for the oil producing companies is to develop better techniques to address these challenges facing the heavy oil production. Recent techniques include the addition of chemicals and thermal methods to reduce the viscosity of heavy oil and improve recovery, but these methods suffer from limited applicability and economic feasibility issues.

For several years, researchers have studied the mechanism driving the heavy oil recovery process and has identified viscosity reduction as the primary mechanism responsible for heavy oil recovery. However, the following research questions are yet to be answered.

- The injection of CO₂ in heavy oil leads to the formation of bubbles, viscosity reduction and ultimately improved recovery. What are the role(s) of perforation diameter and the generated CO₂ bubble size distribution in the process?
- How can these parameters be altered to improve the CO₂ utilisation efficiency
- Can the perforation diameter and CO₂ bubbles be regulated to improve recovery? If they can, will the recovery be economically viable?

1.2 Research Contributions

- To provide a novel technique for in situ reduction of heavy oil viscosity and improved recovery in homogeneous and heterogeneous reservoirs.
- To reduce the cost burden associated with large purchases of CO₂ for heavy oil recovery process by improving the CO₂ utilisation efficiency.

1.3 Aims

The aims of this research work are to:

- Enhance viscosity reduction and heavy oil recovery during the immiscible CO₂ injection process.
- Improve CO₂ utilisation in heavy oil recovery process
- Ascertain the economic viability of the technique used in this study for enhanced viscosity reduction and heavy oil recovery.

1.4 Objectives

The objective of this experimental study is as follows:

- Model the flow of CO₂ in heavy oil at different perforation diameter to
 - Examine the CO₂ bubble sizes generated
 - Measure the corresponding viscosity of the CO₂- heavy oil mixture
- Conduct an experimental simulation of the immiscible CO₂ heavy oil recovery process on homogeneous and heterogeneous reservoir models using different perforation to
 - Examine the effect of perforation diameter on oil recovery
 - determine the ratio of CO₂ injected to the oil produced
- Conduct an economic analysis using the discounted net present value and payback period evaluation tool to determine the economic viability of the application of micro-perforation in heavy oil recovery process.

1.5 Thesis Outline

Chapter 1: Introduction

The chapter introduces the challenges facing conventional oil production and presents heavy oil as a strategic alternative resource to address the rising energy demand. It also presented CO₂ enhanced oil recovery method as a viable technique for recovering heavy oil

Chapter 2: Background Details

The chapter introduces the reader to the background of the field of heavy oil recovery processes. It discusses the various method of heavy oil production and well as their challenges. It also presents a brief description of the concept of perforation in well completion process as well as the generation of gas bubbles in liquids.

Chapter 3: Literature Survey

The chapter discusses the literature that directly relates to the area of research conducted in this thesis. It includes an assessment of the formation and dissolution of CO₂ bubbles under multiphase flow conditions in micro channels, formation and immiscible dissolution of multiphase flow in micro channels, an evaluation of the techniques for heavy oil viscosity reduction, and an appraisal of research into the application of carbon dioxide for immiscible heavy oil recovery.

Chapter 4: Methodology

The chapter presents the methodology applied in the present study. It provides a phase description of the experimental apparatus, procedures, materials as well as the errors associated with each phase of the investigation.

Chapter 5 Results and Analyses

The chapter reports the results and analysis of all the phases of experimental investigation conducted in chapter 4. It also presents a concise report of the economic analysis of a CO₂ heavy oil recovery project using the results obtained in chapter 4; to evaluate the economic viability of implementing the system developed in this research study.

Chapter 6: Conclusion and Recommendations

The chapter summarises the main findings and conclusion obtained from the research and proposes area of further study

Chapter 2

Background Details and Literature Survey

2.1 Introduction

The chapter presents the background details and literature survey. The background details provide the reader with an appreciation of the current world energy mix and its challenges. It discusses the current state of conventional oil production, it presents heavy oil as a viable alternative and addresses the challenges associated with its production. It focuses on the application of CO₂ immiscible flooding and compares the results of various CO₂ laboratory and field application to other heavy oil production methods. The background details conclude with the introduction of the reader to the concept of well casing perforation and bubble generation. The later part of the chapter deals with key literatures reviewed on the subject of investigation.

2.2 Petroleum Resources and World Energy Mix

The increase in world population coupled with industrial developments has resulted in a surge in demand for energy. The situation is worsening since the global production from conventional oil reserves, which is a significant source of energy, is on a steady decline [11]. In September 2017, the United States Energy Information Administration made a twenty-five-year projection of the world energy consumption. In the report illustrated in Figure 2.1, the world energy consumption is expected to rise by 28% within the stated period.

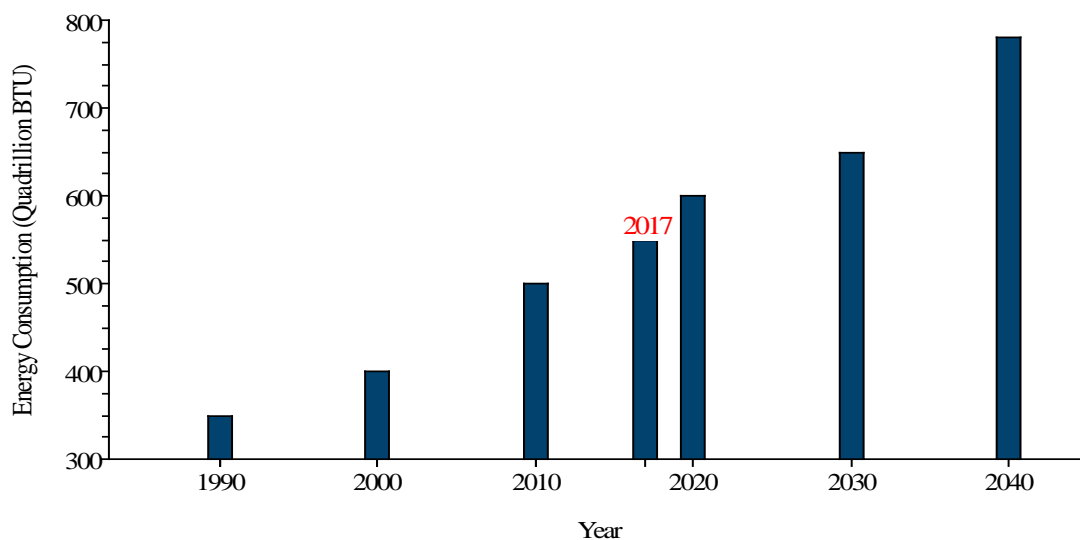


Figure 2.1: International energy outlook [12]

In June 2017, a report on the Statistical Review of World Energy by British Petroleum stated that the global energy mix consists primarily of oil, coal, natural gas, hydro-electricity and renewables. Among these energy sources, oil remains the world's dominant fuel making up a third (33%) of all the energy consumed (see Figure 2.2).

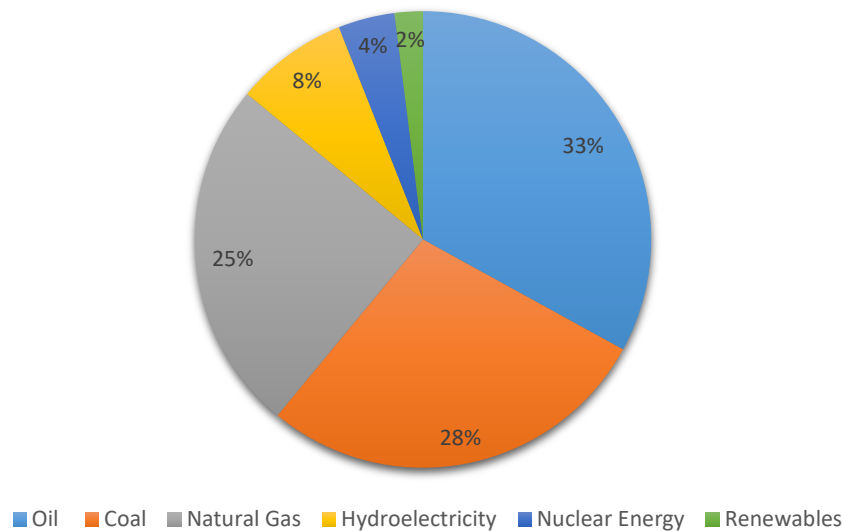


Figure 2.2: World energy mix[13]

However, in November 2017, the International Energy Agency 2017 World energy Outlook reports that conventional oil production is expected to decline from 67.6 million barrels per day in 2016 to 64.1 million barrels per day in 2040 (see Figure 2.3). Currently, discoveries of the conventional resource are scarce and inadequate to meet the surge in energy demand. The difficulty associated with finding this resource has resulted in a worldwide energy supply gap with global economic impacts. To overcome the challenge, oil companies must transform potential energy sources into exploitable commercial reserves. In this context, the development of new techniques for the production of oil that were once considered uneconomical is very crucial[3].

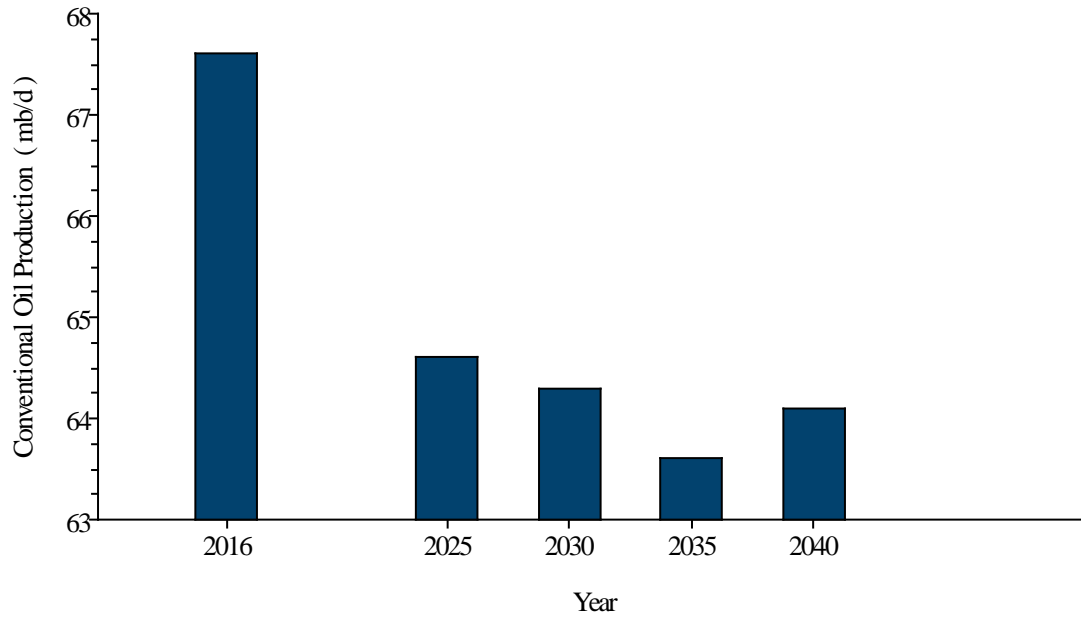


Figure 2.3: History and forecast of world conventional oil discoveries[14]

Parallel to the steady decline of conventional oil reserves, the discoveries possess distinct nature from those inherent to light oils [3, 15-17]. Hence, these oils are called unconventional. The primary distinction is that unconventional oils cannot be recovered in their natural state by the exclusive application of traditional production methods. In most cases, they cannot be produced and transported without heating and dilution which ultimately increases recovery costs[18]. The high resistance to flow exhibited by these unconventional oils is another impediment to natural flow. They are entirely different from conventional oils in that they possess higher viscosity, higher density, a higher content of nitrogen, oxygen, sulphur and heavy metals and a more extensive quantity of heavier oil fractions. As a result, unconventional oil requires specific technology to refine. Recent studies have shown that unconventional oil reserves, including heavy oils, extra-heavy oils and bitumen exceed 6 trillion barrels. According to reports from Oilfield Review Summit, 2006, the amount represents 70% of all energy resources derived from fossil fuels in the world[19]. Figure 2.4 shows the distribution of conventional and unconventional reserves in the world.

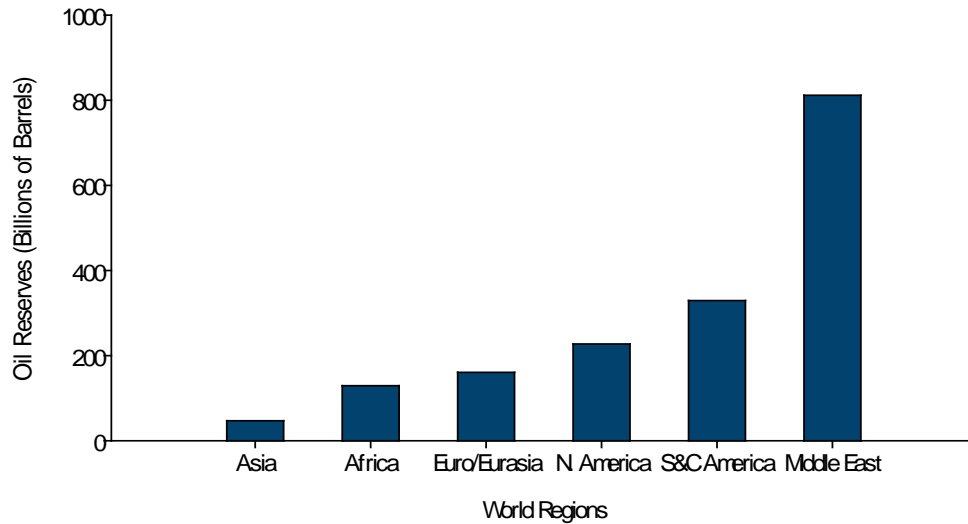


Figure 2.4: Illustrates the regional distribution of proven and recoverable reserves of unconventional oils [16, 20].

Reports from the United States Geological Survey shows that South America has the most extensive deposit of heavy oil reserves in the world, among which the Orinoco river basin in Venezuela accounts for over 60% [16, 20]. Table 2.1 illustrates the distribution of heavy of heavy oil and bitumen around the world.

Table 2.1: Regional distribution of heavy oil and bitumen reserves [16]

Regions	Heavy oil		Bitumen	
	Recovery Factor	Reserve (BBO)	Recovery Factor	Reserve(BBO)
North America	0.19	35.30	0.32	530.90
South America	0.13	265.70	0.09	0.10
Africa	0.18	7.20	0.10	43.00
Europe	0.15	4.90	0.14	0.20
Middle East	0.12	78.20	0.10	0.00
Asia	0.14	29.60	0.16	42.80
Russia	0.13	13.40	0.14	33.70
Total		434.30		650.70

The International Energy Agency projects that heavy oil and bitumen production from Venezuela and Canada is anticipated to reach 6 million barrels per day by 2030 [21]. Just recently, the total volume of unconventional oils in Canada was estimated to be similar to conventional oil reserves in the Middle East [21]. Athabasca oil sands deposit is the world's most abundant known petroleum resource, which contains more than 1.3 trillion barrels in the ground. The Cold Lake oil sands contain 200 billion barrels, and the Peace River deposit is estimated to have a deposit of 155 billion barrels [22]. In Brazil, the recoverable heavy oil reserves amount to 2.9 billion barrels. Also, four billion other barrels would be immediately incorporated if resources previously discovered became technically and economically feasible. Confirmed feasibility would mean that heavy oils could represent 40% of the proven Brazilian reserves in the medium term [15]. Furthermore, Petrobras, the Brazilian oil company, reports that heavy oil represents about 20% of the total volume of oil produced in the country in 2010 [23]. Besides the inherent adversities for the production and transport of viscous oils, the largest reserves of heavy oils in Brazil are located in water deeper than 1500 m and usually in shallow reservoirs with temperatures between 40 and 60°C. The rock existing in these Brazilian reservoirs is typically unconsolidated with high permeability. In fact, significant volumes of heavy oil found in recent discoveries have API gravity between 13 and 17 degrees and a viscosity ranging from 20 to 400 cP under reservoir conditions. The new scenario led Petrobras to create a technology program to focus on offshore reserves of heavy oil with the objective of developing technologies for the production of these oils [23].

2.3 Heavy Oil

The U.S. Geological Survey (USGS) defines heavy oil as a type of crude oil characterised by a dense, viscous, and asphaltic content. It also contains impurities such as waxes and carbon residue that must be removed before being refined [16]. There are various classifications of heavy oil. However, the most widely used description for heavy oil is the one proposed by the American Petroleum Institute. The institute uses the API scale as the basis for oil classification. However, while the API scale method employed by the institute is broadly accepted, its range of values (API less 20°) for heavy oil is not. The World Petroleum Conference classifies heavy oil as those having API of less than 22.3°. The Brazilian National Petroleum Agency (ANP) uses a similar index for its classification as shown in Table 2.2.

Table 2.2: Crude oil classification (Brazilian National Petroleum Agency)[24]

Oil Class	°API
Light	$^{\circ}\text{API} \geq 31$
Medium	$22 \leq ^{\circ}\text{API} < 31$
Heavy	$10 \leq ^{\circ}\text{API} < 22$
Extra-Heavy	$^{\circ}\text{API} \leq 10$

2.4 Origin of Heavy Oil

Heavy oils are derivatives. They are formed by the degradation of light and medium oils that have migrated into shallower traps. Over geologic timescales, micro-organisms metabolise these conventional oils (light and medium oils) by a bio-degradation process to produce methane and heavy hydrocarbons. The process increases the density, acidity, viscosity and sulphur content of the conventional oils. Optimal biodegradation process occurs at temperatures lower than 80 °C. Hence, the formation of heavy oil is restricted to reservoirs depths of around 1.5 to 2 km. Heavy oil is found in large shallow formations of marginal geological basins formed by unconsolidated sand. The recovery factor for heavy oil reservoir is low when compared with light oil reservoir because they are usually at low reservoir pressure and have a low gas-oil ratio (GOR). Notwithstanding the complicated and expensive extraction process of heavy oil, its high permeability location makes the method of producing it worthwhile.

2.5 Properties of Heavy Oil

2.5.1 Physical Properties of Heavy Oil

Heavy oil displays a wide range of physical properties. Some properties such as viscosity, density, and boiling range vary widely, while others like the ultimate or elemental analysis vary over a narrow range for a large number of samples. Heavy oil differs from one another due to the differences in the hydrogen and heteroatom contents. However, the carbon content is relatively constant. The heteroatom content of heavy oil is mainly responsible for the recovery process. Hence, the initial examination of the physical properties is necessary. The analysis makes it possible to ascertain the propensity of easy or difficult recovery. In fact, evaluation of heavy oil from physical property data to determine which recovery sequences should be employed for any specific heavy oil is a predominant part of the initial examination [25].

2.5.1.1 Sampling of Heavy Oil

Heavy oil is very complicated in its composition and therefore require proper sampling [26] [27]. The homogeneity of the heavy oil sample affects properties like elemental analysis, metal content, density (specific gravity), and viscosity. Also, adequate documentation of the circumstances and conditions during sampling have to be properly done. For example, during the sampling from oil field separators, the temperatures, pressures of the separation plant and the atmospheric temperature must be noted. Most importantly, an accurate sample handling and storage log should be maintained and should include information such as:

- i. The precise source of the sample, i.e., the exact geographic location or refinery locale from which the sample was obtained
- ii. A description of the means by which the sample was collected
- iii. The protocols used to store the sample
- iv. Chemical analysis, such as elemental composition
- v. Physical property analyses, such as API gravity, pour point, and distillation profile.
- vi. ASTM methods used to define the properties of items 4 and 5
- vii. The number of times that the sample has been reclaimed from storage to extract a portion. That is the indications of exposure to air or oxygen

The strict adherence to these procedures enables standardised evaluations to be made when subsequent samples are taken [28-31].

2.5.1.2 Elemental Analysis

Elemental analysis is the process of analysing a sample of a material or chemical compound to determine its elemental or isotopic composition. For heavy oil, the method is used to ascertain the percentages of carbon, hydrogen, nitrogen, oxygen, and sulphur in the feedstock. The overall character of the heavy oil is reflected by the atomic ratios of the various elements to carbon (i.e., H/C, N/C, O/C, and S/C) [25]. Trace elements such as vanadium and nickel are also analysed because these materials can have serious deleterious effects on the performance of the catalyst during the partial upgrading in the recovery or transportation process. The procedures for conducting an elemental analysis is described in the annual book of the American Society for Testing Materials (ASTM, 2012) [32]. The main components of the heavy oil are carbon and hydrogen, and they are usually present in amounts of the order of 83%w/w and 10% w/w respectively. The aromatic or aliphatic nature of the heavy oil is

estimated using the hydrogen to carbon ratio. Nature, together with the functional group of the heavy oil, gives an indication of the fluidity of the oil as well as its affinity to the reservoir rock [25]. Nitrogen occurs at levels in the order of 0.5–1% w/w and tends to concentrate in the highest boiling fractions as both basic and neutral type functional groups. The basic types are primarily aliphatic, aromatic amines and pyridines. While the neutral classes are in the form of indole derivatives, carbazole derivatives, imides, and porphyrin nitrogen [18]. The percentage of oxygen present in heavy oil is in the order of 1.0–1.5% w/w. It exists mainly as hydroxyl-type groups like phenols, alcohols, and carboxylic acids. Oxygen concentrates on the most polar constituents of the heavy oil such as resin constituents and asphaltene constituents. Naphthenic acids make up a class of oxygen-containing components and are essential compounds because of the corrosive properties. In infrequent occasions, oxygen can appear in the form of ethers or cyclo-ethers, or coupled with other heteroatoms to form sulfoxide derivatives and amide derivatives [25]. The most common heteroatom present in heavy oil is sulphur. It is usually in amounts in the order of 2–35 w/w but can reach values in the order of 6–8%w/w. It is distributed in increasing quantity according to the boiling points of the oil. Sulphur is present as thiophene type sulphur in condensed structures and as aliphatic sulphur in sulphide and di-sulphide functional groups [25].

2.5.1.3 Specific Gravity and Density

The specific gravity and density of heavy oil are essential properties [33–37]. Moreso, because they are used in the preliminary assessment of the character of the oil. Specifically, heavy oils with high content of asphaltene and resin constituents have poor mobility at ambient temperature and pressure and may have a specific gravity (density) of about 0.95. The chemical composition of the heavy oil influence the specific gravity, but the quantitative correlation is difficult to establish. However, it is acknowledged that increased amounts of aromatic compounds increase density, whereas an increase in saturated compounds decreases the density. There are also certainly preferred trends in the API gravity of heavy oils and one or more of the other physical parameters. For instance, a correlation exists between the API gravity and sulphur content, Conradson carbon residue, and viscosity [38, 39]. Despite these parallels, the derived relationships between the density of heavy oil and its fractional composition are valid only for some heavy oils and may lose their significance when applied to heavy oils from different sources. The nature of the heavy oil sample determines the property (density, specific gravity or API gravity) to be measured. The measurement, in any case, is done with the aid of a hydrometer or pycnometer [33, 35–37]. Most heavy oils are sold by volume. Thus, the

knowledge of its coefficient of expansion is essential. The coefficient of expansion is considered a significant parameter because, at a fixed temperature, it is assumed to be a function of only density.

The gas oil ratio (GOR) and reservoir temperature have a significant influence on the viscosity of the heavy oil. So much so that, oils with similar API gravity can have a different viscosities in the reservoir. Oil having a low API at a higher temperature in the reservoir may be easier to produce when compared to the same oil at a lower temperature. Moreover, for a given API, the viscosity of heavy oil can vary widely depending on the depth of the reservoir [38, 40, 41]. Also, the presence of dissolved gases in the oil affects the in situ viscosity of the oil. Hence, saturated oil will typically have a lesser viscosity than corresponding dead oil.

2.5.1.4 Viscosity of Heavy Oil

The heavy oil viscosity is a critical property in oil recovery prediction as it determines the ease of flow of the oil from the reservoir pay zone to the surface. For most heavy oil with API gravity of 15° and below, a thermal method is employed as a means of reducing the viscosity. Such methods include in-situ combustion, steam injection, hot water injection among others [42]. The viscosity of heavy oil varies distinctly over a wide range of values. It values can range from several centipoises at room temperature to several hundreds of centipoise at the same temperature [43]. The choice of a measurement device for heavy oil viscosity rely mainly on the properties of the oil. Consequently, much effort has to be spent converting from one scale to another; especially from Saybolt to kinematic viscosity [44-47]. Finally, the classification of heavy oil into different categories such as heavy oil, extra heavy oil, tar sand bitumen is based on their viscosity, specific gravity, a method of production, and the amount of high molecular and polar constituents. Heavy oil has a lesser viscosity and higher API gravity than extra-heavy oil, but they are both movable in the reservoir; unlike tar sand bitumen that is immobile [25, 38, 41].

2.5.1.5 Metal Content

Metals such as Vanadium and Nickel are found in most crude oils [48]. The proportion of metals in heavy oil is relatively high. They are either in the form of salts or as organometallic constituents such as the metalloporphyrins which are extremely difficult to remove from the feedstock or heavy oil sample. These metallic components often volatilize under thermal recovery operations and appear in the reservoir or the production lines. The American Society for Testing and Materials developed a series of test designated for the determination of metals

in heavy oil, petroleum and petroleum products [49-60]. The determination of metals in a feedstock can then be accomplished by combusting the sample to produce organic ash. The ash residue is digested with an acid and the resulting solution analysed for metals species by atomic absorption (AA) or by inductively coupled argon plasma spectrometry (ICAP).

2.5.1.6 Solubility

Crude oil solubility, especially the asphaltene fractions, has been the subject of many research owing to its importance [38]. The occurrence of phase separation during thermal recovery of heavy oil can be explained using the solubility parameter. Recent data shows that there is a connection between the atomic hydrogen/carbon ratio and the solubility parameter for hydrocarbons and the constituents of the lower-boiling parameter of petroleum. Hydrocarbon liquids can dissolve polynuclear hydrocarbons with less than a three-point difference between the lower solubility parameter of the solvent and higher solubility parameter of the solvent. Hence, a correlation can be assumed that allows for the solubility parameter of the asphaltenes and the resins to be estimated. Figure 2.5 illustrates this correlation.

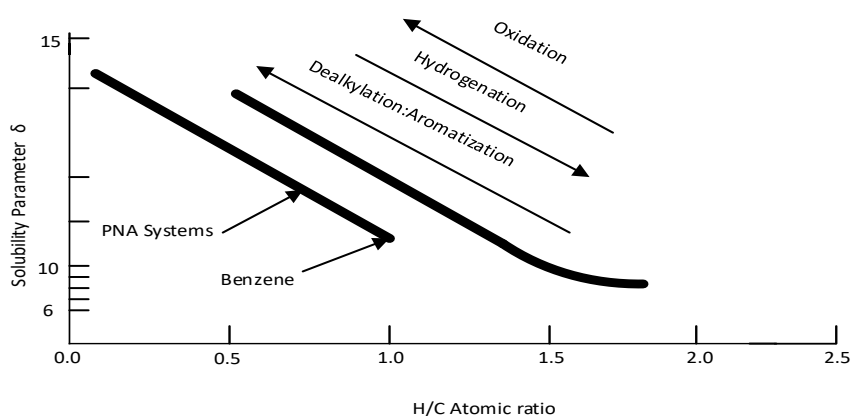


Figure 2.5: Representation of the variation of the solubility parameter of petroleum fractions with the H/C ratio of benzene and polynuclear aromatic systems [38, 61].

The solubility parameter of asphaltenes is estimated to be in the range 9 to 12. The parameter is so because asphaltenes are composed of a mixture of different compound types with a variation in polarity. During thermal recovery involving superheated steam, the alkyl side chain is removed from the asphaltenes resulting in a decrease in the hydrogen to carbon atomic ratio and increasing the solubility parameter (see Figure 2.6). Concurrently, changes occur in the

oil medium, but they are of lesser overall effect. The results of these changes lead to a higher solubility parameter differential between the reacted asphaltene constituents, the resin constituents and the oil, producing a deposited material. The material is usually a product of the action of the highest molecular weight and the highest-polarity constituents in the asphaltene and resin fractions. It benefits the refiner of the produced oil, but often a disadvantage as the deposit causes blockage of the reservoir flow channels.

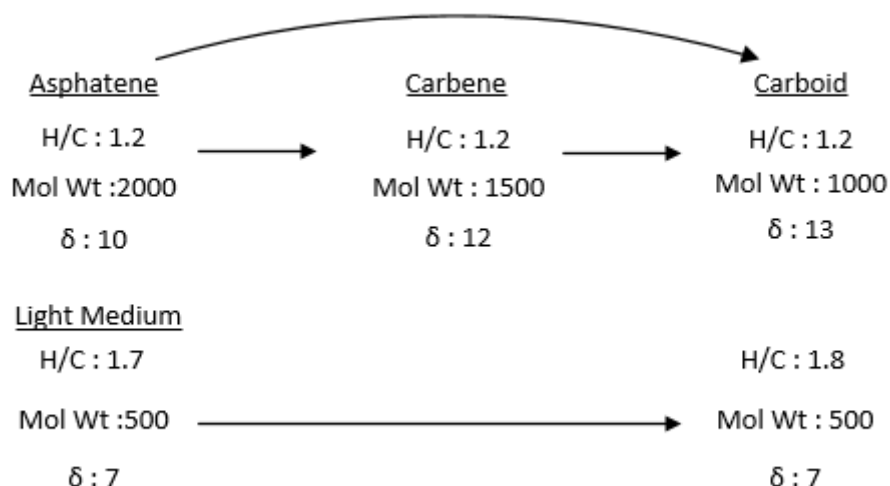


Figure 2.6: Variation of the solubility parameter of the asphaltene fraction and the oil with reaction progress [61]

As shown in Figure 2.7, the order of deposition relative to models applied to the system is another aspect of this reaction. The amphoteric constituents (i.e. the polar constituents of the asphaltene) and the resin fractions are more thermally liable than the lower-polarity constituents (i.e. the neutral polar constituents) are. Consequently, products from the amphoteric constituents exceed the solubility parameter differential more quickly and separate from the oil medium first earlier than could be predicted if an average property is used for any model applied to the system.

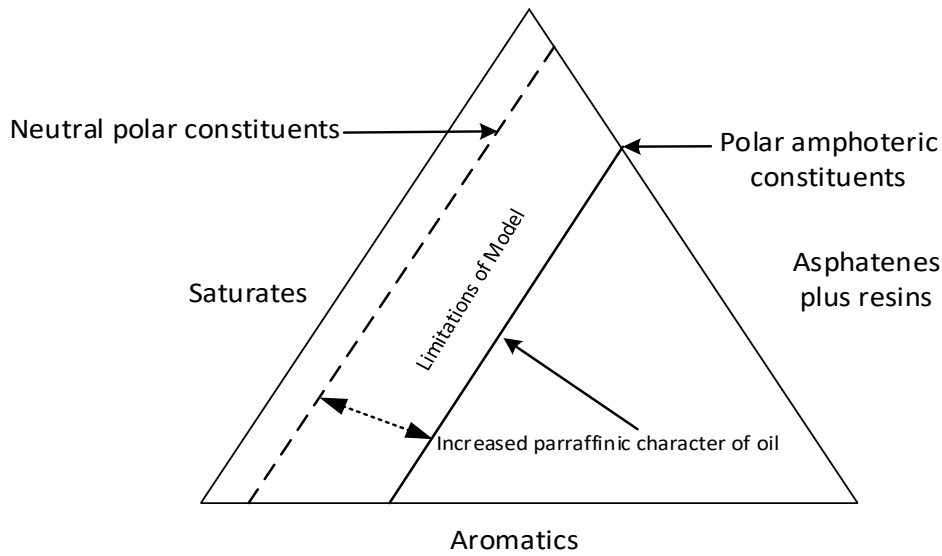


Figure 2.7: Order of deposition of asphaltene constituents during thermal alterations [61].

2.5.2 Thermal Properties

The thermal properties of heavy oils are the carbon residue, specific heat, the heat of combustion and, volatility. Only a summary of these properties will be presented here. The details of these properties are not discussed because they are used for thermal methods of heavy oil recovery which are beyond the scope of the current study.

2.5.2.1 Carbon Residue

Carbon residue refers to the measure of combustibility and deposit forming tendencies of the oil. It is used to evaluate the carbonaceous depositing characteristics of heavy oil during thermal recovery [61-64].

2.5.2.2 Specific Heat

Specific heat is the quantity of heat required to raise a unit mass of material through one degree of temperature. It is used in all calculations related to the heating and cooling of the heavy oil. [61, 65]. It is computed using the equation 2.1:

$$C = \frac{1}{d} \{0.388 + 0.00045t\} \quad (2.1)$$

Where C = Specific Heat (J); d = Specific Gravity(gm per cc);

t = Temperature in fahrenheit

2.5.2.3 Heat of Combustion

The heat of combustion is the energy released when a compound undergoes complete combustion with oxygen under standard conditions. The gross heat of combustion of heavy oil is given with a reasonable degree of accuracy by the equation 2.2 [61]:

$$Q = 12400 - 2100d^2 \quad (2.2)$$

Where Q = Heat of combustion (J), d = Specific Gravity (gm / cc)

2.5.2.4 Volatility

The volatility of a liquid or liquefied gas can be defined as its tendency to vaporise. That is to change from the liquid to the vapour or gaseous state. It is used to estimate the ability of the heavy oil to distil, or steam distil during thermal recovery methods [61].

2.6 Types of Oil Recovery

Oil recovery is classified as primary, secondary and tertiary oil recovery process. Historically, these stages described the production from a reservoir in chronological order [66]. The primary production which is the initial production stages resulted in the displacement energy naturally existing in the reservoir. Secondary recovery represented the second stage of operations and was usually implemented after primary production declined. Tertiary recovery considered as the third stage of production was that obtained after water flooding or any other secondary process was used. The drawback to this chronological classification is that many production operations are not conducted in the specified order. A typical example is the production of heavy oils that are discussed in this study. Heavy oil is viscous and may not flow in economical rates under regular energy drives, thus primary and sometimes secondary production would be negligible [66].

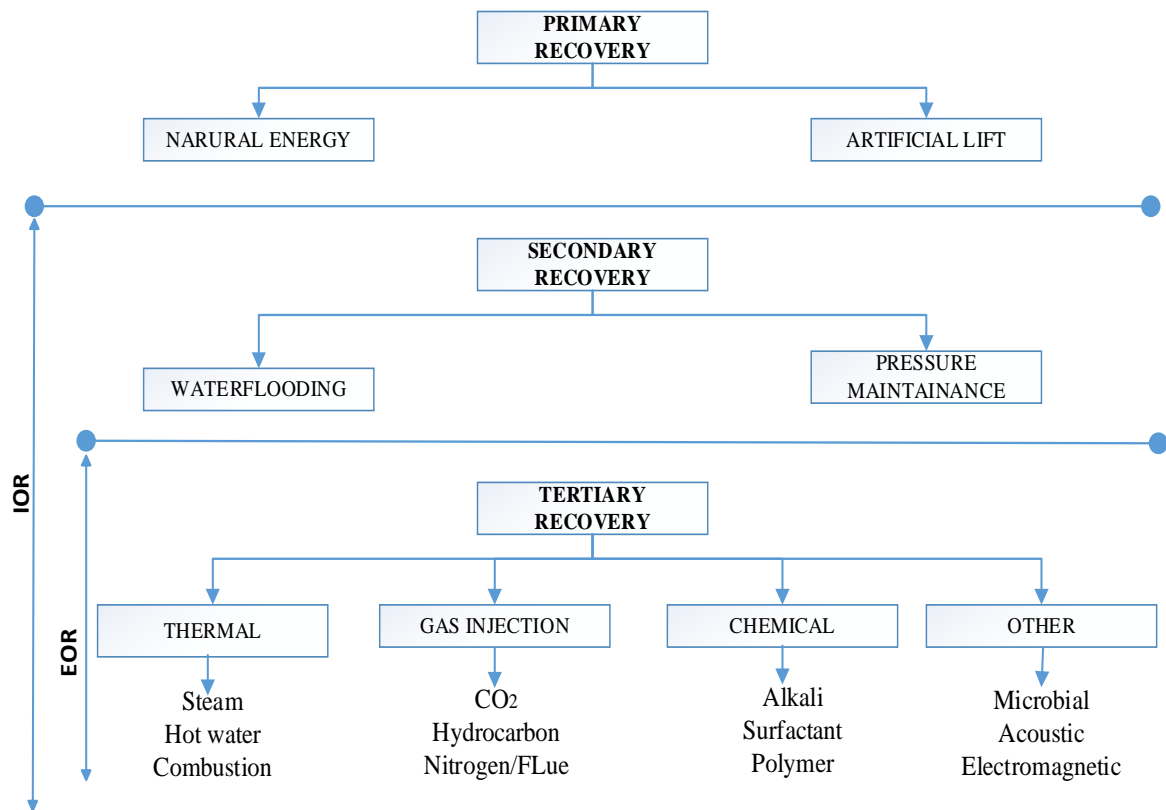


Figure 2.8: A chart showing the different stages and terminology of the oil recovery process

For such reservoirs, a method considered a tertiary process in a standard chronological depletion sequence would be used as the initial and perhaps the final method of recovery. Consequently, the term ‘tertiary recovery’ fell into disfavour in petroleum engineering literature and the term ‘enhanced oil recovery (EOR)’ became more accepted [66]. Another descriptive designation commonly used is ‘improved oil recovery (IOR)’. The term includes EOR and a broad range of activities such as reservoir characterisation, improved reservoir management, and infill drilling. An illustration of the oil recovery processes is shown in Figure 2.8.

2.7 Principles of Heavy Oil Recovery

Oil is retained in the reservoir as a result of the capillary, gravitational and viscous forces. The relative interface between these forces during the flow of oil in the porous media can be estimated by the capillary number and the mobility ratio [67]. The capillary number (Ca) is defined as the dimensionless number that describes the relative effect of viscous forces to the interfacial tension acting across an interface between a liquid and a gas or two immiscible liquids. It is expressed mathematically as shown in equation 2.3.

$$Ca = \frac{\eta \cdot v}{\gamma} \quad (2.3)$$

$Ca = \text{Capillary Number}$; $\eta = \text{Dynamic Viscosity (cP)}$; $v = \text{Velocity(m/sec)}$, $\gamma = \text{Surface Tension}$

The mobility of fluids in porous media is defined by the Darcy equation. The value k represents the permeability of the reservoir rock. For single phase flow, k represents the absolute permeability, while for multiphase flow it denotes the effective permeability. Darcy's equation is illustrated in equation 2.4 as:

$$u = \frac{k}{\mu} \cdot \frac{dP}{dx} \quad (2.4)$$

From which the phase fluid mobility is given in equation 2.5 as $\lambda = \frac{k}{\mu}$ (2.5)

Where: $u = \text{Flow velocity (m/s)}$; $k = \text{Rock Permeability(mD)}$; $\mu = \text{Dynamic Viscosity(cP)}$;

$\frac{dP}{dx} = \text{Pressure Gradient } \left(\frac{\text{psia}}{\text{m}}\right)$, $\lambda = \text{Fluid Mobility}$

The mobility ratio (M) is defined as the ratio of the displacing fluid to the displaced fluid, and it is expressed in equation 2.6 as:

$$M = \frac{\lambda_2}{\lambda_1} \quad (2.6)$$

$M = \text{Mobility ratio}$; $\lambda_2 = \text{Mobility of displacing fluid}$;

$\lambda_1 = \text{Mobility of displaced fluid}$

The mobility ratio (M) is a dimensionless viscosity ratio. It is an essential index in displacement process as it affects both the areal and vertical sweep and classifies the displacement process. Mobility ratio values higher than unity refer to an unfavourable ratio, while values lower than unity refer to a favourable ratio [68].

2.8 Heavy Oil Recovery Methods.

Heavy oil has low mobility due to its high viscosity, even though the relative permeability may be close to unity (i.e. high). Hence, primary recovery method may not be feasible. Also from previous experiences, heavy oil recovery method from conventional waterflooding usually record value far below 10% [69, 70]. This section, therefore, will focus on modern EOR methods that have been applied together with the challenges encountered.

2.8.1 Chemical flooding Methods

Chemical flooding involves the application of chemicals to enhance the oil displacement process by improving the mobility ratio and capillary number (see Figure 2.9). There are three main types of chemical flooding: polymer flooding, surfactant flooding and alkaline flooding. Other forms of chemical flooding methods such as micellar flooding and alkaline-surfactant-polymer flooding are not applicable to viscous oil [71].

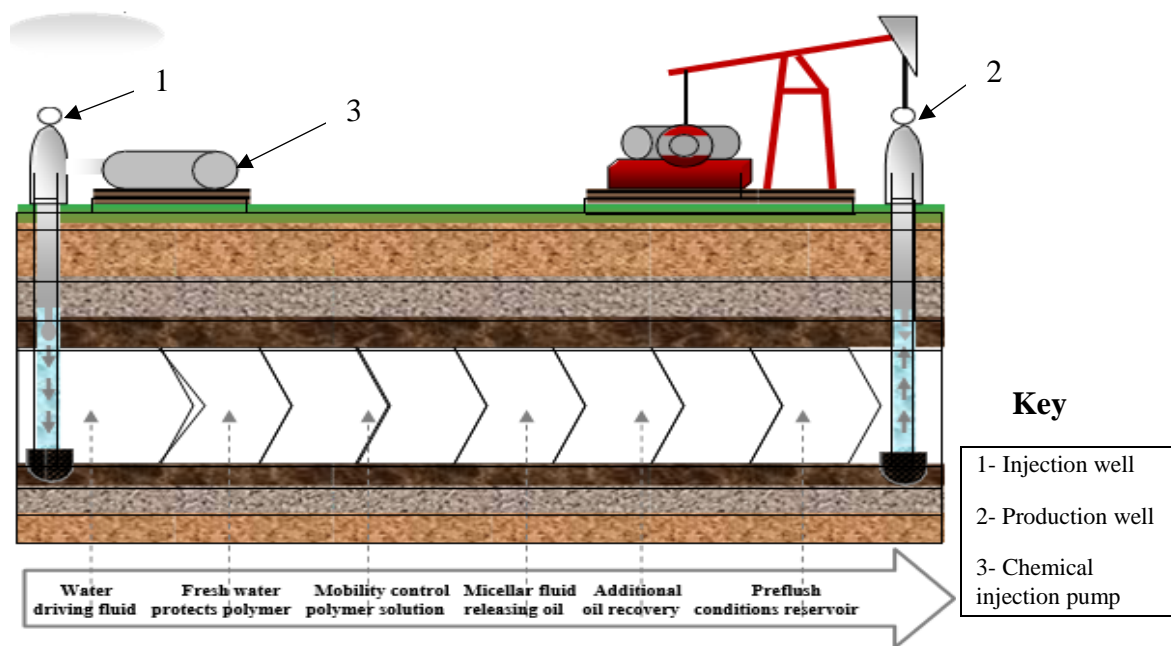


Figure 2.9: Principles of chemical flooding. Water is used as the supporting fluid to drive the polymer into the reservoir pay zone to affect mobility control[72].

2.8.1.1 Polymer Flooding

In Polymer flooding, a nominal quantity of a water-soluble, high molecular weight polymer is added to the invading water to increase the apparent viscosity of water, thus lowering the mobility ratio [73, 74]. Heavy oils have a wide range of viscosity, and so there is a limit to

which the application of polymer may be practicable, both for reasons of cost and mechanical considerations of injection pressure [75].

2.8.1.2 Surfactant Flooding

Surfactant flooding involves the injection of suitable surfactants to mobilise the oil from the reservoir. Surfactants are a chemical substance that absorbs on or concentrate at a surface or fluid/fluid interface when present at low concentration. They modify the interfacial properties by significantly decreasing the interfacial tension (IFT) [76]. The formation of an emulsion in the reservoir also helps in improving the mobility ratio. The main problem with surfactants is the loss to the rock matrix through several mechanisms.

2.8.1.3 Alkaline Flooding

In alkaline flooding, a chemical system with a high potential of hydrogen (PH) is injected into the reservoir. If the crude oil has sufficient saponifiable components, a reaction will occur in which surfactants are formed in situ [66]. The reduction of IFT enhances the recovery of oil and increase in the oil displacement efficiency due to the surfactants formation.

2.8.1.4 Limitation of Chemical Flooding Methods

There are cost and reservoir flow limitations associated with chemical flooding methods. The cost of surfactants can significantly vary from \$1.10 to \$4.40 per kilogram. Consequently, the risk of incurring losses is likely [71]. From the standpoint of reservoir flow, loss of surfactant because of adsorption and reaction with minerals are of great concern. Such losses increase as the clay content increases. Gravity segregation of the surfactant is also a substantial factor, given the slow injection rates and large areas involved in the field. Mixing of the surfactant with water can make the surfactant ineffective particularly where the process commences after a waterflood. The environmental aspect of injection of chemicals and production of fluids containing these chemicals can also add to the cost [77]. The application of polymer flooding for heavy oil recovery presents somewhat different sets of challenges. Polymer degradation due to the shearing, salinity and high temperature is an obvious obstacle to commercial applications. In Dalia field, Angola, shearing at the wellhead chokes resulted in polymer viscosity loss of 50% [78-81]. Again, in Daqing field, China, the application of polymer flooding with brine as base water, produced a tertiary recovery rate of only 5.48% [82-84].

2.8.2 Thermal Methods

Thermal methods rely on the use of thermal energy to increase the reservoir temperature. The intent is to reduce the viscosity of the oil and to displace the oil to a producing well. Figure 2.10 illustrates the process. There are three main types of thermal recovery processes: cyclic steam stimulation, steam drive, and in situ combustions. The details of all other thermal methods can be found in standard petroleum engineering textbooks.

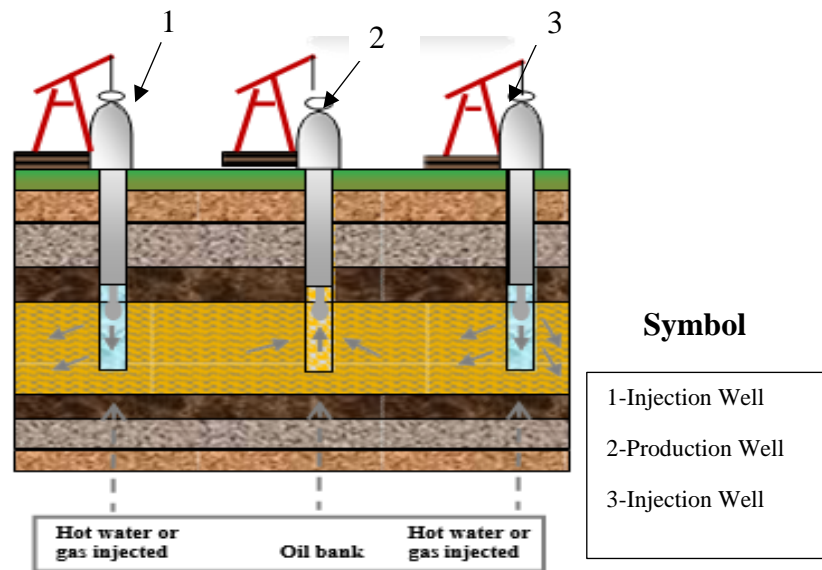


Figure 2.10: Thermal recovery method. Hot water or steam is pumped through the injection well to reduce the viscosity of the heavy oil and to mobilise it into the production well[72].

2.8.2.1 Cyclic Steam Stimulation (CSS)

Cyclic steam stimulation otherwise known as CSS relies on heat energy supplied to the formation to change the rock and fluid properties at a particular time to increase well productivity. The process is carried out in three phases. In the first phase, steam is injected into the formation through the wellbore with certain steam quality and injection rate. The quantity of heat injected depends on the reservoir volume and characteristics. The second phase is the soaking phase. Here, the heat energy already supplied is allowed to spread all over the formation. The aim is to mobilise the less viscous oil into the production well. The third and final phase is the production phase where production is maintained until the oil recovery reaches the initial condition of the reservoir.

2.8.2.2 Steam Drive

In the steam drive method, steam generated at the surface is injected into the reservoir through specially distributed injection wells. The injected steam heats up the crude oil and distills the light components of the crude oil, which had condensed in the oil bank ahead of the steam front. The consequence is the reduction of the oil viscosity. The steam together with hot water resulting from condensation generate an artificial drive that sweeps the oil toward the producing wells. Another contributing factor to recovery is the near wellbore clean up. Here steam reduces the interfacial tension between paraffin, asphaltenes and the rock surface. Also, the steam distillation of the crude oil light ends creates a small solvent bank that can miscibly remove trapped oil. The steam drive method is also called continuous steam injection or steam flooding [85].

2.8.2.3 In-Situ Combustion

In situ combustion (also known as fire flooding) is the process of injecting a gas containing oxygen such as oxygen to generate fire inside the reservoir. The well is fitted with a unique heater, which ignites the oil. The heat produced by the burning heavy hydrocarbons causes hydrocarbon cracking, vaporisation of light hydrocarbons and reservoir water. Heavier hydrocarbons known as coke are also produced in the process. As the fire travels, it creates a burning front, which pushes ahead the mixture of hot combustion gases, steam and hot water. The process reduces the oil viscosity displacing it towards the production wells. Also, the lighter hydrocarbons and the generated steam move in advance of the burning front, condensing into liquids; thus producing a miscible displacement and hot water flooding [85].

2.8.2.4 Limitation of Thermal Recovery Methods

Thermal methods have been proven as a viable method for heavy oil recovery. However, its applicability is restricted to shallow reservoirs with thick pay zone. Heat losses in the thin and deep reservoir can become excessive making the process economically unprofitable. More so, most heavy oils are contained in relatively thin reservoirs. For example, Canada has abundant heavy oil resources, but more than 90% of the proven resources are located inside pay zones that are less than 10 meters thick, and 55% of this are in reservoirs that are less than 5 meters thick [69, 86].

2.8.3 Carbon-Dioxide (CO₂) Flooding

Carbon dioxide flooding has achieved results in cases where other methods are inapplicable or uneconomical. In carbon dioxide flooding, CO₂ is injected into the reservoir to mix and displace the oil to the production well (see Figure 2.11). Carbon dioxide flooding can be either miscible or immiscible. Miscibility is achieved when CO₂ is injected at a pressure above the minimum miscibility pressure (MMP). The MMP is the lowest pressure at which the injected gas can develop first or multiple contact miscibility with given reservoir oil at reservoir temperature. Miscibility occurs at high pressures, and most heavy are found in shallow formations. Consequently, miscible flooding is commonly applied to light oils.

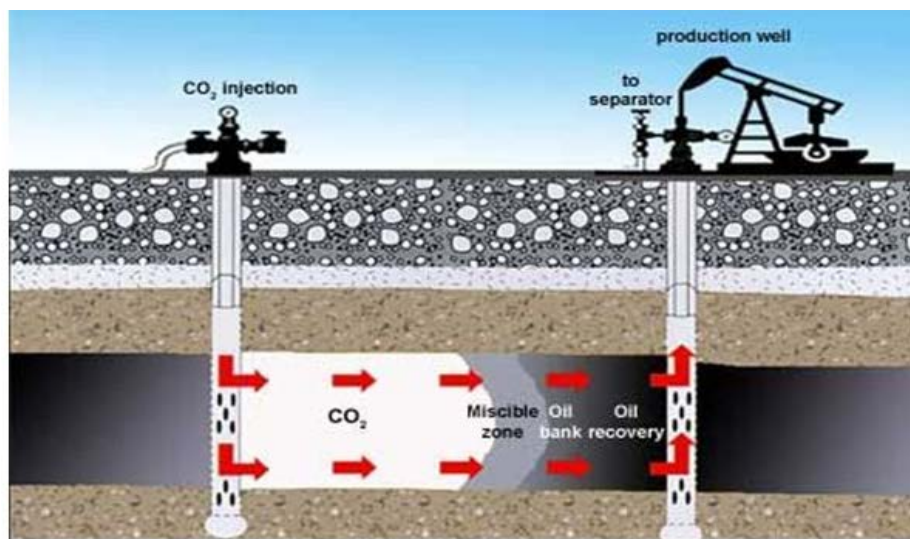


Figure 2.11: Carbon-dioxide EOR process[87]

2.8.3.1 Mechanism of Carbon-dioxide Immiscible Flooding

The recovery of heavy oil is determined by the physical, chemical and flow properties of the heavy oil and the injected CO₂. The three main mechanisms driving the oil recovery process are viscosity reduction, oil swelling and reduction of the interfacial tension between the oil and the formation water.

2.8.3.1.1 Viscosity Reduction

CO₂ dissolves in crude oil causing a significant drop in oil viscosity. The reduction of the oil viscosity depends on the reservoir pressure and its effect on the mobility ratio is favourable in viscous oils than in less viscous oils [88-90].

2.8.3.1.2 Oil swelling

The solubility of CO₂ is a critical parameter in the recovery process. Gaseous CO₂ dissolves in crude oil causing an increase in the oil volume. The swelling factor of the oil is determined by the pressure, temperature and composition of the oil. It was discovered that 123.8 m³ of CO₂ dissolved in 1 m³ of crude oil yielded about 10-40% increase in oil volume [91].

2.8.3.1.3 Interfacial Tension Reduction

Immiscible flooding process is characterized by the interfacial tension between the reservoir and the injection fluids. However, the presence of CO₂ has been shown to decrease the interfacial tension between the oil and formation water by about 30% [92].

2.8.4 Laboratory Reports of Immiscible CO₂ Flooding

Lloydminster and California heavy oil have an API gravity of 14° and a viscosity of 3000cp. Laboratory tests conducted by Earlougher Engineering showed that the CO₂ drive process is an effective method for heavy oil recovery. At 1250 psia, CO₂ flooding after carbonated water flooding recovered up to 54% of the residual oil. The CO₂ utilisation factors ranged from 1.6-6.7 Mscf/bbl (a thousand standard cubic feet per barrel of oil) [93]. West Sak crude oil has an API of 10.5° to 22.5° and a viscosity ranging from 50 to 3000cP. A numerical simulation conducted using values from laboratory model showed that continuous CO₂ injection is the most effective of various CO₂ injection methods [94]. In Saskatchewan, Canada, oil with 14-17° API and viscosity 1430 at 28°C was subjected to immiscible flooding process. Two methods were particularly employed in the process: CO₂ slug injection and CO₂-water alternating gas (WAG). The results obtained from the experiments indicated that the WAG process was more effective in improving recovery [92]. The purity of CO₂ used in the process is also a contributing factor. A Saskatchewan crude oil with a viscosity of 1058cp was also flooded with pure carbon dioxide (CO₂), pure nitrogen (N₂) and a mixture of both. The results showed that oil recovery was highest with pure CO₂ having a value of 51.3% followed by the CO₂-N₂ mixture with a nitrogen mole percentage of 5% [95]. Figure 2.12 illustrates the results obtained from the experiment.

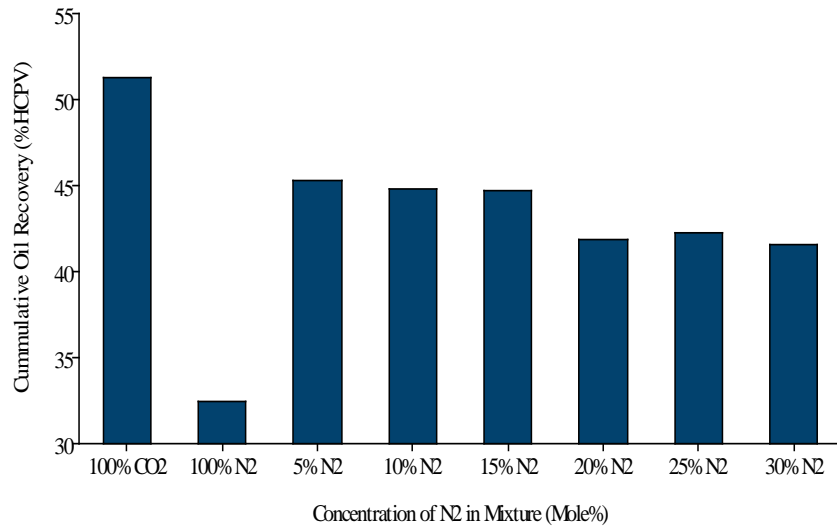


Figure 2.12: Effect of nitrogen content on oil recovery[95]

2.8.5 Field Reports of Immiscible CO₂ Flooding

However, it must be noted at this point that the cumulative percentages obtained in the various laboratory experiment described above, represents values obtained by flooding the reservoir model without proper consideration for the CO₂ utilisation. For field projects, where the amount of CO₂ injected affects the economics of the process oil recoveries are still well below 15% PV (Hydrocarbon Pore Volume) in most cases. A good example is the application of CO₂ immiscible flooding method in Forest and Oropouche fields in Trinidad and Tobago.

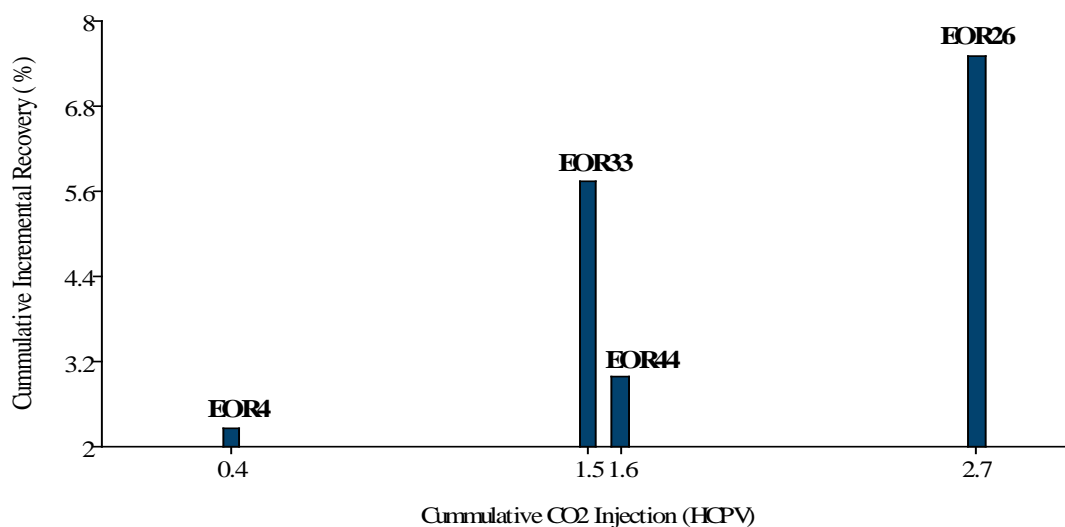


Figure 2.13: Performance evaluation of Forest and Oropouche Field Projects[96]

The fields contain crude oil with gravity ranging from 17 to 29° and are situated at depths between 2160ft to 4200ft. Four CO₂ immiscible flooding were conducted in fields EOR4, EOR26, EOR33 and EOR44 and their performance were evaluated [96]. The result obtained is shown in Figure 2.13. EOR26 recorded the highest value regarding cumulative incremental recovery but the volume of carbon dioxide injected is factored into the process, EOR4 gave the best performance, producing 5.625% per one hydrocarbon pore volume. (PV).

2.8.6 Challenges Facing Immiscible CO₂ Flooding Process

Farouq Ali along with some researchers investigated the performance of 113 field test conducted using non-thermal methods for heavy oil recovery. Among the tests were 54 polymer flooding, 25 Carbon dioxide flooding, 15 caustic flooding and 19 other flooding methods. The outcome of the investigation is exemplified in Figure 2.14. From the methods investigated carbon dioxide performed the best producing an incremental recovery of about 11% [97].

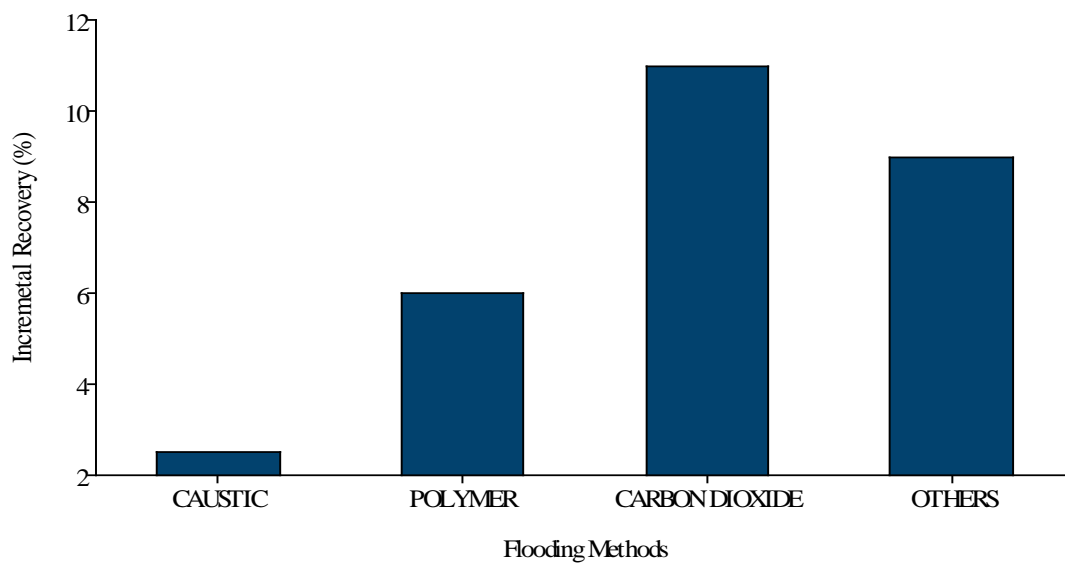


Figure 2.14: Performance evaluation of non-thermal methods for heavy oil recovery[98]

Despite its performance, immiscible CO₂ flooding is still saddled with technical and economic challenges. The relatively low viscosity of CO₂ compared to heavy oil causes viscous fingering and channelling leading to process inefficiencies. A typical case is the Lick Creek oilfield. The field yields oil with 17°API and 160cp viscosity. Barely two weeks after production, has a CO₂ breakthrough occurred as most of the oil was being bypassed by the injected gas. The result was a recovery of 11.1% as against the 16% projected [99]. On the economic front, the total

cost for CO₂–EOR projects is governed by the cost of CO₂, investment in the infrastructure for the injection, separation and transportation cost including operation cost [99]. Consequently, the quantity of CO₂ utilised for the injection process is very crucial.

2.9 Perforation diameter and CO₂ Bubbles

Perforation diameter and CO₂ bubbles forms the conceptual framework for this study. The impact of perforation diameter and CO₂ bubble sizes, and how they affect changes in viscosity and heavy oil recovery in a sandstone reservoir. Therefore, a brief overview of these factors are necessary.

2.9.1 Perforation

Perforations are holes made through the steel casing and cement sheath in order to establish communication that allows for the flow of reservoir fluids into the wellbore. The fate of an oil well hinge on years of exploration, months of well planning and weeks of drillings, but it eventually relies on executing the optimal completion, which begins with perforation. As shown in Figure 2.15, perforation forms channel into the reservoirs that not only allows hydrocarbon recovery but influences it [100]. There are four geometrical parameters governing flow efficiency in perforated completion: shot density, phase angle, perforation penetration, and perforation diameter.

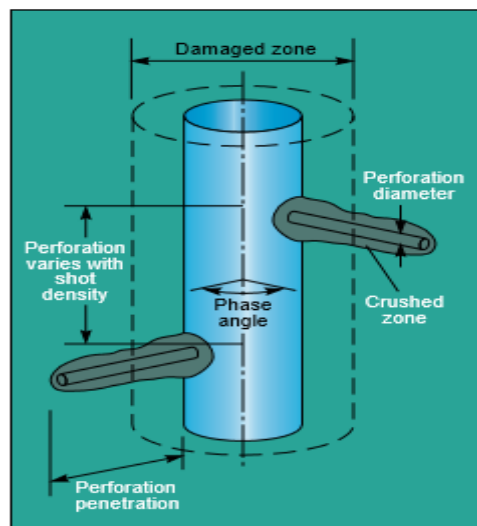


Figure 2.15: Geometric parameters of a completed perforation [100].

Shot density, also known as perforation density, refers to the number of shots made per foot. Not all shots contribute to fluid flow; the portion of the total shot density contributing to the production or injection of fluids is regarded as the effective shot density. Phase angle is the

radial distribution of the successive perforation charges around the gun axis. Usually, the gun assemblies are phase at 0° , 60° , 90° , 120° and 180° . Perforation penetration is a measure of the length a functional perforation tunnel extends past the casing or liner into the reservoir formation. In most completion process, a high penetration is required so that fluid flow access can be made through the damaged zone of the formation. Perforation diameter is the diameter of the hole generated from the casing or liner into the reservoir formation.

2.9.2 Bubble Formation

Bubbles are gas-filled cavities having an internal pressure that is at least that of its external environment. Figure 2.16 typifies a gas bubble formed in a liquid solution. The interface of each bubble possess properties that are different to the bulk solution. Smaller bubbles have higher internal pressure and release gas to dissolve under pressure into the surrounding under saturated solution while larger bubbles grow by absorbing gas from the supersaturated solution. Hence, large bubbles grow while small bubbles shrink. In CO_2 -EOR, bubble formation is achieved through a process known as sparging.



Figure 2.16: Gas bubbles in a liquid[101]

2.10: Literature Survey

The section aims to introduce the reader to the work of other researchers and authors that are related to the present study and to provide additional information to the materials presented in chapter two. The literature survey is divided into three sections:

- Bubbles dissolution in channels: The study of the effect of perforation diameter on the distribution of CO₂ bubble size distribution is novel. Hence, there is little or no literature available on the subject matter. However, the physics of bubble formation and dissolution mass transfer has been well studied in the field of multiphase flow. Therefore, this section of the review is concerned with the detailed presentation of the works of authors in the field of multiphase flow regarding the dissolution of bubbles within a viscous fluid in micro channels. It examines the physics of multi-phase bubble dissolution and tracking of the dissolved CO₂ bubbles
- Viscosity reduction: This section presents an in-depth review of the literatures of authors on the subject of CO₂-heavy oil viscosity reduction in enhanced oil recovery processes.
- Oil recovery and CO₂ utilisation: This section presents an assessment of the work done by authors on the laboratory investigation of the application of carbon dioxide flooding for heavy oil recovery processes. The CO₂ utilisation for each case of the process is also considered.
- Finally, a section summarizing the literature is presented that exposes the gaps in the studied literatures that necessitated the current investigation.

2.10.1 Review of Literatures on CO₂ Bubbles in Micro-channels

This section of the literature review looks particularly at published material in the area of CO₂ bubble formation, dissolution in micro-channels in the context of the current study. A summary of these literatures can be found in Appendix A.

Timoshenko et al., (2017) conducted a numerical simulation to study the formation and dissolution of CO₂ bubbles within silicon oil in a micro-channel. The authors utilised a coupled multiphase multi component computational fluid dynamics model to investigate the effects of varying surface tension, diffusion coefficient and flow rates on the initial length of bubble formed, mass transfer coefficient and the period of bubble formation. The results from the study showed that increasing the surface tension causes the bubble cap to be less curved and that the initial bubble length and bubble formation were strongly affected by the flow rate [102].

Ganapathy et al., (2015) studied the hydrodynamics and mass transfer performance of a micro-reactor for enhanced gas separation process. The results showed that the decrease in channel diameter resulted in an enhancement in the absorption performance[103].

Suazade et al., (2013) investigated the initial micro fluidic dissolution regime of CO₂ bubbles in viscous oil. The authors conducted an experimental investigation of bubble morphology from low to large capillary numbers and measured the effective mass diffusion flux across the interface by tracking and monitoring. Their findings showed that it was possible to control and main[104].

Tan et al., (2011) studied the mass transfer performance of gas-liquid segmented flow in micro channels. The authors conducted an experimental investigation of the influence of channel geometry on the overall dissolution mass transfer coefficient. The results showed that the dissolution was higher for curved surfaces than at straight surfaces and the gas bubbles were considerably smaller during dissolution mass transfer and accounting for 30 to 40% of the dissolved solute during the formation stage[105].

Haining et al., (2009) studied the effect of design and operating parameters on CO₂ absorption in microchannel contactors. The authors conducted an experimental investigation to determine the feasibility of using microchannel contactors for the absorption of CO₂ by PZ activated MDEA. The results from the experiment showed that the mass transfer rate was enhanced when smaller microchannel were used. The mass driving force also increased with the increase of the operation pressure[106]

2.10.2 Review of Literatures on Heavy Oil Viscosity

This section of the literature is concerned with the works of authors on the subject of the impact of perforation diameter and CO₂ bubbles on the viscosity of heavy oil.

Sasaki et al., (2015) investigated the swelling and viscosity reduction of heavy oil by CO₂-gas foaming in immiscible conduction. The authors measured experimentally, the apparent foam viscosity to the foam swelling for a temperature range of 20 to 50 °C and draw down pressure of 1.0 to 10 MPa. The result from the experiment showed that the viscosity of the heavy oil was not only affected by temperature but by the concentration of the dissolved CO₂ in the oil[107]

In a similar study, Chanmoly et al., (2014) studied the viscosity of foamy oil by analysing CO₂ microbubbles in hexadecane. They reported that by exposing the generated foamy oil under the shear rate of 76.8 s⁻¹ for 5 minutes the bubble volume density profile changes from broadband towards a Gaussian distribution. The changes was caused by the disappearance of the larger sizes of CO₂ bubbles; that is the bubble diameter of the maximum probability density of the bubble volume density profile reduced from 80 to about 10µm. However, the ratio of the viscosity did not indicating a strong dependence of the apparent viscosity to microbubbles less than 10µm in diameter[108].

Emadi et al., (2011) conducted a series of flow visualisation experiments using a high-pressure micro model rig. The aim was to investigate the performance of CO₂ injection in heavy oil recovery and CO₂ storage. The result from the flow visualisation study showed that the colour of the heavy oil brightened during the CO₂ injection process indicating CO₂ dissolution and viscosity reduction[109].

Abivin et al., (2009) examined the rheological behaviour of foamy oils. The authors conducted an experiment to study of the kinetics of bubble evolution in heavy oil. The viscosity and visco-elastic properties were measured from the nucleation and disengagement of the bubbles from the heavy oil. Results from the experiment indicated that under low shear rates, the presence of bubbles leads to an increase in the heavy oil viscosity. However, under high shear rate, the viscosity appears lower in the direction of the flow. In conclusion, the authors argued that the influence of bubbles on the foamy viscosity depends on the shear conditions[110].

2.10.3 Review of literatures on CO₂ Bubbles and Oil Recovery

Hiroko et al., (2016) conducted a comparative core-flooding test to investigate the effects of micro bubble CO₂ injection on oil recovery. Two test cases were applied in this study: Case I and Case II. In Case I, normal CO₂ was injected into Berea sandstone core sample after water flooding. In Case II, CO₂ microbubbles generated with a special filter was injected into the same core sample used in case I. The sweep efficiency in both cases were determined with the aid of an X-ray CT scanner. The results from these experiments showed that the CO₂ bypassed most part of the Berea micromodel in Case I, but gravity segregation was remarkably suppressed in case II. The recovery factor in Case II was also greater than that of case I by 13%[111].

Mehdi et al., (2015) conducted a laboratory study to examine the performance of dense intermittent CO₂ injection as an enhanced oil recovery method for extra heavy oil reservoirs. The authors performed two core flooding tests using liquid and supercritical CO₂ as the injectant for the first and second experiment respectively. The viscosity of the live oil used in the first experiment was about 7 times higher than second. In both cases, the injection was stopped for a period of 24 hours. The results obtained from the experiment showed that injecting 1 PV of liquid CO₂ recovered 21% of OOIP while the supercritical CO₂ produced 19%[10].

Sixu et al., (2013) conducted experimental and numerical simulation to evaluate the performance of pressure maintenance and improving oil recovery with immiscible CO₂ in heavy oil reservoirs. Three well design configuration were used to examine the effects on recovery. In the first scenario, a five spot well pattern consisting of four vertical injectors and one vertical producer was used. In the second scenario, four vertical injectors and one horizontal producer were used. The third scenario consist of one horizontal injector and horizontal producer. Result from the experiments showed the recovery of 4, 16 and 16% OOIP for the CO₂ flooding at 50PV. At 1PV, there was basically no appreciable change in the recovery value from the recovery obtained from a water flooding that was conducted before the CO₂ injection[112].

2.11 Research Gaps

The general subject area of carbon dioxide enhanced oil recovery is well studied. Also, there are various authors in the field of multiphase flow and enhanced oil recovery whose works provide useful information relevant to this study. Appendix A presents a bibliography of references in the order stated in section 3.1, specifying the authors, titles, and the extent of their investigation. However, it can be seen from the survey that more work needs to be done regarding the overall mechanism driving the immiscible CO₂ injection process in heavy oil reservoirs; especially in the area of the role of CO₂ bubble dynamics and well completion perforation where there is paucity of literature. Consequently, this research study focuses on the effect of CO₂ bubble size distribution on heavy oil viscosity and recovery during enhanced oil recovery processes. It also aims to investigate the role of casing perforation diameter on the CO₂ bubble size distribution.

2.12 Chapter Summary

The chapter presented an overview of the global energy mix in the context of the current energy challenges and emphasized the major role of conventional oil resources in dealing with the energy challenges. However, it also assessed the future prospects of the use of conventional oil resources in the energy mix and offers heavy oil as a viable option in dealing with the short and long term energy situation. In the concluding sections, it presented the methods, scope, and the limit of the investigation conducted by several authors on key areas that are indirectly or directly related to the aims of this current study. The review was deliberately restricted to the work of researchers within the last ten years. This was done to ensure that the material and methods applied by these authors are consistent with current trend in research methodology. The gaps identified from the literature survey forms an integral part of the current study. Consequently, the succeeding chapters would focus on the series of experimental plan designed to close these gaps.

Chapter 3

Methodology

3.1 Introduction

This chapter introduces the reader to the apparatus, materials, and procedures used in the study, as well as the errors associated with it. It consists of three sections, with each section describing a phase of the experimental work. The first phase of the experiment describes the preliminary investigation. The second phase is particle characterisation and viscosity measurement, while the third and final phase is the reservoir petrophysics and oil recovery experiment. In each of the phases, the apparatus subsection describes the design and function (s) of the equipment and its constituent parts. The section is followed by the material subsection, which represents the materials used. The procedure subsection explains the steps taken to conduct the experiments. A chart of the experimental process and phases is illustrated in Figure 3.1

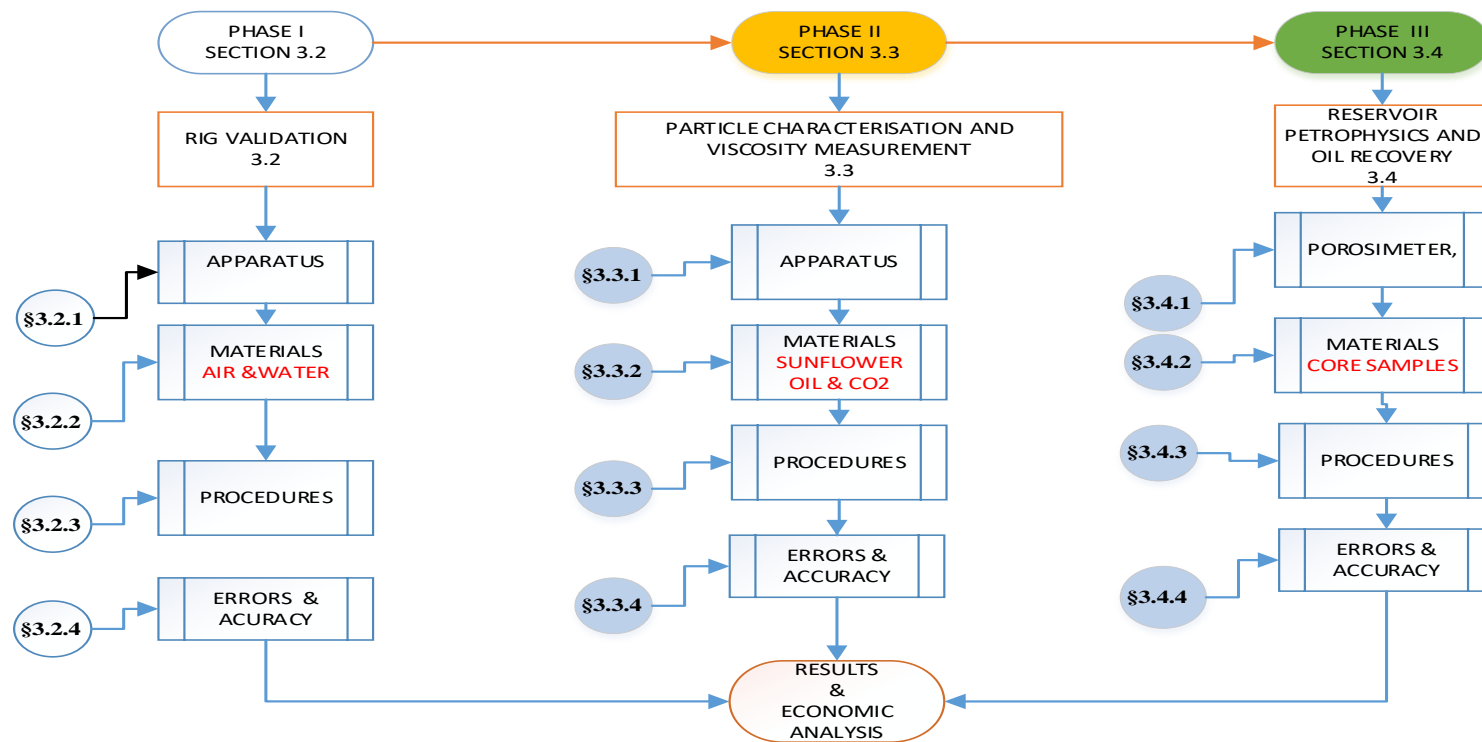


Figure 3.1 Sequence of experimental investigation

3.2 Phase I: Rig Validation

The laboratory work for this study was conducted with the aid of an experimental rig. The construction of the rig was necessary because the standard equipment used in reservoir fluid flow experiments of this kind do not offer the option of simultaneous in-situ imaging of gas bubbles and heavy oil viscosity measurement. Consequently, a preliminary test was conducted to ensure the safety and reliability of the rig. Two particular tests were carried out. The rig was first pressure-tested and subsequently used to conduct a trial particle characterisation experiment.

3.2.1 Apparatus

3.2.1.1 Rig Setup

The rig consists of an assembly of a transparent perspex tube, pressure gauge, pressure regulator, pressure relief valve, L-shaped copper pipe serially connected with a polyamide calibre tubing of the same diameter. For this phase of the experiment, the supply end of the polyamide calibre tubing was attached to a compressed air cylinder, while the discharged end was connected to the horizontal section of the L-shaped copper pipe. The horizontal section consist of the gas inlet nozzle. Figure 3.2 and 3.3 shows the schematic and snapshot of the rig. The design specifications of the gas inlet nozzle as well as the cylindrical tube section of the rig are detailed in Appendix B.

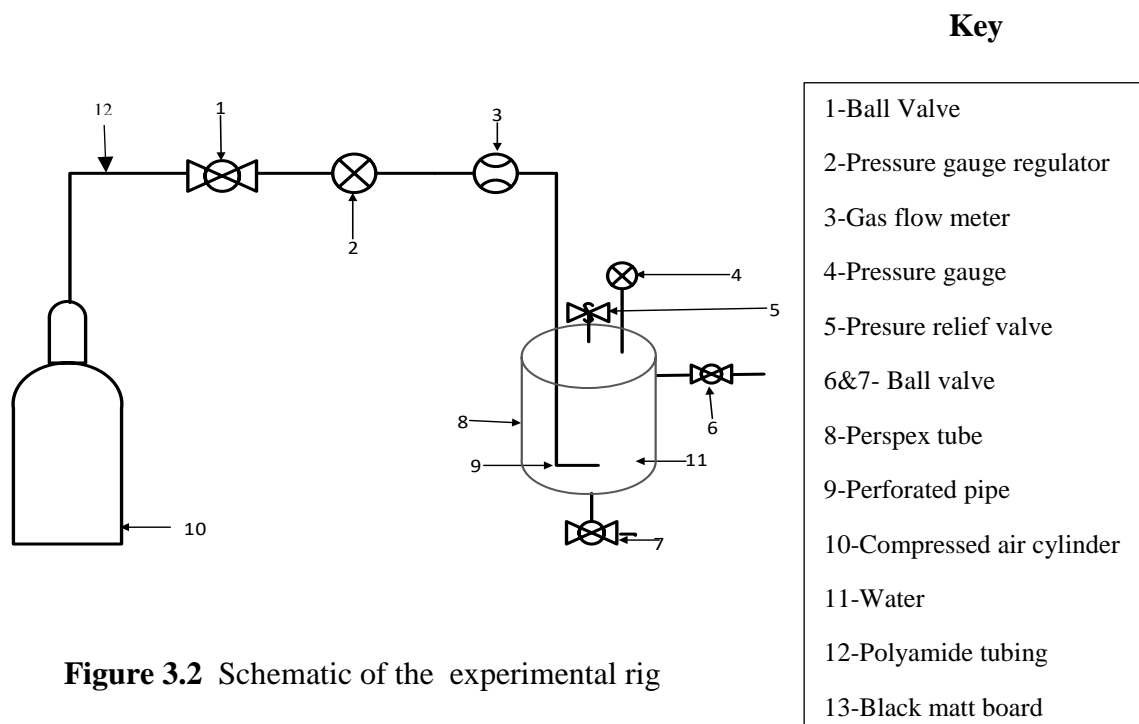


Figure 3.2 Schematic of the experimental rig

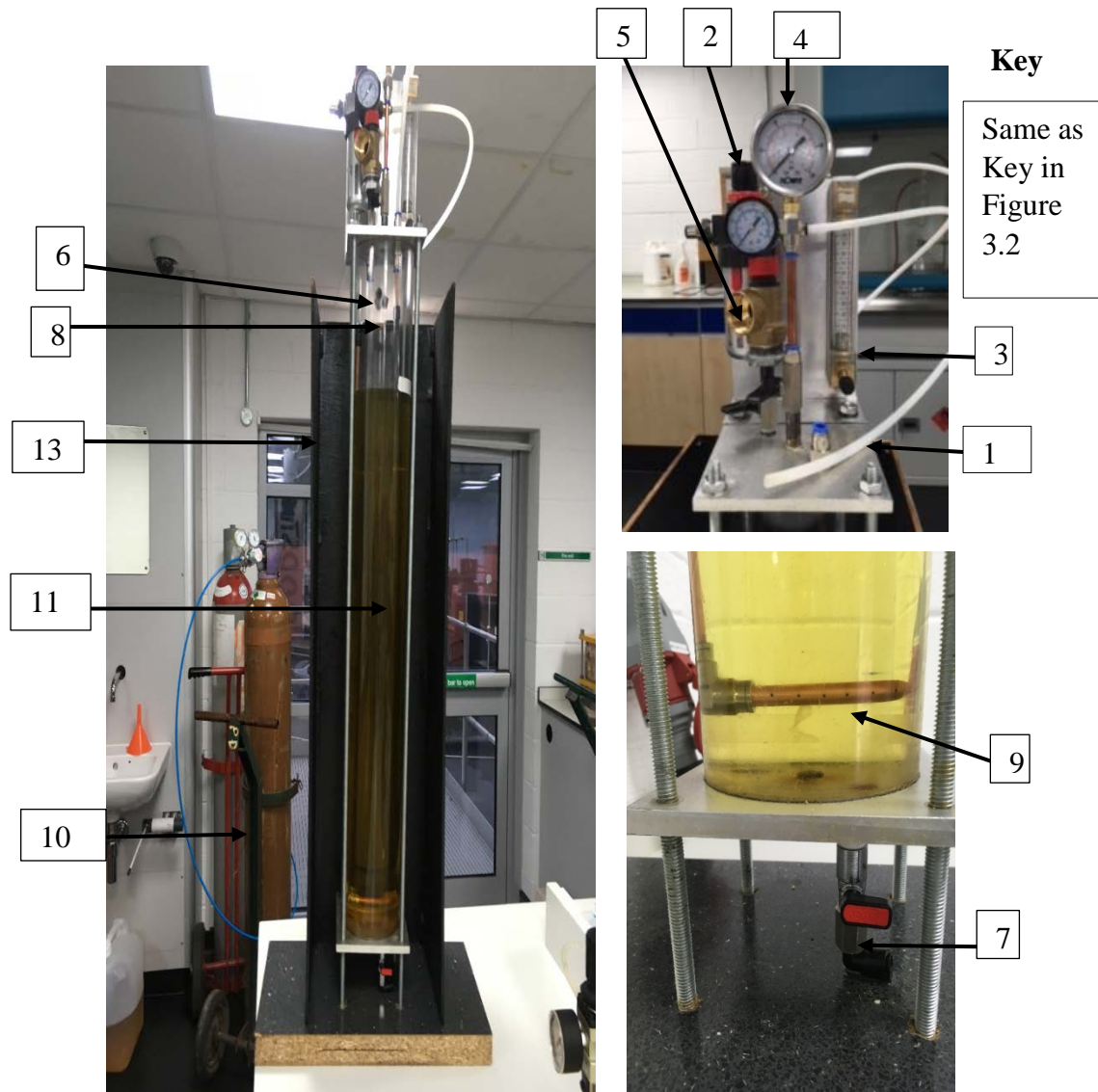


Figure 3.3 Snapshot of the experimental rig

The ball valve was used to provide on/off control of the flow of air from the compressed air cylinder. The design of the ball valve makes it suitable for gas applications where leakages are not tolerated. The function of the pressure gauge regulator was to match the flow of air through the regulator to the desired output pressure. The pressure relief valve limits the pressure within the system to a maximum working pressure of 3bar. The flow meter and totaliser display the volume flow rate of the gas entering the transparent tube section.

3.2.1.2 Imaging Setup

The images of the air bubbles in water during the fluid flow process in the transparent Perspex tube was acquired using a high-speed Canon EOS 700D camera with a frame speed of 25 frames per second (fps). The continuous phase was illuminated by two low powered light-emitting diode (LED). The camera was supported by a tripod stand placed 40cm from the perspex tube. The black painted board shown in Figure 3.3 was placed around the tube to minimise the effect of reflection from the led lightings. The setup for the image acquisition is shown in Figure 3.4. The videos obtained during the experiment was converted to frames using the Adobe Photoshop Software. Appendix C shows the detail specification of the high-speed camera.

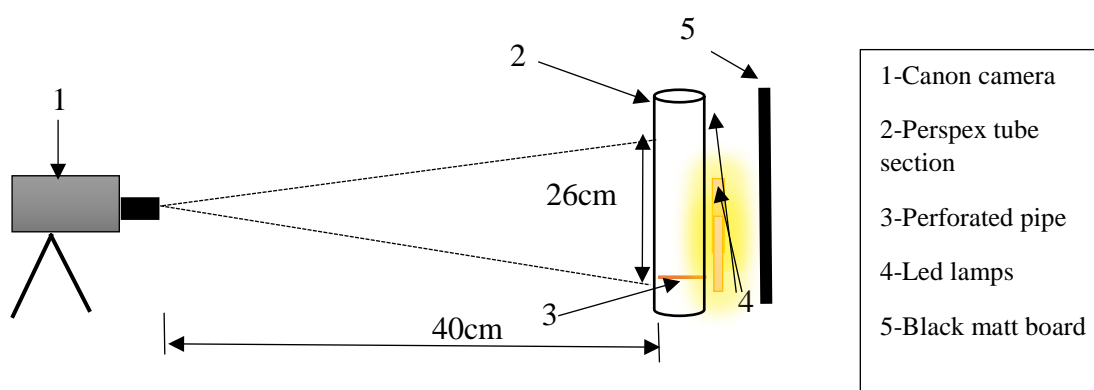


Figure 3.4: Setup for image acquisition

3.2.2 Materials

As stated in section 3.2.1.2, the reagents used for the preliminary experiment were water and air. The reagents were chosen because of their suitability, availability, and cost. The Table 3.1 shows the specification of the reagents used.

Table 3.1: Material specifications

Materials	Temperature (°C)	Pressure (bar)	Density (kg/m ³)
Air	23.8	1 - 6	1.2041
Water	23.8	Atmospheric	1000

3.2.3 Procedures

The rig setup for the experiment was connected as shown in Figure 3.2. The transparent cylinder was filled with distilled water at a laboratory temperature of 23.8 °C to a height of 70 cm, resulting in a hydrostatic pressure of 0.0686 bar. A feed connected to a compressed air cylinder at 120 bar supplies air into the system. The 120 bar pressure was regulated by a series of pressure reducing valves to 10 bar. The minimum air injection pressure used was 1.2 bar. Two reasons necessitated the choice of a minimum pressure of 1.2bar. First, for air bubbles to be generated and for flow to occur, the air injection pressure must be greater than the hydrostatic pressure in the water column in the Perspex tube. Secondly, the air injection pressure has to be low enough to generate images of bubbles that can analysed accurately.

3.2.3.1 Pressure Testing

The first part of the preliminary experiment is the pressure testing of the rig. The testing was necessary to ascertain the suitability of the rig to withstand build-up of pressure up to a maximum of 6 bar during the main experiment. A certified technician did the testing in line with the Provision and Use of Work Equipment Regulations 1998 (PUWER).

- i. The pressure regulator was adjusted to supply air at 2bar to the system while the ball valve is shut
- ii. The pressure gauge was monitored while the system is kept closed for one hour
- iii. The system was checked for signs of air and water leakage
- iv. The process was repeated for pressure 3,4,5 and 6 bar.
- v. At 6 bar, the system was kept shut and the pressure monitored for 8hours

3.2.3.2 Particle Imaging

The rig set up for the fluid flow pre-testing required the use of additional devices. To begin with, the experiment was conducted with the lightings in the laboratory turned off. The water filled Perspex tube section was illuminated by two light emitting diode bulbs and covered with a U-shaped matt black wooden board to minimise the effect of reflection. Once the setup was completed, the following steps were used for the experimental process results obtained.

- i. The temperature of the laboratory was first measured and recorded.
- ii. The camera and the led lightings were positioned as described in Section 3.2.1.2.
- iii. Compressed air from the cylinder was released and adjusted to a pressure of 1.2bar.it was injected into the cylinder by opening the flow meter already connected to the copper pipe with a perforation diameter of 0.5 mm.
- iv. The images of the air bubbles generated in water were recorded for 5 mins.
- v. The process above is repeated for 1.4 bar, 1.6 bar, 1.8 bar, 2.0 bar, and 2.2 bar.
- vi. Once the reading was taken, the 0.5 mm perforated pipe was replaced, and the steps from two to five were repeated for pipes of the diameter: 1.0 mm, 1.5 mm, 2.0mm, 2.5 mm, and 3.0 mm.

3.2.4 Errors and Accuracy

The accuracy of the pressure gauge, volumetric gas flow rate and meter rule are $\pm 4\%$ FSD, $\pm 2.5\%$ FSD, and $\pm 0.5\text{mm}$ respectively. Where FSD means full-scale deflection. The following steps were taken to ensure that experimental errors were minimised.

- i. The flow meter, pressure regulators, and gauges were all tested and calibrated before use.
- ii. The temperature and humidity of the laboratory were kept constant throughout the experiment.
- iii. The measurements were repeated and the mean value calculated.
- iv. The laboratory lighting was switched off during the image acquisition process.
- v. Measurement from these analogue devices were taken at the same level of the markings to avoid parallax error.

3.3 Phase II: Particle Characterisation and Viscosity Measurement

This phase of the experiment aims to examine the effect of the perforation diameter and the resulting CO₂ bubbles size distribution on the viscosity of sunflower oil under varying pressure conditions. The experiment represents a laboratory model that simulates the application of CO₂ Immiscible flooding in a heavy oil reservoir. However, the focus at this stage is to investigate the pore-scale mechanism behind the changes in heavy oil viscosity.

3.3.1 Apparatus

3.3.1.1 Rig Setup

The rig setup for the particle characterisation and viscosity measurement is a slight modification to the preliminary test rig. Here, a Viscolite 700HP viscometer replaces the pressure gauge in section 3.2.1.1 while a flow totaliser was serially attached to the flow meter. The shaft end of the viscometer was immersed into the Sunflower oil to a depth of 35mm. Also, the compressed air cylinder was replaced with a carbon-dioxide cylinder while the water in the perspex tube was changed to Sunflower oil. The areas in the rig setup affected by these changes are highlighted in green colour as shown in Figure 3.5.

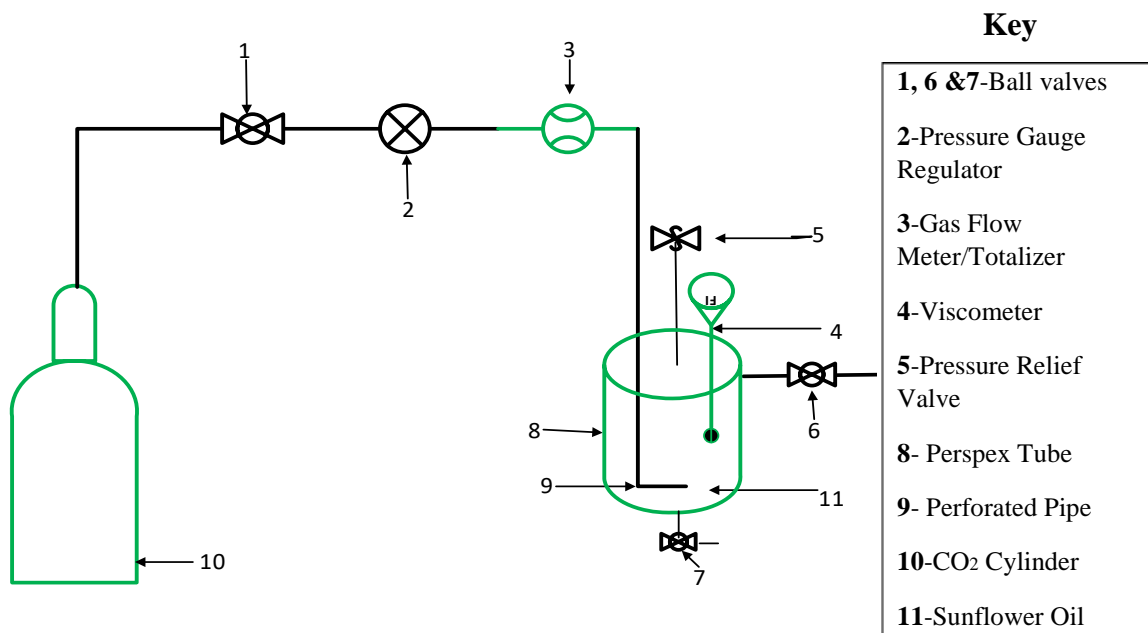


Figure 3.5 Schematic of a section of the rig showing how the various instruments are connected.

3.3.1.2 Viscometer

The Sunflower oil viscosity was measured with the aid of the Viscolite 700HP viscometer. The Viscolite 700HP is a handheld or bench-mounted instrument. It is used for the instant measurement of fluid viscosity by insertion. The sensor has a solid construction with no moving parts. It is connected to a microprocessor unit by a flexible cable, and the whole instrument is powered by a transformer/adaptor unit. The design of the instrument makes it suitable for in-line or in-situ measurement of viscosity. Figure 3.6 shows the Viscolite 700HP viscometer.

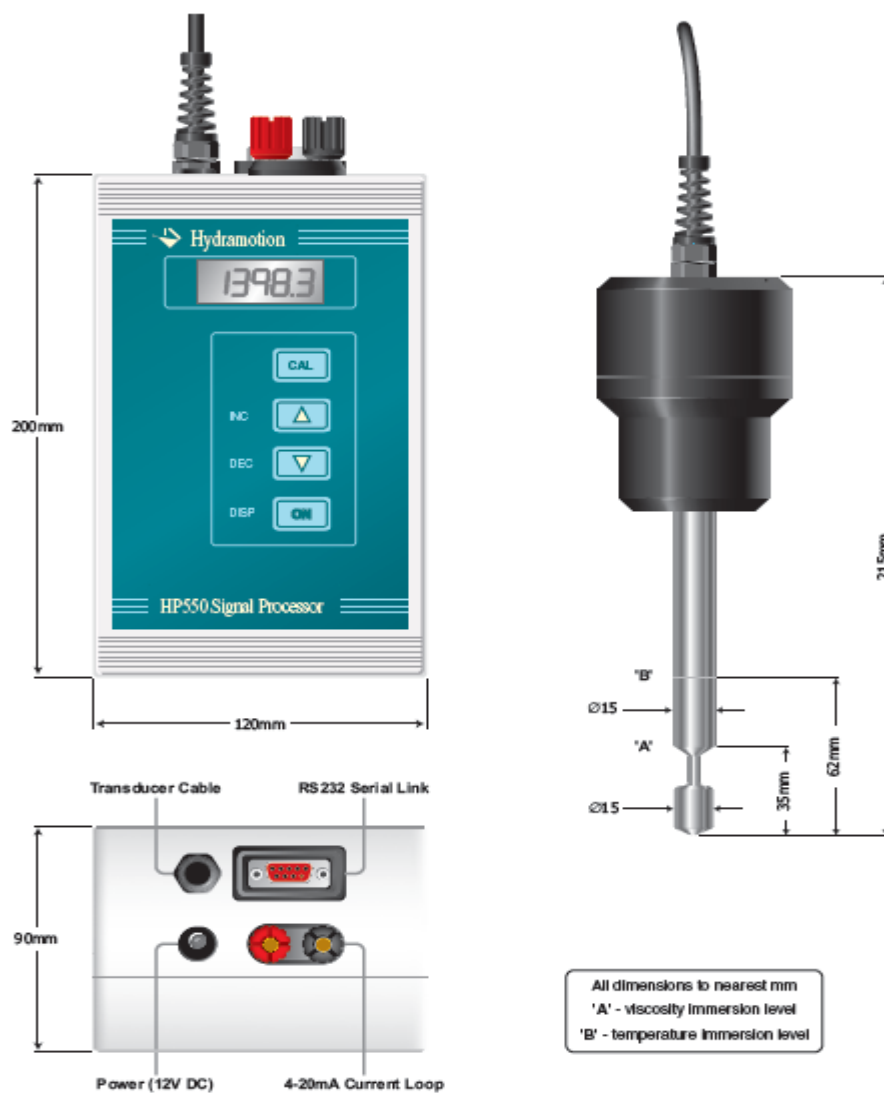


Figure 3.6 Viscolite VL 700HP Portable Viscometer[113]

3.3.1.2.1 Working Principle of Viscolite Viscometer

The sensor element consists of a shaft with an end mass, or bob, which was made to vibrate (also called resonate) at its natural frequency. When vibrating, the moving parts of the sensor shear through the fluid. As this shearing takes place, energy is lost to the drag forces on the sensor caused by the viscosity of the fluid. The loss of energy in each cycle of vibration is measured by the sensor electronics and the microprocessor in the display unit. From this energy loss, the actual viscosity of the fluid is determined. The Viscolite is therefore in a class of instruments sometimes called resonant or vibrational viscometers. The response of these devices is not purely with viscosity but with the product of viscosity and density. In practice, viscosity changes on a far more significant scale than density, and the fluid density can be accommodated by merely entering its nominal value in the display unit.

3.3.1.2.2 Determination of Viscosity

The transformer was first connected to the main supply before the power was switched on. Once powered, the microprocessor in the display unit goes through its start-up routine. The display runs through all its digits and settles on the display of viscosity, with the letters 'VL' shown briefly, in units of centipoise ($\text{cP} = \text{mPa}\cdot\text{s}$). This display is called Normal Mode. If the sensor is in the air, and perfectly clean, the instrument should read zero. VL means live viscosity. Viscosity was measured by inserting the shaft end of the viscometer into the fluid to be measured to the depth of 35 mm (see Figure 3.6), and the reading of viscosity in centipoise will appear on the VL display.

3.3.1.3 Dantec Dynamic Studio Software 5.0

DynamicStudio has a range of methods and techniques for imaging measurements within the field of fluid dynamics, spray diagnostics, particle characterisation, mixing and combustion diagnostics. For imaging experiments, DynamicStudio provides easy setup and control of hardware devices, data acquisition and storage, fast analysis and professional presentation of results in the form of graphs and images. The intuitive user interface features plug-and-play hardware devices and wizards for easy setup, automated measurement capabilities, and smart data processing. This study focuses on the examination of the flow of CO_2 bubbles in Sunflower Oil. Hence, the next section addresses the working principle and application of the Interferometric Particle Imaging techniques applied in the characterisation process.

3.3.1.3.1 Interferometric Particle Imaging (IPI)

IPI is a technique used in determining the size of spherical, transparent particles through the fringes patterns observed in a defocused image. The diameter of the particle is obtained using a single image. Before performing IPI data analysis, the image must be calibrated to ensure that the images are correctly overlapped. It must be noted that the setup for the camera and lighting used in section 3.2.1.2 was used here. Also, the settings of the Canon EOS 700D camera were adjusted to meet the image specification of the FlowSense EO 4M-32 already incorporated into the dynamic studio software. The process flow chart for the IPI is shown in Figure 3.7 while the detailed steps taken is shown in Appendix E.

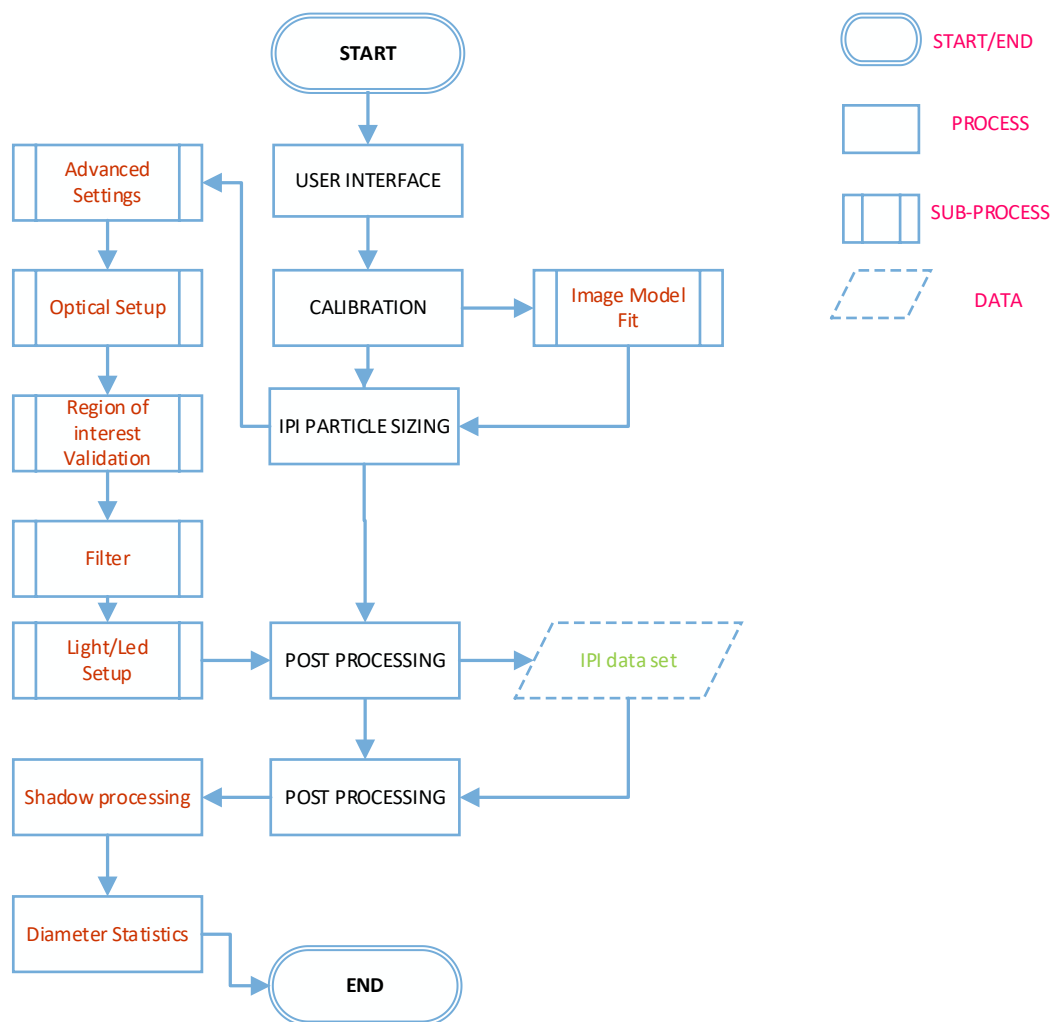


Figure 3.7 Process flow chart for the interferometric particle imaging[114]

3.3.2 Materials

The materials used for this phase of experimental work were sunflower oil and carbon dioxide. The CO₂ and Sunflower oil were used to simulate the injection and reservoir fluids respectively. The carbon dioxide used for this research work has a purity of 99.9% and a dynamic viscosity of 0.015 cP at 20 °C. The sunflower has a specific gravity of 0.91g/cm³ at 20 °C and an API gravity of 21.77°.

3.3.3 Procedures for Particle Characterisation and Viscosity Measurement

The temperature of the laboratory was measured and recorded before the start of the experiment. The temperature of the lab was kept constant at 20°C for the entire length of the investigation. Maintaining the constant temperature was an integral part of the experiment as a slight change in temperature can significantly alter the viscosity of the Sunflower oil. The setup for the test was connected as shown in Figure 3.5, while the camera was positioned as shown in Figure 3.4. The perforation diameter of the horizontal section of the copper pipe used to begin the experiment was 0.5mm. The transparent cylinder section of the rig was filled with Sunflower oil to the 70cm mark. The 16.5cm space above the tank was deliberately left to ensure that only the required length of the viscometer shaft was immersed in the fluid. The reading on the viscometer was recorded at this point. The led lighting was turned on to illuminate the region in the cylinder to be investigated. On the other hand, the laboratory lightings were switched off. The steps described hereunder were taken to conduct the particle characterisation and viscosity measurement. The flow totalizer is powered by a 12 volts battery and was pre-set to stop the flow when the volume of CO₂ gas into the sunflower solution reaches 3 litres.

- i. The CO₂ feed was opened, and the pressure regulator was adjusted to supply gas at 1.2 bar pressure into the Sunflower solution.
- ii. The camera records the flowing CO₂ bubbles generated until the flow is stopped.
- iii. The viscosity of the oil is read off from the Viscometer display.
- iv. The cylinder is emptied and refilled with Sunflower oil.
- v. The steps 1-4 is repeated for 1.4 bar, 1.6 bar, 1.8 bar, 2.0 bar and 2.2 bar consecutively.
- vi. The steps 1-5 was repeated for pipe perforation diameter of 1.0 mm, 1.5 mm, 2.0 mm, 2.5 mm and 3.0 mm.
- vii. The video recordings obtained were converted to frames using Adobe Photoshop software. The frames were subsequently imported into the Dynamic Studio software for processing as described in section 3.3.1.3.

The results obtained were tabulated and plotted on a graph to determine the relationship between the perforation diameter, CO₂ bubble distribution and heavy oil viscosity.

The tabulated result are presented in Appendix D.

3.3.4 Error and Accuracy

The accuracy of the additional instrument used for this experiment is presented here. For the accuracy and errors of instruments, not listed here, please refer to section 3.2.4. The Viscometer has the capacity of producing a reading accuracy of $\pm 0.1\text{cp}$ under the following conditions. The viscosity of the fluid sample must be in the range of 0 - 10,000cp. The temperature of the sample must fall within -20°C to 120°C. Finally, the sample must not be less than 100 ml. The XFM gas flow meter has a flow accuracy and repeatability of $\pm 1\%$ and $\pm 0.15\%$ of full scale within a temperature range of -10°C to 50°C.

The following steps were taken to minimise experimental errors:

- i. The viscometer was calibrated prior to use.
- ii. The measurement was repeated and the mean value obtained
- iii. The lightings in the laboratory were switched off and the temperature was maintained at 20°C throughout the experiment.
- iv. The error associated with the measurements were analysed by computing the standard error of the mean using the following equation[115]:

$$\sigma_m = \frac{\sigma}{\sqrt{n}} \quad (3.1)$$

Where: σ_m = standard error of the mean ; σ = standard deviation ; n = sample size

At 1.2 bar and 0.5mm perforation diameter, the reading on the viscometer for three experimental runs were 42.00cP, 41.90cP, and 42.00cP. The standard deviation of these data $\sigma = 0.058\text{cP}$ while the sample size $n = 3$. Therefore, the standard error of the mean: $\sigma_m = \pm 0.03\text{cP}$. The same procedure was repeated to compute for the standard error for all pressure and diameter condition.

3.4 Phase III: Reservoir Petrophysics and Core Flooding

In Phase II, the scope of the experiment was limited to the examination of the dynamics between the injection fluid (CO_2) and the reservoir fluid (Sunflower Oil). The estimation of the amount of oil recovered was not considered at the time. In this phase, however, a Boise and Castlegate core samples were used to model a homogeneous and heterogeneous reservoir to experimentally simulate the effect of the perforation diameter on the amount of oil recovered in a heavy oil reservoir under immiscible conditions.

3.4.1 Apparatus

3.4.1.1 Core Flooding Experimental Setup

The setup for the particle characterisation and viscosity measurement as described in section 3.3.1 was modified for use in this section. The modified rig was obtained by disconnecting a section (section A) in the former rig and reconnecting it to a core holder as shown in Figure 3.8. Figure 3.9 illustrates the disconnected section and the core holder.

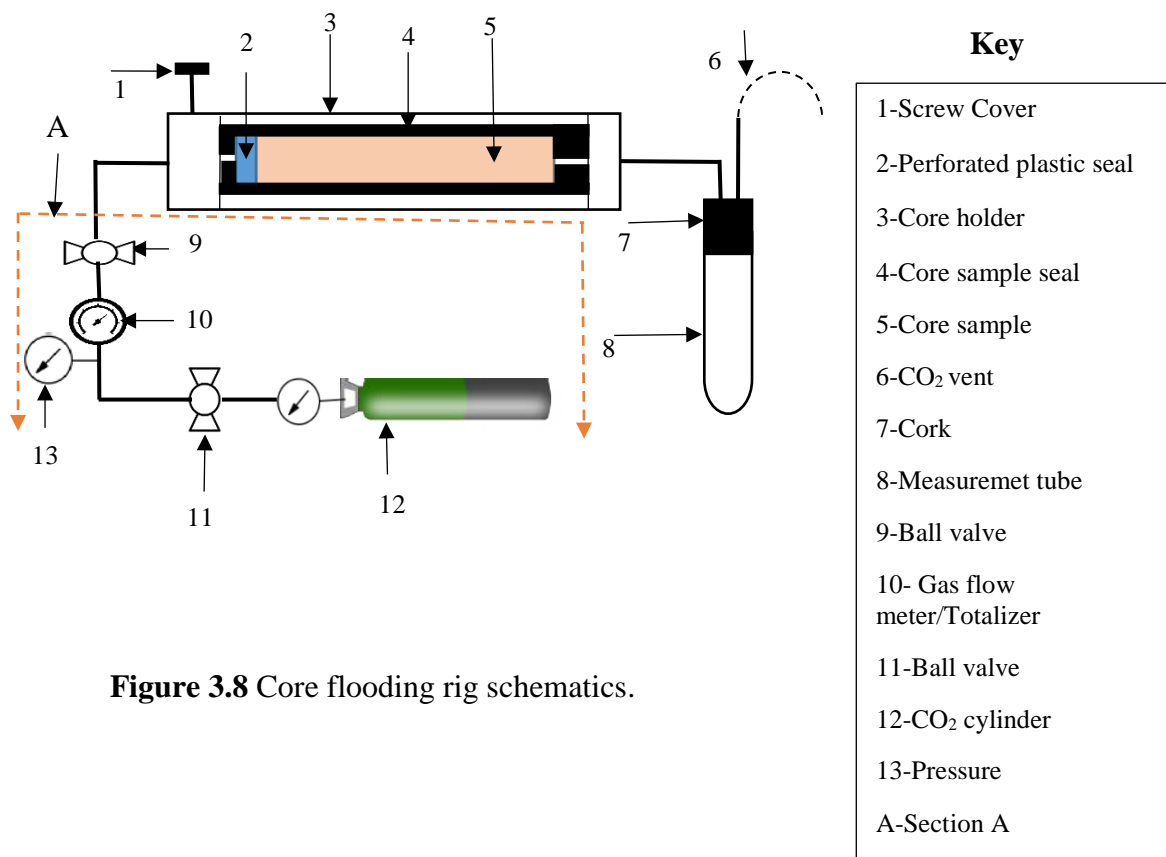


Figure 3.8 Core flooding rig schematics.

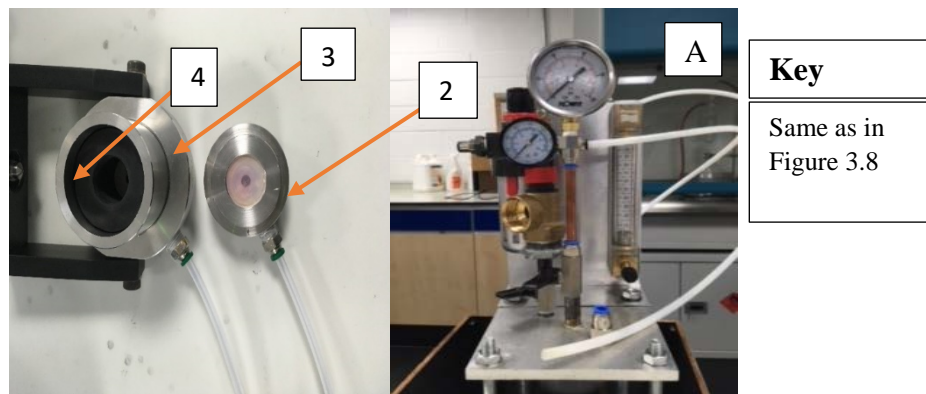


Figure 3.9 Snapshot of the core holder, the perforated seal and section A.

3.4.1.2 Reservoir Saturation System.

The reservoir saturation system consists of a Smo-King Vacuum Chamber connected, as shown in Figure 3.10 and 3.11, to a vacuum pump and a conical flask containing the Sunflower Oil. The Vacuum pressure inside the chamber was controlled by the ball valve A. The flow of oil from the accumulator was controlled by ball valve B. The core samples used as the reservoir was saturated by placing the core plug into the chamber and degassing the chamber at 10bar pressure for twenty seconds. Once the pressure was stabilised, the Valve B was slowly opened to allow for the flow of oil into the chamber. The pump was switched off, and the core sample removed just when the oil level in the chamber was above the sample

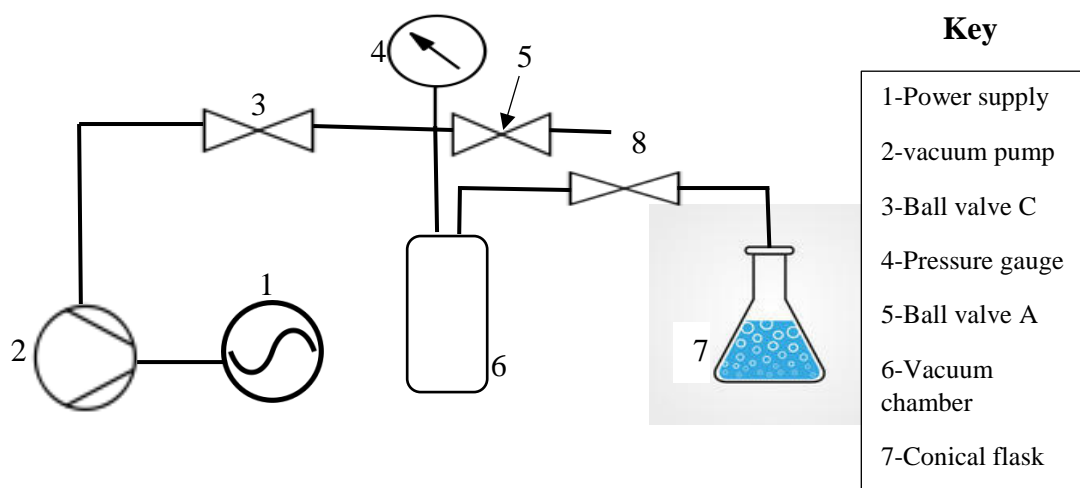


Figure 3.10 Schematics for reservoir saturation system

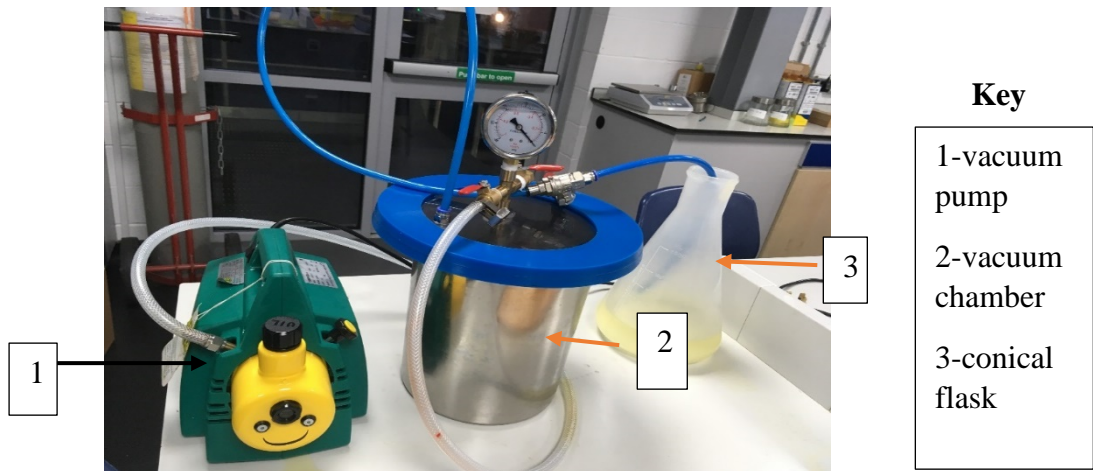


Figure 3.11 Snapshot of reservoir saturation system

3.4.1.3 Mud Balance

The mud balance is an instrument used primarily for the measurement of the density and weight of a given volume of liquid. The balance is graduated in four different scales allowing it to measure in pounds per gallon, pounds per cubic feet, grams per cubic centimetres (specific gravity) and kilogram per metre cube. Before taking the reading, the mud balance was first calibrated. The reading on the balance when taken when the volume cup at one end of the beam was balanced by a forced counterweight at the other end. To balance the beam, the slider was gently moved along the graduated scale until the level bubble on the beam was stabilised. The specific gravity of the oil was measured using the Ofite mud balance illustrated in Figure 3.12. The value obtained was used to compute the API gravity of the oil.



Figure 3.12 Mud balance[116]

3.4.1.4 PORG -200 Porosimeter

The PORG-200 porosimeter was used in the study to determine the grain volume of the core samples. The apparatus consists of the PORG-200 with a Matrix Cup for core samples with one inch in diameter and up to 3 inches in length and a set of steel calibration disks. The Figure 3.13 shows the PORG 200 porosimeter and its front panel respectively

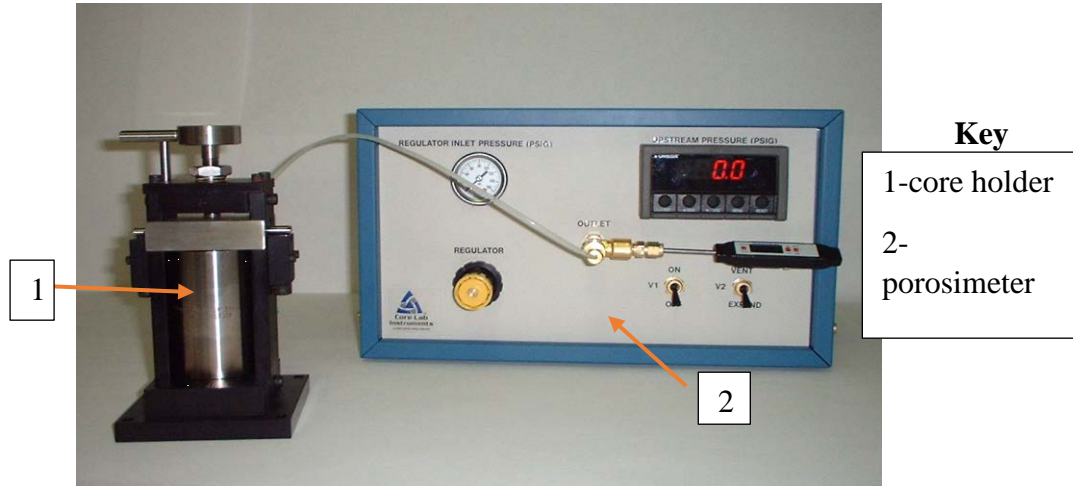


Figure 3.13: PORG-200 Porosimeter and core holder[117]

3.4.1.4.1 Principles of Operation

Porosity (\emptyset) is defined as the ratio of the pore volume to the bulk volume of a rock sample expressed in percentage. It is written mathematically in Equation 3.2[117] as:

$$\emptyset = \frac{V_p}{V_b} \times 100\% \quad (3.2)$$

Where: \emptyset = Porosity; V_p = Pore volume (cc); V_b = Bulk volume(cc)

Pore volume (V_p) is the void space in the rock. Bulk volume or Matrix volume is the volume that the rock occupies. Grain volume (V_g) is the volume of the rock grains excluding the pore volume. Equation 3.3 illustrates pore volume as

$$V_p = V_b - V_g \quad (3.3)$$

Where: V_g = grain volume of the rock sample(cc)

Bulk volume (V_b) is usually determined by a calliper or displacement method. In this study, the calliper method was used. The grain volume as previously stated was determined with the aid of the porosimeter. The porosity can then be calculated using the Equation 3.4 [117].

$$\phi = \frac{V_b - V_g}{V_b} \times 100\% \quad (3.4)$$

3.4.1.4.2 Principles of Grain Volume Determination using PORG-200

The porosimeter operates on the principle of Boyles Law. The law states that the volume of a given mass of gas is inversely proportional to its pressure provided the temperature remains constant. The grain volume of a rock sample is determined by expanding a known volume of helium into a calibrated sample holder or matrix cup. Mathematically, the general gas law is represented in Equation 3.5 [117] as follows:

$$\frac{P_1 V_1}{T_1} = \frac{P_2 V_2}{T_2} \quad (3.5)$$

Where:

P_1 = Initial Absolute Pressure (psig); V_1 = Initial Volume (cc)

T_1 = Initial Absolute Temperature (°K) T_2 = Expanded Absolute Temperature (°K)

P_2 = Expanded Absolute Pressure (psig); V_2 = Expanded Volume (cc)

The reference volume is pressured to 90 psig and expanded into the matrix cup sample holder containing the core sample to be analysed. A second pressure is read, and it is used to calculate the unknown volume using Equation 3.6 [117]:

$$V_g = V_c - V_r \left\{ \frac{P_1 - P_2}{P_2 - P_a} \right\} + V_v \left\{ \frac{P_2}{P_2 - P_a} \right\} \quad (3.6)$$

Where:

V_g = Grain Volume (cc); V_c = Sample Chamber Volume (cc);

V_r = Reference Chamber Volume (cc); V_v = Valve Displacement Volume (cc)

P_1 = Absolute Initial Reference Volume Pressure (psig)

P_2 = Absolute Expanded Pressure (psig)

P_a = Absolute Atmospheric Pressure Initially in Sample Chamber (psig)

3.4.1.4.3 PORG-200 Porosimeter Panel Description

The Figure 3.14 shows the front panel of the porosimeter. The function of the various components required for the measurement of the porosity of the core samples is described hereunder.

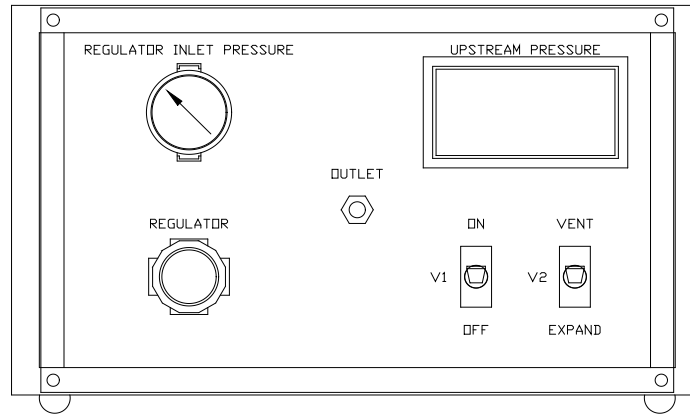


Figure 3.14 Front Panel of PORG-200 Porosimeter[117]

(a) Helium Inlet Port

The helium inlet port allows for the connection of the porosimeter to the helium source

(b) Helium Outlet Port with Temperature Sensor

The outlet port allows the connection of the porosimeter to the matrix cup for grain volume measurement. The temperature sensor measures the temperature of the helium passed into the porosimeter

(c) Regulator Inlet Pressure

The regulator inlet pressure displays the inlet pressure from the helium cylinder.

(d) Upstream Pressure

The upstream pressure reads the reference pressure in pounds per square inch gauge (psig).

(e) Regulator

The regulator allows for the adjusting of the input gas pressure to the desired reference pressure.

(f) Valve 1 (V1)

The valve V1 controls the flow of helium from the regulator to the reference cell.

(g) Valve 2 (V2)

The valve V2 performs two functions. It directs the helium from the reference cell to the matrix cup and vents the cup once the measurement is completed.

3.4.1.4.4 Determination of Porosity

The helium gas cylinder was connected to the helium supply port at the rear of the instrument. The pressure from the cylinder was regulated to supply 120 psig to the helium port. The helium outlet was connected to the matrix cup with a short tubing. The tubing had to be short to minimise the effect of dead volume. Before the porosity measurement, the porosimeter was leak tested and zeroed.

(a) System Grain Volume Calibration

Once the leak test and zero checks had been completed, the instrument was ready for grain volume calibration. A reference disk with an identification number (1) was placed into the matrix cup. Valve V2 was turned to the Vent position while the valve V1 was switched on. The system was pressurised to 90 psig by adjusting the regulator. The reference pressure (P1) was read off the display once the gas inlet valve was switched off. The expanded pressure (P2) was obtained by turning the valve V2 to Expand. The pressure in the display was observed until the reading was stabilised. The stabilised pressure is the expanded pressure. The valve V2 was switched to Vent, and the calibration disk was removed. The process was repeated for all the calibration disk and its combination. The readings obtained were recorded accordingly.

(b) Grain Volume Determination

The grain volume of the Boise and Castlegate core samples were determined using the procedure for the grain volume calibration described in 3.4.1.5.4(a). In this case, however, the calibration disk was replaced by the actual sample. The values for the reference and expanded pressure obtained from the calibration and the core samples were inputted into an excel spreadsheet for the computation of the grain volume.

3.4.1.5 PERG -200 Permeameter

The PERG-200 permeameter was used in the study to ascertain the gas permeability of the Boise and Castlegate core samples. The apparatus consists of the PERG-200 permeameter connected to a Fancher core holder as shown in Figure 3.15. It incorporates a digital pressure transducer, flow rate meter, thermometer, valves and flow system that enables the measurement of gas permeability of one-inch core samples.

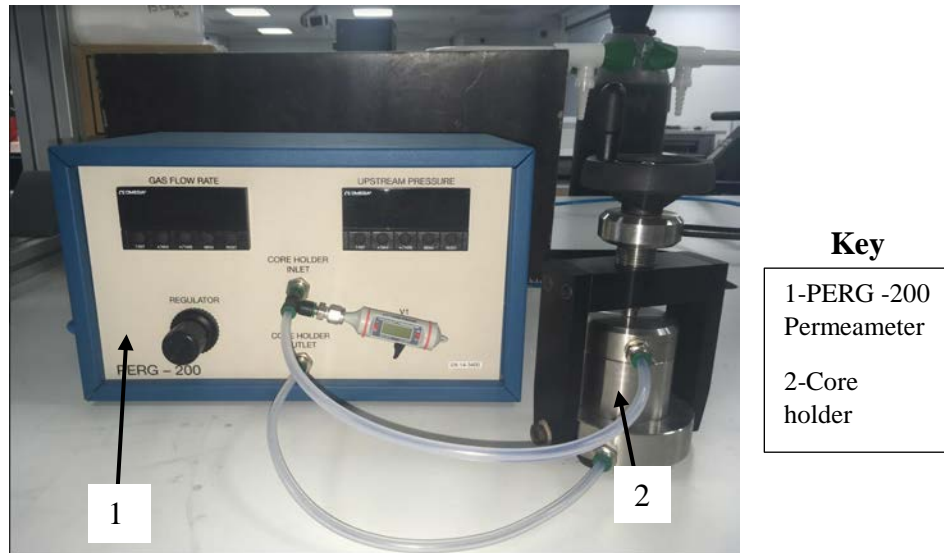


Figure 3.15 PERG-200 Permeameter connected to a core holder[118]

3.4.1.5.1 Theory of Gas Flow in Porous Media

In 1895, Henry Darci empirically established the flow of fluid in porous media as a function of the differential pressure per unit length. Darci represented the findings using the following the Equation 3.7 [118] expressed as:

$$Q = \frac{kA\{P_1 - P_2\}}{\mu L} \quad (3.7)$$

Where:

Q = Flow Rate (cc per sec); k = Permeability in darcies; μ = Viscosity(cP)

A = Cross – Sectional Area of Flow(sq.cm); P_1 = Upstream Pressure (atm)

P_2 = Downstream Pressure (atm); P_1 = Upstream Pressure (atm)

Further studies, however, revealed that the equation described in 3.7 was only valid at low flow rates. It was therefore classified as a particular case of the more characteristic Forchheimer equation where the second order term has been reduced to zero. Consequently, a Darcian region of flow is referred to as linear laminar. The complete Forchheimer equation of non-linear laminar flow is expressed in Equation 3.8 [118] as:

$$\frac{\delta P}{\delta L} = \frac{\mu v}{k} + \beta \rho v^2 \quad (3.8)$$

Where:

$\frac{\delta P}{\delta L}$ = Pressure Drop Across Sample (; μ = Viscosity(cP); v = Darcian Velocity

k = Permeability (D) ; β = Forchheimer Factor ; ρ = Density (gm per cc)

In the mid-1800's, Kundt and Warburg discovered the phenomenon called molecular slip while studying the flow of fluids in conduit and porous media. It was discovered that gases move at a higher flow rate when compared to liquids. Further investigation revealed that the gas molecules closer to the wall of the conduit were in motion, unlike liquids where the molecules were stationary. The amount of slip was also found to be dependent on the molecular mean free path. The molecular mean free path on the hand depends on the pressure, temperature, and molecular size of the gas. Klinkenberg applied these principles to fluid flow in porous media and discovered that the permeability of a gas depends on these same factors. The dependency is shown in Equation 3.9. In particular, he posited that the mean pressure of which the measurement was determined should qualify air permeability. Accordingly, the error introduced by not qualifying the permeability in this way increases as the permeability decreases, and it is significant for values less than one millidarcy as shown in Equation 3.9 [118]

$$k = k_s \left\{ 1 + \frac{b}{P_m} \right\} \quad (3.9)$$

Where:

k = Permeability(darcies); k_s = Permeability at Infinite Mean Pressure

b = Klinkenberg Factor; P_m = Mean Pressure (psia)

3.4.1.5.2 Principles of Permeability Determination using PERG-200

The key to accurate computation of the gas permeability measurement using PERG -200, therefore, is to ensure that the flow rates are in the darcian region. The flow rate is controlled by the upstream gas pressure regulators while the resultant flow rate through the sample is measured by the flow meter.

3.4.1.5.3 PERG-200 Permeameter Panel Description

Figure 4.16 depicts the front panel of the permeameter. The function of the various components required for the measurement of the core samples permeability to air is described hereunder.

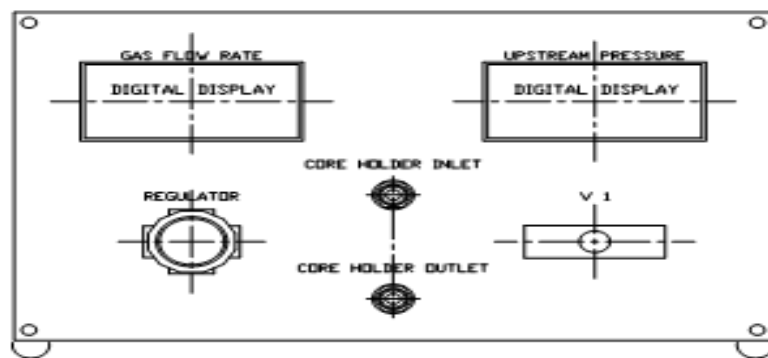


Figure 3.16 Front Panel of PERG-200 Permeameter[118]

(a) Core Holder Gas Outlet Port with Temperature Sensor

The outlet port allows the connection of PERG-200 to the downstream post of then Fancher core holder

(b) Upstream Pressure

The upstream pressure measures the inlet pressure in psig

(c) Gas Regulator

The regulator allows for the adjustment of the gas inlet pressure

(d) Valve V1

Valve V1 controls the flow of gas from the external regulator to the regulator

(e) Rear Gas Inlet Port

The gas inlet port connects the PERG-200 to the regulated air source

(f) Rear Gas Out

The gas out is the discharge port of the gas flow meter

3.4.1.5.4 Determination of Gas Permeability

The permeameter was first connected to the air supply using one-quarter nylon tubing, and the power was switched on. The core holder inlet port on the front panel was connected to the inlet of the Fancher core holder using two feet, one-quarter diameter tubing. The choice of the two feet tubing was deliberate to minimise pressure drop. Before the permeameter was used, it had to be calibrated.

(a) Gas Permeability Measurement

The length and the area of the core samples were determined from the dimensions obtained by a vernier calliper. The Permeability of the Boise and Castlegate samples was measured using the steps described hereunder. A compressed air feed regulated to a supply pressure of 20 psig was connected to the permeameter. The valve V1 was opened, and the flow rate was adjusted by slightly rotating the regulator. Once the upstream pressure and the flow rate was stabilised, the temperature and the pressure was recorded. The process was repeated for several values of flow rates and the stabilised upstream pressure, and flow rate reading was recorded accordingly. The values obtained alongside the length and area of the core samples earlier obtained were inputted into an excel computational spreadsheet where the measurement of the permeability was calculated. The results obtained are presented in chapter four.

3.4.1.6 PERL-200 Permeameter

The PERL-200 permeameter was used in the study to determine the liquid permeability of Boise and Castlegate core samples. The instruments consist of a PERL-200 permeameter and a core holder. The Corelab permeameter is specifically designed to be used with water or brine only. In the case of this study, water was used. The permeameter is shown in Figure 3.17.



Figure 3.17 PERL-200 permeameter[119]

43.4.1.6.1 Theory of Liquid Flow in Porous Media.

The principles of the flow of fluids in porous media as described in section 3.4.1.5.4 apply here also. For liquids, however, the concept of molecular slippage does not hold, because the molecules of the liquid in contact with the wall of the porous media are at rest. Here, Darcy equation for permeability of liquid is better expressed by changing the unit of pressure to psig and the unit of permeability to millidarcy as shown in Equation 3.10 [119].

$$k = 14500 \frac{\mu l V}{T A \delta P} \quad (3.10)$$

where :

k = Permeability (mD); μ = Viscosity (cP) ; l = Length of Flow (cm)

T = Time(s) ; A = Cross Sectional Area of Flow(sq. cm);

δP = Differential Pressure(psig)

3.4.1.6.2 Principle of Permeability Determination using PERL-200

The upstream gas pressure regulator controls the flow rate of the gas. The resultant liquid flow rate through the sample is determined by measuring the time required for the liquid meniscus to pass between the calibrations marks of the calibrated measurement tube (see Figure 3.18). The measurements are made at different flow rates to ensure that the rates are in the Darcian region.

3.4.1.6.3 PERL-200 Permeameter Panel Description

The function of the various components used for the measurement of the core sample permeability to liquid is briefly described here. Figure 3.18 shows the diagram of the PERG-200 permeameter used for the study.

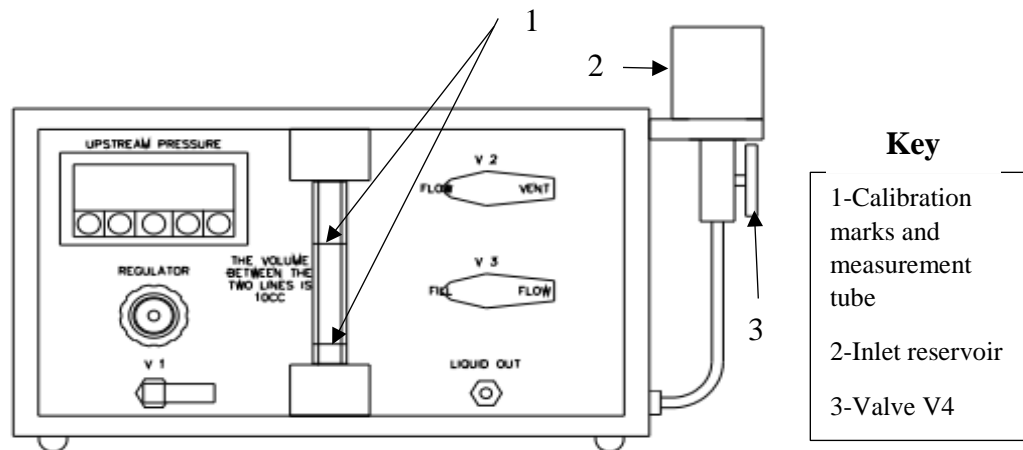


Figure 3.18 Front panel of PERL-200 Permeameter[119]

(a) Liquid out Port

The liquid out port allows for the connection of the permeameter to the bottom part of the Fancher, core holder.

(b) Upstream Pressure

The upstream pressure reads the inlet pressure of the sample in psig

(c) Regulator

The regulator allows for the fine-tuning of the inlet gas pressure. The maximum pressure from the regulator is 25 psig

(d) Valve V1

Valve V1 controls the flow of gas from the supply feed to the instrument regulator. The recommended pressure supplied to the regulator should not exceed 100 psig.

(e) Valve V2

Valve V2 is a three-way valve. When it is in the flow position, it directs the gas from the regulator to the flow tube. In the vent position, however, it vents air from the flow tube when it is filled with liquid.

(f) Valve V3

Valve V3 is also a three-way valve. In the flow position, it directs the liquid from the flow tube to the core sample. In the fill position, it directs the flow of liquid from the fill reservoir to the flow tube.

(g) Measurement Tube

The measurement tube is located on the front panel of the instrument. It has two calibration marks (see Figure 3.18). The tube volume between the marks is 10 cc. A 10cc liquid volume is reached when the liquid level rises from the bottom to the top mark of the measurement tube.

(h) Gas Inlet Port

The gas inlet port is located at the rear end of the instrument. It allows for the connection of the instrument to the air supply source.

(i) Inlet Reservoir and Valve V4

The inlet reservoir and valve V4 is mounted on the right side of the instrument as depicted in Figure 3.18. Valve V4 is attached to the bottom of the reservoir. The inlet reservoir contains the liquid used to fill the measurement system before the initiation of the fluid flow.

3.4.1.6.4 Determination of Liquid Permeability

The air supply was connected to the gas-in port, and the instrument was powered. The liquid-out fitting was connected with a one quarter nylon tubing to the bottom of the Fancher, core holder. The other end of the core holder was connected to a two feet tubing while the free end of the nylon tubing was inserted into a 50 ml plastic beaker. Before the start of the experiment, the instrument was calibrated. The dimension of the core samples was obtained using a vernier calliper. The core samples were saturated with brine with 10% concentration using the method described in section 3.4.1.2.

(a) Liquid Permeability Measurement

Once the saturated core sample was placed in the core holder, the air supply regulator was adjusted to supply 25 psig to the instrument. Valve V1 was opened, and the pressure was gently fine-tuned by rotating the regulator to ensure that the flow rate through the system was between the range of 1 and 6 cc/min. Hereafter, the upstream pressure was allowed to stabilise and valve V3 and V2 were turned to the 'flow' positions. A stopwatch was started when the level of brine in the measurement tube reaches the upper calibration mark. The timer was stopped when the brine meniscus reaches the lower calibration mark. At that point, the valve V3 and V2 were set to 'fill' position to stop the flow of brine through the core sample. The time taken for 10cc of brine to flow through the sample was recorded with the corresponding upstream pressure.

The experiment was repeated by opening the valve V4 to allow for the refilling of the measurement tube to the level of the upper calibration mark and pressure stabilisation. Valve V4 was shut, and valve V3 was turned to the ‘flow’ position. The pressure regulator was adjusted again to obtain the new flow rate. Valve V2 was turned to flow position and the time and upstream pressure measurement during flow were recorded. The valve V3 was turned to ‘fill’ position to end the experiment and to unload the sample. The process demonstrated above was repeated three times for each core samples at different flow rates. The values obtained during the experimental run were inputted into an excel software for the computation of the liquid permeability.

3.4.1.7 Phoenix V|tome|x S Scanner

The Phoenix V|tome|x S shown in Figure 3.19 was used in the study to scan the Boise and Castlegate core samples. The aim was to ensure that the structural integrity of the samples was intact. The Phoenix V|tome|x S is a high-resolution system for 2D X-ray inspection, 3D computed tomography (CT), and 3D metrology. The instrument is equipped with a 180kV/15W high powered Nano focus X-ray tube and a 240kV/320W microfocus tube to allow for high flexibility. The combination of nano and micro-focus tubes enables the scanner to be reliably applied for a wide range of applications. V|tome|x can be used for applications from extreme high-resolution scans of low absorbing materials to the 3D analysis of high absorbing objects.

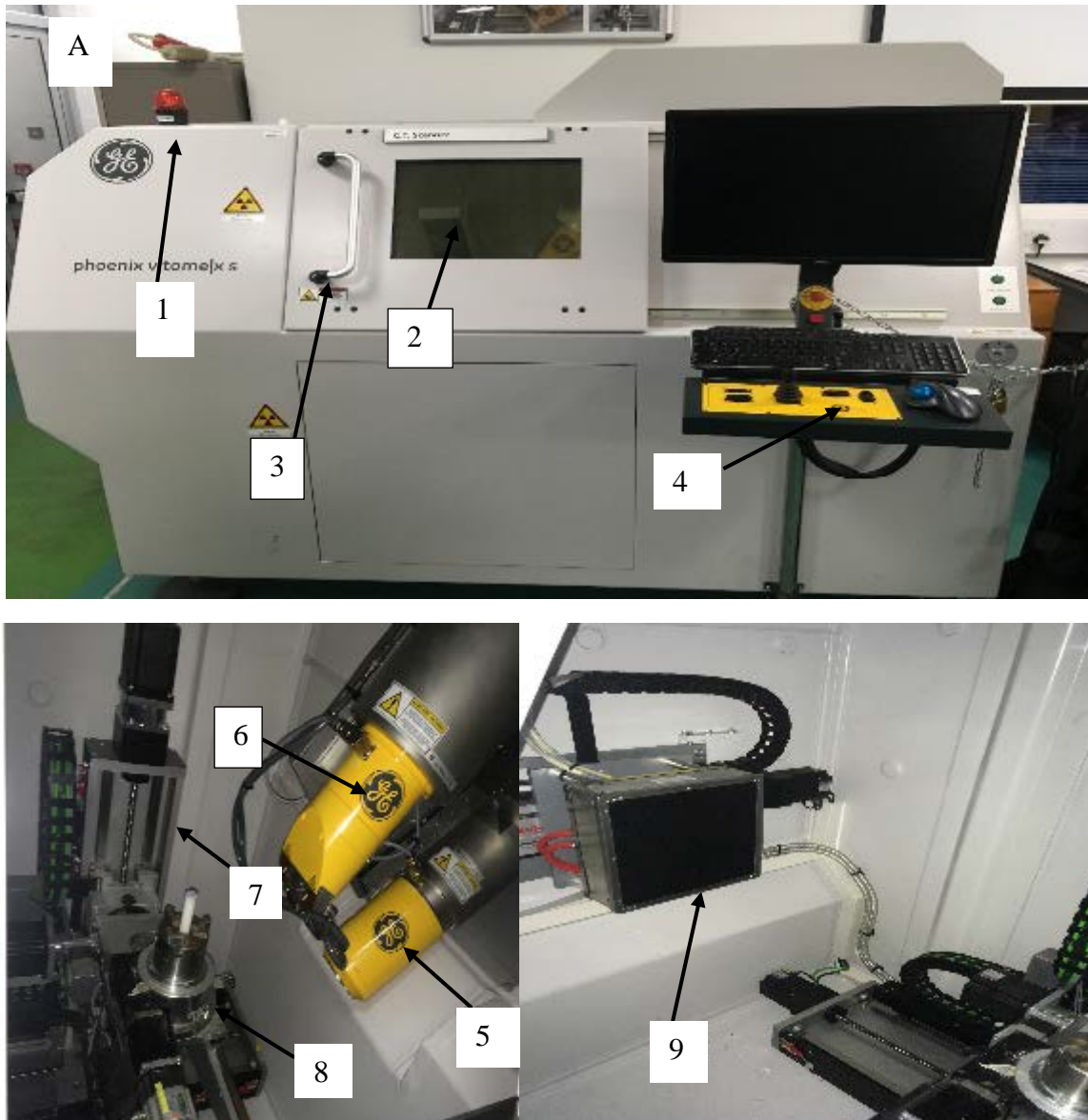


Figure 3.19 Phoenix V|Tome|x S Scanner

1-Alarm Light 2-Radiation chamber 3- Sliding door 4-Control console 5-Transmission tube
6-Direct tube 7-Sample manipulator 8-Sample holder 9- X-ray detector

The scanner features a sample manipulator, radiation protection cabinet, two x-ray tubes, x-ray detector and control console. The sample manipulator is a powered device capable of moving in five directions (x-y-rotate and tilt). It is used for positioning a sample before a scan is carried done. The radiation cabinet houses the holder where samples to be x-rayed are kept. The cabinet is accessed through a sliding door equipped with an integrated pane of lead glass; which prevents the system operator from being exposed to the X-rays while providing a clear view.

The x-ray tubes are termed direct and transmission tube (see Figure 3.19). They are located inside the radiation cabinet and consist of the cathodes, which generates the x-rays. X-rays are electromagnetic waves with a wavelength lesser than 10nm. A smaller wavelength, therefore, corresponds to higher energy as demonstrated by Plank in the equation [120]:

$$E = hf = \frac{hc}{\lambda} \quad (3.11)$$

Where h is Plank's constant ($h=6.63 \times 10^{-34} \text{js}$), c is the speed of light ($c=3 \times 10^8 \text{m/s}$), and λ is the wavelength of the X-ray. Conversely, x-rays with longer wavelengths have lower energies. X-ray energy is usually expressed in electron volts, eV. $1\text{eV} = 1.602 \times 10^{-19} \text{j}$. X-rays are produced when a metal object retards an accelerated beam of electrons. X-ray source consists of a hot cathode (tungsten filament) and an anode inside a vacuum tube with an electric potential. Electrons ejected from the surface of the cathode accelerates towards the anode. When these electrons impinge on the target, they interact with the target atoms and transfer their kinetic energy to the anode. These interactions occur within a small penetration depth into the target as the interactions continues, the electrons finally decelerates and finally come to rest; at which time they are conducted through the anode and out into the associated electric circuit [120]. The X-ray detector is used to measure the transmission of the rays through the object along the different paths. It measures the x-rays by converting the incident x-ray flux into an electric signal that can be processed by electronic technique. The control console is the operational panel located in front of the instrument. It consists of a keyboard, mouse rocker switches, joystick an electrostatic discharge socket that diverts electrostatic discharge to prevent damage of sensitive components. The console connects to a computer monitor that visualises the x-ray images in real time.

3.4.1.8.1 Working Principle of the Phoenix V|Tome|x S Scanner

In principle, computer tomography creates cross-sectional images by projecting a beam of emitted photons from a defined angle position through one plane of an object performing one revolution. As the x-rays (emitted photons) pass through the object, some of the rays are absorbed, some are scattered, and some is transmitted. The process by which the intensity of the scattered or absorbed rays is reduced as a result of interaction with the object is termed attenuation. The attenuated rays do not reach the deflector. Instead, the photons transmitted through the object at each angle are collected on the detector and visualised by a computer by creating a reconstruction of the scanned object. The reconstruction is shown as a grey value

data structure which denotes the electron density distribution of the measured object [121]. The illustration of the working principle of computer tomography process is shown in Figure 3.20.

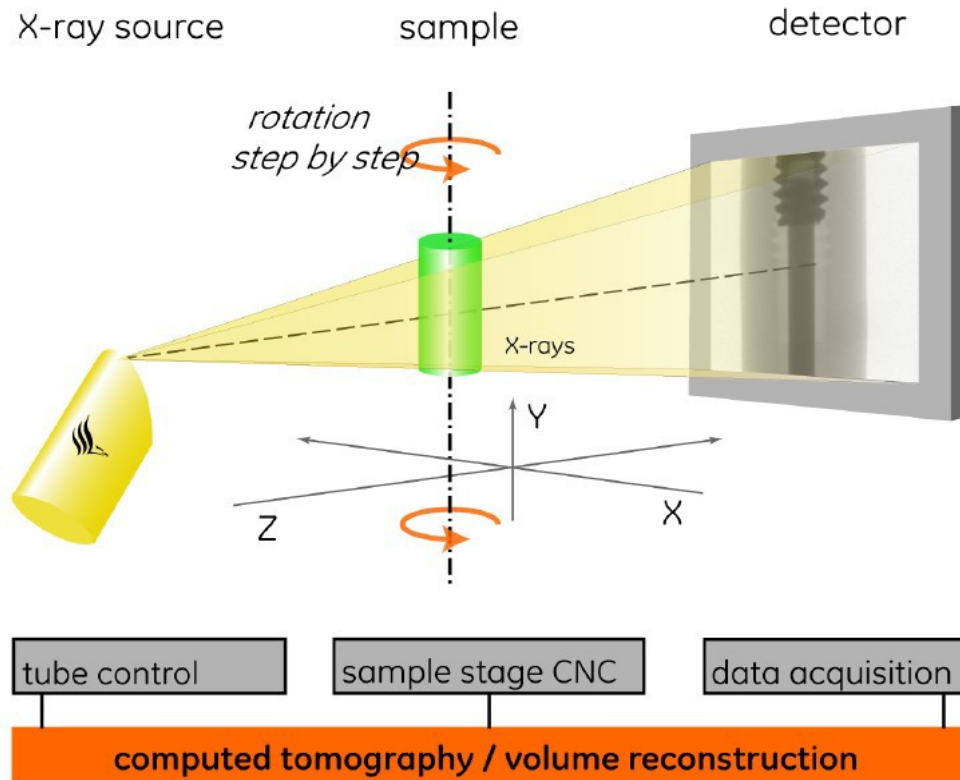


Figure 3.20 3D Computer Tomography with Flat Panel Detector[122]

3.4.1.8.2 Influence Factors

Influence factors are parameters that determine the quality of the computer tomography output. Figure 3.21 illustrates these factors. Details of each of the factors illustrated, and the techniques for compensating and or reducing their effect on the CT output can be found in the German guidelines VDI/VDE 2630 part 1.2 [123]

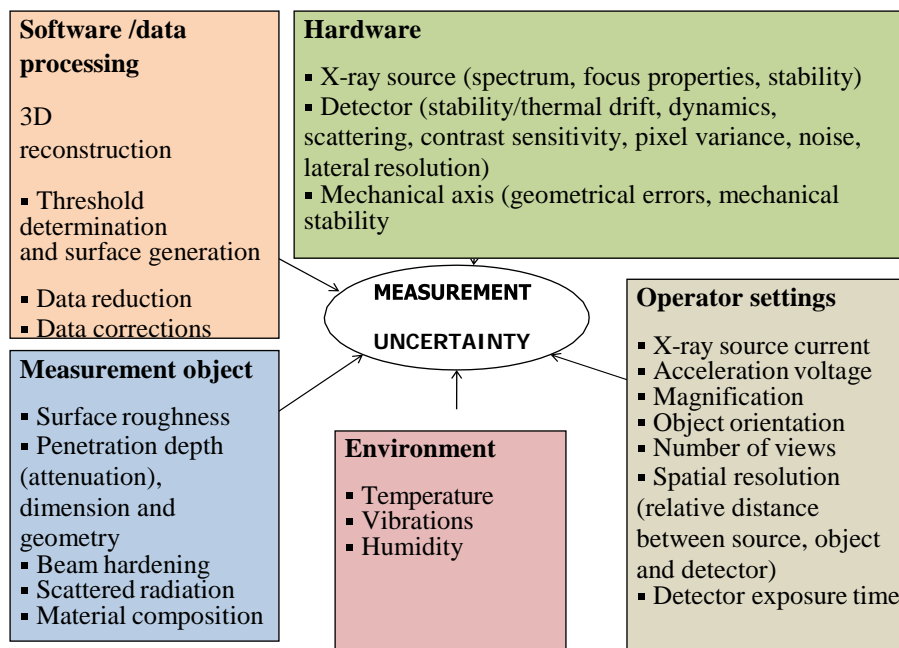


Figure 3.21 Influence factors in Computer Tomography [122]

3.4.1.8.3 CT Scan Data Acquisition and Processing

The process chain for the entire computer tomography described here was derived from the Phoenix V|tome|x S and VGstudio max 22 reference manual. As the sub-heading suggests, the process chain consists of two separate stages: data acquisition and data processing or reconstruction. The first stage involves scanning the core samples. The core samples are placed in the sample manipulator and adjusted to the best position with the aid of the control console. The input parameters for the scanning process is set at this stage. Table 3.2 shows the input parameters used for the Boise and Castle gate core samples. The second stage is the data processing. The images acquired were automatically imported into a computer for reconstruction. It is at this stage the property in question ascertained. Here, the focus is to examine the core samples to ensure that they are not fractured.

Table 3. 2 Input parameters for Boise and Castlegate core samples

Input parameters	Core samples	
	Boise	Castle gate
Dimension	1x1	1x1
voltage	165	140
Current	75	90
Power	12.4	12.6
Timing	333	200
Average	3	3
Skip	1	1
Bining	1x1	1x1
Sensitivity	4000	2000
Vsensor	1	1
focus	standard	standard
filter	0.1	1000

3.4.2 Materials

The following materials were used for the phase III of the experimental study: Boise and Castlegate samples were used to model homogeneous and heterogeneous reservoirs. While CO₂ and Sunflower Oil were used to model the injection and reservoir fluid respectively. Figure 3.22 shows the snapshot of Castlegate and Boise core sample used in this study

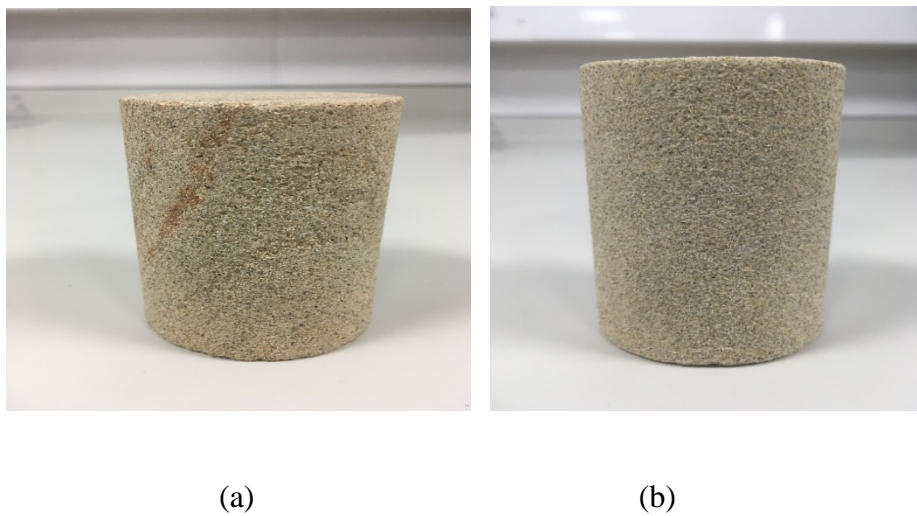


Figure 3.22 Boise (a) and Castlegate sample (b)

3.4.3 Procedures

The flooding of a reservoir is usually preceded by reservoir characterisation. The properties of a reservoir formation are not generic, hence it necessary for a reservoir to be screened and the appropriate recovery method ascertained before production is initiated. Properties such as the porosity, permeability, temperature, pressure, depth of the reservoir rock as well the viscosity and API gravity of the reservoir fluid are among the critical properties required for the screening process. The procedures for the characterisation of the models applied in this study is described from section 3.4.1.2 to 3.4.1.8.

This section, however, will focus on the experimental procedures for the core flooding process. The following represents the steps and the order taken to simulate the core flooding process.

- i. The weight of the six Boise core plugs were measured and recorded using the weighing balance using the steps described in section 3.4.1.4.
- ii. The plug was saturated with a brine of 5% concentration using the method described in section 3.4.1.2. The saturated sample is weighed
- iii. The brine-saturated sample was displaced by Sunflower oil to obtain the initial water saturation. The resulting sample was weighed and allowed to settle for 72hours.
- iv. The core holder was fitted with a with a 0.5mm centrally perforated seal (see Figure 3.9)
- v. The sample was gas flooded using the set up shown in Figure 3.8 by injecting CO₂ at 1bar until the gas-oil ratio was 100:1.
- vi. The volume of oil displaced was recorded. The volume of CO₂ used was also noted.
- vii. The core sample was removed from the core holder and weighed.
- viii. Steps 1-7 were repeated with the other five plus for CO₂ injection pressure of 2-6bar.
- ix. The core plugs were cleaned with Tuolene and Methanol and heated to its original weight
- x. The process was repeated for 1.0mm,1.5mm,2.0mm,2.5mm,3.0mm perforation diameter
- xi. The steps 1-10 were repeated for six Castlegate core plugs. The results obtained is shown in Appendix F and G

3.4.4 Errors and Accuracy

The accuracy of some of the instrument has been discussed in section 3.3.4. Hence, the description will be concerned with the additional instruments used here. The porosimeter PORG-200 has a non-linearity of ± 0.045 . At zero output pressure, its percentage error is within 0.2%FS. At full output voltage, it is about $\pm 0.2\%$ FSD. The parameters are more sensitive as fluctuations of temperature up to 1°C can affect its measurements. Hence they have to be properly grounded and provided an adequate supply of gas.

The following steps were taken to minimise experimental errors:

- i. The porosimeter and permeameters were calibrated prior to use.
- ii. The readings on the equipments were stabilised before they were recorded.
- iii. The samples were weighed before and after the reading to ensure that the integrity of the weight of the sample has not been compromised.
- iv. The samples were degassed after the characterisation with the aid of a vacuum pump to ensure that gases were expelled from within its pores
- v. The core flooding experiments were repeated thrice and the mean value computed.
- vi. The error in measurement for the core flooding tests were analysed using the equation for the standard error of the mean illustrated in equation 3.1.

At 1bar, 0.5mm perforation diameter, the data set obtained for the percentage of oil recovered (%OOIP) in heterogeneous and homogeneous core flooding tests after three run were 0.12, 0.12, 0.11 and 0.070, 0.071, 0.071. Using equation 3.1, the standard error of the mean was computed to be ± 0.006 and ± 0.0006 for the heterogeneous and homogeneous tests respectively.

3.4.5 Chapter Summary:

The experimental methods for the study was conducted in this chapter with special focus on:

- Conducting a preliminary experiment to ensure that the integrity of the experimental rig was maintained throughout the study as well as the validation of the use of low powered light emitting diode for bubble particle visualization.
- Investigating the nature of correlation between well casing perforation diameter on CO₂ bubble size distribution in a heavy oil reservoir.
- Experimental simulation of the immiscible CO₂ -heavy oil recovery process with emphasis on the impact of perforation diameter and carbon dioxide bubbles on heavy oil viscosity and recovery.

Chapter 4

Results and Discussion

4.1 Overview

This chapter presents the results obtained from the experimental investigation conducted in the sequence illustrated in Figure 4.1. The focus of this study is to investigate the role of the perforation diameter and CO₂ bubbles in heavy oil viscosity reduction and recovery in an enhanced oil recovery process. The results are analysed with the goal of ascertaining firstly, the technical implication, and subsequently, the economic implication of the technique employed in the study. The technical analysis is presented in the phase and order in which the experiment was conducted

- ❖ **Phase I:** Experimental Rig Validation: Section 4.2 reports the results and analysis of the pressure testing of the experimental rig as well as a trial particle-imaging test conducted in Section 3.2. Although the validation of the experimental rig is vital for obtaining accurate results in a subsequent experiment, the results and its analysis are outside the scope of this study.
- ❖ **Phase II:** Particle Characterisation and Viscosity measurement: Section 4.3 discusses the result and analysis of the experiment conducted in Section 3.3 to examine the effect of perforation diameter on the viscosity of heavy oil. It also aims to study the link between the generated CO₂ bubble sizes, perforation diameter and heavy oil viscosity. The focus at this stage is to gain an appreciation for the fluid-fluid dynamics within the pore spaces in a heavy oil reservoir.
- ❖ **Phase III:** Reservoir Petrophysics and Core flooding. Section 4.4 presents the outcome of the reservoir fluid and rock characterisation study as well as the results and analysis of the experimental simulation of an immiscible CO₂ EOR heavy oil recovery process conducted in Section 3.4. It aims to address the extent to which perforation diameter can influence the recovery of heavy oil.
- ❖ **Economic Analysis:** A discounted net present value and payback period was used to ascertain the economic viability of using a smaller perforation diameter for heavy oil recovery projects.

4.2 Results of Preliminary Experiment (Phase I)

4.2.1 Pressure Testing of Experimental Rig

The design of the experimental rig allows for the build-up of pressure inside the Perspex tube. Pressure build-up can result in the uncontrollable release of fluids, deformation or fracture of the test item. Consequently, the rig had to be tested. The test was conducted to ensure the safety and reliability of the rig setup. Section 3.2 describes the procedures used for the pressure testing. The rig was filled with coloured water up to the 70 cm mark and subjected to pressures from injected air ranging from 1-6 bar. It was observed for leaks and signs of failure for 2 hours. No leaks or deformation was observed for pressures from 1 to 3 bar, and the pressure inside the tube was constant. At 4 bar however, there was air and water leakage at section A and B respectively (see Figure 4.3). The cause of the leak was found to be due to a defective seal at point B and a faulty tube fitting at point A. These were replaced, and the test was repeated successfully to the maximum test pressure of 6 bar. Once the simulation was completed, trial experimentation of the particle characterisation schedule for phase II experiment was conducted.

4.2.2 Particle Imaging: Choice of Led Light Source

Most particle imaging techniques require the application of laser light sources. These sources are capable of producing high power, short duration pulses that allow the instantaneous marking and capture of seed particles and their scattered light by an imaging system. Currently, lasers are costly despite their relatively slow repetition rates[124]. An alternative approach provided for by researchers, allows low power illumination devices such as light emitting diodes (LED) to be used in place of lasers in many particle imaging processes [124-128]. Besides the benefits of reduced cost, led lighting is compatible with less expensive commercial cameras in auto-correction or two-colour mode, unlike lasers that must be used with expensive cross-correlation cameras [124]. Figure 4.1 shows results of an experimental work conducted by Jordi Estevadeordal and Larry Goss to proof the validity and feasibility of the concept of LED lightings for particle imaging.

The concept was applied in this study and the results obtained further validates the position of these researchers on the subject. Figure 4.2 shows the original and processed image of air bubbles in light yellow coloured water used in this study. The colouring was done deliberately to mimic the colour of the reservoir fluid model to be used in phase II of the experimental process

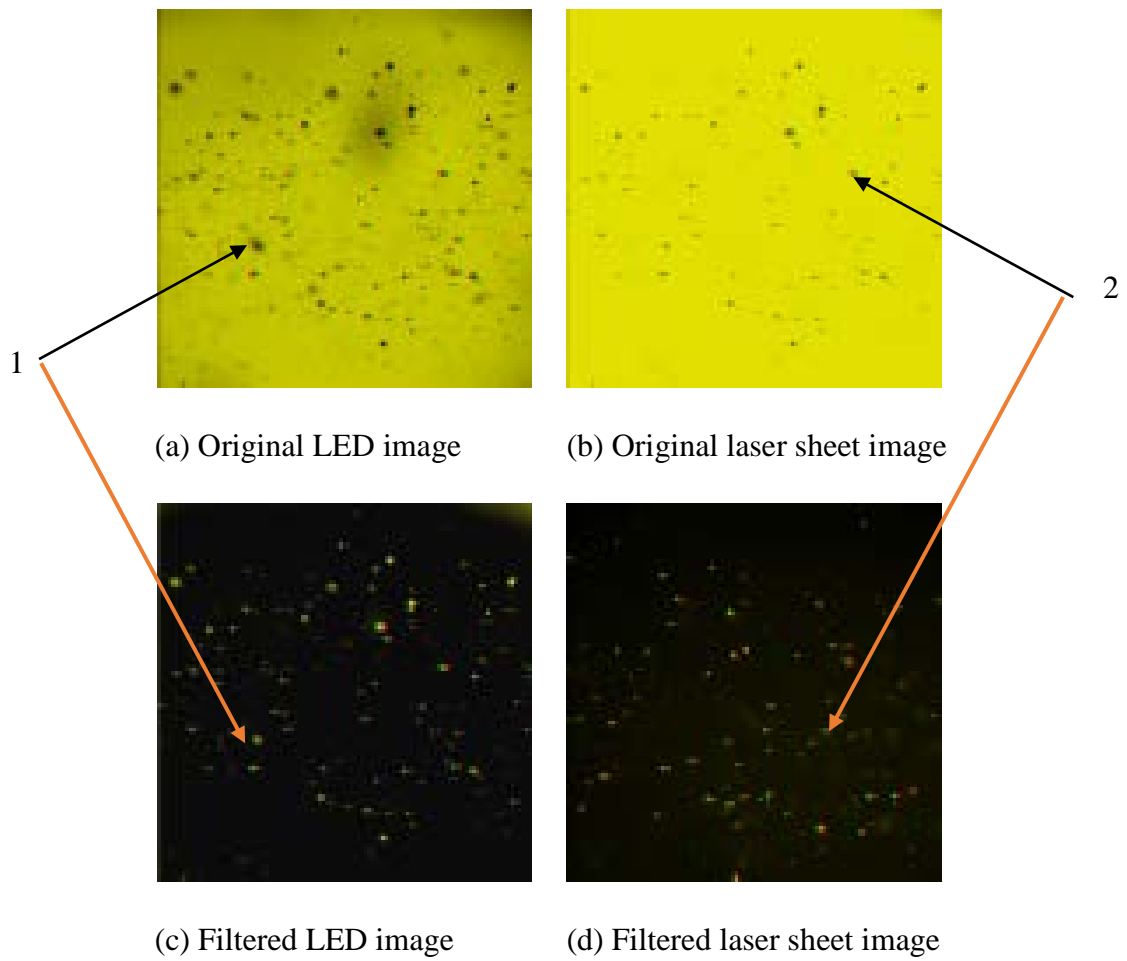


Figure 4.1 Original and filtered image from water jet bubbles [124]

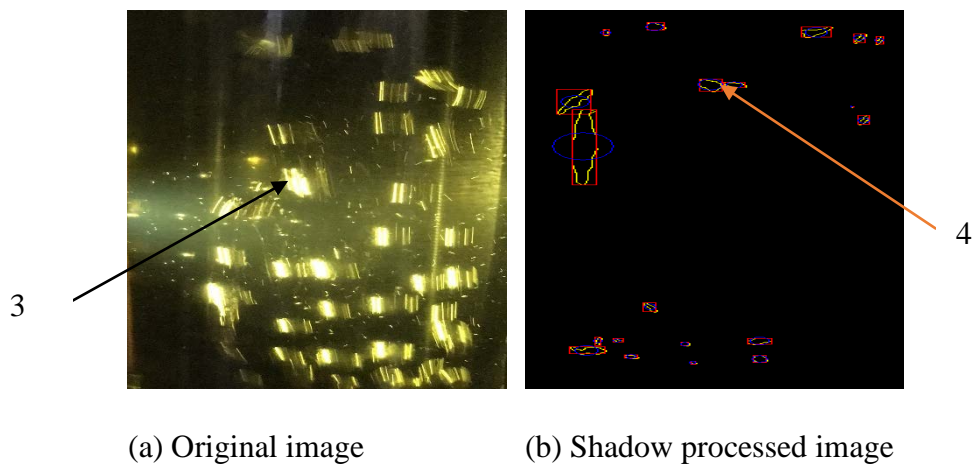


Figure 4.2 Original and processed image of air bubbles in water

Key: 1,2,3,4 are bubbles

4.3 Result of Particle Characterisation Experiment (Phase II)

4.3.1 Effect of Perforation Diameter on CO₂ bubble Size distribution

The investigation of the effect of perforation diameter on the distribution of CO₂ bubbles in heavy oil recovery process forms an integral part of this research. This is particularly so, because understanding the relationship between the perforation diameter, CO₂ bubble size distribution within the oil and the viscosity will ultimately determine the applicability of perforation diameter in the oil recovery process.

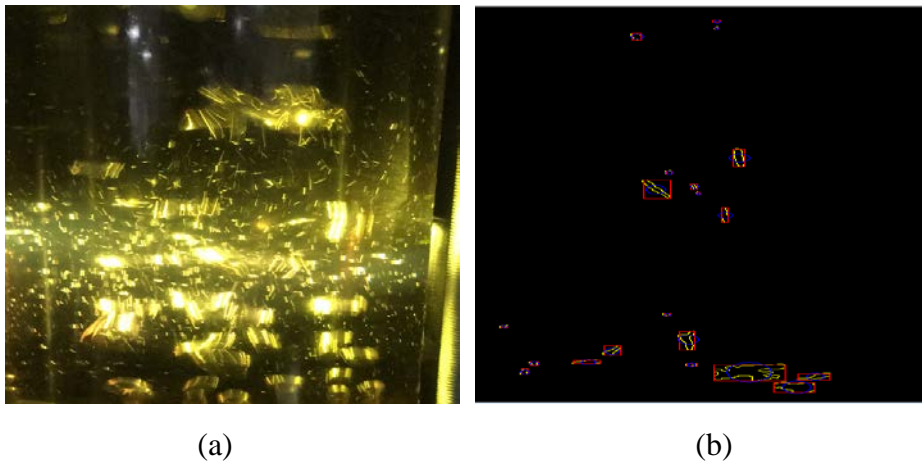


Figure 4.3 (a) Original image (b) Processed image

Figure 4.4 describes the result of the experiment conducted in section 3.2 to examine the impact of perforation diameter on the distribution of CO₂ bubbles in heavy oil recovery process. The results shown in Figure 4.4 were obtained by importing the original images (shown in Figure 4.3a) into the Dantec dynamic studio software described in section 3.3.1.3. Figure 4.4(a) shows the distribution of CO₂ bubbles in Sunflower oil when gaseous CO₂ was injected at a pressure of 1.2 bar through a perforation diameter of 0.5mm in. it was observed that the quantity of bubbles in the range of 0-100 μ m reduced from 151 to 116 as the perforation diameter increased from 0.5mm to 3.0mm. A similar trend was also noticed for the 100-500 μ m as it showed a corresponding decrease from 73 to 60. However, for bubbles with sizes greater than 500 μ m, the relationship between the size distribution of the CO₂ bubbles and the perforation diameter could not be establish because of the inconsistency in variation

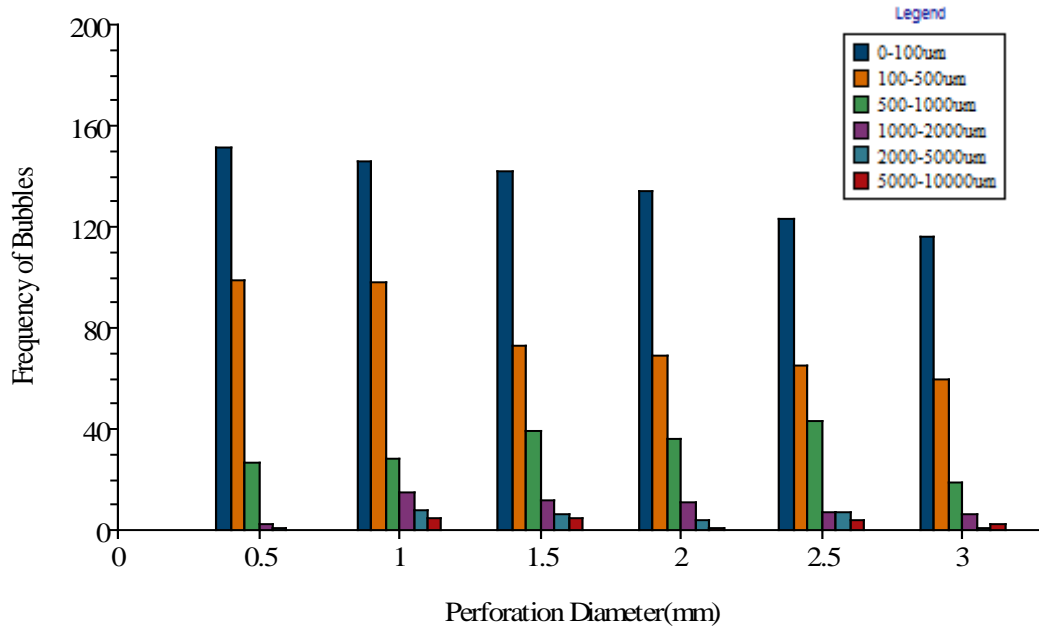


Figure 4.4: (a) Variation of CO₂ bubbles size with perforation diameter at 1.2bar

In other plots, (b) – (f), shown in Appendix H, the trend remained the same. In Figure 4.4 (b), the pressure of the injected CO₂ was increased from 1.2 bar to 1.4bar .Again, the bubble sizes in the range of 0-500 µm collectively decreased from 275 to 176 as the perforation diameter used for the injection was increased from 0.5 to 3.0 mm. In Figure 4.4(c), the injection pressure was raised further to 1.6bar. While the reduction of the frequency of 0-500 µm bubble sizes continued as the perforation diameter was increased, there was also an appreciable increase in the number of the CO₂ bubbles generated in the sunflower oil owing to the increase in pressure. In Figure 4.4(a), (b) and (c) the concentration of the bubbly particles with sizes of (0-100 µm) in sunflower oil increased from 151 in Figure (a) to 166 in figure (c). The effect of pressure and the perforation diameter on the distribution of CO₂ bubble sizes as observed in Figure 4.4(a) to (c) for bubble sizes 0-500 µm, was also noticed in Figure 4.4 (d) to (f). That is, the frequency of these bubbles decrease as the perforation diameter was increased and increased with the injection pressure. In Figure 4.4(d), the distribution of bubbles in the range of (0-100 µm) dropped from 167 at 0.5mm diameter to 133 at 3.0mm. For bubble with sizes ranging from 100-500 µm, the reduction of the frequency was from 131 at 0.5mm to 73mm. The behaviour of the bubbles with diameter greater than 100µm remained inconsistent.

In Figure 4.4(e), the distribution of CO₂ bubbles sizes in the order of 0-100 µm contained the highest number of particles. The frequency of these bubbles was 174 at 0.5 mm perforation diameter as against 140 at 3.0 mm. Similarly, the 100-500µm bubbles was reduced from 144 to 76. In Figure (f), the number of bubble particles within the range of (0-100µm) present in the sunflower oil dropped from 189 at 0.5 perforation diameter to 141. While that of (100-500µm) decreased from 156 to 81.

4.3.1.1 Comparative Analysis of the Effect of Perforation Diameter on CO₂ Bubble Size Distribution

Findings from this study has shown that, the injection pressure, and perforation diameter are two key factors driving the bubble size distribution process. This position is consistent with the outcome of some researchers. In 2009, Haining et al investigated the effect of design and operating parameters on CO₂ absorption in multichannel contactors. They discovered that the mass transfer rate improved with the reduction of the microchannel diameter and with the CO₂ injection pressure [106]. In 2011, Tan et al added that gas bubbles were considerably smaller during dissolution mass transfer.

4.3.2 Effect of Perforation Diameter on Heavy Oil Viscosity

The recovery mechanisms for oils during immiscible flooding are viscosity reduction, oil-swelling effect, reduction of interfacial tension and blowdown recovery[129]. For heavy oils, viscosity reduction is the primary and most important mechanism driving its recovery process[130]. The effect of CO₂ on oil viscosity is well researched and documented. In 2011, Emadi and Sohrabi reported the results of a visualisation experiment conducted using CO₂ during immiscible displacement and recovery of heavy oil [131]. The results indicated that despite the enormous contrast between CO₂ and heavy oil, the injection of CO₂ effectively reduced the heavy oil viscosity. The results showed that the colour of the heavy oil brightened as the injection of CO₂ continued, indicating CO₂ dissolution and reduction of viscosity. In a similar study, Emadi and Sohrabi investigate the effect of CO₂ foam injection on heavy and extra- heavy oil. The results showed an increment in the reduction of oil viscosity, with more incremental reduction observed in the extra-heavy oil sample [132]. In 2009, Albin et al. experimented with the rheological behaviour of foamy oil. They concluded that the pressure, dissolved gas content and the presence of bubbles control the viscosity of the foamy oil [133]. In 2014, Chanmoly, Sasaki et al. studied the viscosity of foamy hexadecane by analysing CO₂ micro-bubble in hexadecane during depressurisation. The result which supported the work of

Albin indicated that large bubbles are unstable and contribute to swelling, unlike the microbubbles that are more stable and effective for viscosity reduction [133] [134]. In 2015, Sasaki, Sugai et al. repeated the experiment conducted in 2014 with a heavy oil sample having API gravity of 13.06. The result of the experiment confirmed the position of the previous study and showed that the solubility of CO_2 dissolving in heavy oil almost linearly increases with a pressure less than 5.5Mpa but decreases with increase in temperature [107].

This study, however, focuses on the effect of the perforation diameter on the viscosity of heavy oil during the injection process. Figure 4.4 describes the result of the experiment conducted in section 3.2 for this study. The result from the investigation showed a marked reduction of the sunflower viscosity as perforations with smaller diameters were used. At 2.2bar, 0.5mm perforation diameter, the dynamic viscosity of sunflower was reduced from its original value of 54cP at 20°C to 39cP; representing a reduction of 27.7%. At 2.2bar, 3.0mm perforation diameter, the percentage of viscosity reduction was 5.4%. For all conditions of pressure, the percentage of viscosity reduction varied inversely as the perforation diameter. It must be noted however that the highest percentage of viscosity reduction was obtained at the highest pressure and highest perforation indicating a complementary relationship between the injection pressure and the perforation diameter.

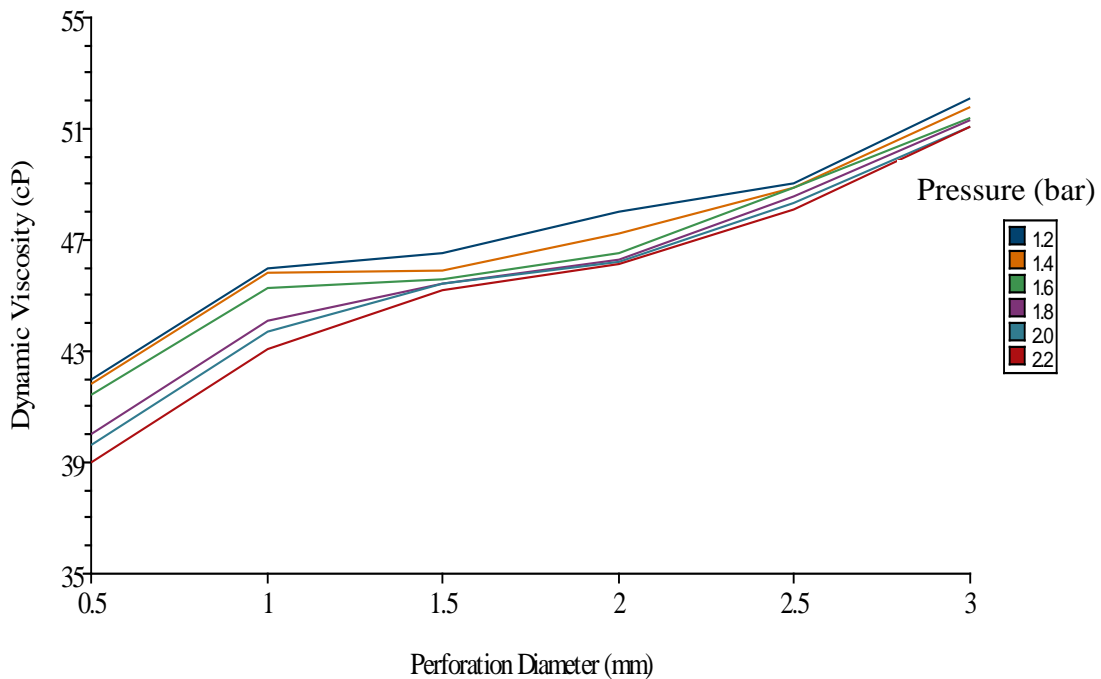


Figure 4.5 Variation of dynamic viscosity of sunflower oil at different injection pressure

4.3.2.1 Comparative Analysis of Viscosity Reduction Methods

The effect of pressure on the viscosity of heavy is well studied, and the findings from this study are consistent with the work of Albin and Sasaki on this subject[107, 133]. Another interesting observation was that the bubble size distribution coincided with the point in the experiment where CO₂ was injected at a pressure of 2.2bar and 0.5mm perforation diameter. Again, this finding agrees with the results of Chamnoly,s investigation of the role of the CO₂ bubble sizes on the swelling effect and viscosity of heavy oil [134].

However, while the findings from this study correlate with the results of the researchers above, they differ in the value performance. For instance, in Sasaki's study, the viscosity of the heavy oil sample was reduced from 175cP to 132cP (24.5%) when CO₂ was dissolved in heavy oil at 15.6bar [107]. Also, the result of an experiment conducted by Bora on the rheology of foamy oil showed a reduction of heavy oil viscosity from 5,500MPa.S to 4500MPa.S representing a reduction of 18.8%[135]. Figure 4.6 compares the result of this work with that of Sasaki and Bora [107, 135].

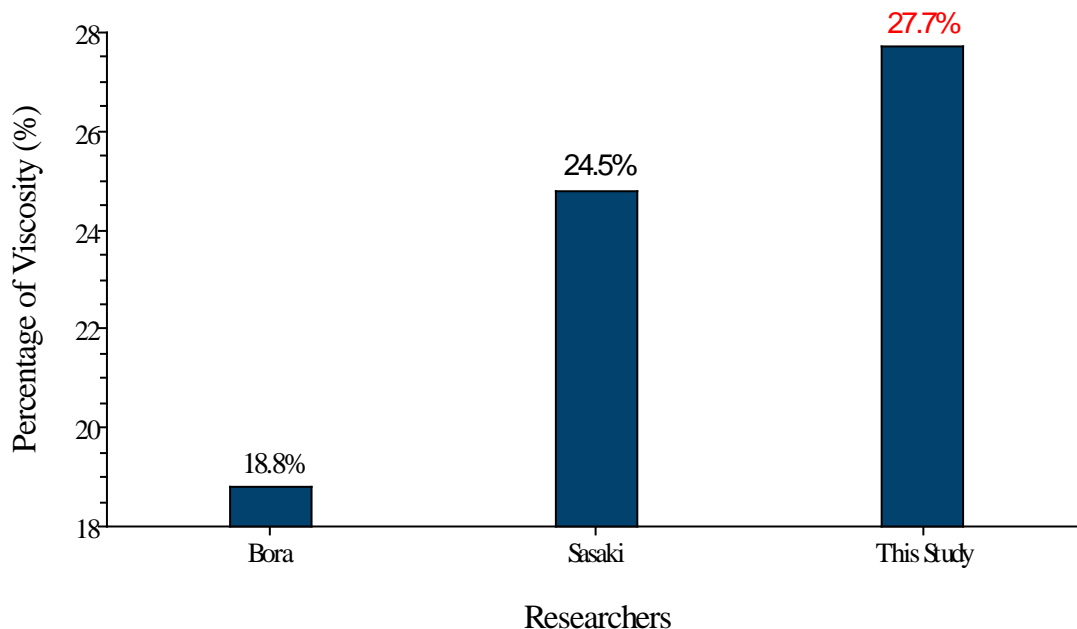


Figure 4.6 A comparative chart showing the results of other researchers and this work[107, 135].

As previously stated, heavy oil viscosity reduction is a key factor in heavy oil recovery process. Other mechanisms that may be investigated include the interfacial tension and swelling factor, although they are beyond the scope of this current study. The values in Figure 4.6 indicates that the viscosity of heavy oil can be better reduced just by using a smaller perforation diameter in the injection well. The next phase of the experimental process was to ascertain the extent to which recovery can be enhanced using the same perforation diameter. Two reservoir models were selected, and the goal was to simulate experimentally the CO₂-heavy oil recovery process using homogenous and heterogeneous core sample models. The result obtained is detailed in section 4.4

4.4 Results of Reservoir Petrophysics and Core flooding (Phase III)

4.4.1 Reservoir Petrophysics

The petrophysical examination otherwise known as reservoir characterisation of the reservoir rock and fluid is an essential requirement for the core flooding process. Reservoir properties are not generic. Therefore the conditions of the reservoir have to be predetermined before any production process can commence. Reservoir rock properties such as thickness, depth, porosity, permeability, reservoir pressure, temperature, reservoir type have to be known. In this study, the flooding was conducted under standard atmospheric condition. The model used were not subjected to overburden pressure other than the confining pressure within the core holder. Six Boise core plugs and six Castlegate core plugs were used to model the reservoir rocks. The fluid properties are also fundamental. The API gravity, specific gravity and viscosity of the reservoir fluid has to be determined.

4.4.1.1 Dimension and Weight of Core Samples

The dimension of the cores samples was measured using Vernier calliper. Table 4.1 shows the dimension of the twelve samples used for this experimental work.

Table 4.1: Weight and Dimension of the Experimental Core Samples

Type	Name	Length (inch)	Diameter (inch)	Weight (g)
BOISE	A	1.0110	0.9715	21.57
	B	1.0270	0.9650	21.65
	C	1.0175	0.9705	21.71
	D	1.0055	0.9760	21.81
	E	1.0165	0.9710	21.66
	F	1.0084	0.9780	21.62
CASTLEGATE	1	1.0110	0.9780	23.03
	2	1.0031	0.9822	23.01
	3	1.0002	0.9783	23.04
	4	1.0244	0.9714	23.02
	5	1.0140	0.9705	23.05
	6	1.0220	0.9862	23.03

4.4.1.2 Porosity Measurement

The essence of porosity measurement is to enable the computation of the original oil in place (OOIP) in the reservoir model. It is also required to quantify the injected gas volume during flooding operations since the injected gas volume is measured as a percentage of the pore volume of the reservoir. Section 3.4.1.5 describes the apparatus and procedures used for the porosity measurements. An example of the computation procedure for porosity is shown in this section using one Boise and one Castlegate sample. The values of the other samples are presented in Table 4.5. Table 4.2 provides the calibration and sample data obtained.

Table 4.2 Calibration table and sample input data

Disc No.	Volume cc	Reference Pressure psig (P1)	Expanded Pressure psig (P2)	P1/P2
empty	0.000	90.70	10.60	8.557
1	1.596	90.60	10.99	8.244
2	4.791	90.54	11.87	7.628
3	6.408	90.51	12.25	7.389
4	9.615	90.47	13.11	6.901
5	16.024	90.48	15.41	5.872
5+1	17.620	90.44	16.08	5.624
5+3	22.431	90.45	18.66	4.847
5+4	25.639	90.44	20.82	4.344
5+4+3	32.047	90.45	27.01	3.349
5+4+3+2	36.838	90.41	35.00	2.583
Boise C	12.290	90.39	12.84	7.040
Castlegate 1	12.450	90.37	13.03	6.936

A graph of the calibration disk volume was plotted against the ratio of the reference pressure to the expanded pressure. Figure 4.7 illustrates the graph obtained from the plot. The reference and expanded pressure values of samples and the values from a coefficient table obtained from the regression equation (see Equation 4.1) is inputted into an excel software termed “testing table”. The test table computes the grain value of the sample based on equation 3.5 [117]:

$$f(x) = ax^3 + bx^2 + cx + d \quad (4.1)$$

The values for a,b,c and d shown in Table 4.3 are constant all the core samples. R^2 is a statistical termed called coefficient of determination. It shows how the regression line approximates the real data. An R^2 of 1 means the regression line perfectly fits the data.

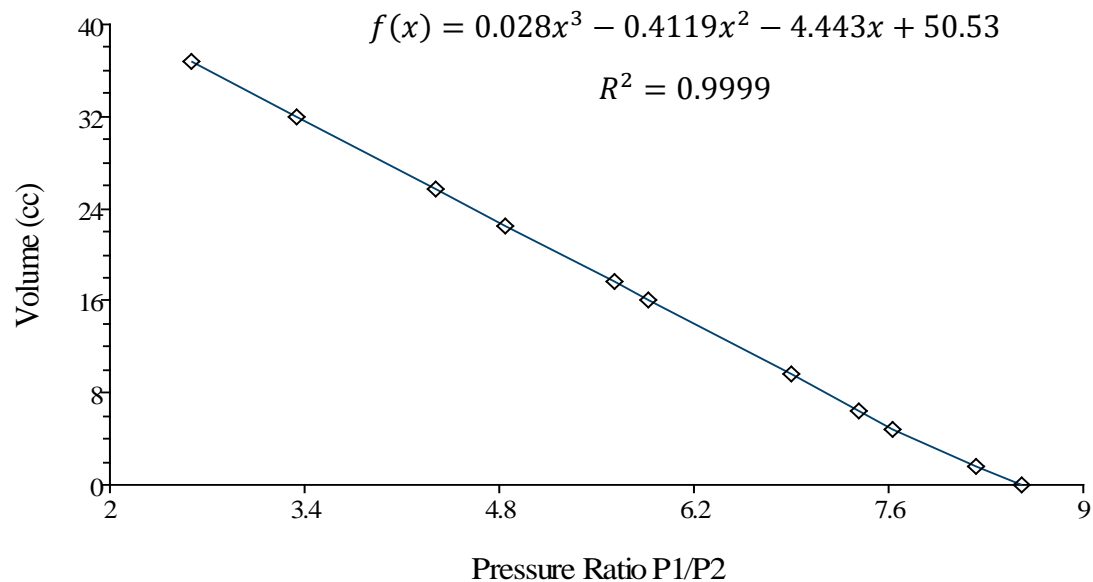


Figure 4.7 Calibration graph showing the disk volume versus the pressure ratio

Table 4.3 Coefficient table

a	b	c	d
0.028	-0.4	-4.443	50.53

Table 4.4 Testing Table

	PI	P2	P1/P2	Grain Volume
Boise	90.39	12.84	7.0397	8.608
Castlegate	90.37	13.03	6.9355	9.243

The porosity and pore volume of the samples is calculated using equation 4.2 and 4.3 respectively.[117]

$$\phi = \frac{V_p}{V_b} \times 100\% \quad (4.2)$$

$$V_p = V_b - V_g \quad (4.3)$$

The bulk volume V_b is given by equation 4.4:

$$V_b = \pi r^2 h \quad (4.4)$$

Where r is the radius of the sample and h the length of the sample. Table 4.5 shows the values of the grain volume, pore volume, bulk volume and porosity of the entire sample used.

Table 4.5 Core Sample Petro-physical Properties

Sample	Name	Grain Volume(cc)	Bulk Volume(cc)	Pore Volume(cc)	Porosity (%)
Boise	A	8.61	12.29	3.68	29.96
	B	8.61	12.29	3.68	29.97
	C	8.61	12.29	3.68	29.96
	D	8.61	12.29	3.68	29.96
	E	8.61	12.29	3.68	29.98
	F	8.80	12.45	3.66	29.31
Castlegate	1	9.24	12.45	3.21	25.76
	2	9.24	12.45	3.21	25.76
	3	9.24	12.45	3.21	25.78
	4	9.24	12.45	3.21	25.81
	5	9.10	12.29	3.19	25.94
	6	9.24	12.45	3.21	25.78

4.4.1.2 Gas Permeability Measurement

The gas permeability of a reservoir rock is defined as the ability of the rock to transmits gases. It is measured in darcies(D) or millidarcies (mD). The samples were tested for its permeability to gas using the procedure described in section 3.1.6.4(a). The flow rate and the differential pressure obtained was inputted into Darcy's equation expressed in equation 3.6. Table 4.6 presents the factory and measured permeability values.

Table 4.6 Measured and Factory Gas Permeabilities.

Sample	Name	Measured Permeability (mD)	Factory Permeability (mD)
Boise	A	2500	2500
	B	2500	2500
	C	2499	2500
	D	2500	2500
	E	2500	2500
	F	2501	2500
Castlegate	1	1350	1350
	2	1351	1350
	3	1351	1350
	4	1351	1350
	5	1351	1350
	6	1351	1350

4.4.1.3 Liquid Permeability Measurement

Like gas permeability, the liquid permeability is defined as the ability of the reservoir rock to transmit liquids. Section 3.4.1.7.4 describes the procedure for the measurement of liquid permeability. Equation 3.9 was used to compute the value of the liquid permeability once the input parameters such as the differential pressure have been read off from the permeameter. Table 4.7 presents the measured and factory values for the liquid permeability.

Table 4.7 Measured and factory Liquid Permeability

Sample	Name	Measured Permeability (mD)	Factory Permeability (mD)
Boise	A	675	675
	B	674	675
	C	674	675
	D	674	675
	E	674	675
	F	675	675
Castlegate	1	750	750
	2	749	750
	3	750	750
	4	750	750
	5	750	750
	6	751	750

4.4.1.4 Computer Tomography (CT) Scan

It is often a good practice to examine a core sample for defects as part of the characterisation process. The topological and geometrical analysis of the rock provides detailed information about the internal rock features that cannot be determined by darcy's method. Defects such as fractures can alter the permeability and productivity of the rock. In this study, a computer tomography scan was conducted on the samples to examine their internal structures for fractures. The procedure used for the examination is described in section 3.4.1.8.3. Figure 4.7 and 4.8 shows a sample of the Boise and Castlegate model examine and the result obtained.

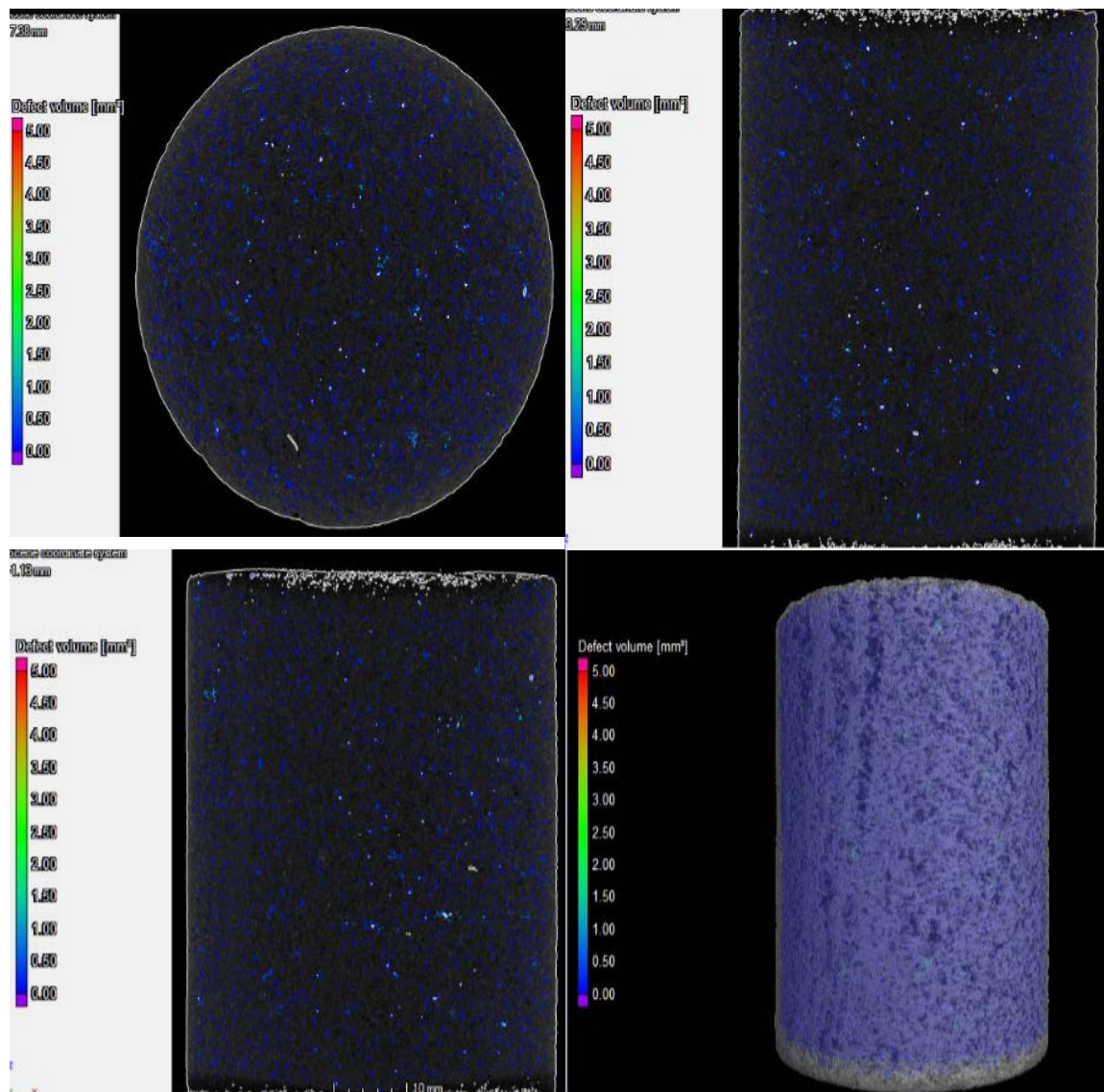


Figure 4.8 CT scan of Boise core sample.

The defect volume obtained from the scan shows that the range of the volume of voids within the sample is between 0 -5cubic millimetre. The volume of these voids can be estimated from the colour code displayed in the diagram. The volumes of these voids are within the dark blue region in the colour code. This range of values is consistent with the pore throat size distribution for sandstone. The scan also reveals that the reservoir model is not fractured. Similar results were obtained from the Castlegate core samples. Figure 4.9 the result of the defect volume analysis of the castle gate core samples used in this study. Due to the homogeneous internal structure of the Castlegate sample, a wall thickness analysis method was chosen. The method scans the sample from the radial plane and reveals any discontinuity found in the internal structure.

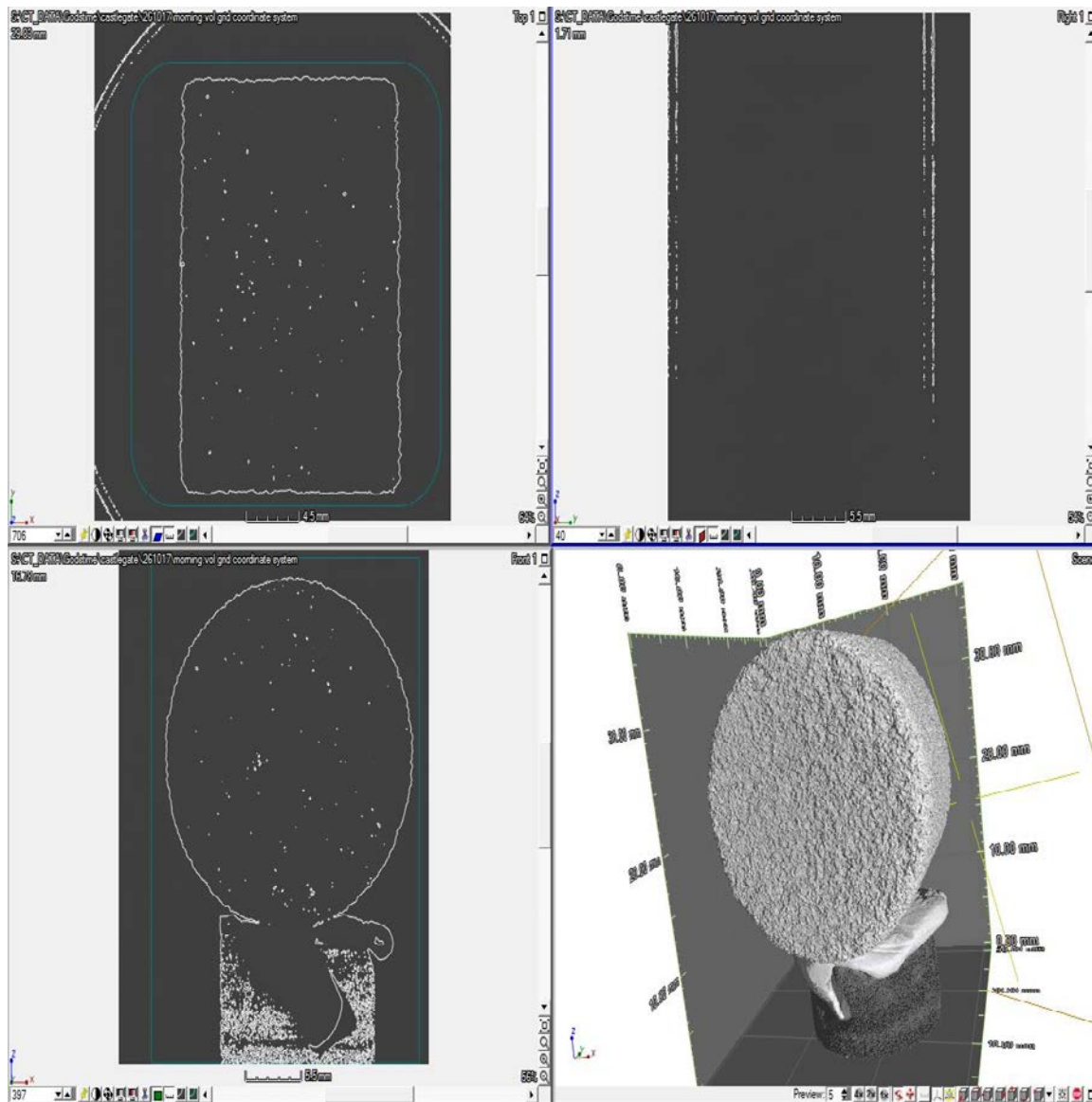


Figure 4.9 CT scan of Castlegate core sample

4.5 Result of Core Flooding Tests (Phase III)

This aspect of the study aims to investigate the effect of perforation diameter on heavy oil recovery. The struggle to increase the performance of non-thermal methods for heavy oil recovery is gaining momentum within the research circle. Thermal methods cannot be applied in a wide range of heavy oil reservoirs owing to the thin and shallow pay zone of these heavy oil deposit. Even when the reservoir meets the screening criteria for thermal production, the economics of the project may not be feasible. Thermal methods are associated with wellbore heat losses, and the cost of sustaining production is very high

Over the years, CO₂ has proven to be a viable means of recovering heavy oil. However, the large viscosity contract often results in viscous fingering and channels leading to early breakthrough of CO₂. Currently, cold production of heavy oil using CO₂ is still well below 20%. In 2015, Mehdi et al. experimented hydrocarbon recovery enhancement by intermittent CO₂ injection. The result showed that the increase in residence time of CO₂ in the reservoir has a direct impact on production. They also reported a recovery of 15.5% [136]. In a different study, Sixu et al. investigated the effect of pressure maintenance on heavy oil recovery. The results showed that recovery was highest at 15.7% when a conventional five-spot well configuration was used [86]. However, the impact of the casing perforation diameter on heavy oil recovery has never been explored.

In this study, homogenous and heterogeneous reservoirs were modelled using six Castlegate core samples and six Boise core samples respectively. Section 3.4 describes the apparatus and procedures used in conducting the core flooding experiment.

4.5.1 Effect of Perforation Diameter on Heavy Oil Recovery in Homogeneous Reservoirs

Figure 4.10 (a) –(f) shows the results of the laboratory simulation of the immiscible carbon dioxide-heavy oil injection process in homogeneous reservoirs (see Appendix I for figure 4.10 [b]- [f]). The core samples used as the reservoir model were of roughly the same porosity and permeability. The oil recovery of the time-based production curves is quantified as a percentage of the original oil in place (OOIP). For each test, the OOIP represents the volumetric difference between the dry sample and the oil saturated sample before flooding.

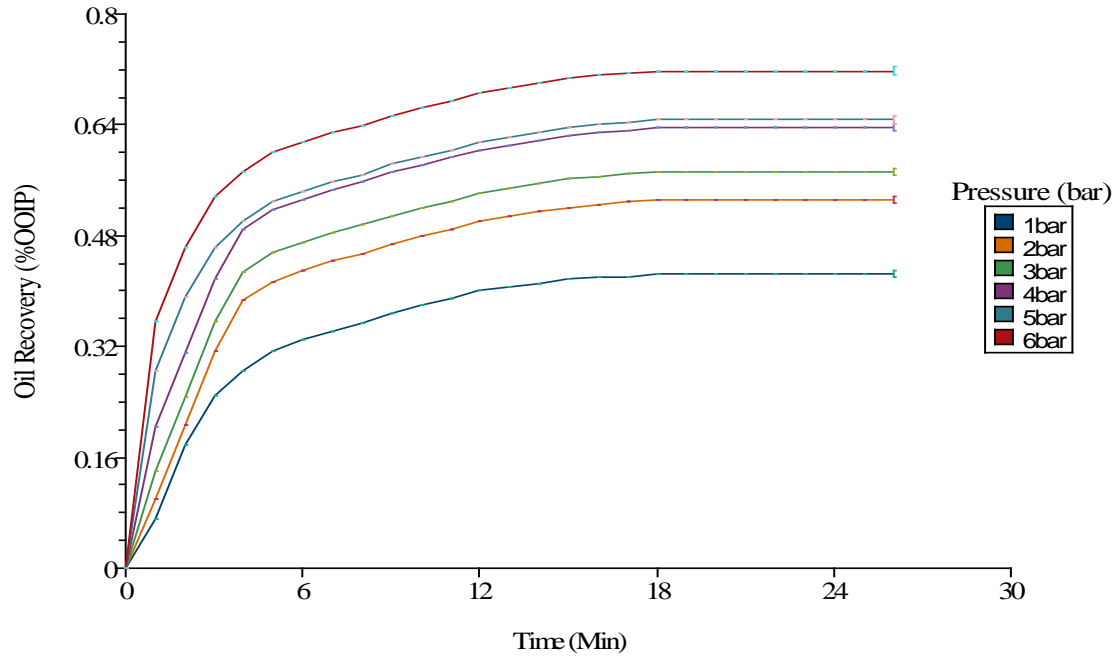


Figure 4.10: (a) Oil recovery at 0.5mm perforation diameter

The effect of perforation diameter on heavy oil viscosity and recovery in a homogeneous reservoir can be explained using Figure 4.10 (a)-(f) (see Appendix I for Figure 4.10 (b)-(f)). In Figure 4.10(a), the highest recovery obtained was 71.8% OOIP at an injection pressure of 6bar. The sharp curves show the impact of injection pressure on the recovery process. The oil recovery values increased with a corresponding increase in injection pressure. Also, the performance of the oil recovery process varied with the injection pressure. In Figure 4.10(a), the oil recovery at just 1 minute from the start of production was recorded to be 35.7 %. It took the same reservoir 8 minutes to produce 35.45% of heavy oil when operating at 1bar injection pressure. As perforation diameter was increased from 0.5mm in Figure 4.10(a) to 1.0mm in Figure 4.10(b), a slight difference scenario started to emerge. Peak production that was initially 71.8% at 6bar dropped to 68%. The performance of the reservoir was also affected. The oil recovery performance dropped from 35.7% to 31.7%. Further reduction in recovery and performance was continued as the perforation diameter was increased. In Figure 4.10(c), the perforation diameter used for the CO₂ injection process was increased to 1.5mm. The maximum oil recovery recorded at 6bar dropped from 68% to 61.1%. The performance of the reservoir also dropped from 31.7% to 25%. The drop in performance and recovery values continued as the perforation diameter increased. The final stage of the experiment was

conducted using a perforation diameter of 3.0mm. The highest oil recovered at this stage at 6bar was 47.3%. The performance of the reservoir was also reduced to 11.1%.

During the period of investigation, it was noticed that the oil recovery fell by 24.5% while the performance of the reservoir dropped to 24.6% by increasing the perforation diameter from 0.5mm to 3.0mm. Figure 5.11 compares the highest oil recovery at different perforation diameter.

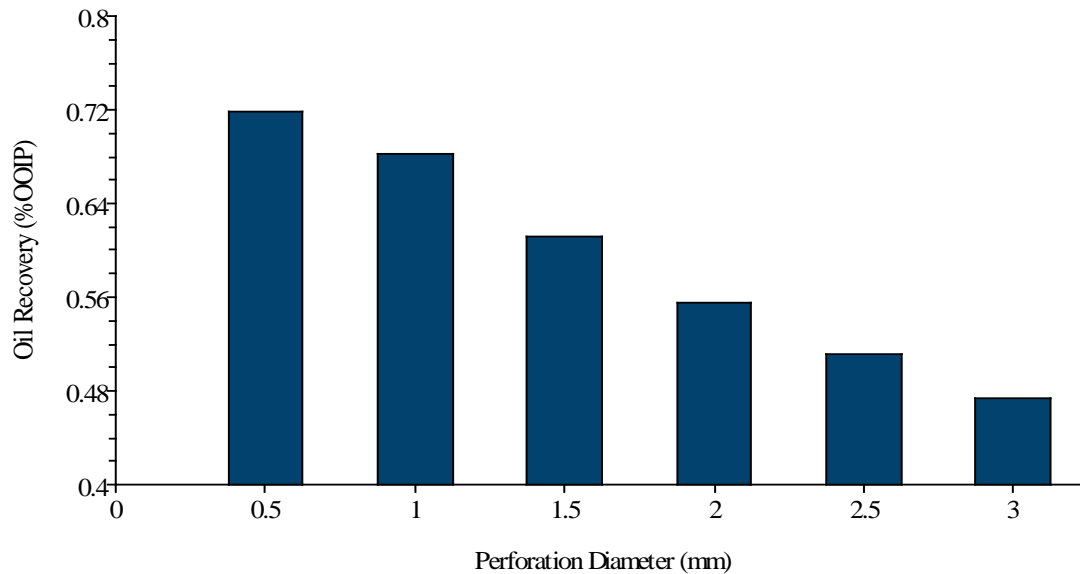


Figure 4.11 Heavy oil recovery at different perforation diameter for the homogeneous model.

Figure 4.11 shows an inverse relationship between the oil recovery and the perforation diameter. This can be attributed to the generation of more rheological stable CO₂ bubbles at smaller perforation as shown in phase II of the experimental study. These stable microbubbles decrease the viscosity of the heavy oil making it more mobile to flow out of the reservoir. The next step in this investigation was to conduct the same test on a heterogeneous sample. One of the advantages of using a heterogeneous sample is that the process of viscous fingering which is a significant barrier in the CO₂ heavy oil recovery process is amplified in micromodels with heterogeneous pore patterns [132].

4.5.2 Effect of Perforation Diameter on heavy oil Recovery in Heterogeneous Reservoirs

In this part of the study, a laboratory simulation was conducted to examine the effect of perforation diameter on oil recovery in heterogeneous formation. The setup for the flooding operation was the same as that used for the homogenous sample. The experiment was

conducted using the sample range of perforation diameter previously used. The results obtained from the study are illustrated in Figure 4.12(a) – (f) (see Appendix J for Figure 4.12(b) – (f). Figure 4.12(a) describes the production pattern at different injection CO₂ injection pressure at 0.5mm perforation diameter. It was observed that the highest oil recovery value of 66% was recorded at an injection pressure of 6bar. The performance of the reservoir was also high producing 43% of OOIP in one minute. The performance at pressures above one bar was observed to be within the range of 37-39% in one minute. The perforation diameter used to inject CO₂ into the model was increased from 0.5mm to 1.0mm, and the flooding process was repeated. Figure 4.12(b) shows the result obtained with the new diameter. A noticeable change in the oil recovery values and the reservoir performance was observed. The oil recovery values drop from 66% to 53% accompanied by a drop in performance from 43% to 31%. The reduction in performance and recovery values continued as the perforation diameter increased. At 1.5mm diameter, Figure 4.12(c) shows peak oil recovery values of 51% and a performance of 21% in the first minute. At 2.0, 2.5 and 3.0mm, perforation diameter, Figure 4.12(d)-(f) oil recovery values to be 57%, 50%, and 54%. The performance of the reservoir under these conditions was 34%, 27% and 14% for the respective perforation diameters.

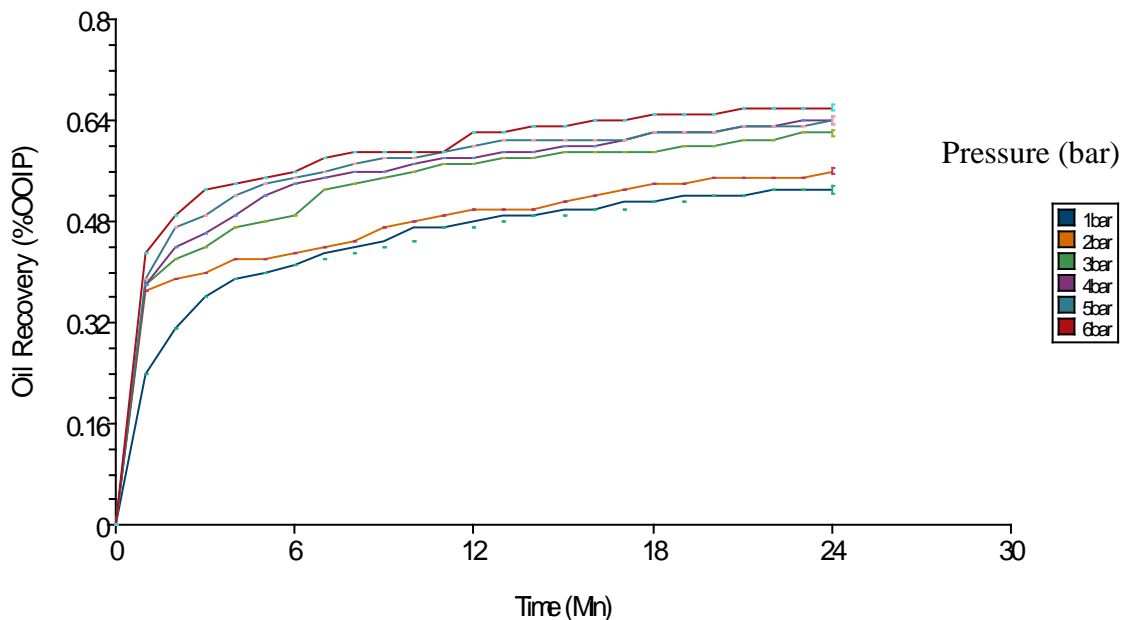


Figure 4.12 :(a) Oil recovery at 0.5mm perforation diameter

The diameter of the perforation used for the test in Figure 4.12(a) was 0.5mm. The sample was flooded at six different pressure ranging from 1-6bars. The results showed highest heavy oil recovery of 66%OOIP at a CO₂ injection pressure of 6bar. In Figure 4.12(b), the diameter of the perforation used was 1.0mm and the highest recovery value recorded was 57% at 6bar injection pressure. For Figures 4.12(c)-(f), the perforation diameter used was 1.5mm, 2.0mm, 2.5mm, and 3.0mm respectively, and the oil recovery at 6bar was 54%, 53%, 51% and 50% respectively. A bar chart of the oil recovery recorded at the different perforation diameter is shown in Figure 4.13.

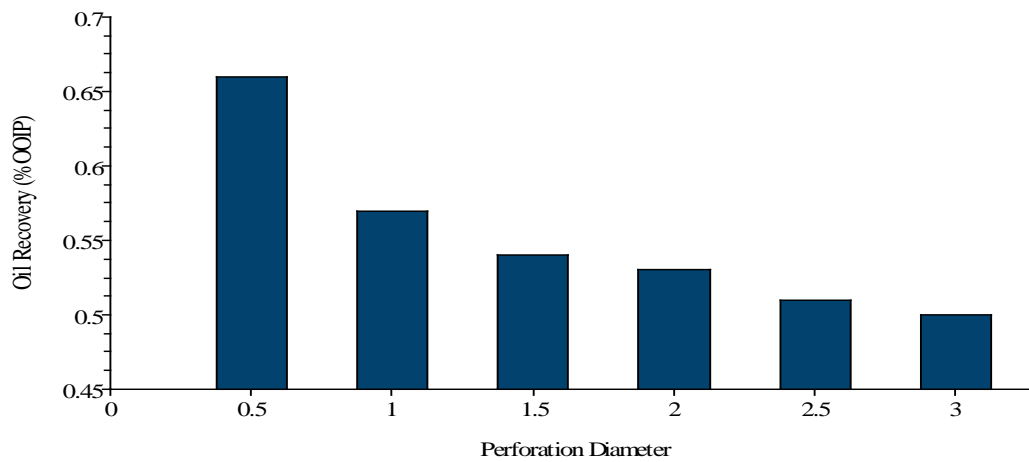


Figure 4.13 Heavy oil recovery obtained in this study at different perforation diameter

Figure 4.13 shows an inverse relationship between the oil recovery and the perforation diameter. This can be attributed to the generation of more rheological stable CO₂ bubbles at smaller perforation as shown in phase II of the experimental study. These stable microbubbles decrease the viscosity of the heavy oil making it more mobile to flow out of the reservoir. It must be noted however that at 1 bar injection pressure, the effect of perforation diameter is not as consistent as it was at pressures from 2bar to 6bar. This may be due to the effect of reservoir heterogeneity at low pressures.

4.5.3 Comparative Analysis of Heavy Oil Recovery Process and CO₂ Utilisation

As stated in section 1.1, CO₂ purchases during EOR project accounts for about 68% of the entire project cost. Therefore, efficient use of CO₂ is required to ensure that the project is profitable. At the laboratory level, CO₂ utilisation is quantified regarding the pore volume of the reservoir model. To compute the volume of CO₂ injected regarding the pore volumes(PV), readings from the XFM flow totalizer is taken. Figure 4.12 (a) shows the highest recovery value

at the start of the production process. Hence it is used for the computation of the CO₂ utilisation for the heterogeneous core-flooding test case. The pore volume of the Boise sample (heterogeneous model) was measured to be roughly 3.68cc. Readings from the flow totalizer showed that 3.65cc of CO₂ was injected in 26seconds (0.44minutes) which corresponds to oil recovery value of about 0.19 (19%OOIP). For the homogeneous model, Figure 4.10(a) recorded the highest. The pore volume of the castle gate sample was measured to be 3.21cc. Again readings from the totalizer showed 3.34 cc of CO₂ was injected in 38sec (0.64minutes). The 0.64minutes corresponds to a recovery value of 23%OOIP. Regarding pore volume, 0.99PV of CO₂ was injected to recover 19% of the original oil in place (OOIP) when the heterogeneous model was flooded. For the homogeneous model, 1.04PV of CO₂ was injected to recover 23% of the OOIP. The results obtained here show that the reservoirs performed better by simply by reducing the perforation diameter. Interestingly, the amount of CO₂ utilised in this study was lesser than the 1.1PV and 1.3PV used by Mehdi and Sixu [86, 136]. Figure 4.14 compares the result of this study with the work of these researchers. HT and HM as shown in the plot represents, heterogeneous and homogeneous model respectively.

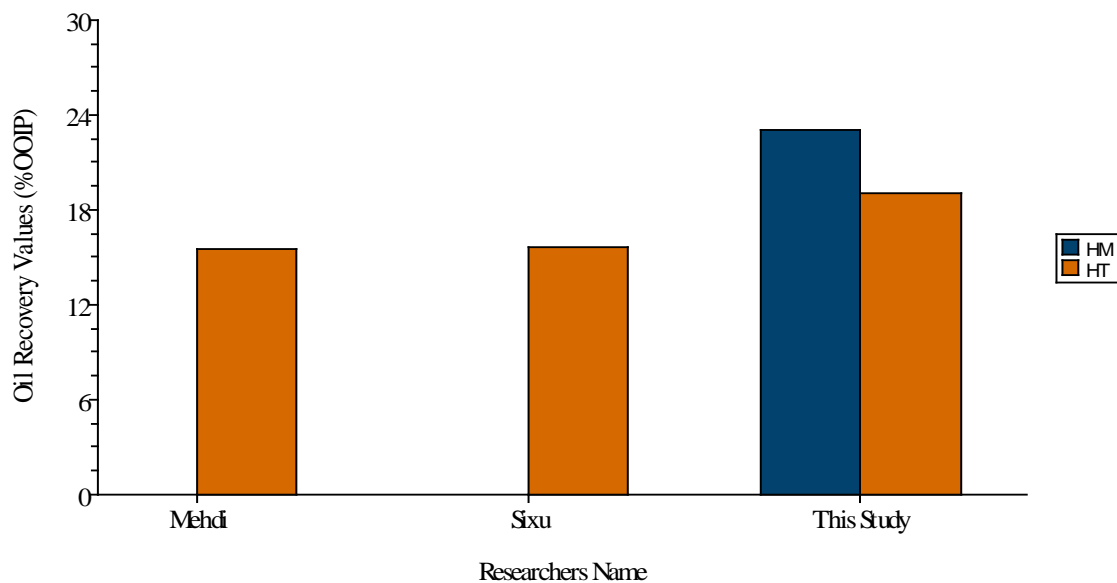


Figure 4.14 A chart comparing the results of this study to other researchers[112, 136].

4.6 Economic Analysis

This section presents a concise cost benefit analysis to evaluate the economic viability of CO₂ heavy oil Enhanced Oil Recovery process with specific focus on the technique applied in this study.

4.6.1 Analysis Framework

The framework applied here includes a reservoir performance model, a revenue model and cost model as shown in Figure 4.15. The performance results of the reservoir model integrate into different revenue and cost models that compute the net revenue and the total cost of the project. The Net Present value of the project was calculated by discounting the cash flow.

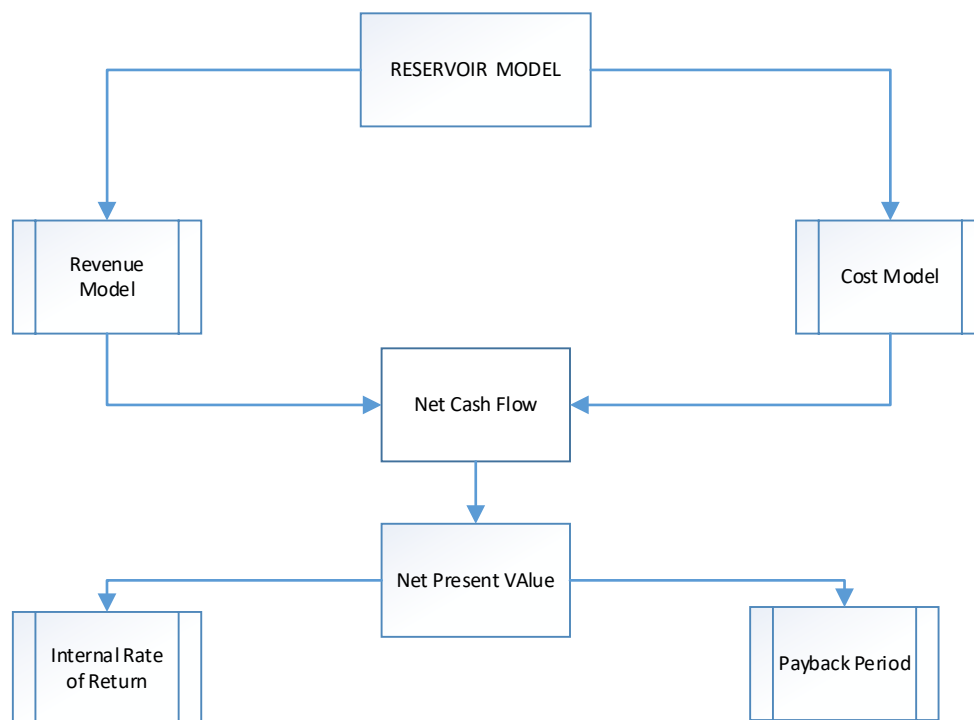


Figure 4.15 Analysis framework used in this study

4.6.2 Reservoir Performance Model.

The economic viability of a CO₂-EOR project depends on the oil recovery, CO₂ injection, production, and recycling performance of the reservoir. In this study, production data from a heavy oil field in Nigeria will be used. For confidentiality, the field will be called “Field X”. Oil recovery results were used to compute the net revenue for the project. The produced water, CO₂ and oil were incorporated into the cost model to estimate the cost of CO₂, capital, operation and maintenance cost (O&M).

4.6.3 Revenue Model.

The revenue model calculates the net revenue obtained from the sale of produced oil after the relevant tax deductions such as royalties, severance tax, and ad valorem tax. The severance and ad valorem tax were deducted from the revenue left after royalties have been deducted. Table 4.8 shows the input and parameters used in the revenue model.

Table 4.8 Revenue model parameters and formulas

Revenue Model Parameter	Input/Definition
Oil Produced(STB)	Volume of incremental or cumulative oil produced during reservoir performance simulations
Oil Price(USD/STB)	Market Price of Oil
Gross Revenue(USD)	Revenue from oil recovered and sold at the specified market price: Oil recovered(STB) x oil price(\$/STB)
Royalty (%)	15% of gross revenue: $0.15 \times \text{gross revenue}(\$)$
Severance Tax (%)	2.0% of revenue after royalty tax : $0.02 \times (0.15 \times \text{gross revenue } \$)$
Ad Valorem tax (%)	1.5% of revenue after royalty tax: $0.015 \times (0.15 \times \text{gross revenue } \$)$
Net Revenue	Revenue after deduction of royalty, severance, and Ad valorem taxes: $\text{Gross Revenue}(\$) - \text{Royalty}(\$) - \text{Severance}(\$) - \text{Ad Valorem}(\$)$

4.6.4 Cost Model

The cost model consists of three costs: well costs, CO₂ costs, operation and maintenance costs (O &M). The well costs are the costs incurred during well design and the installation at the early stage of the production process. The well cost can be subdivided into well drilling and completion costs, production, injection well equipment costs, and well conversion costs. The CO₂ cost includes all cost associated with the purchase, transport, recycling, processing, and recompression of CO₂. The total costs for the site include periodic O&M costs and liquid lifting costs. The periodic O&M costs show the ongoing expense associated with the operation and maintenance of the CO₂-EOR. The cost model shown in Table 4.9 was used for the cost computation in this study. It was developed by six operators for twenty-six well drilled and operated in Ohio between 2005 and 2015 at depths between 1308 and 9200ft.

Table 4.9 Cost model parameters and equations

Cost Parameter	Equations
Well Costs	
Drilling and Completion(D&C)	$\$65703e^{(0.0004 \times \text{depth, ft.})}$
Production Well Equip. EQp)	$(\$10.12 \times \text{depth, ft.}) + \20210
Injection Well Equip. (EQi)	$(\$18.33 \times \text{depth, ft.}) + \11626
Well Conversion	$0.48 \times \$ [D\&C] + (0.50 \times \$ \text{Equipment})$
CO₂ Costs	
CO ₂ transportation and Distribution	$\$187985 + (\text{mi} \times \text{USD/mi})$
CO ₂ Recycling Plant	$\$877264 \times \text{Max. CO}_2 \text{ recycling rate MMscf/day}$
Total O &M Costs	
Periodic O&M	$\$33684e^{(0.0001 \times \text{depth, ft})} \times \text{no of wells}$
Liquid Lifting Costs	$\$0.25 \times (\text{produced BBLs water +oil})$
General & Administrative(G&A)	$0.20 \times (\$[O\&M] + \$\text{Liquid lifting})$

4.6.5: Analysis Scenario and Evaluation Metrics

4.6.5.1 Price Scenario

The choice of this study was to use prices that that is projected to reflect the market realities for a period of fifteen years . Hence, \$60 was chosen as the cost per barrel of oil while the cost of CO₂ was taken as \$40/t CO₂[14, 137].

4.6.5.2 Net Present value

The net present value shows the value of future cash flows accrued incrementally and cumulatively over a period. It is the sum of all cash inflows and outflows discounted to account for the time value of money and the risk associated with future cash flows.

4.6.6 Methodology for Economic Analysis

4.6.6.1. Reservoir Description and simulation parameters

Field X is located in South-South Nigeria. Field X is situated at an average depth of 1750ft. Data from X was considered since it possesses relatively similar properties of the case used in this study. The data presented in Table 4.10 represents the input data for X used to simulate a five-year production history. Immiscible Injection is characterized by piston like displacement processes especially as the composition of the reservoir fluid and the injection fluid is never compromised. Heavy oil are usually located in shallow reservoirs. Consequently, the minimum pressure required for the mixing of carbon dioxide and the oil is highly unlikely. It also means that the a micromodel can be used to simulate recovery processes to an acceptable degree of accuracy. The model for this analysis assumes that the flow processes is driven by the differential pressure between the wellbore and the reservoir and that the effect of reservoir heterogeneity is minimal.

Table 4.10 Reservoir Model Parameters

Parameter	Input
Reservoir	Sandstone
Pattern	5-spot
injection Rate	0.5MMscf/day (26t/day)
PV CO ₂	2
field area	146000acres
Reservoir temperature	107F
Initial Reservoir Pressure	485psia
Reservoir depth	1750ft
Permeability	4.6mD
Porosity	0.27
OOIP	1435
Initial Oil Saturation	0.6
Initial Water saturation	0.3
Initial gas saturation	0.1
Vertical: Horizontal Permeability	0.13
Viscosity of Oil	54cP
Viscosity of water	0.6762
formation volume factor	1.16rb/stb
Solution gas : Oil ratio	284scf/stb
Oil API Gravity	21°

4.6.6.2 Reservoir Production and performance Data.

Table 4.11 shows the result of the simulation conducted to obtain estimates for a five year production history. The data provided here enables the cost and revenue to be computed. It also indicates the performance of the reservoir during the set period. The operational parameter for field X is also shown in Table 4.12

Table 4.11 Results of Eclipse EOR simulation for Field X

Time(Years)	1	2	3	4	5	Cumulative
Oil Produced (MSTB)	23	11	7	6	4	51
Water Produced(MSTB)	15	3	3	2	2	25
CO ₂ Injected (MMscf)	183	183	183	183	183	915
CO ₂ Produced/Recycled (MMscf)	106	153	162	166	170	757
CO ₂ Stored (MMscf)	76	30	22	15	14	157

Table 4.12 Field and Operational input for Field X

Operational Parameters	Input
Field	X
No of Pattern	1
Depth,ft	1750
Distance of trunkline	1
Cost of trunkline \$/mi	33475
Max.CO ₂ recycling rate MMscf/day	0.46
Max.CO ₂ Injection rate	0.49
New injector wells	0.25
New producer wells	0.25
Total wells required	0.5

The values for the new injection and production wells shown in Table 4.12 are obtained by converting the values of the five spot pattern used for the simulation to one pattern. This was done because the cost model used was developed on a per pattern basis but can be upscaled to reflect the pattern of the field development schedule.

4.6.6.3 Project Cost and Revenue.

The cost and revenue were computed by considering a price scenario that reflects the realities of the current oil and gas market. Hence, the price used for oil and CO₂ are \$60/STB and \$40/tonnes respectively. Table 4.13 shows the value obtained for the revenue generated, capital cost and operating cost of the project using the revenue and cost model described in Table 4.8 and 4.9 Two project scenarios (A and B) were chosen to conduct the analysis. Project A describes the performance of field X without any perforation alteration in the well completion process; while project B describes the same field but with the perforation diameter changed by a factor of six as typified in this study. Also in the case of A, 22% OOIP (51MMscf) was recovered using 2PV of injected CO₂ as against B where 34.4% (80MMscf) recovered 22% OOIP of the oil (see Figure 4.10a).

Table 4.13 Revenue and Expenditure of the EOR project

Capital Cost (CAPEX)	Millions of Dollars(\$)	
New Well D &C	0.070000	
Production Well Equipment	0.000948	
Injection Well equipment	0.010926	
CO ₂ recycling Plant	0.403540	
CO ₂ Transport and Distribution	0.221450	
Total CAPEX	0.706864	
Operating and Maintenance Cost		
OPEX		
CO ₂ Recycling O&M	0.45400	
CO ₂ purchase Cost	0.33284	
Periodic O/M	0.13000	
Liquid Lifting	0.01900	
G/A	0.03000	
Total OPEX	0.96584	
Revenue	Project A	Project B
Gross Revenue	3.060000	4.480000
Royalty	0.459000	0.717000
Severance	0.009180	0.014340
Ad Valorem	0.006885	0.010755
Net Revenue	2.584935	4.037905

4.6.6.4 Net Present Value

The net present value (NPV) is calculated as the sum of cash inflows and outflows, discounted to account for the time value of money and the uncertainty associated with future cash flows. The profitability of any venture is usually determined by the net present value equation[138]. It is expressed mathematically as

$$\text{NPV (project)} = A_0 + \sum_{t=1}^n \frac{F_t}{(1 + k + p_t)^t} \quad (4.1)$$

Where,

F_t = the net cash flow in period t

A_0 = initial cash investment (it is negative because it is outflow)

k = the discount rate

t = year of evaluation

n = total number of years of the project life

For this study, an attempt was made to compare the net present values(NPV) at a discount rate of 5% and 10% for field X with (case B) and without perforation reduction(case A). The result from Table 4.14 and 4.15 indicates that case B is economically viable at both discount factor unlike case A which failed at 10% percent discount rate.

Table 4.14 Project A: NPV at 5% discount rate

Year[t]	Cash Outflow(M\$)	Cash Inflow(M\$)	Net Cash flow(M\$) [F _t]	Discount Factor	Discounted Cash(M\$)	Cum NPV(M\$)
0	-0.70686	0.00000	-0.70686	1.000000000	-0.70686000	-0.70686000
1	-0.19317	0.51699	0.32382	0.952380952	0.30840000	-0.39846000
2	-0.19317	0.51699	0.32382	0.907029478	0.29371429	-0.10474571
3	-0.19317	0.51699	0.32382	0.863837599	0.27972789	0.17498218
4	-0.19317	0.51699	0.32382	0.822702475	0.26640752	0.44138969
5	-0.19317	0.51699	0.32382	0.783526166	0.25372144	0.69511114
		2.58495	0.91224	NPV=0.65511114		0.10141729

Table 4.15 Project A: NPV at 10% discount rate

Year	Cash Outflow(M\$)	Cash Inflow(M\$)	Net Cash flow(M\$)[F _t]	Discount Factor	Discounted Cash(M\$)	Cum NPV(M\$)
0	-0.70686	0.00000	-0.70686	1.000000000	-0.70686000	-0.70686000
1	-0.19317	0.51699	0.32382	0.909090909	0.29438182	-0.41247818
2	-0.19317	0.51699	0.32382	0.826446281	0.26761983	-0.14485835
3	-0.19317	0.51699	0.32382	0.751314801	0.24329076	0.09843241
4	-0.19317	0.51699	0.32382	0.683013455	0.22117342	0.31960583
5	-0.19317	0.51699	0.32382	0.620921323	0.20106674	0.52067257
		2.58495	0.91224	NPV=0.52067257		-0.32548572

Table 4.16 Project B: NPV at 5% discount rate

Year	Cash Outflow(M\$)	Cash Inflow(M\$)	Net Cash flow(M\$)[F _t]	Discount Factor	Discounted Cash flow(M\$)	Cum NPV(M\$)
0	-0.70686	0.00000	-0.7068600	1.000000000	-0.70686000	-0.70686000
1	-0.19317	0.80758	0.6144110	0.952380952	0.58515333	-0.12170667
2	-0.19317	0.80758	0.6144110	0.907029478	0.55728889	0.43558222
3	-0.19317	0.80758	0.6144110	0.863837599	0.53075132	0.96633354
4	-0.19317	0.80758	0.6144110	0.822702475	0.50547745	1.47181100
5	-0.19317	0.80758	0.6144110	0.783526166	0.48140710	1.95321809
		4.03791	2.3651950	NPV=1.93521809		3.998378.9

Table 4.17 Project B: NPV at 10% discount rate

Year	Cash Outflow(M\$)	Cash Inflow(M\$)	Net Cash flow(M\$)[F _t]	Discount Factor	Discounted Cash(M\$)	Cum NPV(M\$)
0	-0.70686	0.00000	-0.70686	1.000000000	-0.70686000	-0.70686000
1	-0.19317	0.57950	0.38633	0.909090909	0.55855545	-0.14830455
2	-0.19317	0.57950	0.38633	0.826446281	0.50777769	0.35947314
3	-0.19317	0.57950	0.38633	0.751314801	0.46161608	0.82108922
4	-0.19317	0.57950	0.38633	0.683013455	0.41965098	1.24074020
5	-0.19317	0.57950	0.38633	0.620921323	0.38150089	1.62224109
			1.22479	NPV=1.62224109		3.18837910

4.6.6.5 Payback Period

The payback period of a project is the time in years beyond which the project begins to generate returns. It is also the amount time required to recover the initial investment. The payback period is used to evaluate a project to determine the viability of the project. A project with a shorter payback period is considered to be more economically viable. In this analysis, two project were considered: project A and project B. the net present value of the A and B showed that both projects were viable at a discount rate of 5%. The payback period for both projects was determined by plotting the cumulative net present value against the project years. The results from Figure 4.5 showed that the payback period for case A was 2 years and 5months, while that of case B was 1 year and 2 months. A standard rule of thumb is to accept the project with the project with the shortest payback period [139]. Hence, project case B that requires the reduction of the perforation diameter is considered more viable than project case A.

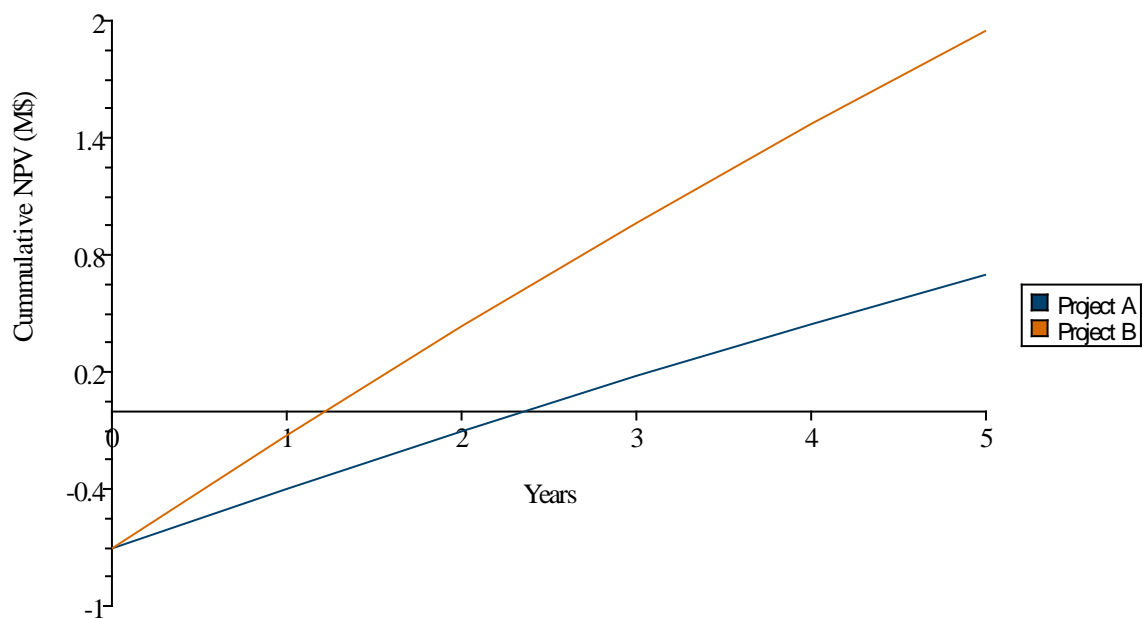


Figure 4.16 Payback period for project case A and B.

4.7 Chapter Summary

This chapter presents and discusses the result of the experiment conducted in chapter three. It records observations and compares it with the work of other researchers. The chapter also presented an economic analysis of two project cases. The first project was a CO₂ –heavy oil recovery project that was performed with the standard well casing perforation diameter. The other project, case B was the same CO₂- heavy oil recovery project, but it was performed with reduced well-casing perforation diameter as typified in this study. The analysis presented in this chapter showed that the project case B was more economically viable than project case A. Chapter five presents the conclusions and recommendations of this study.

Chapter 5

Conclusions and Recommendations

5.1 Conclusions

This experimental study aimed to investigate the effect of perforation diameter and CO₂ bubble size distribution on heavy oil viscosity and recovery. The study was also conducted to examine the CO₂ utilisation involve in the recovery process. Three phases of the experiment were designed for the investigation. The first phase was the rig validation experimentation. The goal at this stage was to ensure that the rig set up and the tools for measurement are appropriate for the investigation. This phase was followed by the second phase. The examination of the effect of perforation diameter and CO₂ bubble size on heavy oil viscosity was done in this phase. The pre-tested rig was set up for particle characterisation and viscosity measurement. A simulation of the fluid-fluid interaction between the injected CO₂ and heavy oil in a recovery process was conducted. The results obtained was presented and analysed in section 4.3 of chapter four. In the third phase, two reservoir models saturated with brine and heavy oil (sunflower oil) was used to conduct 72 core flooding test: 36 for the homogeneous model and another 36 for the heterogeneous model. The focus in this phase was to examine the effect of the perforation diameter on the amount of oil recovery during the CO₂ heavy oil recovery process. The CO₂ utilisation associated with was each of the flooding processes was also noted. The results obtained in phase three was discussed in section 4.5.3 of chapter four. Finally, an economic analysis of the application of perforation with smaller diameter during heavy oil recovery process was conducted, and the results about were presented in section 4.6

The following conclusion can be drawn based on the findings from this study.

PHASE 1

- The CO₂ bubble size distribution is a function of the perforation diameter. The concentration of bubbles with the range of diameter, 0-100µm varied inversely as the perforation diameter.
- Increasing the injection pressure of CO₂ resulted to an additional increase in the concentration of these smaller bubbles (0-100µm)
- The viscosity of the heavy oil was affected by changes in the perforation diameter. The viscosity of Sunflower oil was reduced by 27.7% by changing the perforation diameter from 3mm to 0.5mm.

PHASE II

- The higher the concentration of these microbubbles(1-100 μ m), the lower the viscosity of the oil.

PHASE III

- The recovery values of the oil were affected by changes in the perforation diameter. Higher recovery values were noticed as the perforation diameter was reduced. The injection pressure also had a similar effect on the recovery values. Higher recovery was observed at higher injection pressures. The recovery of oil in the homogeneous model witnessed a 24.5% increment as the perforation diameter was changed from 3mm to 0.5mm. For the heterogeneous model, the increment in oil recovery was 16%.
- The effect of the perforation diameter on recovery values for the heterogeneous model was not consistent at a pressure below 2bar. The recovery values in the heterogeneous model fluctuated after initial production but recorded higher value for smaller perforation decline at the point of peak recovery.
- The CO₂ utilisation varied with the type of the reservoir. The volume of CO₂ required to recover a given quantity of oil is higher for the heterogenous sample than it was for the homogenous sample. One pore volume of CO₂ was required to recovery 23% of the original oil in place(OOIP) for the homogeneous case, unlike the heterogeneous model that recovered 19% OOIP with the same pore volume.
- The CO₂ utilisation reduced with the perforation diameter in both the homogeneous and heterogeneous models.
- Economic analysis showed that heavy oil production project cashflow could be doubled by adopting the application of micro-perforation.

5.2 Recommendations

Carbon dioxide immiscible recovery process is driven primarily by three mechanisms: viscosity and interfacial tension reduction and oil swelling. For heavy oil, the primary driving factor is viscosity reduction. Hence, this research study focussed on how changes in viscosity caused by smaller perforation diameter and CO₂ bubble sizes can ultimately enhance heavy oil recovery. That said, the examination of the role of interfacial tension and swelling may yet complement this investigation. Consequently, further investigation may include:

- Investigating the effect of the perforation diameter on the interfacial tension between the reservoir fluids.
- The effect of perforation diameter and CO₂ bubble size distribution on the interfacial the swelling factor during immiscible carbon dioxide heavy oil recovery.

References

- [1] Poveda, C. A., and Young, R., 2015, "Potential benefits of developing and implementing environmental and sustainability rating systems: Making the case for the need of diversification," *International Journal of Sustainable Built Environment*, 4(1), pp. 1-11.
- [2] Dipietro, J., 2011, "The role of naturally-occurring CO₂ deposits in the emergence of CO₂ enhanced oil recovery."
- [3] Suslick, S. B., Schiozer, D. J., Nepomuceno, F., and Furtado, R., "Forecasting the development of heavy-oil reserves in ultra-deep waters using technological risk models," *Proc. SPE Hydrocarbon Economics and Evaluation Symposium*, Society of Petroleum Engineers.
- [4] Alvarado, V., Manrique, E., 2010, "Enhanced oil recovery: An update review," *Energies*.
- [5] Song, C., and Yang, D. T., 2012, "Optimization of CO₂ flooding schemes for unlocking resources from tight oil formations," *Society of Petroleum Engineers*.
- [6] Jarrell, P. M., Fox, C. E., Stein, M. H., and Webb, S. L., 2002, *Practical aspects of CO₂ flooding*, Society of Petroleum Engineers Richardson, TX.
- [7] Martin, D. F., and Taber, J. J., 1992, "Carbon dioxide flooding."
- [8] Brock, W. R., and Bryan, L. A., 1989, "Summary results of CO₂ EOR field tests, 1972-1987," *Low Permeability Reservoirs Symposium*, Society of Petroleum Engineers, Denver, Colorado.
- [9] 2006, "2006 worldwide EOR survey," *Oil and Gas Journal*, 104(15).
- [10] Seyyedsar, S. M., Farzaneh, S. A., and Sohrabi, M., 2015, "Enhanced heavy oil recovery by intermittent CO₂ injection," *SPE Annual Technical Conference and Exhibition*, Society of Petroleum Engineers, Houston, Texas, USA.
- [11] Suslick, S. B., Schiozer, D. J., Nepomuceno, F., and Furtado, R., 2003, "Forecasting the development of heavy-oil reserves in ultra-deep waters using technological risk models," *Society of Petroleum Engineers*.
- [12] Administration, U. E. I., 2017, "International energy outlook 2017."
- [13] British Petroleum, 2017, "Bp statistical review of world energy,," <https://www.bp.com/content/dam/bp/en/corporate/pdf/energy-economics/statistical-review-2017/bp-statistical-review-of-world-energy-2017-full-report.pdf>.
- [14] International Energy Agency, 2017, November 14, "A world in transformation: World energy outlook 2017," <https://www.iea.org/newsroom/news/2017/november/a-world-in-transformation-world-energy-outlook-2017.html>.
- [15] Trevisan, O., Lisboa, A., França, F., and Trindade, W., "Oil production in offshore fields: An overview of the Brazilian technology development program," *Proc. World Heavy Oil Conference*.

- [16] Meyer, R. F., Attanasi, E. D., and Freeman, P. A., 2007, "Heavy oil and natural bitumen resources in geological basins of the world," Report No. 2007-1084.
- [17] Meyer, R., and Attanasi, E., 2011, "Heavy oil and natural bitumen-strategic petroleum resources, usgs fact sheet 70-03, august."
- [18] Speight, J. G., 2014, The chemistry and technology of petroleum, CRC press.
- [19] Alboudwarej, H., Felix, J., Taylor, S., Badry, R., Bremner, C., Brough, B., Skeates, C., Baker, A., Palmer, D., and Pattison, K., 2006, "Highlighting heavy oil," Oilfield review, 18(2), pp. 34-53.
- [20] Meyer, R. F., and Attanasi, E. D., 2003, "Heavy oil and natural bitumen : Strategic petroleum resources," Report No. 070-03.
- [21] Taylor, P., 2010, "Energy technology perspectives 2010–scenarios and strategies to 2050," International Energy Agency, Paris, 74.
- [22] Clark, B., Graves, W., Lopez-de-Cardenas, J., Gurfinkel, M., and Peats, A., 2007, "Heavy oil, extra-heavy oil and bitumen unconventional oil," Working Document of the NPC Global Oil and Gas Study, TOPIC PAPER, 22.
- [23] Santos, R. G., Loh, W., Bannwart, A. C., and Trevisan, O. V., 2014, "An overview of heavy oil properties and its recovery and transportation methods," Brazilian Journal of Chemical Engineering, 31, pp. 571-590.
- [24] Santos, R., Loh, W., Bannwart, A., and Trevisan, O., 2014, "An overview of heavy oil properties and its recovery and transportation methods," Brazilian Journal of Chemical Engineering, 31(3), pp. 571-590.
- [25] Speight, J. G., 2013, "Chapter 3 - properties and evaluation," Heavy Oil Production Processes, Gulf Professional Publishing, Boston, pp. 37-62.
- [26] D, W. E., 1998, "E.D. Wallace (ed.), a review of analytical methods for bitumens and heavy oils. Austra technical publication series no. 5, alberta oil sands technology and research authority, edmonton, alberta, canada ".
- [27] G, S. J., 2000, The desulfurization of heavy oils and residua (second ed.), marcel dekker inc., new york, ny
- [28] American Society for Testing, M., "Astm d4007. Standard test method for water and sediment in heavy oil by the centrifuge method (laboratory procedure). Annual book of standards. American society for testing and materials, west conshohocken, pa.."
- [29] American Society for Testing, M., "Astm d4006. Standard test method for water in heavy oil by distillation. Annual book of standards. American society for testing and materials, west conshohocken, pa.."
- [30] American Society for Testing, M., "Astm d954. Standard test methods of test for apparent density and bulk factor of nonpouring molding powers (withdrawn 1961). Annual book of standards. American society for testing and materials, west conshohocken, pa."

- [31] American Society for Testing, M., " Astm d1796. Standard test method for water and sediment in fuel oils by the centrifuge method (laboratory procedure). Annual book of standards. American society for testing and materials, west conshohocken, pa.."
- [32] American Society for Testing, M., 2012, Annual book of astm standards : 2012. Section 3, vol. 03.06, section 3, vol. 03.06, Americal Society for Testing Materials, West Conshohocken.
- [33] American Society for Testing, M., "Astm d287. Standard test method for api gravity of crude petroleum and petroleum products (hydrometer method). Annual book of standards. American society for testing and materials, west conshohocken, pa.."
- [34] American Society for Testing, M., "Astm d1555. Standard test method for calculation of volume and weight of industrial aromatic hydrocarbons and cyclohexane. Annual book of standards. American society for testing and materials, west conshohocken, pa.."
- [35] American Society for Testing, M., "Astm d1217. Standard test method for density and relative density (specific gravity) of liquids by bingham pycnometer. Annual book of standards. American society for testing and materials, west conshohocken, pa.."
- [36] American Society for Testing, M., "Astm d1298. Standard test method for density, relative density (specific gravity), or api gravity of crude petroleum and liquid petroleum products by hydrometer method. Annual book of standards. American society for testing and materials, west conshohocken, pa.."
- [37] American Society for Testing, M., "Astm d941. Standard test method for density and relative density (specific gravity) of liquids by lipkin bicapillary pycnometer (withdrawn 1993). Annual book of standards. American society for testing and materials, west conshohocken, pa.."
- [38] Speight, J. G., 2007, "The chemistry and technology of petroleum (fourth ed.), crc-taylor & francis group, boca raton, fl ".
- [39] G, S. J., 2000, "The desulfurization of heavy oils and residua (second ed.), marcel dekker inc., new york, ny ".
- [40] Denney, D., "Development of heavy-oil fields on the u.K. Continental shelf."
- [41] Speight, J. G., 2009, Enhanced recovery methods for heavy oil and tar sands, Gulf Publishing Company.
- [42] M, B. R., 1991, Thermal recovery of oil and bitumen, prentice-hall inc., upper saddle river, nj (1991).
- [43] American Society for Testing, M., "Astm d341. Standard test method for viscosity-temperature charts for liquid petroleum products. Annual book of standards. American society for testing and materials, west conshohocken, pa.."
- [44] American Society for Testing, M., " Astm d88. Standard test method for saybolt viscosity. Annual book of standards. American society for testing and materials, west conshohocken, pa.."

- [45] American Society for Testing, M., "Astm d445. Standard test method for kinematic viscosity of transparent and opaque liquids (and the calculation of dynamic viscosity). Annual book of standards. American society for testing and materials, west conshohocken, pa."
- [46] American Society for Testing, M., "Astm d2270. Standard practice for calculating viscosity index from kinematic viscosity at 40 and 100°C. Annual book of standards. American society for testing and materials, west conshohocken, pa."
- [47] American Society for Testing, M., "Astm d2161. Standard practice for conversion of kinematic viscosity to saybolt universal viscosity or to saybolt furol viscosity. Annual book of standards. American society for testing and materials, west conshohocken, pa."
- [48] G, R. J., 1998, Metals and heteroatoms in crude oils; petroleum chemistry and refining, taylor & francis, washington, dc
- [49] American Society for Testing, M., "Astm d3605. Standard test method for trace metals in gas turbine fuels by atomic absorption and flame emission spectroscopy. Annual book of standards. American society for testing and materials, west conshohocken, pa."
- [50] American Society for Testing, M., "Astm d3341. Standard test method for lead in gasoline-iodine monochloride method. Annual book of standards. American society for testing and materials, west conshohocken, pa."
- [51] American Society for Testing, M., "Astm d3340. Standard test method for lithium and sodium in lubricating greases by flame photometer. Annual book of standards. American society for testing and materials, west conshohocken, pa."
- [52] American Society for Testing, M., "Astm d2788. Method of test for trace metals in gas turbine fuels (atomic absorption method) (withdrawn 1983). Annual book of standards. American society for testing and materials, west conshohocken, pa."
- [53] American Society for Testing, M., "Astm d2599. Methods of test for lead in gasoline by x-ray spectrometry (withdrawn 1992). Annual book of standards. American society for testing and materials, west conshohocken, pa."
- [54] American Society for Testing, M., "Astm d2547 method of test for lead in gasoline, columetric chromate method (withdrawn 1989). Annual book of standards. American society for testing and materials, west conshohocken, pa."
- [55] American Society for Testing, M., "Astm d1549. Standard test method of test for zinc in lubricating oils and additives (polarographic method) (withdrawn 1984). Annual book of standards. American society for testing and materials, west conshohocken, pa."
- [56] American Society for Testing, M., "Astm d1548. Standard test method for vanadium in navy special fuel oil (withdrawn 1997). Annual book of standards. American society for testing and materials, west conshohocken, pa."
- [57] American Society for Testing, M., "Astm d1368. Test method for trace concentrations of lead in primary reference fuels (withdrawn 1994). Annual book of standards. American society for testing and materials, west conshohocken, pa."

[58] American Society for Testing, M., "Astm d1318. Standard test method for sodium in residual fuel oil (flame photometric method). Annual book of standards. American society for testing and materials, west conshohocken, pa.."

[59] American Society for Testing, M., "Astm d1262. Method of test for lead in new and used greases (withdrawn 1990). Annual book of standards. American society for testing and materials, west conshohocken, pa."

[60] American Society for Testing, M., "Astm d1026. Standard test method of test for sodium in lubricating oils and additives (gravimetric method) (withdrawn 1990). American society for testing and materials, west conshohocken, pa."

[61] Speight, J. G., 2009, Enhanced recovery methods for heavy oil and tar sands, Houston, TX : Gulf Pub. Co., Houston, TX.

[62] American Society for Testing, M., "Astm d189. Standard test method for conradson carbon residue of petroleum products. Annual book of standards. American society for testing and materials, west conshohocken, pa."

[63] American Society for Testing, M., "Astm d524. Standard test method for ramsbottom carbon residue of petroleum products. Annual book of standards. American society for testing and materials, west conshohocken, pa."

[64] American Society for Testing, M., "Astm d4530. Standard test method for determination of carbon residue (micro method). Annual book of standards. American society for testing and materials, west conshohocken, pa."

[65] American Society for Testing, M., "Astm d2766. Standard test method for specific heat of liquids and solids. Annual book of standards. American society for testing and materials, west conshohocken, pa.."

[66] Don W Green, P. G. W., 1998, Enhanced oil recovery, Henry L Doherty Memorial Fund of AIME, Society of Petroleum Engineers.

[67] Stalkup, F. I., 1983, Miscible displacement, Society of Petroleum Engineers, Richardson, TX, United States.

[68] Green, D. W., and Willhite, G. P., 1998, Enhanced oil recovery, Henry L. Doherty Memorial Fund of AIME, Society of Petroleum Engineers Richardson, TX.

[69] Kang, S., Gao, C., and Zhang, S., 2013, "Scientific research and field application of co immiscible flooding in heavy oil recovery," Society of Petroleum Engineers.

[70] Zhang, F., Ouyang, J., Feng, X., and Lin, H., "A chemical agent enhancing recovery of the heavy oil reservoir," Society of Petroleum Engineers.

[71] Thomas, S., Ali, S. M. F., Scoular, J. R., and Verkoczy, B., 2001, "Chemical methods for heavy oil recovery."

[72] Sanderson, S. b., 2012, "Enhanced oil recovery by surfactant flooding," Ph.D, Technical University of Denmark, Kongens Lyngby, Denmark.

- [73] Kamal, M. S., Sultan, A. S., Al-Mubaiyedh, U. A., and Hussein, I. A., 2015, "Review on polymer flooding: Rheology, adsorption, stability, and field applications of various polymer systems," *Polymer Reviews*, 55(3), pp. 491-530.
- [74] Tolstikh, L. I., Akimov, N. I., Golubeva, I. A., and Shvetsov, I. A., 1992, "Degradation and stabilization of polyacrylamide in polymer flooding conditions," *International Journal of Polymeric Materials and Polymeric Biomaterials*, 17(3-4), pp. 177-193.
- [75] Asghari, K., and Nakutnyy, P., "Experimental results of polymer flooding of heavy oil reservoirs," *Petroleum Society of Canada*.
- [76] Rosen, M. J., 2004, "Characteristic features of surfactants," *Surfactants and Interfacial Phenomena*, John Wiley & Sons, Inc., pp. 1-33.
- [77] Thomas, S., Scoular, J. R., Verkoczy, B., and Ali, S. M. F., 1999, "Chemical methods for heavy oil recovery," *Petroleum Society of Canada*.
- [78] Morel, D. C., Zaugg, E., Jouenne, S., Danquigny, J. A., and Cordelier, P. R., 2015, "Dalia/camelia polymer injection in deep offshore field angola learnings and in situ polymer sampling results," *Society of Petroleum Engineers*.
- [79] Morel, D. C., Vert, M., Jouenne, S., Gauchet, R., and Bouger, Y., 2012, "First polymer injection in deep offshore field angola: Recent advances in the dalia/camelia field case."
- [80] Morel, D. C., Vert, M., Jouenne, S., Gauchet, R. R. M., and Bouger, Y., 2010, "First polymer injection in deep offshore field angola: Recent advances on dalia/camelia field case," *Society of Petroleum Engineers*.
- [81] Denney, D., 2011, "Polymer injection in a deep offshore field - angola, dalia/camelia field case."
- [82] Wang, D., Han, P., Shao, Z., Hou, W., and Seright, R. S., 2008, "Sweep-improvement options for the daqing oil field."
- [83] Wang, D., Cheng, J., Wu, J., and Wang, Y., 2002, "Producing by polymer flooding more than 300 million barrels of oil, what experiences have been learnt?," *Society of Petroleum Engineers*.
- [84] Wang, D., Dong, H., Lv, C., Fu, X., and Nie, J., 2009, "Review of practical experience by polymer flooding at daqing."
- [85] Schlumberger, 2018, "Oilfield glossary," http://www.glossary.oilfield.slb.com/Terms/s/steam_flood.aspx.
- [86] Zheng, S., Li, H. Z., and Yang, D. T., 2011, "Pressure maintenance and improving oil recovery with co2 injection in heavy oil reservoirs," *Society of Petroleum Engineers*.
- [87] American Pioneer Ventures, 2010, "Carbon dioxide enhanced oil recovery."
- [88] Miller, J. S., and Jones, R. A., 1981, "A laboratory study to determine physical characteristics of heavy oil after co2 saturation," *Society of Petroleum Engineers*.

- [89] Dyer, S. B., Huang, S. S., Ali, S. M. F., and Jha, K. N. N., 1994, "Phase behaviour and scaled model studies of prototype saskatchewan heavy oils with carbon dioxide."
- [90] Saner, W. B., and Patton, J. T., 1986, "Co₂ recovery of heavy oil: Wilmington field test."
- [91] Klins, M. A., and Ali, S. M. F., 1982, "Heavy oil production by carbon dioxide injection."
- [92] Jha, K. N. N., 1986, "A laboratory study of heavy oil recovery with carbon dioxide."
- [93] Sankur, V., and Emanuel, A. S., 1983, "A laboratory study of heavy oil recovery with co₂ injection," Society of Petroleum Engineers.
- [94] Hatzignatiou, D. G., and Lu, Y., 1994, "Feasibility study of co₂ immiscible displacement process in heavy oil reservoirs," Petroleum Society of Canada.
- [95] Nguyen, T. A., and Ali, S. M. F., 1993, "Immiscible carbon dioxide floods, using impure gas in the wag model," Petroleum Society of Canada.
- [96] Mohammed-Singh, L. J., and Singhal, A. K., 2005, "Lessons from trinidad's co₂ immiscible pilot projects."
- [97] Selby, R., Alikhan, A. A., and Ali, S. M. F., 1989, "Potential of non-thermal methods for heavy oil recovery."
- [98] Farouq Ali, S. M., Thomas S., , 1996, "The promise and problems of enhanced oil recovery methods," 7, pp. 57-63.
- [99] Moffitt, P. D., and Zornes, D. R., 1992, "Postmortem analysis: Lick creek meakin sand unit immiscible co₂ waterflood project," Society of Petroleum Engineers.
- [100] Cosad, C., 1992, "Choosing a perforation strategy," Schlumberger Oilfield Review, Schlumberger.
- [101] The Royal Society, 2018, "The potential and limitations of using carbon dioxide," <https://royalsociety.org/topics-policy/projects/low-carbon-energy-programme/potential-limitations-carbon-dioxide/>.
- [102] Soh, G. Y., Yeoh, G. H., and Timchenko, V., 2017, "Numerical investigation of formation and dissolution of co₂ bubbles within silicone oil in a cross-junction microchannel," Microfluidics and Nanofluidics, 21(12), p. 175.
- [103] Ganapathy, H., Shooshtari, A., Dessiatoun, S., Ohadi, M. M., and Alshehhi, M., 2015, "Hydrodynamics and mass transfer performance of a microreactor for enhanced gas separation processes," Chemical Engineering Journal, 266, pp. 258-270.
- [104] Sauzade, M., and Cubaud, T., 2013, "Initial microfluidic dissolution regime of co₂ bubbles in viscous oils," Physical Review E, 88(5), p. 051001.
- [105] Tan, J., Lu, Y. C., Xu, J. H., and Luo, G. S., 2012, "Mass transfer performance of gas-liquid segmented flow in microchannels," Chemical Engineering Journal, 181-182, pp. 229-235.

- [106] Niu, H., Pan, L., Su, H., and Wang, S., 2009, "Effects of design and operating parameters on co2 absorption in microchannel contactors," *Industrial & Engineering Chemistry Research*, 48(18), pp. 8629-8634.
- [107] Or, C., Sasaki, K., Sugai, Y., Nakano, M., and Imai, M., 2016, "Swelling and viscosity reduction of heavy oil by co2-gas foaming in immiscible condition."
- [108] Or, C., Sasaki, K., Sugai, Y., Nakano, M., and Imai, M., 2014, Experimental study on foamy viscosity by analysing co2 micro-bubbles in hexadecane.
- [109] Emadi, A., Sohrabi, M., Jamiolahmady, M., Irland, S., and Robertson, G., 2011, "Mechanistic study of improved heavy oil recovery by co2-foam injection," *Society of Petroleum Engineers*.
- [110] Abivin, P., Henaut, I., Argillier, J.-F., and Moan, M., 2009, "Rheological behavior of foamy oils," *Energy & Fuels*, 23(3), pp. 1316-1322.
- [111] Hiramoto, H., Kuku, K., Kurihara, M., Akai, T., Takakuwa, Y., Sato, K., Tsuchiya, Y., Araki, N., and Shirai, S., 2016, "Experiments of micro-bubble co2 eor using berea sandstone core samples," 22nd Formation Evaluation Symposium of Japan, Society of Petrophysicists and Well-Log Analysts, Chiba, Japan.
- [112] Zheng, S., Li, H. Z., and Yang, D. T., 2011, "Pressure maintenance and improving oil recovery with co2 injection in heavy oil reservoirs," *SPE Heavy Oil Conference and Exhibition*, Society of Petroleum Engineers, Kuwait City, Kuwait.
- [113] Hydramotion, 2017, "Products and industries."
- [114] Dynamics, D., 2010, "Inteferometric particle imaging (ipi) reference manual - 9040u1191".
- [115] Sedgwick, P., 2013, "What is the standard error of the mean?," *BMJ : British Medical Journal*, 346.
- [116] equipment, O. t., 2015, "Products," <http://www.ofite.com/products/product/43-mud-balance-4-scale-metal>.
- [117] Core Laboratory Instruments, 2003, "Porg-200tm manually operated gas porosimeter operating manual."
- [118] TEMCO/CLI, 2003, "Perg-200tm manually operated gas permeameter operating manual."
- [119] Core Laboratory Instruments, 2003, "Perl-200tm manually operated liquid permeameter operating manual."
- [120] Willi, A. K., 2006, "X-ray computed tomography," *Physics in Medicine & Biology*, 51(13), p. R29.
- [121] Ryniewicz, A., 2010, "Accuracy assessment of shape mapping using computer tomography," *Metrology and Measurement Systems*, p. 481.

- [122] Cantatore, A., and Müller, P., 2011, "Introduction to computed tomography," Report, DTU Mechanical Engineering.
- [123] 1.2, V. V. S., 2010, "Computed tomography in dimensional measurement - influencing variables on measurement results and recommendations for computed tomography dimensional measurements,."
- [124] Estevadeordal, J., and Goss, L., 2005, "Piv with led: Particle shadow velocimetry (psv) technique," 43rd AIAA Aerospace Sciences Meeting and Exhibit, American Institute of Aeronautics and Astronautics.
- [125] Buttsworth, D. R., and Ahflock, T. L., 2003, "A pulsed led system for schlieren flow visualisation."
- [126] Chételat, O., and Kim, K. C., 2002, "Miniature particle image velocimetry system with led in-line illumination," *Measurement Science and Technology*, 13(7), p. 1006.
- [127] Hagsäter, S., Westergaard, C., Bruus, H., and Kutter, J., 2008, "Investigations on led illumination for micro-piv including a novel front-lit configuration," *Experiments in fluids*, 44(2), pp. 211-219.
- [128] Willert, C., Stasicki, B., Klinner, J., and Moessner, S., 2010, "Pulsed operation of high-power light emitting diodes for imaging flow velocimetry," *Measurement Science and Technology*, 21(7), p. 075402.
- [129] Rojas, G., and Ali, S. M. F., 1986, "Scaled model studies of carbon dioxide/brine injection strategies for heavy oil recovery from thin formations."
- [130] Al-Abri, A., and Amin, R., 2010, "Phase behaviour, fluid properties and recovery efficiency of immiscible and miscible condensate displacements by scCO₂ injection: Experimental investigation," *Transport in Porous Media*, 85(3), pp. 743-756.
- [131] Emadi, A., Sohrabi, M., Jamiolahmady, M., Ireland, S., and Robertson, G., 2011, "Reducing heavy oil carbon footprint and enhancing production through CO₂ injection," *Chemical Engineering Research and Design*, 89(9), pp. 1783-1793.
- [132] Emadi, A., Jamiolahmady, M., Sohrabi, M., and Ireland, S., 2012, "Visualization of oil recovery by CO₂-foam injection; effect of oil viscosity and gas type," *SPE Improved Oil Recovery Symposium*, Society of Petroleum Engineers, Tulsa, Oklahoma, USA.
- [133] Abivin, P., Henaut, I., Argillier, J. F., and Moan, M., 2009, "Rheological behavior of foamy oils," pp. 1316-1322.
- [134] Chanmoly Or, K. S., Yuichi Sugai, Masanori Nakano, Motonao Imai, 2014, "Experimental study on foamy viscosity by analysing CO₂ micro-bubbles in hexadecane," *International Journal of Oil, Gas and Coal Engineering* 2(2).
- [135] Bora, R., Maini, B. B., and Chakma, A., 1997, "Rheology of foamy oil in porous media," *Technical Meeting / Petroleum Conference of The South Saskatchewan Section*, Petroleum Society of Canada, Regina.

[136] Seyyedsar, S. M., Farzaneh, S. A., and Sohrabi, M., 2015, "Enhanced heavy oil recovery by intermittent co2 injection," Society of Petroleum Engineers.

[137] Economics, S. E., 2015, "2015 Carbon dioxide price forecast."

[138] INVESTOPEDIA, 2018, "Net present value, 2018, february 13, 23:45," <https://www.investopedia.com/terms/n/npv.asp>.

[139] Lyons, W. C., and Plisga, G. J., 2011, Standard handbook of petroleum and natural gas engineering, Gulf Professional Publishing.

Appendix A : Bibliography of Literature Review

A1: Summary of the review of literatures on CO₂ bubbles in micro-channels

Year	Author	Title	Description	Findings	Remarks
2017	Timoshenko et al	Numerical simulation of the formation and dissolution of CO ₂ bubbles within silicon oil in a cross-junction microchannel	Investigated the physics of multiphase bubble formation, dissolution of CO ₂ using a coupled multiphase-multi-component CFD model	Bubble formation is explained. Bubble formation is influenced by flow rate.	The effect of the microchannel diameter on the bubbles was not investigated.
2015	Ganapathy et al	Hydrodynamics and mass transfer of a micro-reactor for enhanced gas separation processes	Experimental analysis of the fluid flow characteristics during the absorption of CO ₂ mixed with N ₂ in aqueous di-ethanolamine (DEA)	Absorption of CO ₂ is explained. Decrease in channel hydraulic diameter resulted in ample enhancement in the absorption performance	Impact of microchannel diameter on CO ₂ dissolution was stated but the bubble sizes were not examined
2013	Sauzade et al	Initial microfluidic dissolution regime of CO ₂ bubbles in viscous oils	Experimental Investigation of bubble morphology from low to large capillary numbers and measured the effective mass diffusion flux across the interface by tracking and monitoring individual bubbles during shrinkage.	Dissolution of CO ₂ bubbles in viscous oil was explained. Findings showed that it was possible to control and explain the interplay of CO ₂ bubbles in viscous oil in small-scale systems.	The dissolution and geometry of individual bubble was examined but the role of the microchannel in the dimension of the bubble was not studied

A2: Summary of the review of the literatures on CO₂ bubbles in micro-channels

Year	Author	Title	Description	Findings	Remark
2011	Tan et al	Mass transfer performance of gas-liquid segmented flow in micro channels.	Experimental investigation of the influence of channel geometry on the overall dissolution mass transfer coefficient	Effect of channel geometry on CO ₂ bubble dissolution is explained. Dissolution was higher for curved surfaces than at straight surfaces. Gas bubbles were considerably smaller during dissolution mass transfer.	The correlation between dissolution, channel type and bubbles sizes was investigated. But the effect of the dimension on the microchannel on the bubble sizes was not examined
2009	Haining et al	Effects of Design and operating parameters on CO ₂ absorption in microchannel contactors	Experimental investigation of the feasibility of utilising microchannel contactors for the separation of CO ₂ from gas stream	Mass transfer rate improved with the reduction of microchannel diameter. Mass transfer driving force increased with CO ₂ pressure	The impact of pressure and the microchannel diameter of on dissolution was studied but the nucleation and distribution was not investigated

A3: Summary of literatures on heavy oil viscosity reduction

Year	Author	Title	Description	Findings	Remarks
2015	Sasaki et al	Swelling and viscosity reduction of heavy oil by CO ₂ gas foaming in immiscible condition	Experimental investigation of the apparent viscosity after depressurisation to atmospheric pressure at 20-50 °C and 1-10 Mpa pressure	The viscosity of heavy oil was reduced by not just temperature increase but by the dissolution of CO ₂ . The concentration of the dissolved CO ₂ in the oil was the primarily responsible for viscosity reduction.	Identified CO ₂ concentration and temperature as factor responsible for viscosity reduction but did not examine the bubbles size distribution and perforation or channel diameter
2014	Chanmoly et al	Experimental study on foamy oil viscosity by analysing CO ₂ microbubbles in hexadecane.	Experimental study to measure the viscosity of foamy hexadecane and CO ₂ gas microbubbles at 20-50 °C and 1-6 Mpa	Findings showed that large bubbles are unstable and contribute to swelling unlike the microbubbles that are more stable and effective for viscosity reduction	The effect of CO ₂ bubble sizes on viscosity during depressurisation or production was examined but not during injection. The role of the perforation diameter was also not studied
2011	Emadi et al	Reducing heavy oil carbon footprint and enhancing production through CO ₂ injection	Experimental investigation of the performance of CO ₂ injection in heavy oil recovery and CO ₂ storage	Visualisation showed that the colour of heavy oil brightened during CO ₂ injection indicating CO ₂ dissolution and viscosity reduction. Extra heavy oil showed more reduction in viscosity under the same conditions	The effect of the dissolution of CO ₂ on heavy oil viscosity was examined, however the role of the CO ₂ bubbly particles and the channel or the perforation was not studied
2009	Abivin et al	Rheological behaviour of foamy oils	Experimental study of the kinetics of bubble evolution and the influence of the bubbles on the heavy oil viscosity	The influence of bubbles on the viscosity of foamy oil depends on the shear conditions. The viscosity of the heavy oil reduced at high shear rate but increased at low shear rate.	The role of CO ₂ bubbles on heavy oil viscosity with respect to shearing conditions during depressurisation was examined but the effect of the channel or perforation diameter was not studied

A4: Summary of review of literatures on heavy oil recovery and CO₂ utilisation

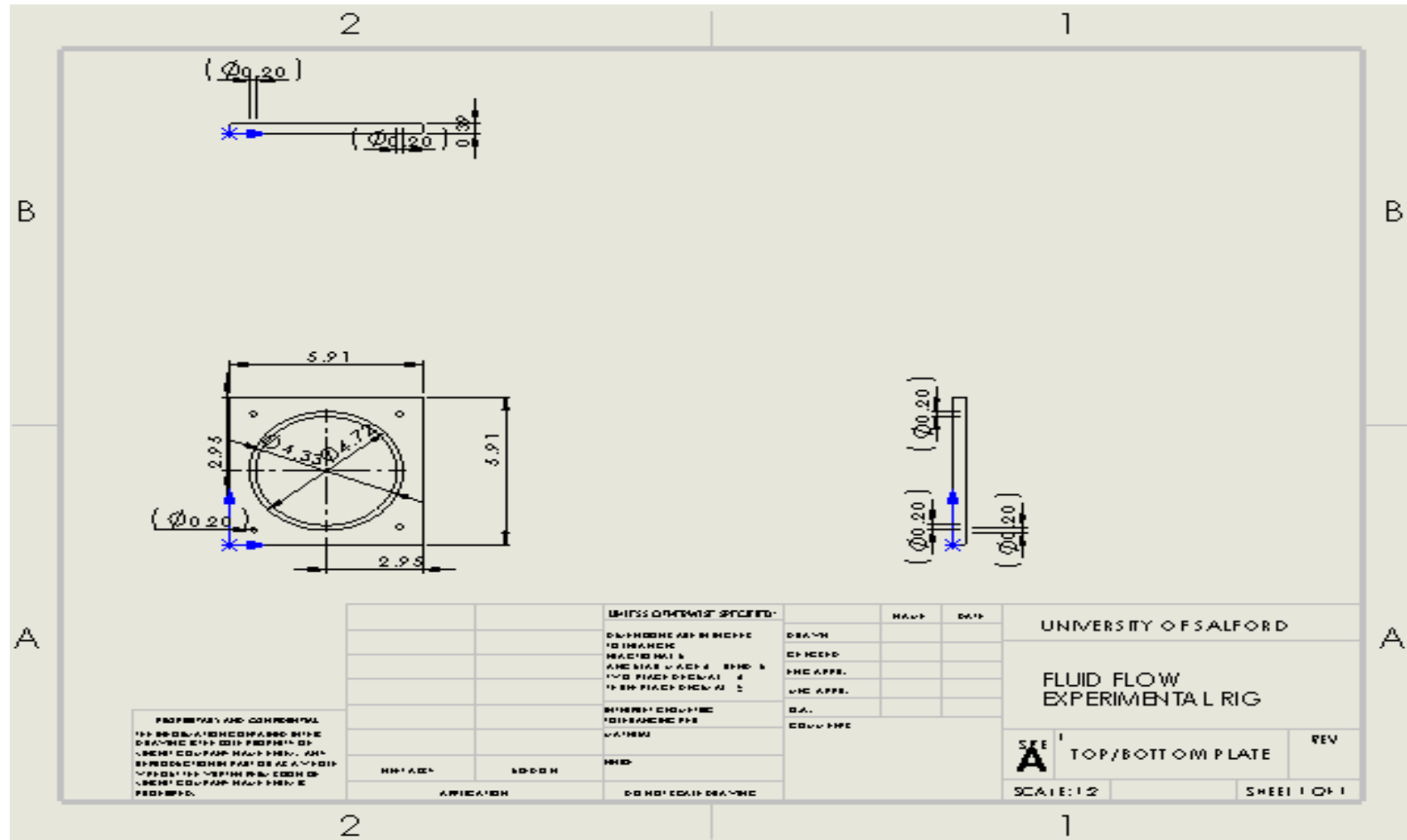
Year	Author	Title	Description	Findings	Remark
2016	Hiroko et al	Experiment of micro-bubble CO ₂ EOR using Berea sandstone core samples	Experimental investigation of the effect of micro bubble CO ₂ injection in oil recovery	Oil recovery was significantly better with CO ₂ microbubbles than with the normal CO ₂	Effect of microbubble on recovery was investigated but the microbubble was generated using a special filter
2015	Mehdi et al	Enhanced heavy oil recovery by intermittent CO ₂ injection	Experimental study to investigate the performance of liquid and supercritical CO ₂ injection in heavy oil recovery process	Heavy oil recovery improved with intermittent CO ₂ injection. CO ₂ utilisation reduced significantly. These improvements were due to the increase in the residence time of CO ₂ in the porous medium	The study focused on the performance of the flooding process and not the bubble sizes or perforation
2013	Sixu et al	Pressure maintenance and improving oil recovery with immiscible CO ₂ injection in thin reservoirs	Experimental investigation and numerical simulation of the performance of pressure maintenance and improving oil recovery with immiscible CO ₂ injection	The effect of well configuration on heavy oil recovery during pressure maintenance with CO ₂ was explained. Recovery was highest for horizontal injector and producer; followed by vertical injector and horizontal producer. Oil recovery was least for vertical injector and producer well pattern	The study was limited to the investigation of impact of well pattern on the recovery of heavy oil.

Appendix B: Rig Design Specifications

B1: Dimension of Nozzle and Cylindrical Section of the Rig

Material Type	Length (mm)	Internal Diameter (mm)	Thickness (mm)	Perforation diameter (mm)	Perforation Spacing	Number of Perforation
Perspex Transparent Cylinder	87.5	115	2.5	NA	NA	NA
Copper Pipe	87.40	8.0	1.0	0.5,1.0,1.5,2.0,2.5,3.0	10	7

B2: Cylindrical Section of Rig Design(Technical Specification)



Appendix C: Camera Specification

Image Sensor

Effective pixels	18megapixels
Aspect ratio	03:02

Focusing

AF system/points	9 cross-type AF points(f/28 at the centre)
AF range	EV-0.5-18(at 23°C \$ISO 100)

Exposure Control

ISO Sensitivity	H:12800
-----------------	---------

Shutter

Speed	1/4000 sec
Frame rate	60fps

Appendix D: Particle Characterisation and Viscosity Data

D1: Data for Bubble Size Distribution vs Perf. Diameter (1.2-1.6bar)

Perforation Diameter (mm)	Frequency of CO ₂ Bubbles						Pressure(bar)
0.5	151	99	27	2	1	0	1.2
1.0	146	98	28	15	8	5	
1.5	142	73	39	12	6	5	
2.0	134	69	36	11	4	1	
2.5	123	65	43	7	7	4	
3.0	116	60	19	6	1	2	
Range of Bubble Diameter (μm)	0-10μm	10-100μm	100-500μm	500-1000μm	1000-5000μm	5000-10000μm	
Perforation Diameter (mm)	Frequency of CO ₂ Bubbles						
0.5	154	110	51	8	5	2	1.4
1.0	151	105	38	10	8	2	
1.5	145	81	34	8	4	2	
2.0	140	72	41	10	5	2	
2.5	124	71	51	5	2	1	
3.0	121	66	42	5	2	0	
Range of Bubble Diameter (μm)	0-10μm	10-100μm	100-500μm	500-1000μm	1000-5000μm	5000-10000μm	
Perforation Diameter (mm)	Frequency of CO ₂ Bubbles						
0.5	166	124	63	5	2	0	1.6
1.0	163	121	42	8	5	2	
1.5	161	92	37	5	0	1	
2.0	151	83	43	7	2	1	
2.5	132	74	56	4	2	2	
3.0	130	71	46	4	3	0	
Range of Bubble Diameter (μm)	0-10μm	10-100μm	100-500μm	500-1000μm	1000-5000μm	5000-10000μm	

Perforation Diameter (mm)

D2: Data for Bubble Size Distribution and Perf. Diameter (1.8-2.2bar)

Pressure(bar)

Frequency of CO ₂ Bubbles							1.8
0.5	167	131	74	1	1	1	
1.0	165	124	49	9	6	1	
1.5	161	111	39	5	1	1	
2.0	158	88	52	4	0	2	
2.5	137	81	62	4	2	1	
3.0	133	73	48	4	0	1	

Range of Bubble Diameter (μm)	0-10μm	10-100μm	100-500μm	500-1000μm	1000-5000μm	5000-10000μm	
Perforation Diameter (mm)	Frequency of CO2 Bubbles						
0.5	174	144	91	3	0	1	2.0
1.0	172	141	49	7	0	2	
1.5	161	118	42	3	3	0	
2.0	158	94	54	4	1	1	
2.5	142	87	67	5	1	0	
3.0	140	76	51	2	1	0	

Range of Bubble Diameter (μm)	0-10μm	10-100μm	100-500μm	500-1000μm	1000-5000μm	5000-10000μm	2.2
Perforation Diameter (mm)	Frequency of CO2 Bubbles						
0.5	189	156	90	2	0	1	
1.0	186	150	53	6	1	0	
1.5	182	126	51	2	1	1	
2.0	163	96	57	2	0	1	
2.5	144	92	73	4	1	0	
3.0	141	81	56	1	3	2	

Range of Bubble Diameter (μm)	0-10 μm	10-100 μm	100-500 μm	500-1000 μm	1000-5000 μm	5000-10000 μm
---	--------------------	----------------------	-----------------------	------------------------	-------------------------	--------------------------

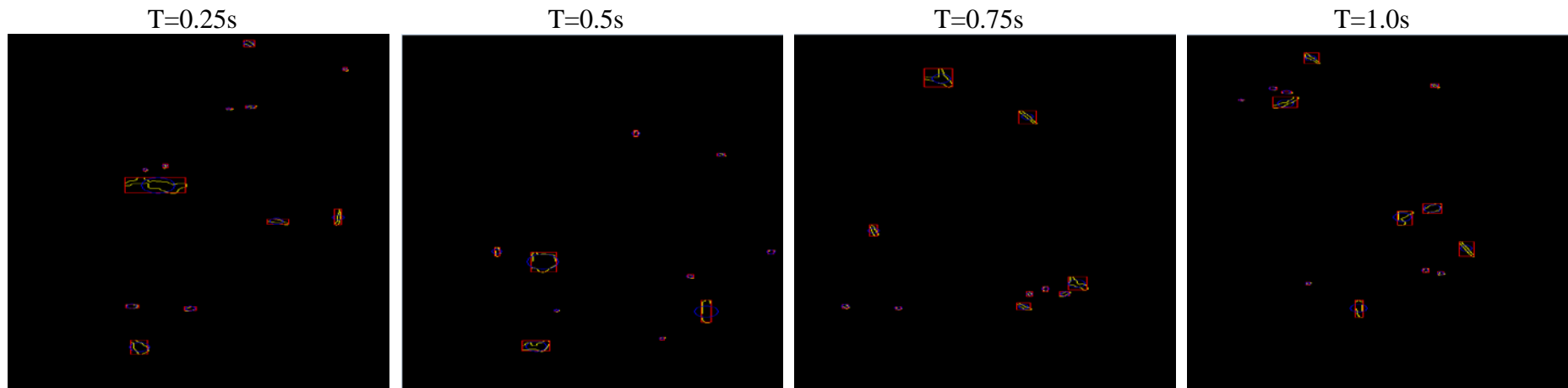
D3: Dynamic Viscosity vs perforation Diameter

Perforation Diameter (mm)	Dynamic Viscosity (cP)					
0.5	42.00	41.90	41.40	40.00	39.60	39.00
1.0	46.10	45.80	45.30	44.10	43.70	43.10
1.5	46.50	45.90	45.60	45.40	45.40	45.20
2.0	48.00	47.20	46.50	46.30	46.20	46.10
2.5	49.00	48.90	48.90	48.60	48.30	48.10
3.0	52.10	51.80	51.40	51.30	51.10	51.10
CO2 Injection Pressure (bar)	1.2bar	1.4bar	1.6bar	1.8bar	2.0bar	2.2bar

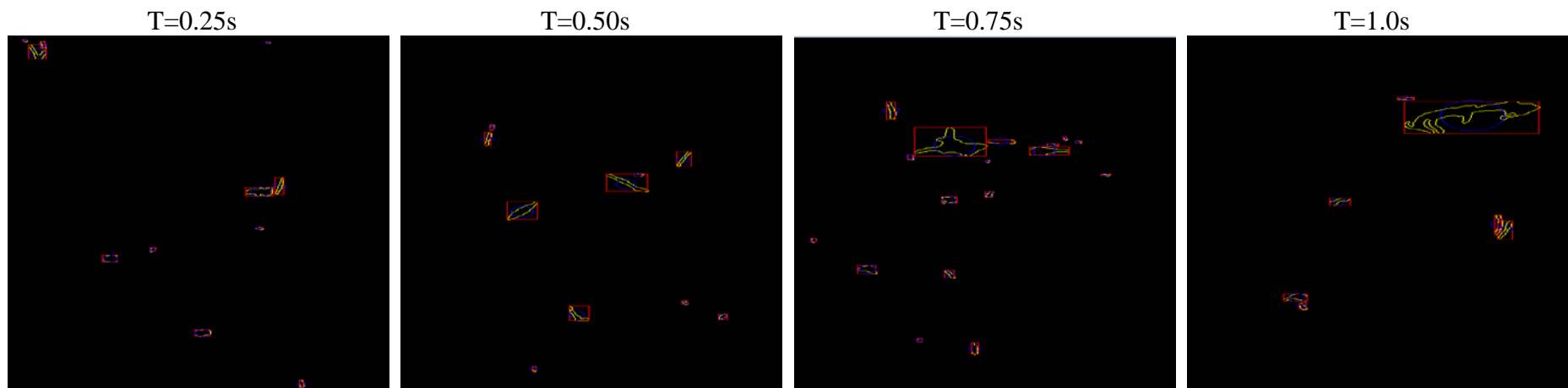
Note: Appendix D4

The images shown in appendix **D4-D39** represent frames captured at four different timesteps within one second of complete saturation of the CO₂ bubbles in the Sunflower oil. The morphology of the CO₂ bubbles is highlighted by the yellow contours shown in each frame. The total number of bubbles in the solution were obtained by the summation of all the bubbles in the timesteps analysed.

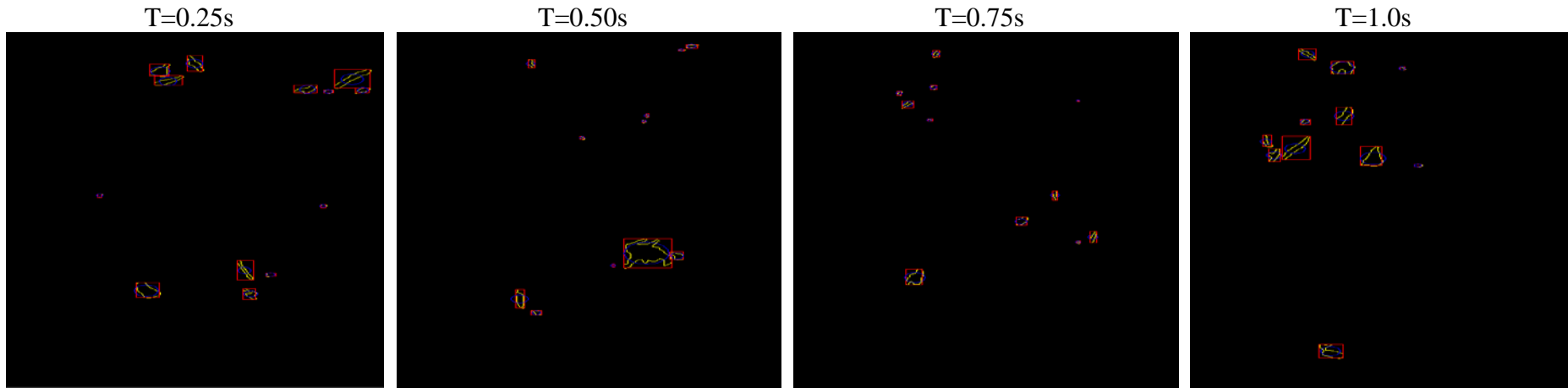
D4: Processed Images of CO₂ Bubbles in Sunflower Oil at 0.5mm Perforation diameter and 1.2bar Injection pressure



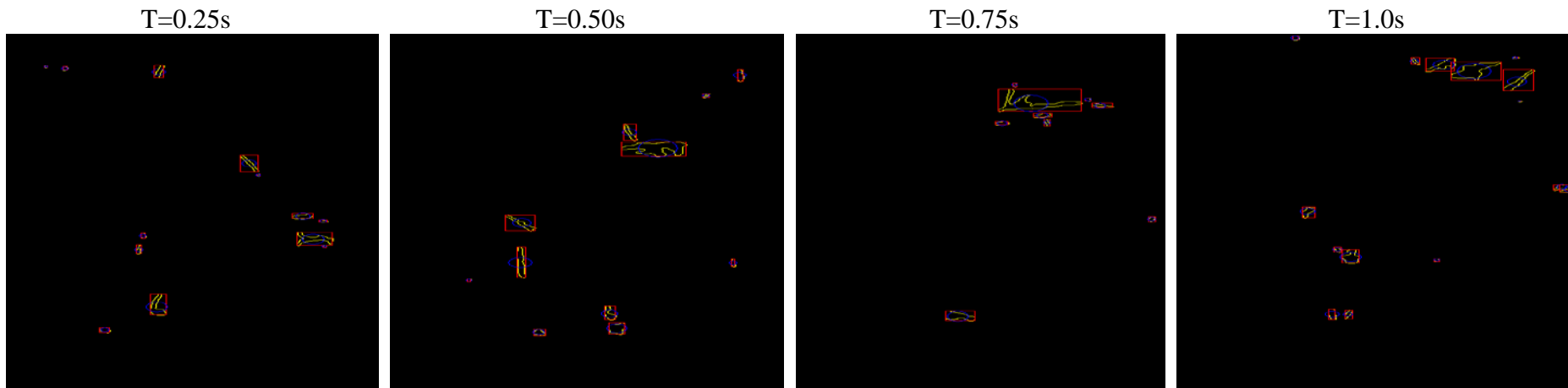
D5: Processed Images of CO₂ Bubbles in Sunflower Oil at 0.5mm Perforation diameter and 1.4bar Injection pressure



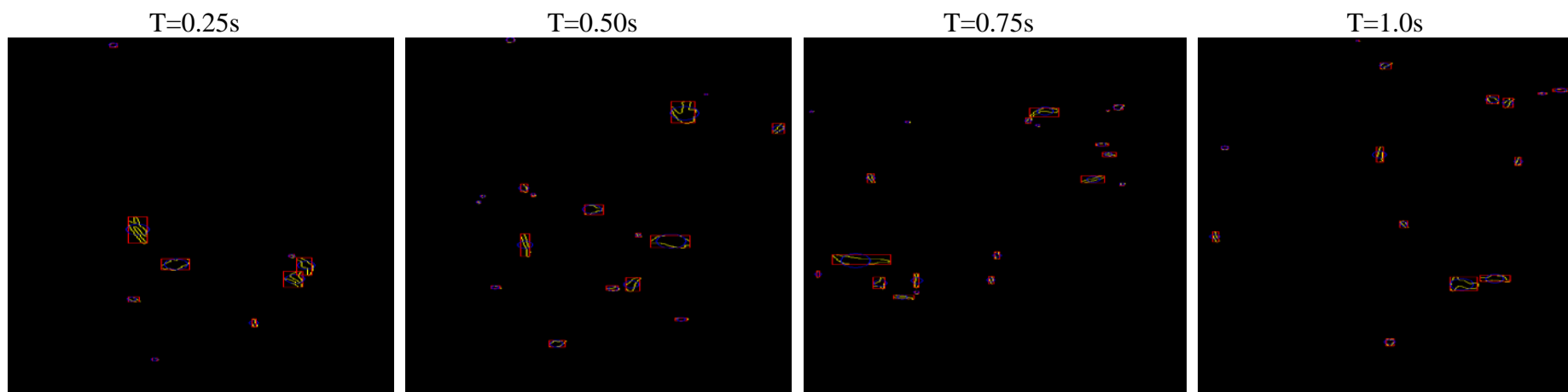
D6: Processed Images of CO₂ Bubbles in Sunflower Oil at 0.5mm Perforation diameter and 1.6bar Injection pressure



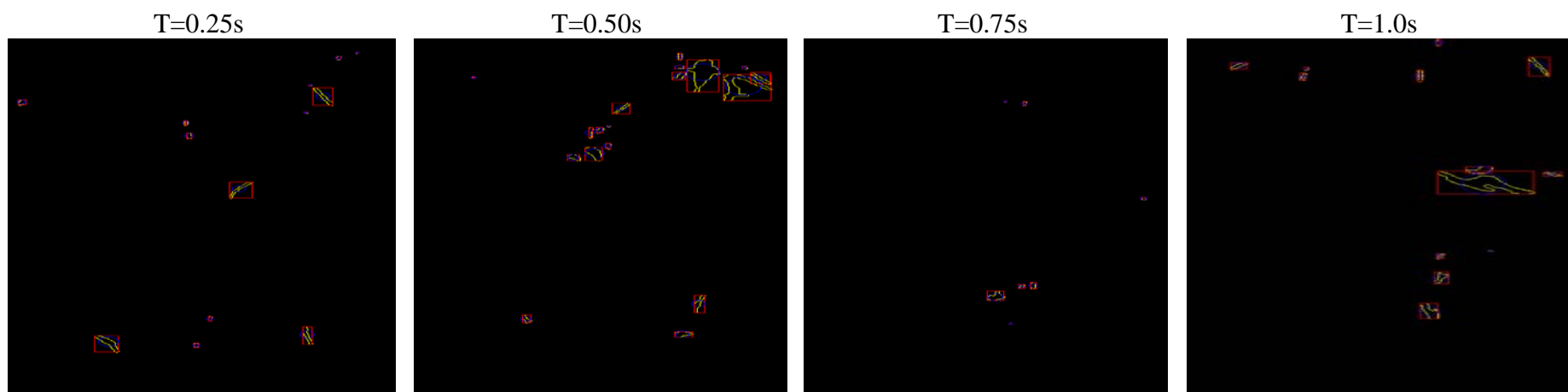
D7: Processed Images of CO₂ Bubbles in Sunflower Oil at 0.5mm Perforation diameter and 1.8bar Injection pressure



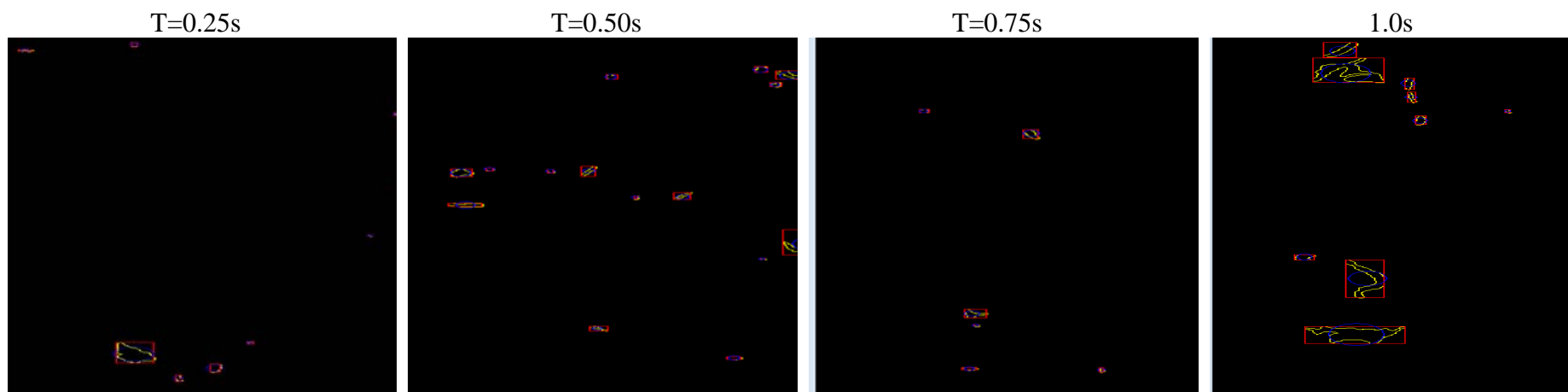
D8: Processed Images of CO₂ Bubbles in Sunflower Oil at 0.5mm Perforation diameter and 2.0bar Injection pressure



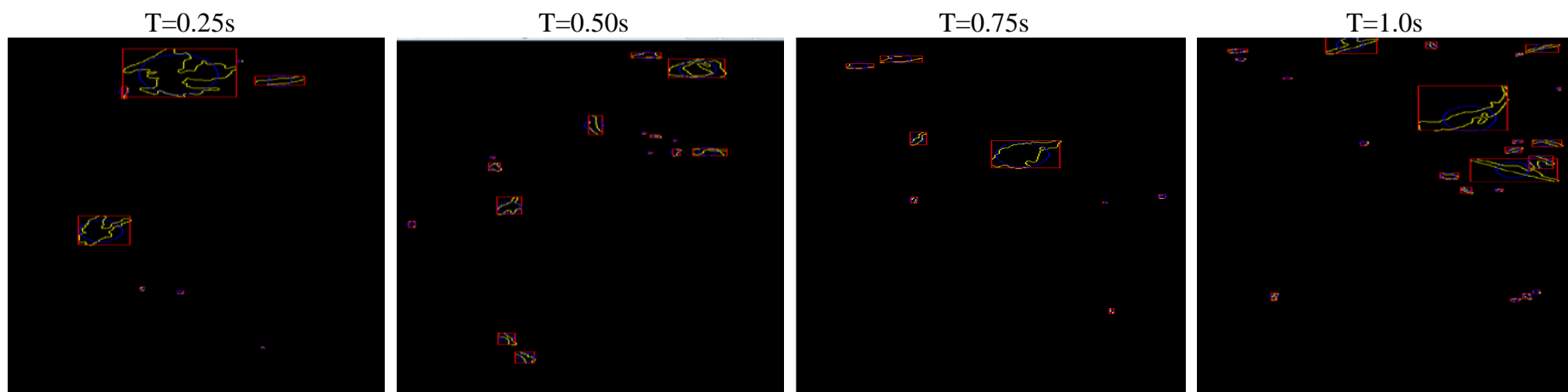
D9: Processed Images of CO₂ Bubbles in Sunflower Oil at 0.5mm Perforation diameter and 2.2bar Injection pressure



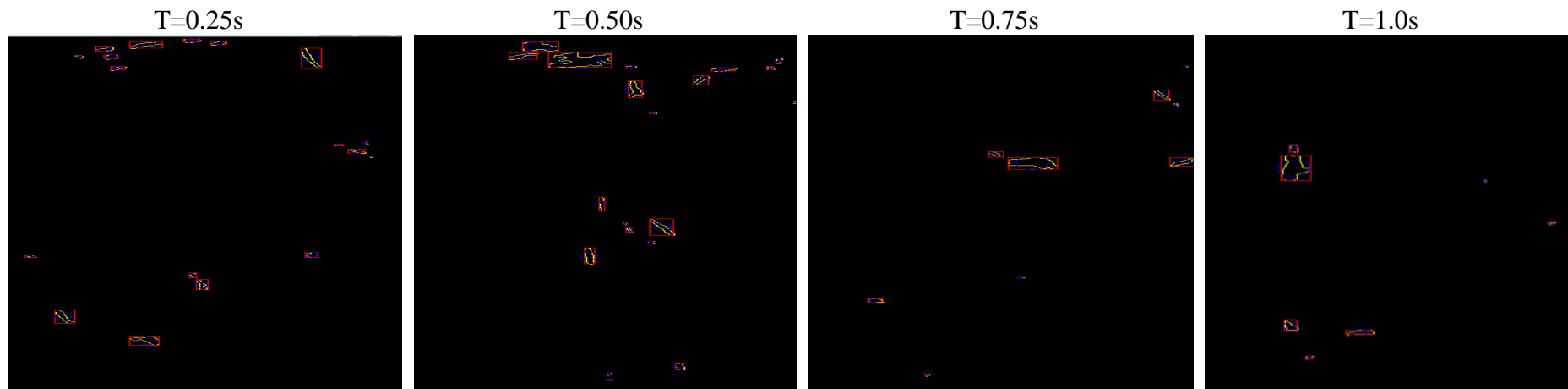
D10: Processed Images of CO₂ Bubbles in Sunflower Oil at 1.0mm Perforation diameter and 1.2bar Injection pressure



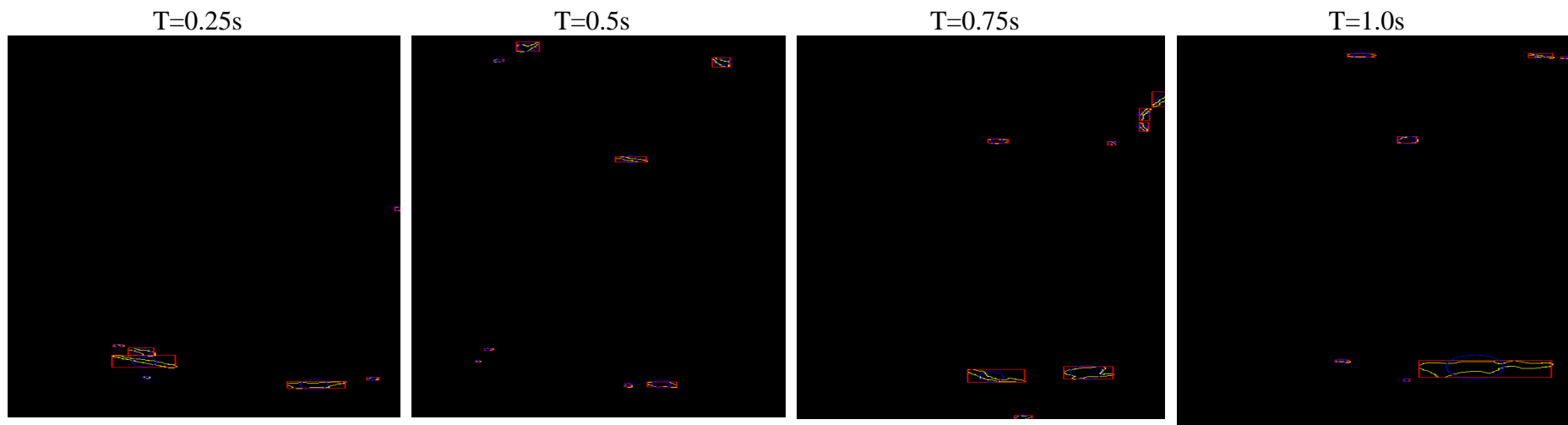
D11: Processed Images of CO₂ Bubbles in Sunflower Oil at 1.0mm Perforation diameter and 1.4bar Injection pressure



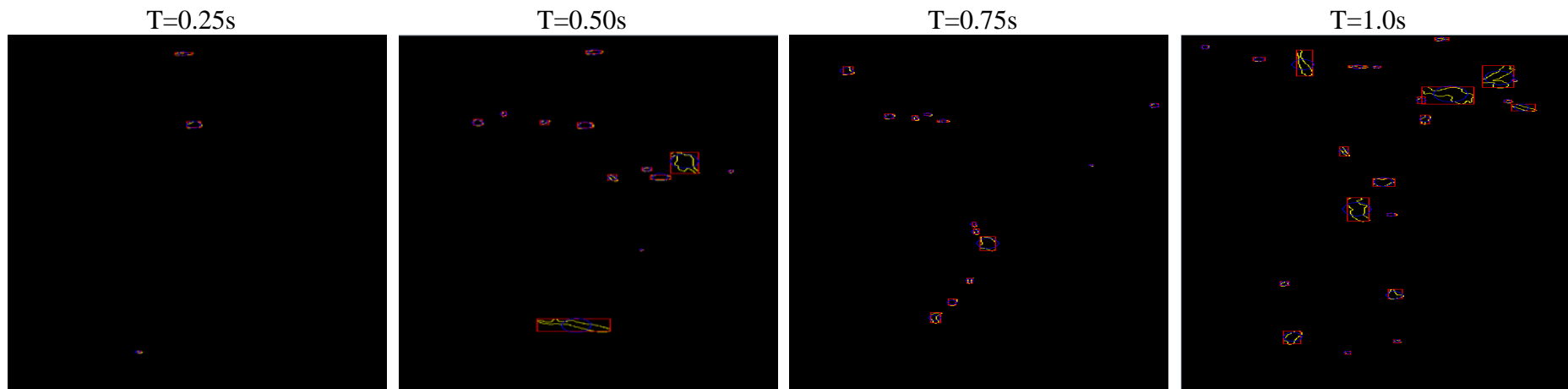
D12: Processed Images of CO₂ Bubbles in Sunflower Oil at 1.0mm Perforation diameter and 1.6bar Injection pressure



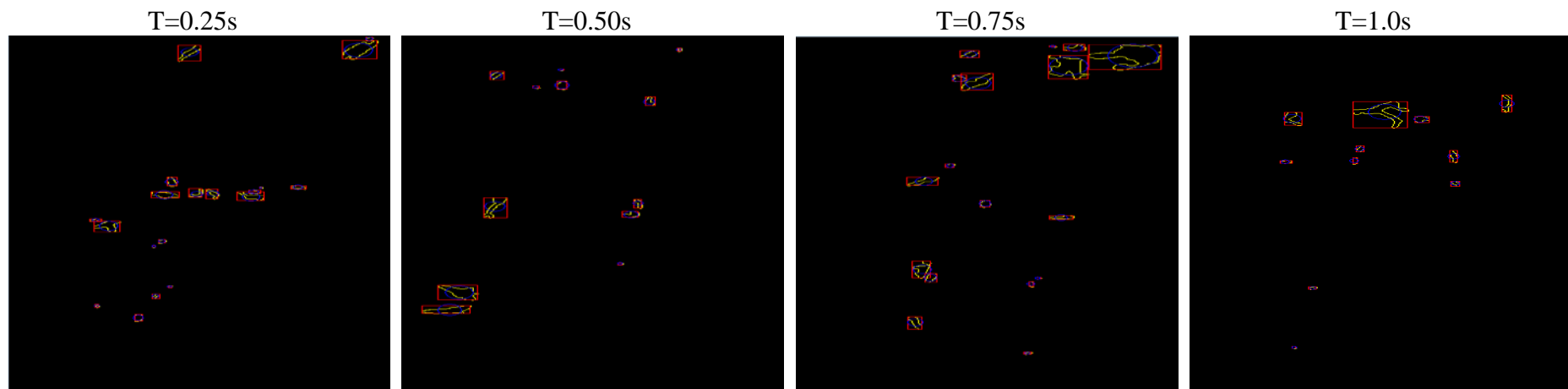
D13: Processed Images of CO₂ Bubbles in Sunflower Oil at 1.0mm Perforation diameter and 1.8bar Injection pressure



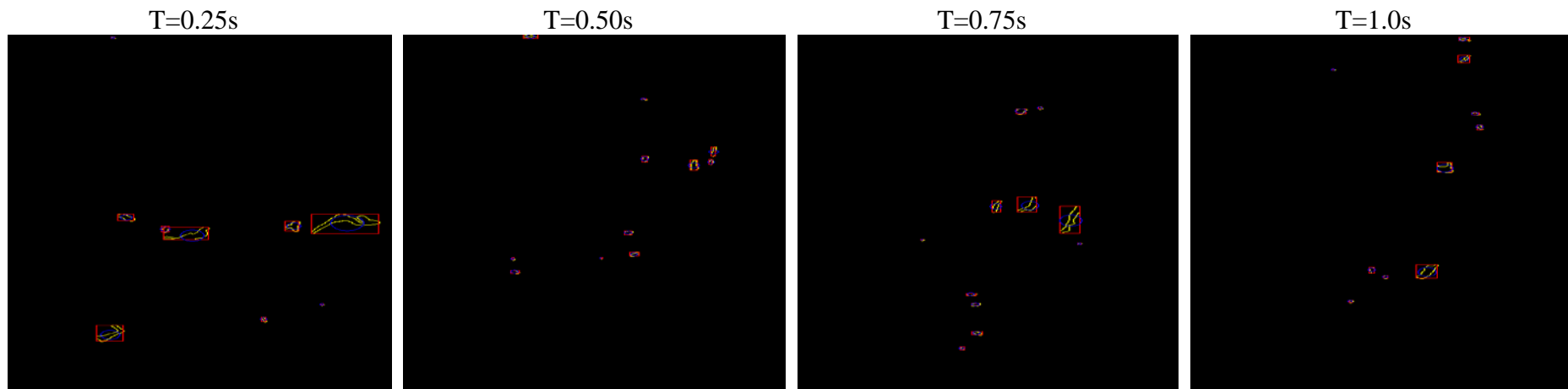
D14: Processed Images of CO₂ Bubbles in Sunflower Oil at 1.0mm Perforation diameter and 2.0bar Injection pressure



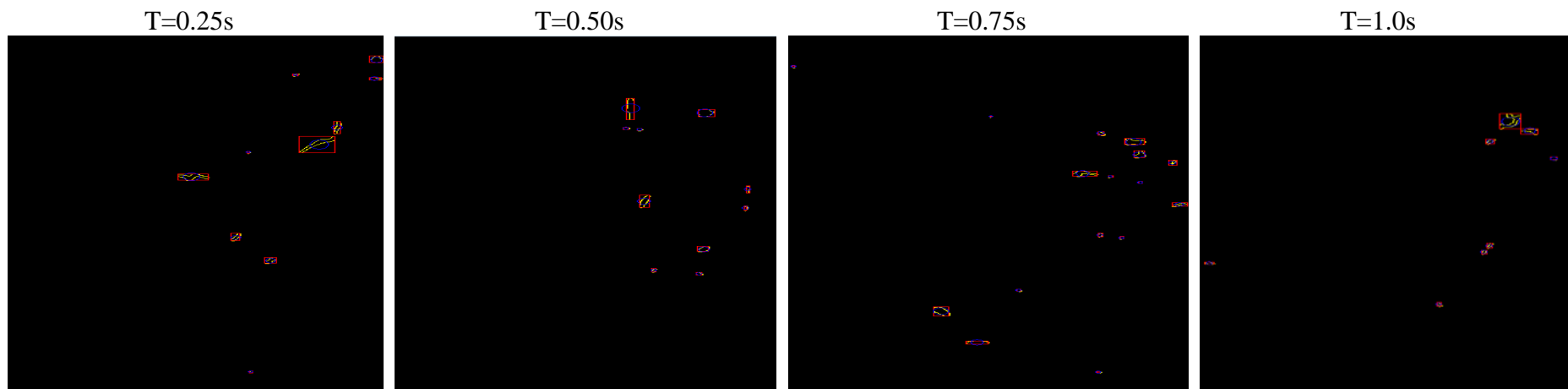
D15: Processed Images of CO₂ Bubbles in Sunflower Oil at 1.0mm Perforation diameter and 2.2bar Injection pressure



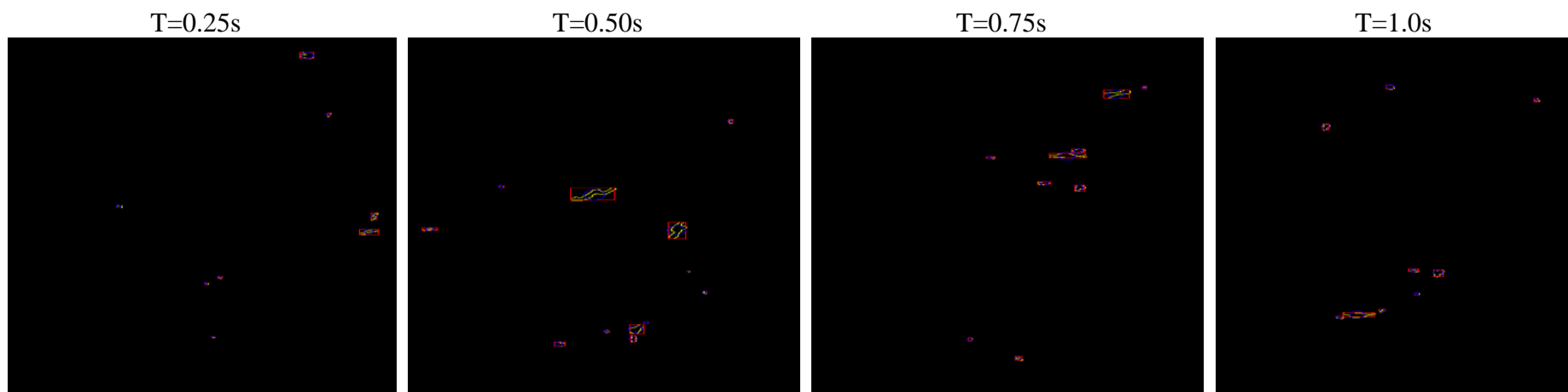
D16: Processed Images of CO₂ Bubbles in Sunflower Oil at 1.5mm Perforation diameter and 1.2bar Injection pressure



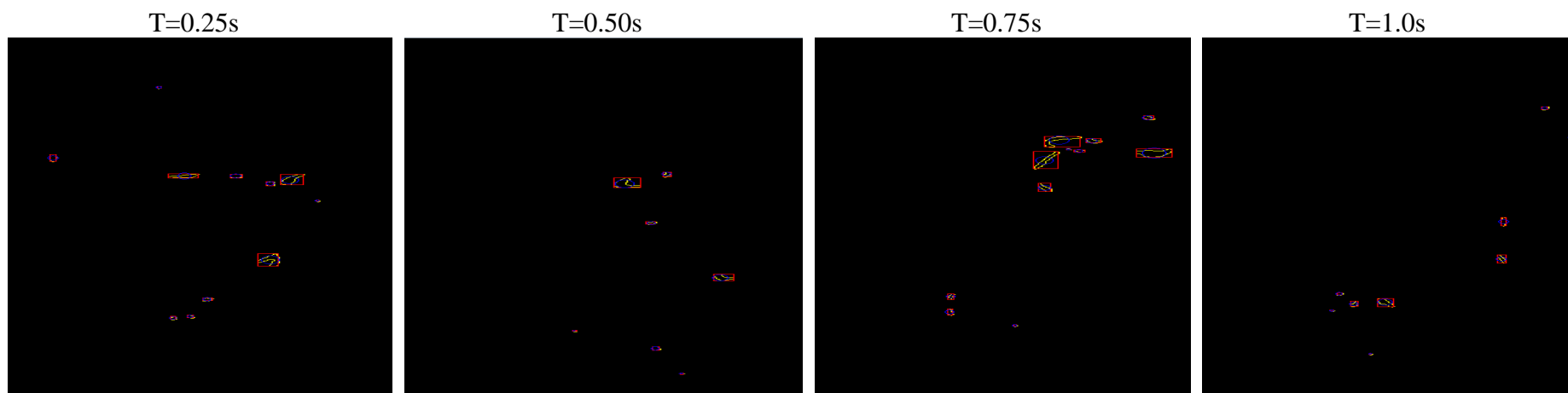
D17: Processed Images of CO₂ Bubbles in Sunflower Oil at 1.5mm Perforation diameter and 1.4bar Injection pressure



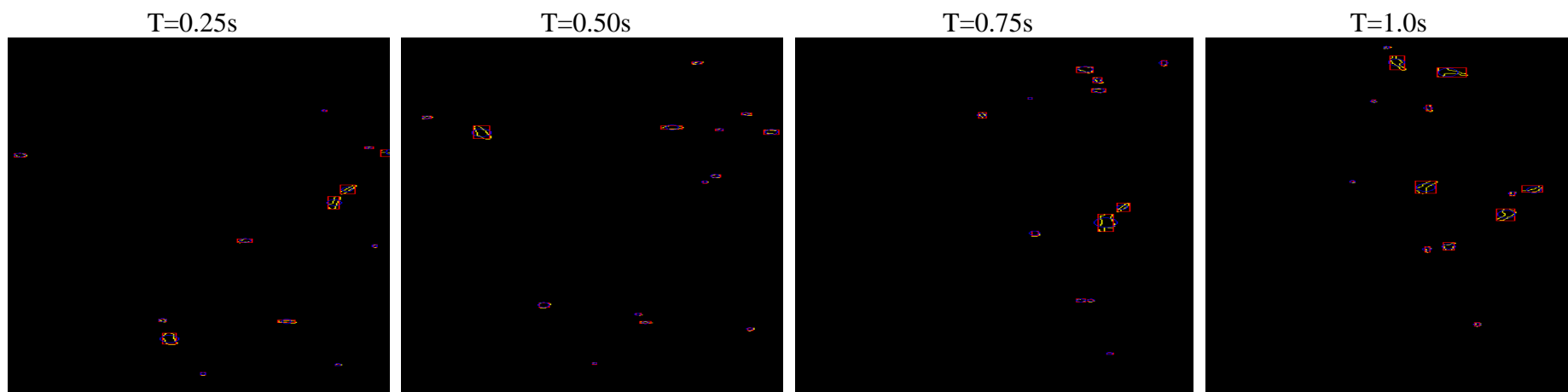
D18: Processed Images of CO₂ Bubbles in Sunflower Oil at 1.5mm Perforation diameter and 1.6bar Injection pressure



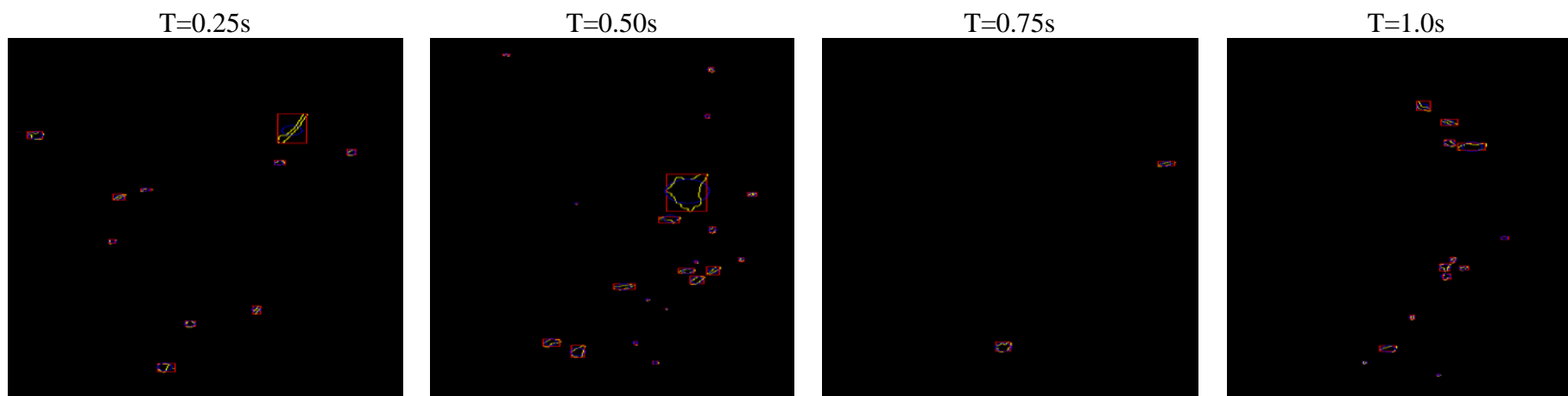
D19: Processed Images of CO₂ Bubbles in Sunflower Oil at 1.5mm Perforation diameter and 1.8bar Injection pressure



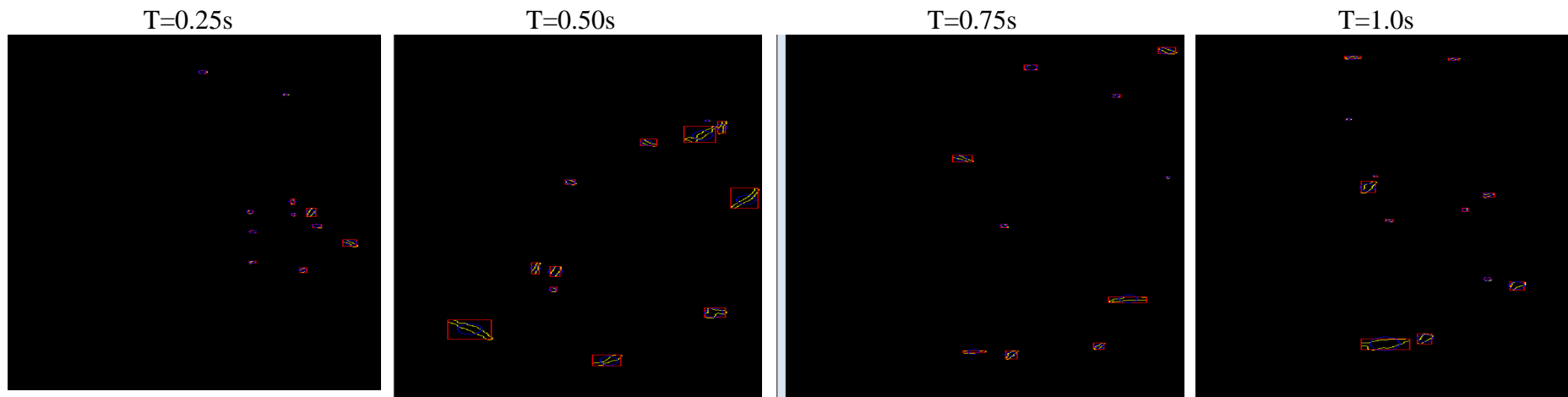
D20: Processed Images of CO₂ Bubbles in Sunflower Oil at 1.5mm Perforation diameter and 2.0bar Injection pressure



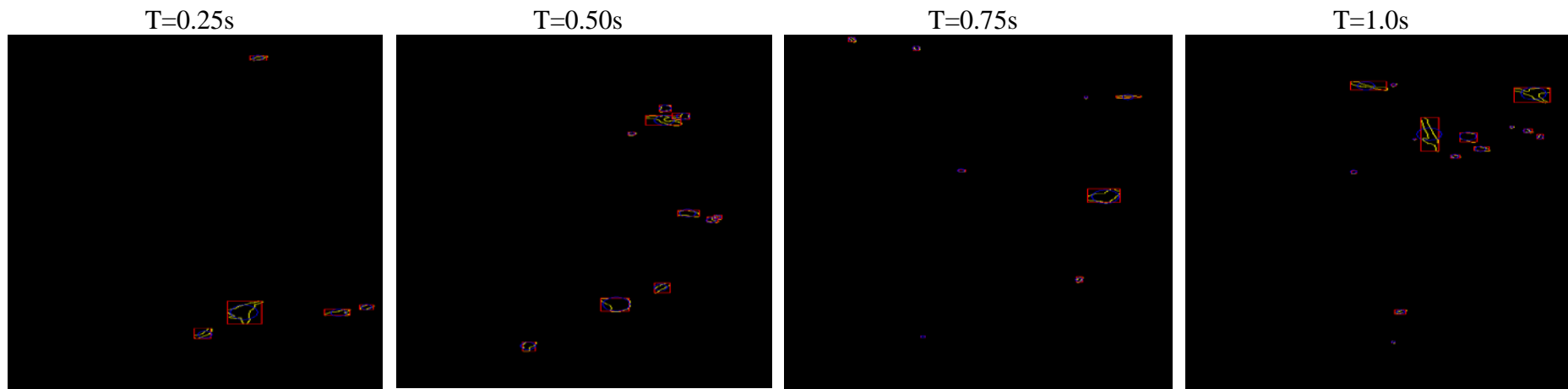
D21: Processed Images of CO₂ Bubbles in Sunflower Oil at 1.5mm Perforation diameter and 2.2bar Injection pressure



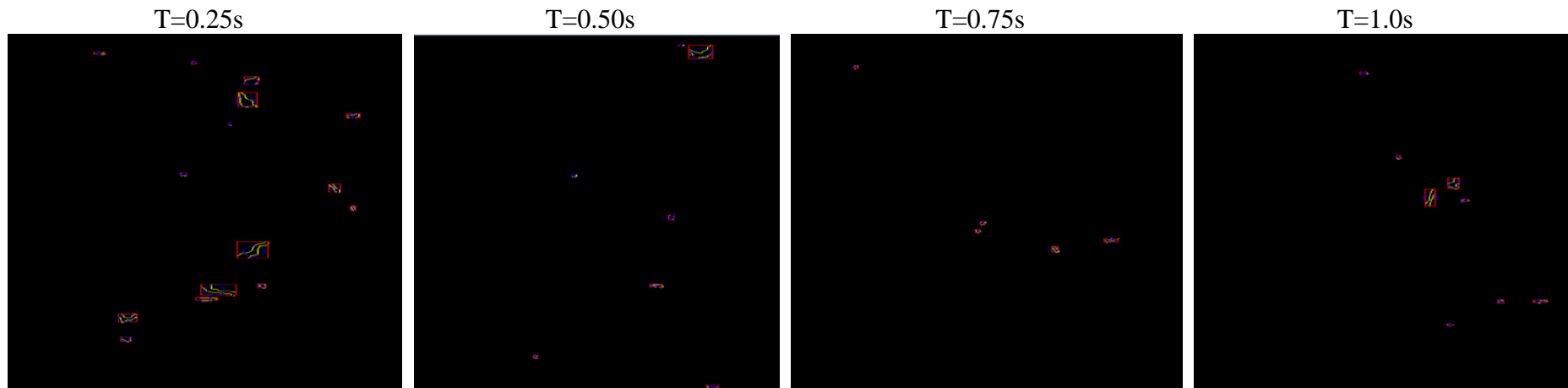
D22: Processed Images of CO₂ Bubbles in Sunflower Oil at 2.0mm Perforation diameter and 1.2bar Injection pressure



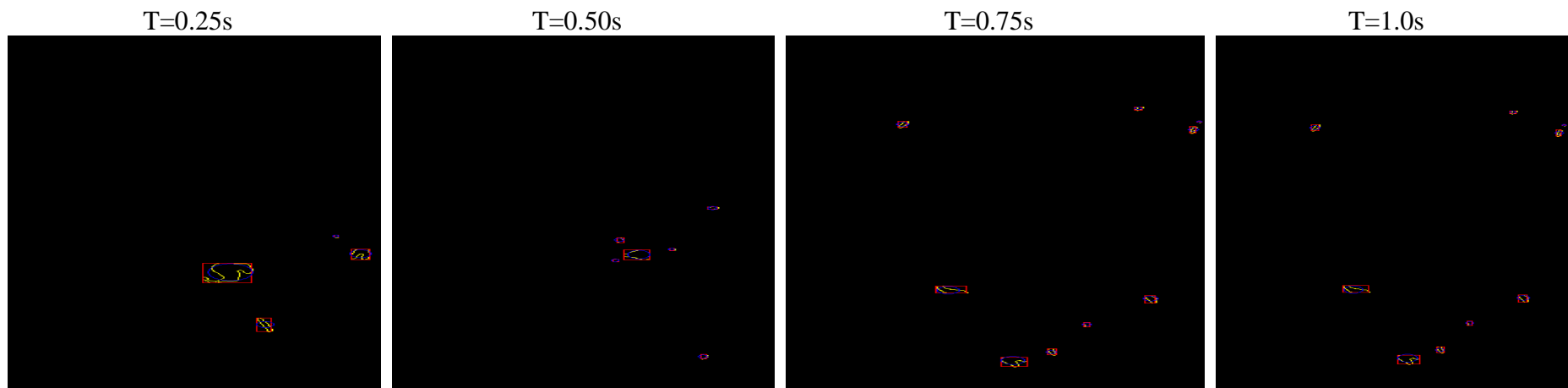
D23: Processed Images of CO₂ Bubbles in Sunflower Oil at 2.0mm Perforation diameter and 1.4bar Injection pressure



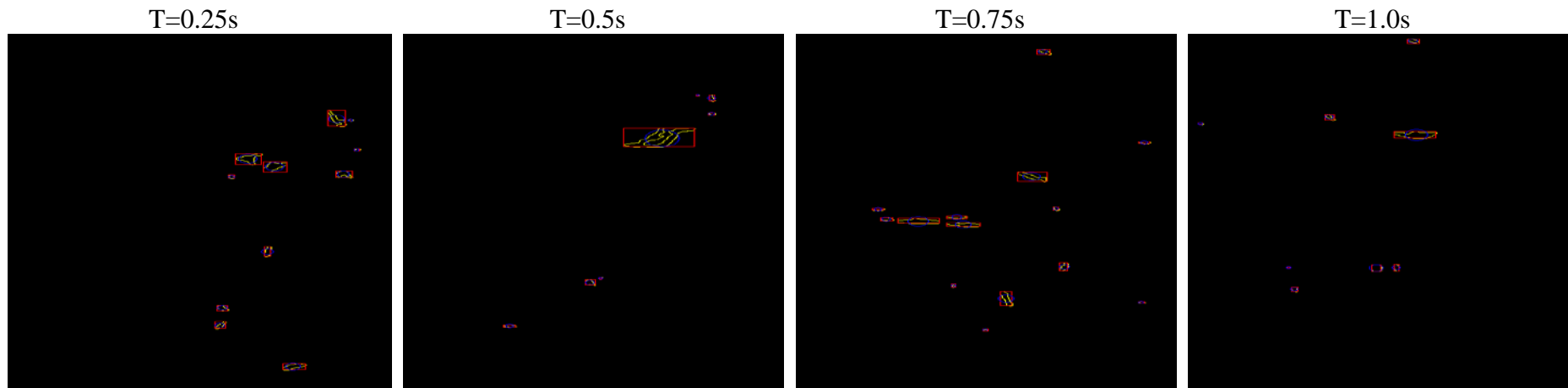
D24: Processed Images of CO₂ Bubbles in Sunflower Oil at 2.0mm Perforation diameter and 1.6bar Injection pressure



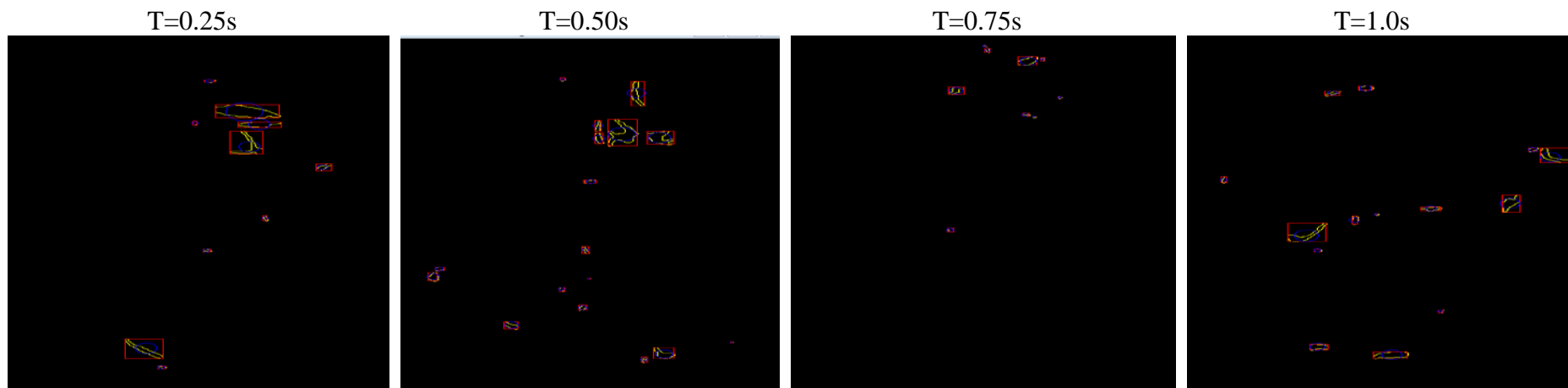
D25: Processed Images of CO₂ Bubbles in Sunflower Oil at 2.0mm Perforation diameter and 1.8bar Injection pressure



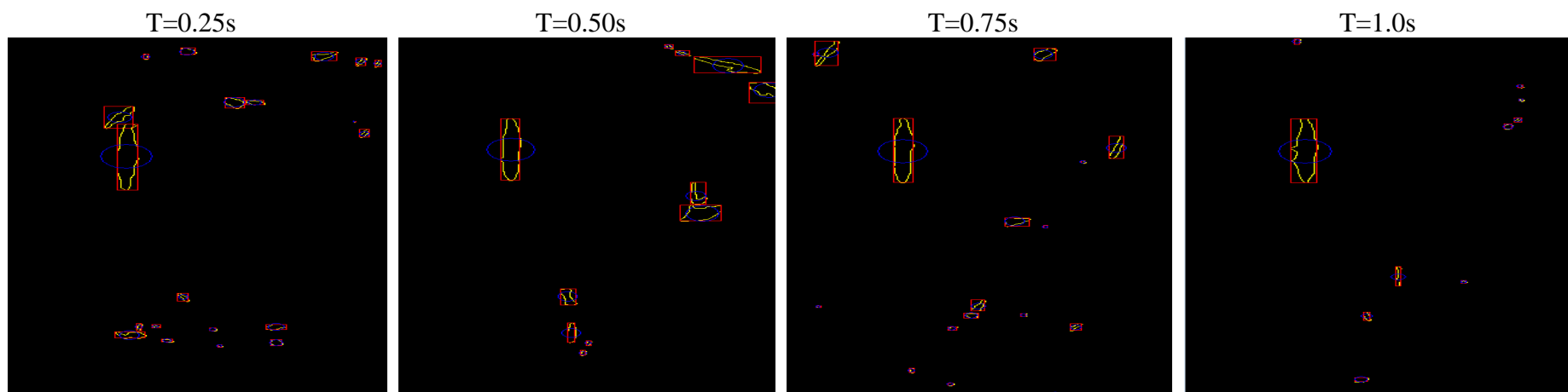
D26: Processed Images of CO₂ Bubbles in Sunflower Oil at 2.0mm Perforation diameter and 2.0bar Injection pressure



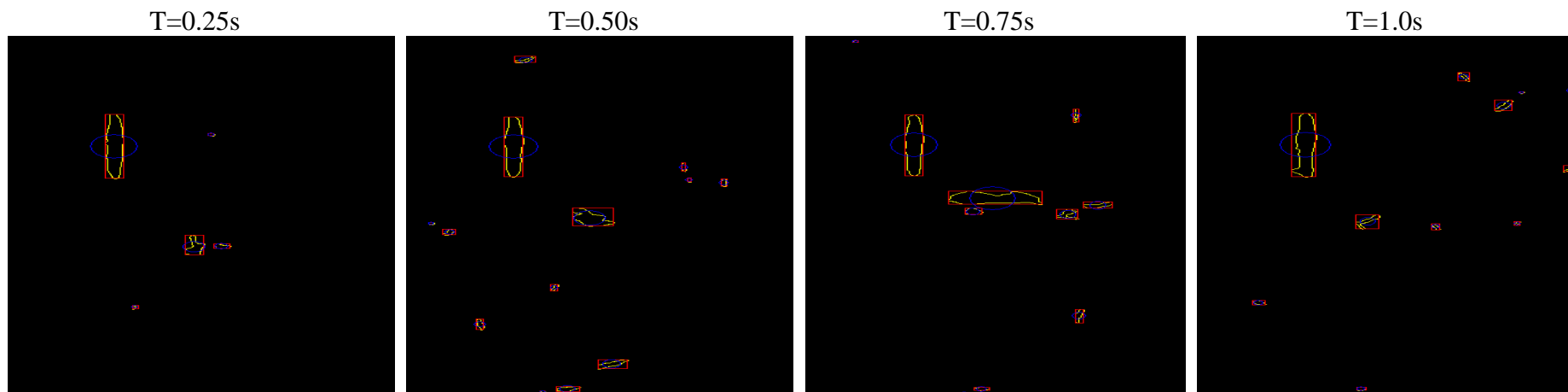
D27: Processed Images of CO₂ Bubbles in Sunflower Oil at 2.0mm Perforation diameter and 2.2bar Injection pressure



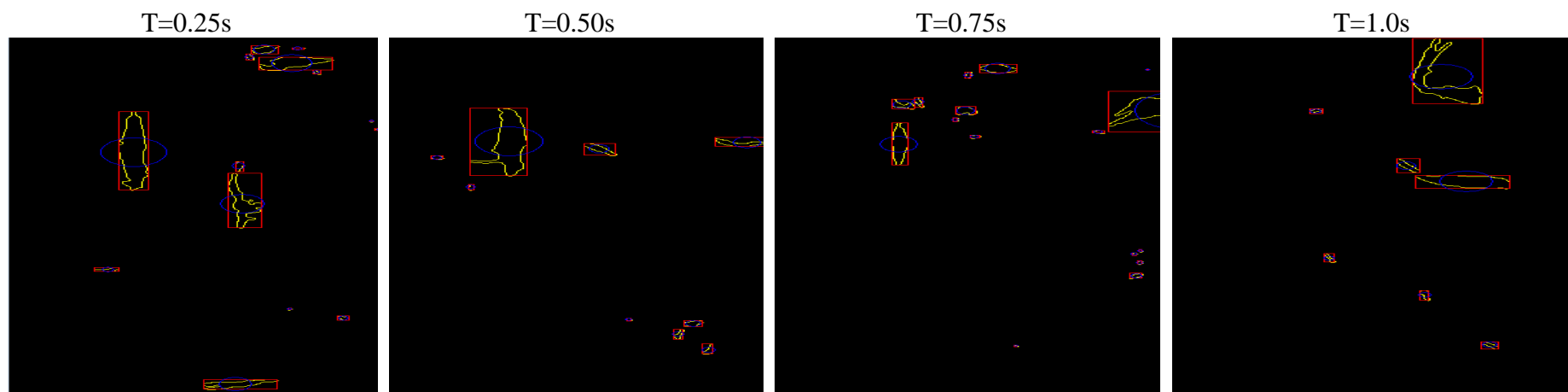
D28: Processed Images of CO₂ Bubbles in Sunflower Oil at 2.5mm Perforation diameter and 1.2bar Injection pressure



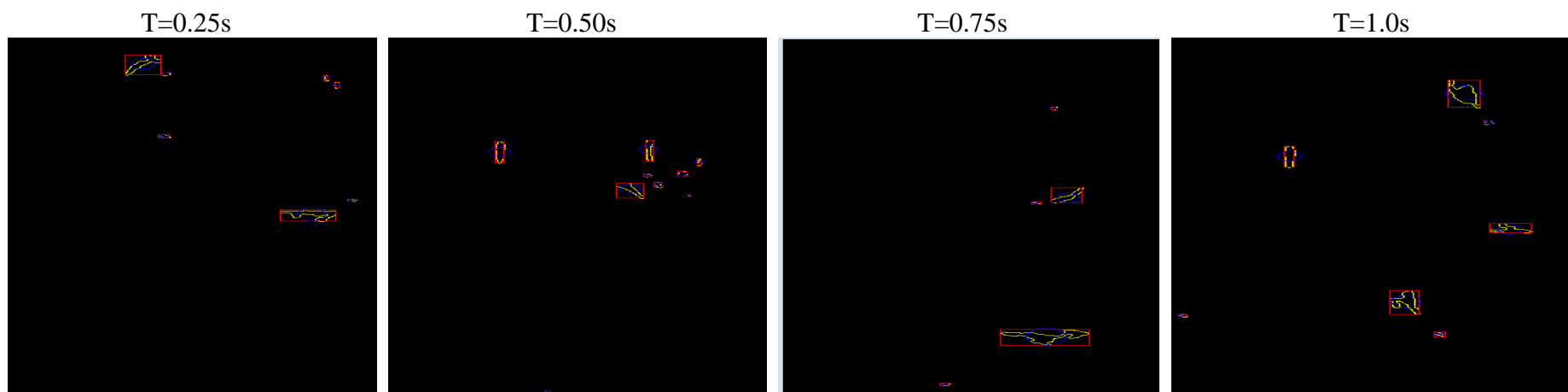
D29: Processed Images of CO₂ Bubbles in Sunflower Oil at 2.5mm Perforation diameter and 1.4bar Injection pressure



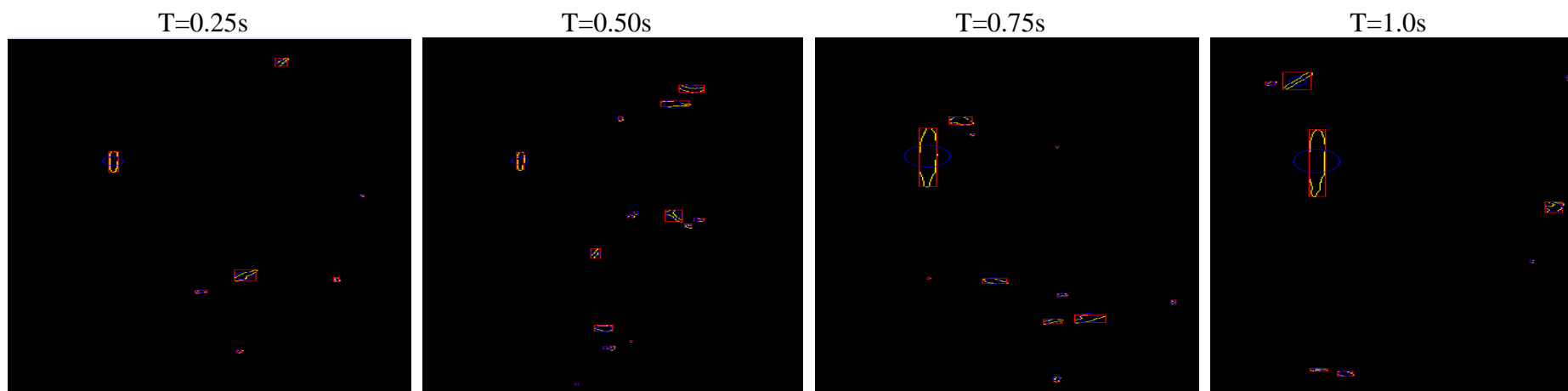
D30: Processed Images of CO₂ Bubbles in Sunflower Oil at 2.5mm Perforation diameter and 1.6bar Injection pressure



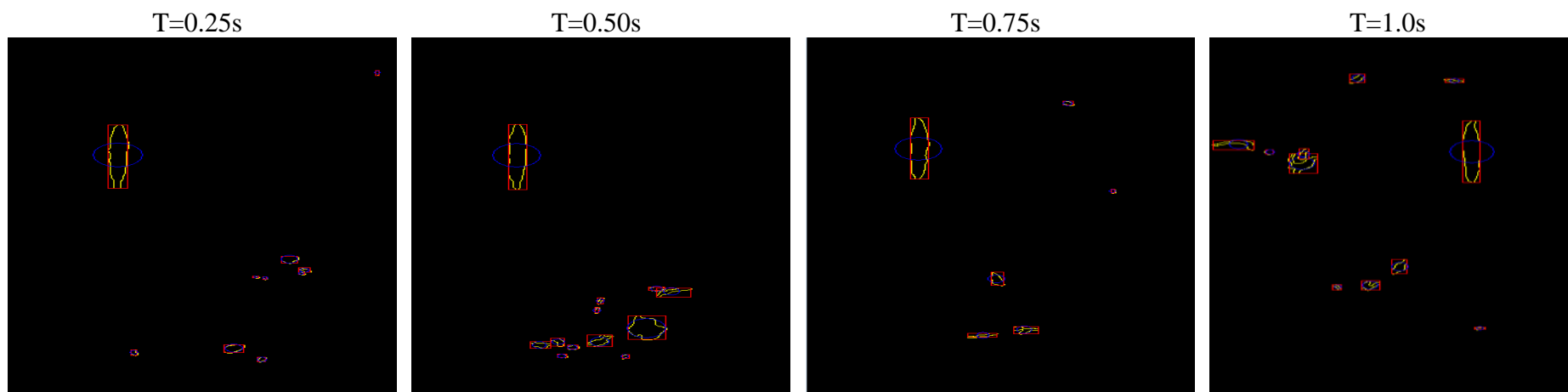
D31: Processed Images of CO₂ Bubbles in Sunflower Oil at 2.5mm Perforation diameter and 1.8bar Injection pressure



D32: Processed Images of CO₂ Bubbles in Sunflower Oil at 2.5mm Perforation diameter and 2.0bar Injection pressure

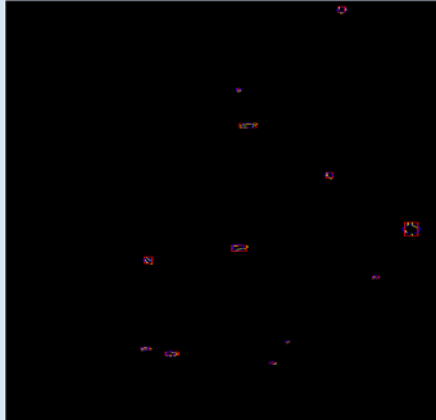


D33: Processed Images of CO₂ Bubbles in Sunflower Oil at 2.5mm Perforation diameter and 2.2bar Injection pressure

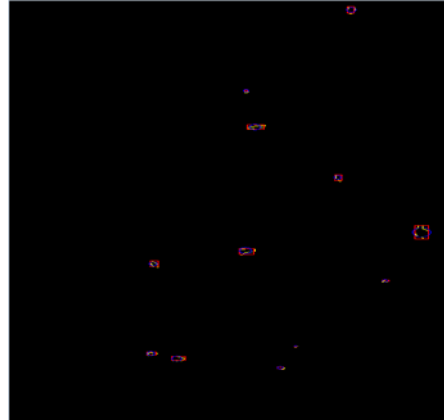


D34: Processed Images of CO₂ Bubbles in Sunflower Oil at 3.0mm Perforation diameter and 1.2bar Injection pressure

T=0.25s



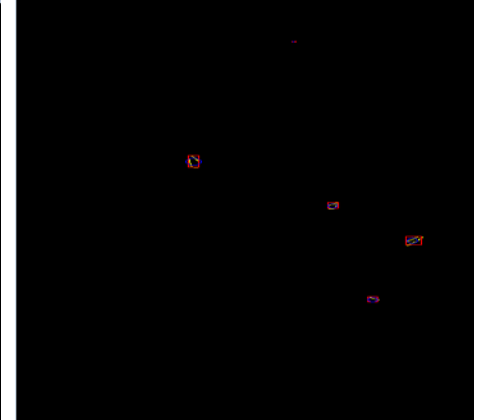
T=0.50s



T=0.75s

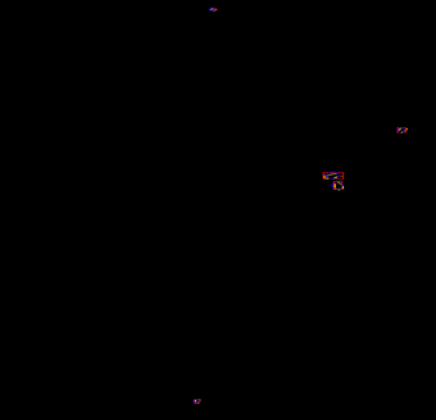


T=1.0s

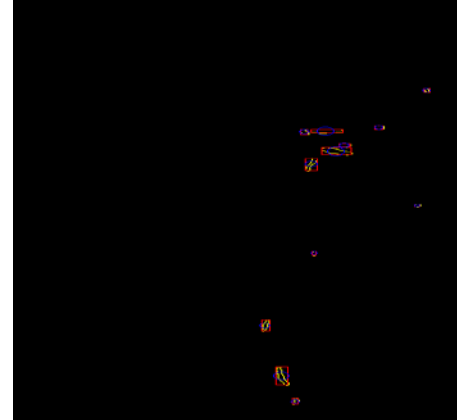


D35: Processed Images of CO₂ Bubbles in Sunflower Oil at 3.0mm Perforation diameter and 1.4bar Injection pressure

T=0.25s



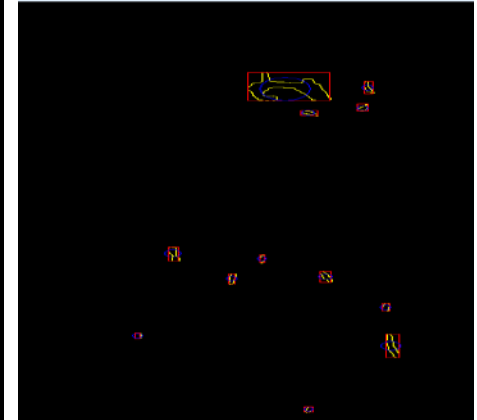
T=0.5s



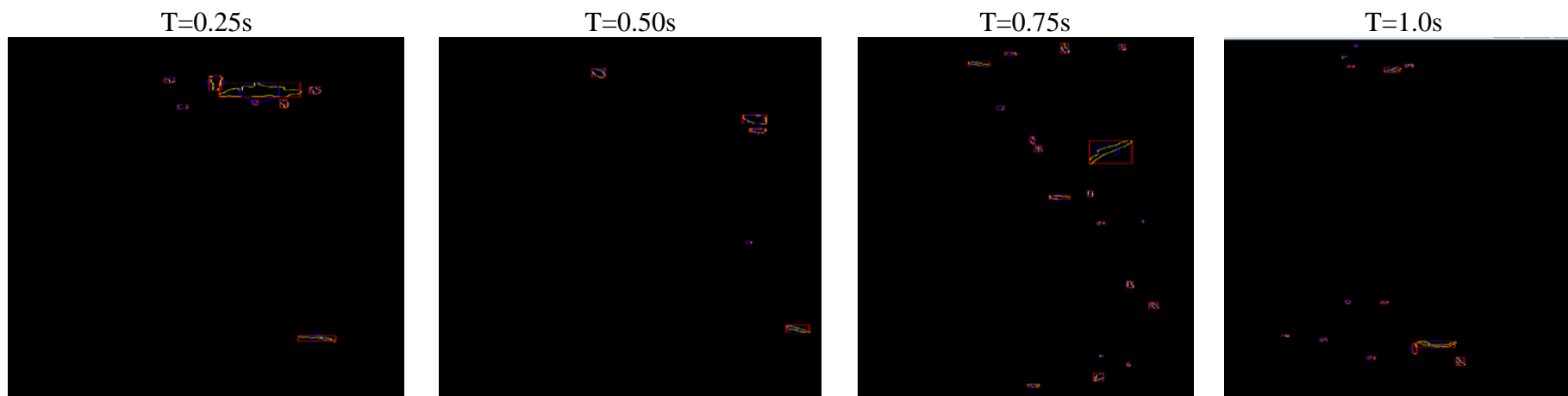
T=0.75s



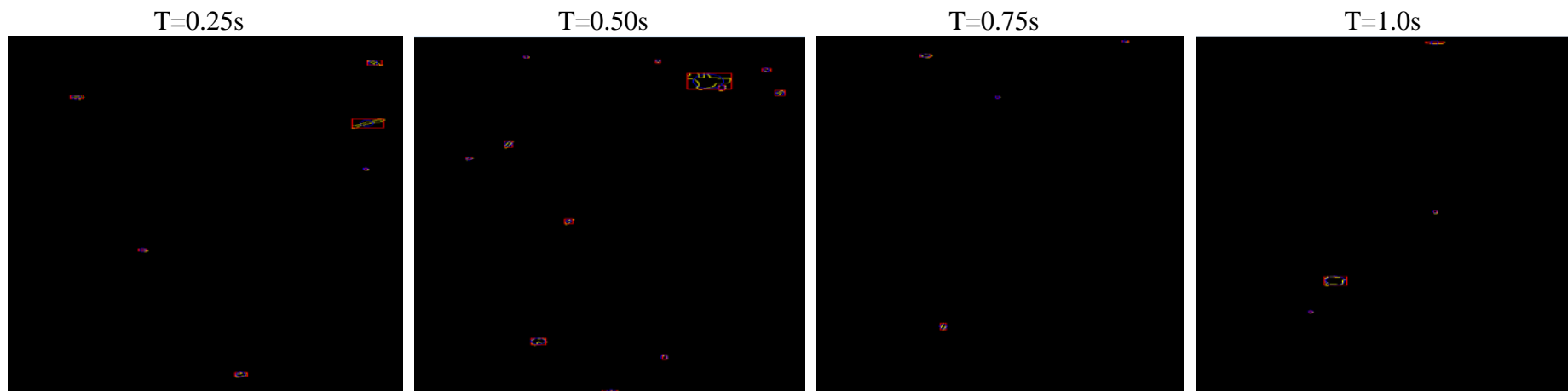
T=1.0s



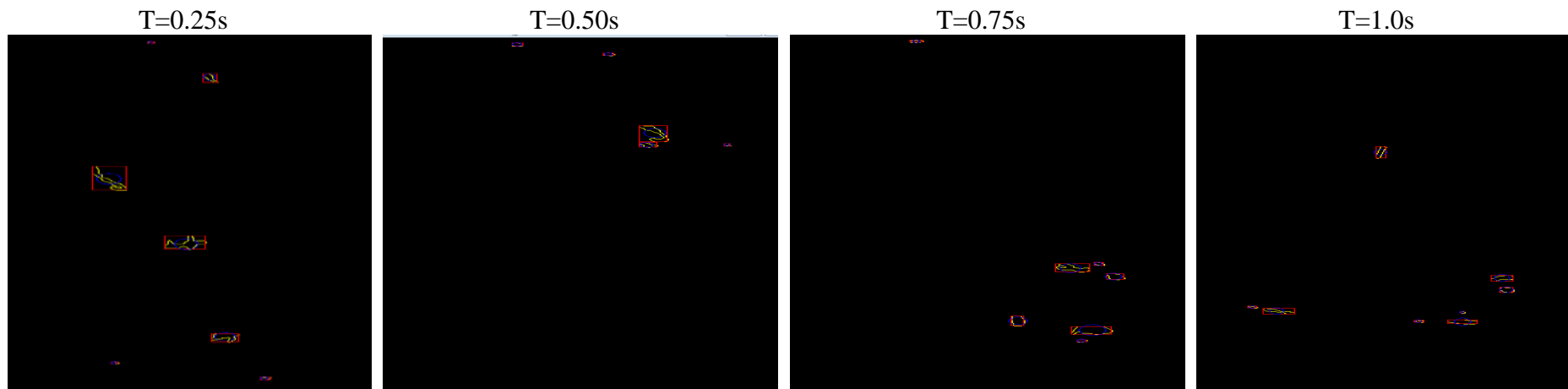
D36: Processed Images of CO₂ Bubbles in Sunflower Oil at 3.0mm Perforation diameter and 1.6 bar Injection pressure



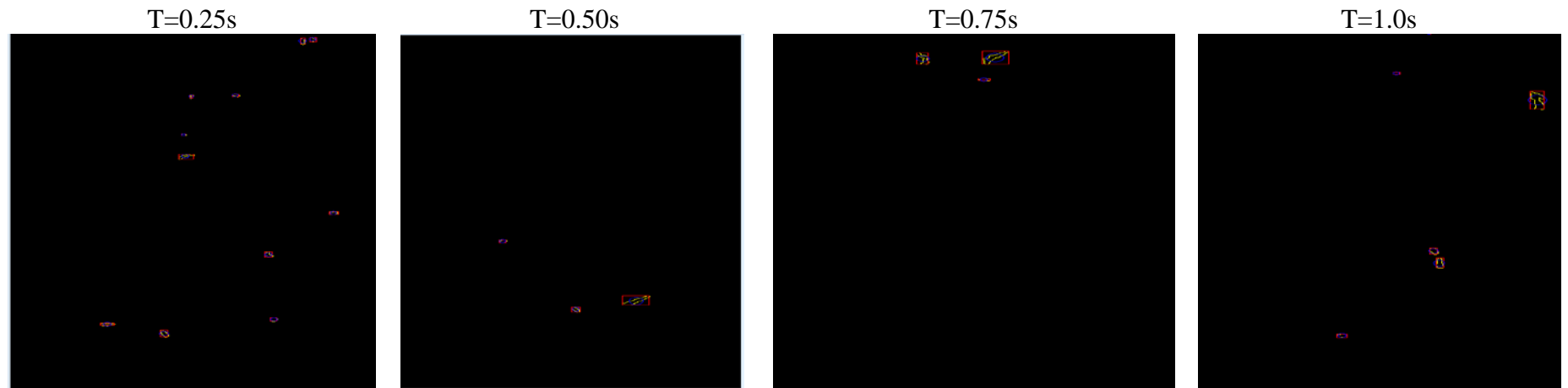
D37: Processed Images of CO₂ Bubbles in Sunflower Oil at 3.0mm Perforation diameter and 1.8 bar Injection pressure



D38: Processed Images of CO₂ Bubbles in Sunflower Oil at 3.0mm Perforation diameter and 2.0 bar Injection pressure



D39: Processed Images of CO₂ Bubbles in Sunflower Oil at 3.0mm Perforation diameter and 2.2 bar Injection pressure



Appendix E: Image Processing Process

User Interface

Select the two target images as shown in Figure 1 highlight calibration image. Do a right click and select “analyse” or from the toolbar press the “analyse” icon.

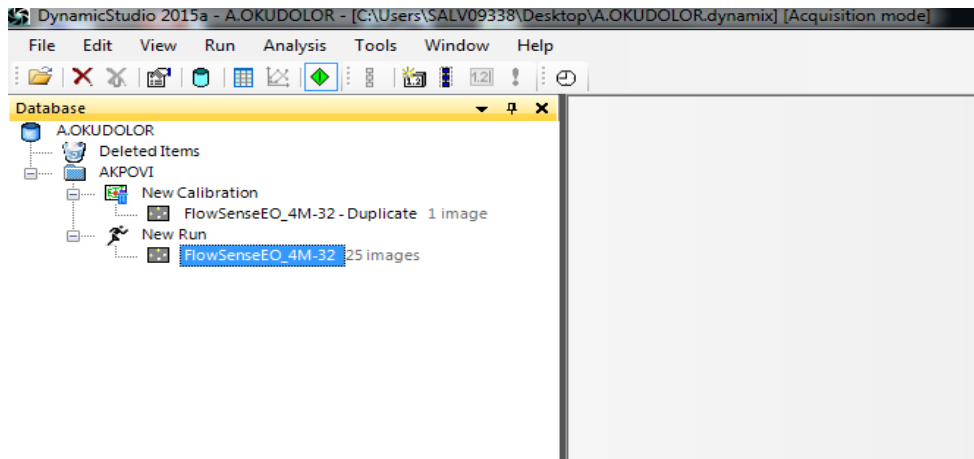


Figure 1: Screenshot for user interface window .



Analysis Method

The following dialogue box opens. Select “particle characterisation” as the method and highlight IPI processing as shown in Figure 2

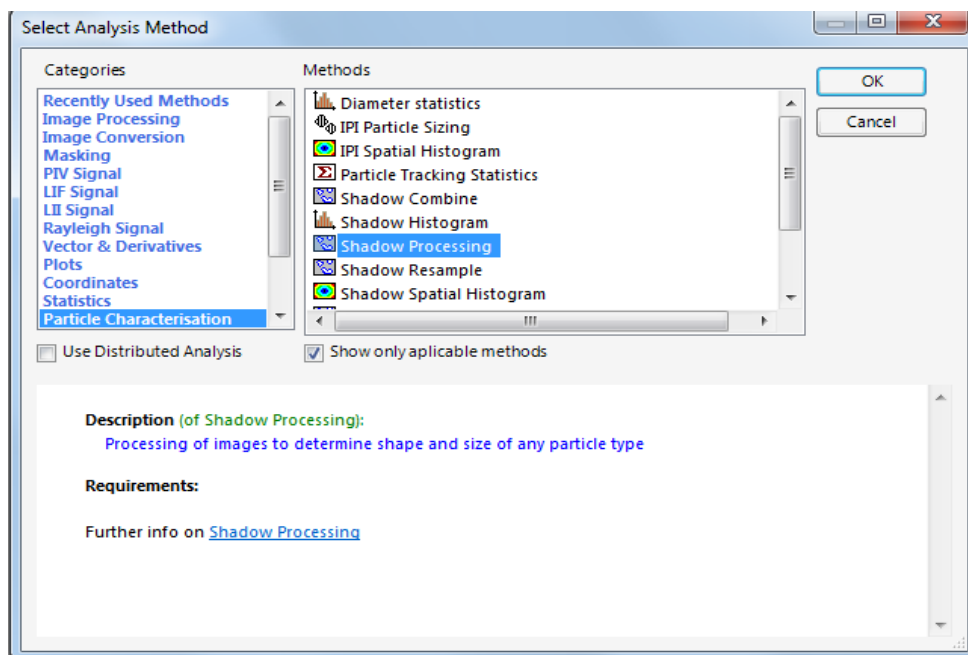


Figure 2: Screenshot of analysis method

(a) Calibration



Calibration Image

Acquire a set of images (see the black arrow and Figure 3) from the camera and save the images as calibration image. Highlight the calibration image, do a right mouse click and select “calibrate”.

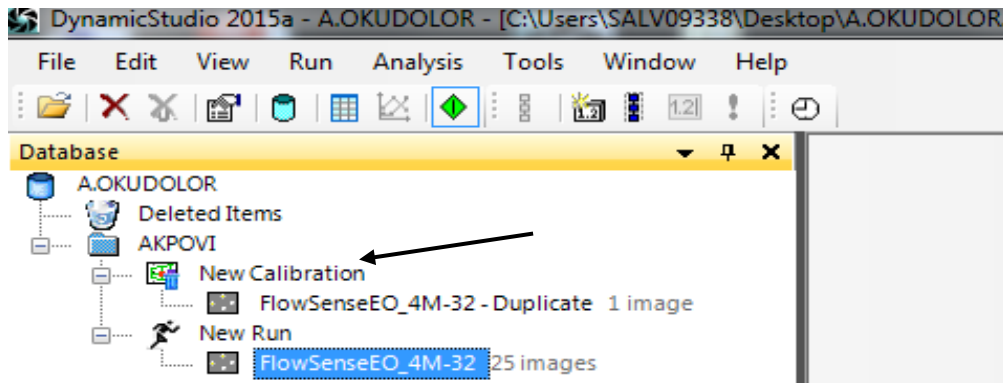


Figure 3: Screenshot for calibration



Calibration Method

From the calibration window shown in Figure 4, select calibrations under the categories and highlight “Image Model Fit” under methods.

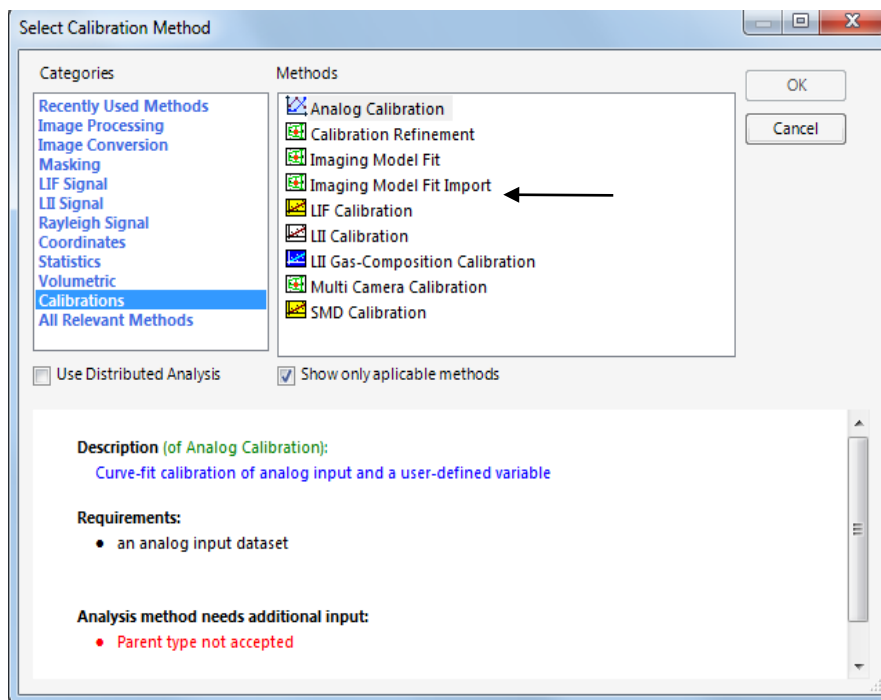


Figure 4: Screenshot for calibration method.

Image Model Fit

The Imaging Model Fit is a mathematical model that describes how points in object space (millimetre coordinates) is transported to the image plane (pixel coordinates). The purpose of the Imaging Model Fit is to enable measurements in real-world metrics such as millimetre in the object space by pixel coordinates in acquired images. Hence, an Imaging Model Fit is a required input to the following numerical methods: Stereo PIV vector processing, Image Dewarping, Vector Dewarping, and IPI particle Sizing. The procedures for Image model fit is detailed in the dynamic studio user manual.

(b) IPI Particle Sizing

General Settings

Under 'select image order' shown in Figure 5, select the image that represents the defocused camera and input values for the minimum and maximum size of the defocused image. The selected values must match closely with those observed in the actual model. The step size controls the integration frequency of the iterative process. The size of Fourier filters (FFT) to be used must be larger than the maximum circle size.

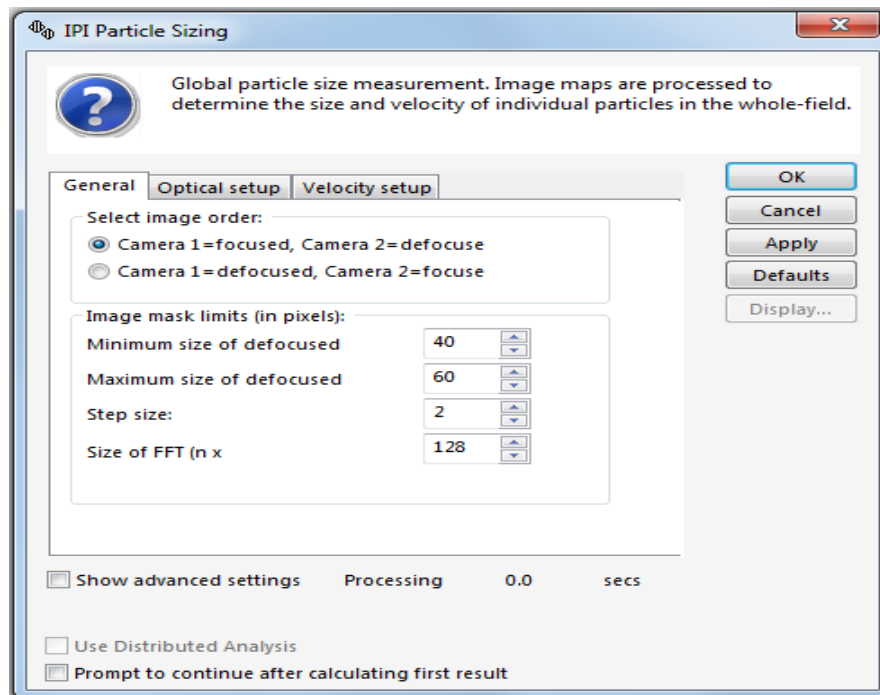


Figure 5: Screenshot for IPI processing general setup

Optical Setup

Enter the optical parameters that best reflect the actual setup as shown in Figure 5. The scattering angle is usually left at 90 degrees to avoid the effects of image warping. The aperture diameter is focal length divided by the aperture. Figure

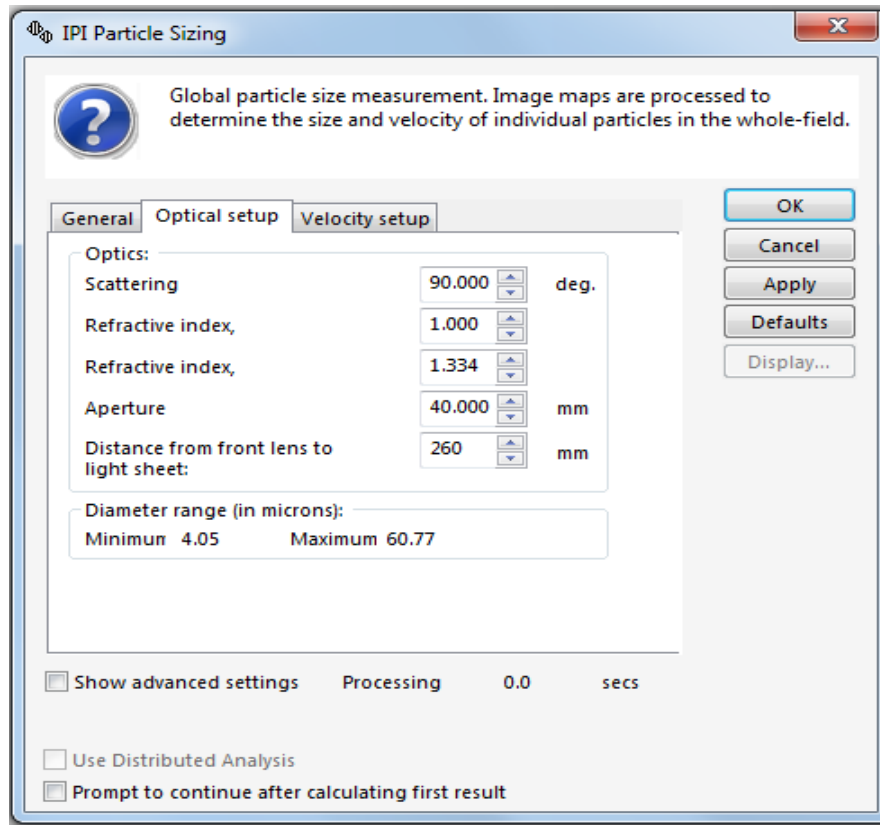


Figure 6: Screenshot for Optical Setup

(c) Advance Settings

To perform the advanced settings, click on the 'show advanced settings' checkbox at the bottom of the dialogue box shown in Figure 6. The setting allows the user to perform further operations such as a Region of Interest, Laser or Lighting setup, Window Setup and Filter.

Region of Interest (ROI)

In this measurement, it is only required to process a portion of the measured area. The area of interest was limited by entering the dimensions or selecting one of the pre-defined areas. Figure 7 illustrates how the ROI is performed.

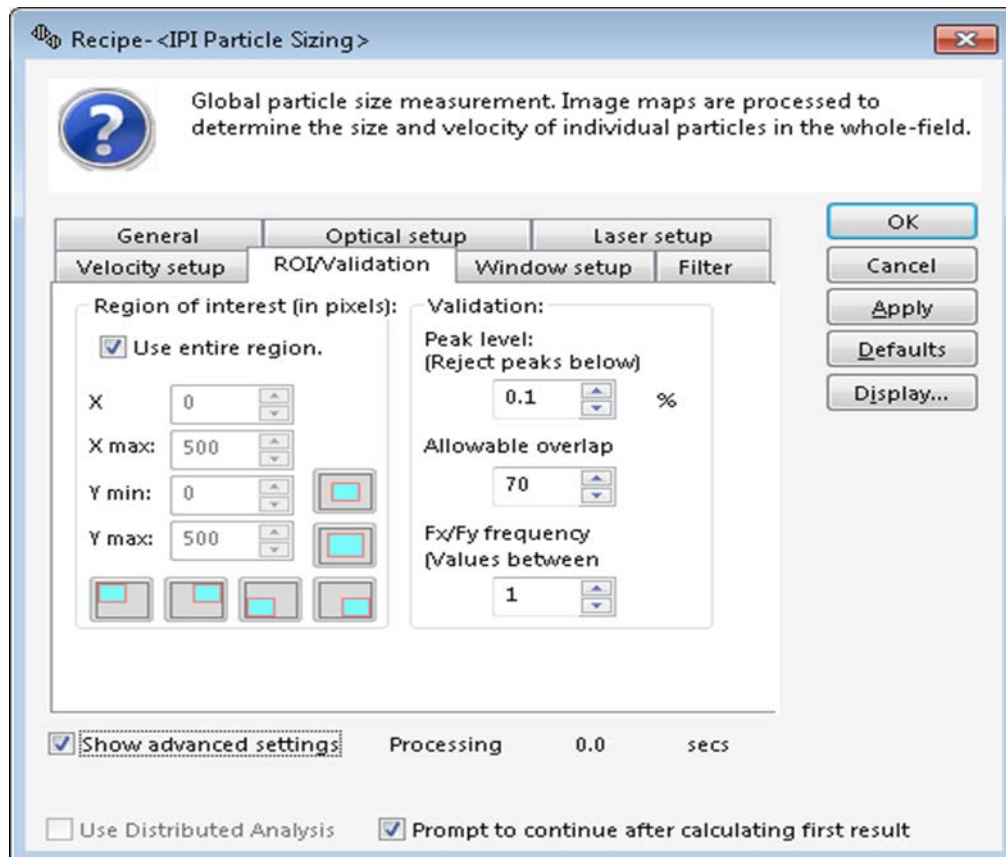


Figure 8: Screenshot for region of interest

The peak level validation rejects particles based on the percentage peak height of the maximum peak determined. The overlap will reject particles with too little useable area. Setting a value of 70% would mean that any particle with more than 70% of its area overlapped would not be accepted. The frequency ratio in the x- and y-direction is another validation tool. Fringes in the x-direction will show small frequency peaks in the y-direction, and therefore a high fringe ratio. Images without fringe information usually exhibit poor fringe ratios.

Window Setup

The processing of the defocused image yields the fringe frequency, which in turn yields the particle diameter. Information about the frequency is determined by applying a 2D filter over the selected area and identifying the dominant frequency peaks. It is often useful to apply a filter over the input data before processing to smoothen the peaks. The built-in window is a familiar type known in signal processing as a Hanning Window. While this window has a precise definition and fixed parameters, a strength factor has been built-in that affects the quality of the output data.

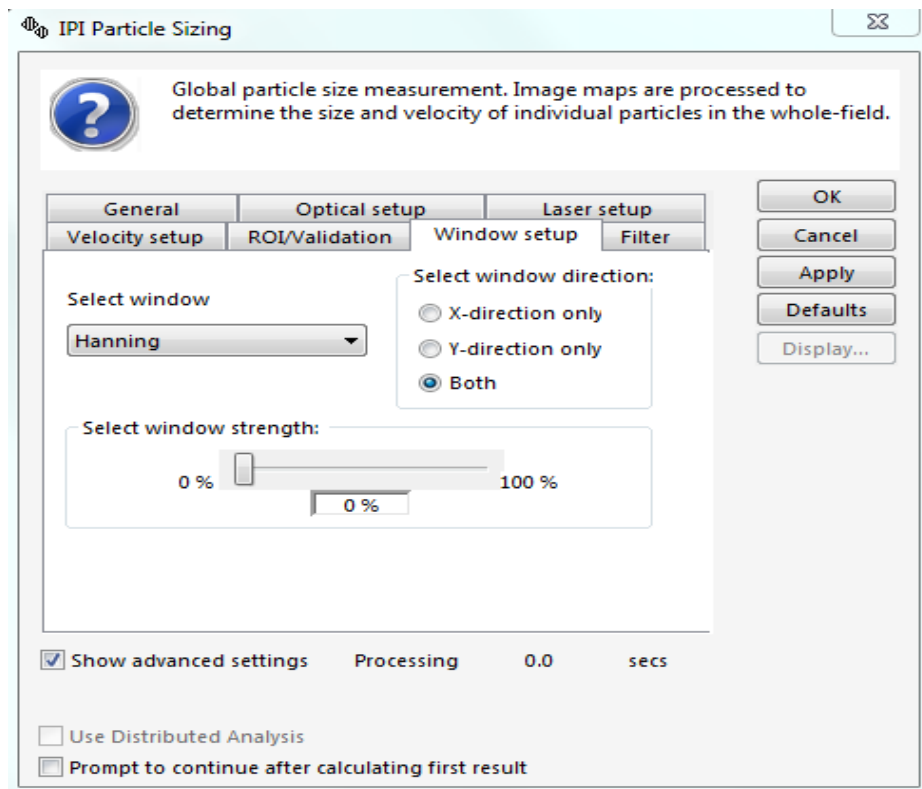


Figure9: Screenshot for window setup

Also, the window can be applied horizontally, vertically or in both directions. Since fringes are oriented according to the optical configuration, it is advantageous to apply the window in the direction perpendicular to the orientation of the fringes. In Figure 9 however, both directions were specified since the intent of the study is to analyse the CO₂ bubbles in both directions.

Filter

In high concentration particle flows, the number of particles can be so high as to reduce the overall validation just because the overlap is too substantial. The solution to this is to artificially reduce the detection such that particle neighbours within a user-specified bound are not accepted. By default, the filter is disabled. Figure 10 shows the screenshot for the input parameters of the filter.

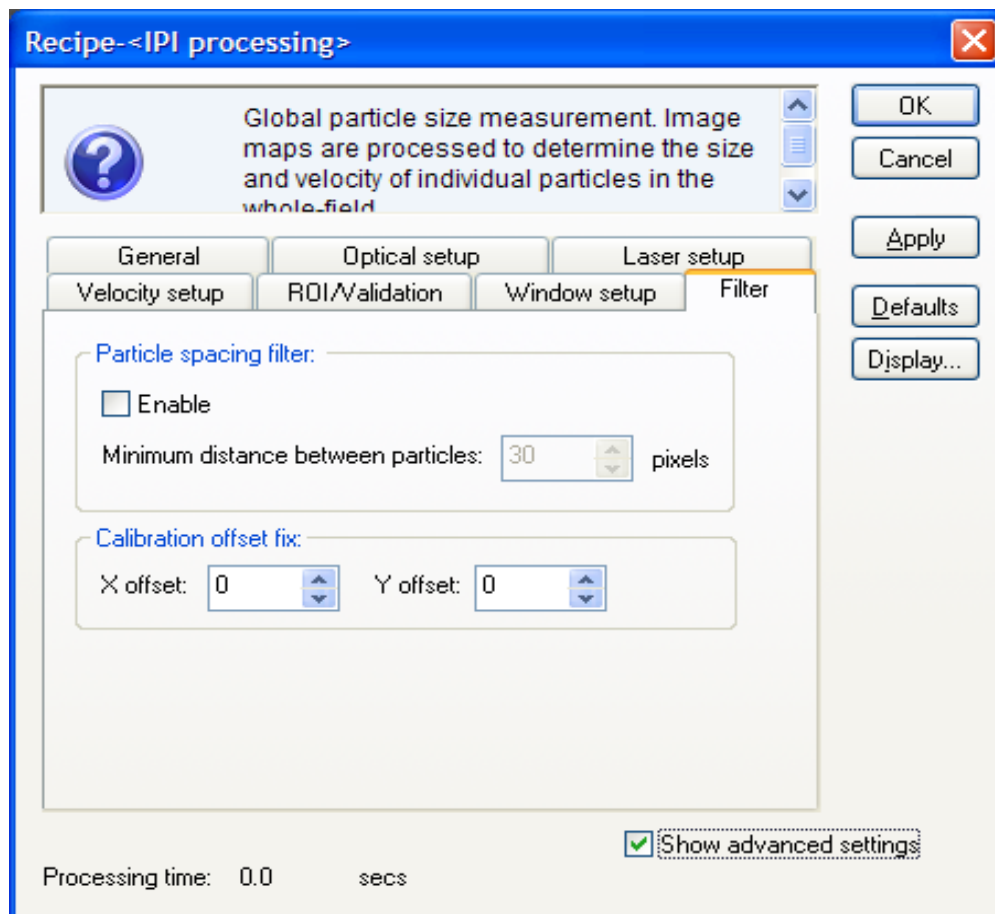


Figure10: Screenshot for filter

Lighting Setup

Led lightings are also used to set the validation criteria. The position of the origin of incident light plays a role in how the fringes are rotated as a function of particle position in the image. The position of the light source is measured from the front of the light sheet optics to the front lens on the camera. Figure 11 shows the input parameters applied for the light setup.

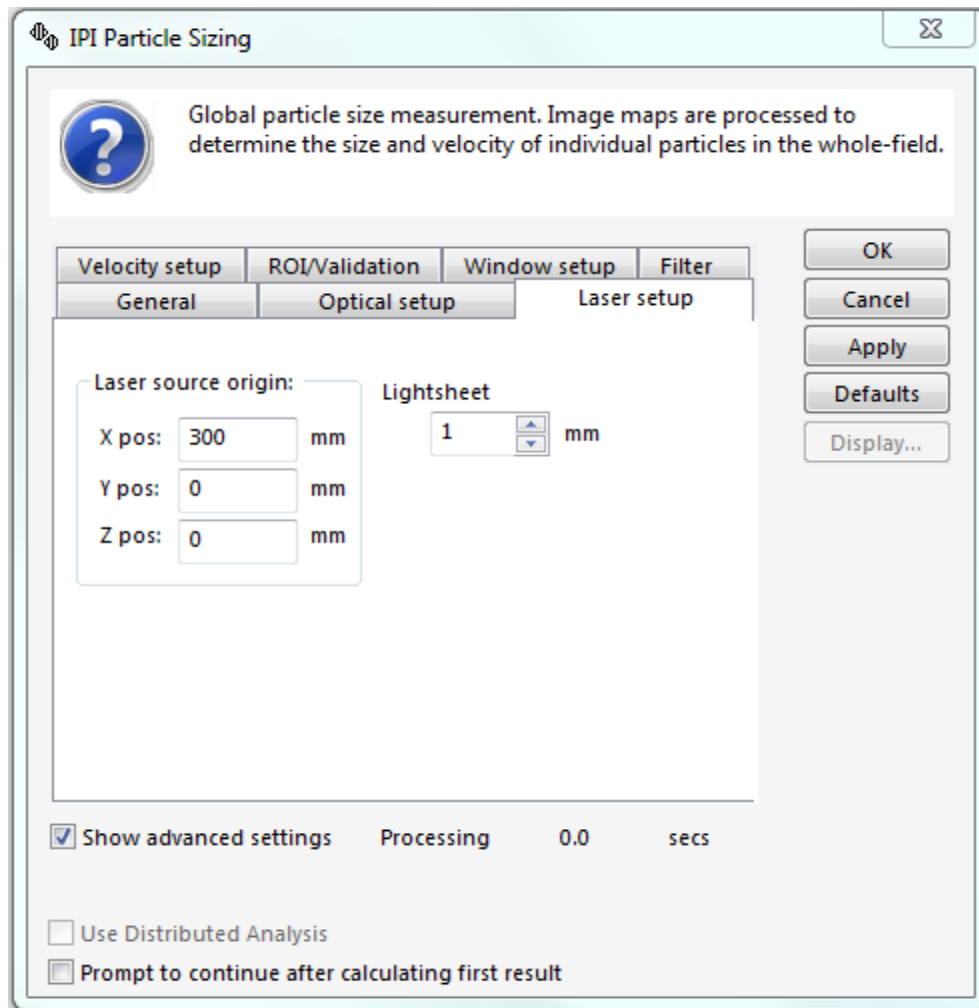
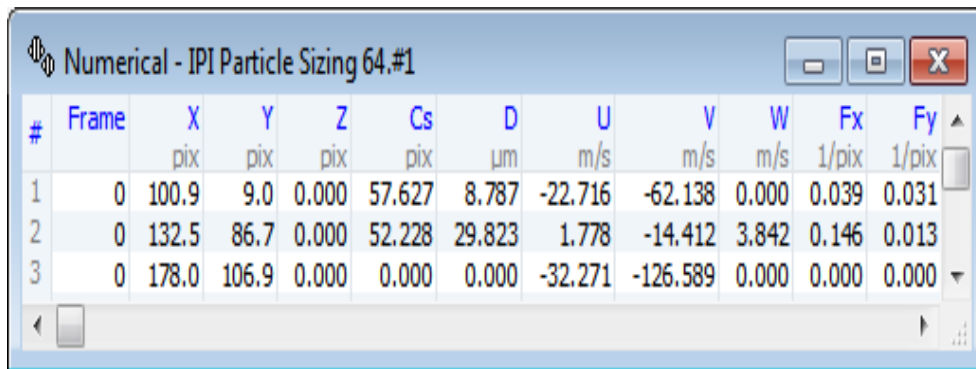


Figure11: Screenshot of Led Setup

(d) Processing and Presentation

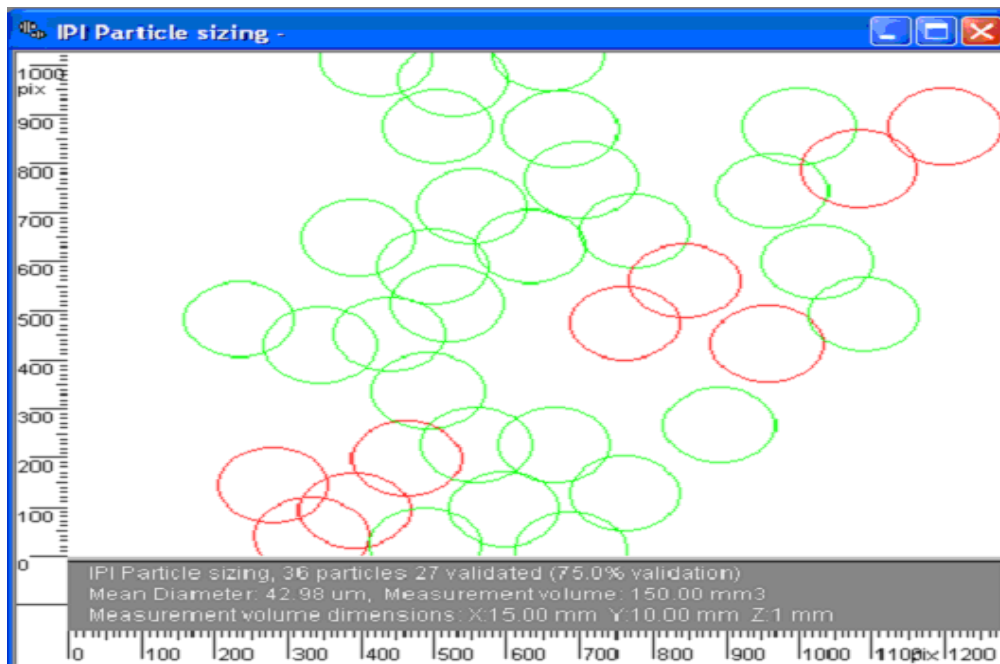
Once the “apply” command shown in Figure 11 is given, the IPI processing will execute, adding an IPI record beneath the selected image datasets. The resulting data can be displayed in tabular form by clicking on the spreadsheet icon in the toolbar, or in graphical form by double-clicking the mouse directly on the IPI record. Figure 12 and 13 a sample of the numerical and graphical presentation of the IPI dataset



The screenshot shows a window titled "Numerical - IPI Particle Sizing 64.#1". It contains a table with 12 columns: #, Frame, X (pix), Y (pix), Z (pix), Cs (pix), D (μm), U (m/s), V (m/s), W (m/s), Fx (1/pix), and Fy (1/pix). The table lists three particles (rows 1, 2, and 3) with their respective coordinates and physical properties.

#	Frame	X pix	Y pix	Z pix	Cs pix	D μm	U m/s	V m/s	W m/s	Fx 1/pix	Fy 1/pix
1	0	100.9	9.0	0.000	57.627	8.787	-22.716	-62.138	0.000	0.039	0.031
2	0	132.5	86.7	0.000	52.228	29.823	1.778	-14.412	3.842	0.146	0.013
3	0	178.0	106.9	0.000	0.000	0.000	-32.271	-126.589	0.000	0.000	0.000

Figure 12 : Numerical presentation of IPI data set



(b)

Figure 13: Graphical presentation of IPI data

(e) Post Processing

Once the IPI datasets are processed, the user can apply the following post-processing procedures. To process a series of datasets, select the IPI datasets to be included in the histogram. In this case, particle characterisation and diameter statistics were selected as shown in Figure Then, right-click the mouse over diameter statistics and select “analysis”.

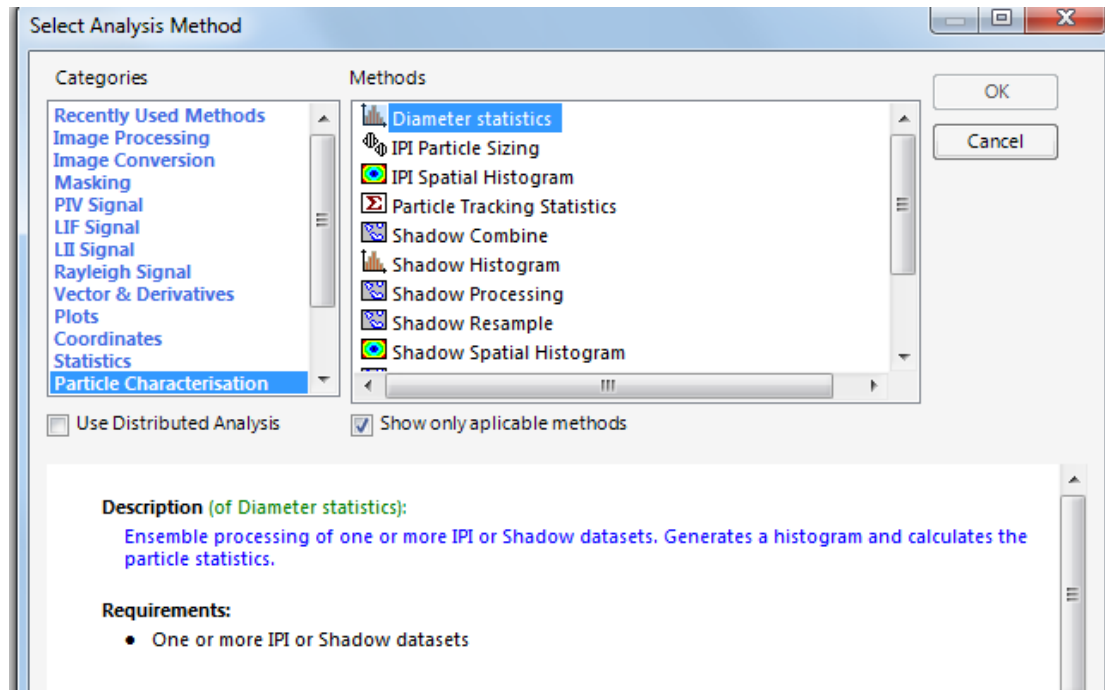


Figure 14: Screenshot for diameter histogram

The CO₂ bubble size distribution in the Sunflower solution was determined to analyse the diameter statistics. To generate the diameter histogram, the input parameter shown in Figure 15 was applied. Figure 16 shows a sample of the diameter histogram generated. The IPI dataset was processed further with the shadow size processing tool. The aim is to generate the graphical representation of the bubbles. The steps taken to conduct the shadow sizer process is detailed in the Dynamic studio manual.

Recipe - <Diameter statistics>

Ensemble processing of one or more IPI or Shadow datasets.
Generates a histogram and calculates the particle statistics.

Histogram setup:

Minimum sort: um

Maximum sort: um

Number of:

Process:

☒ Image A

☐ Image B

☐ Both

Region:

☒ Use entire area

Xmin:

Xmax:

Ymin:

Ymax:

OK
Cancel
Apply
Defaults
Display...

Figure 15: Diameter Statistics Input Window

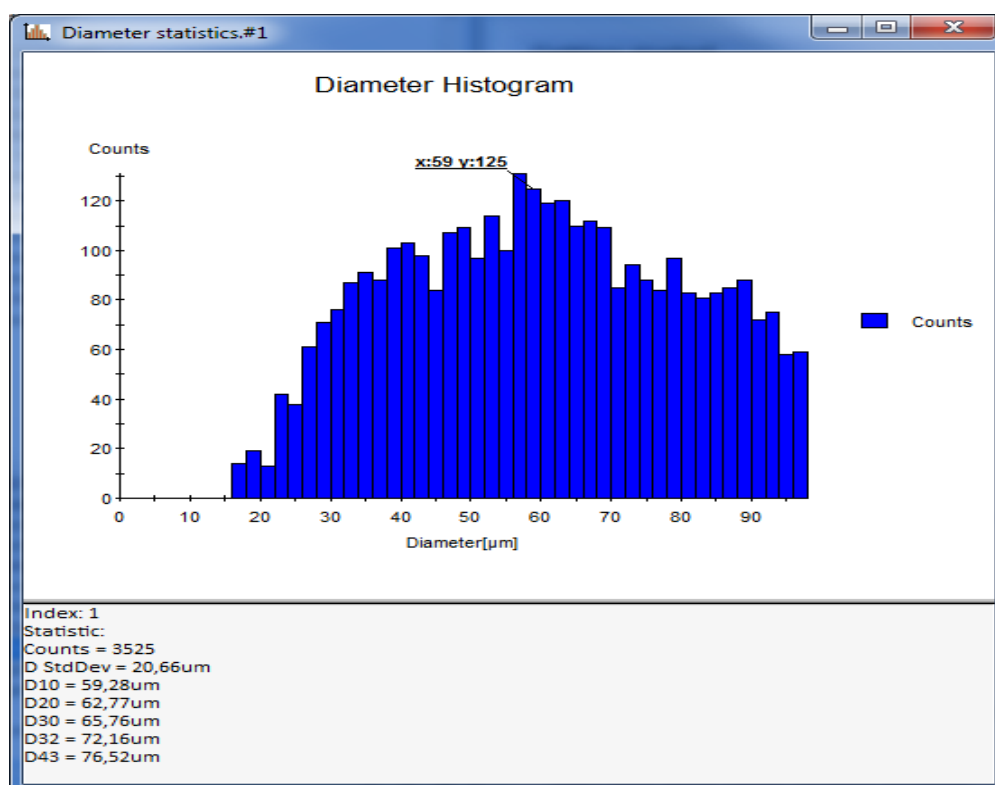


Figure 16: Diameter Histogram

Appendix F: Core Flooding Test Heterogeneous Model

F1: Data for Core flooding Test 1

Injection Pressure = 1bar Mass of Oil sat. sample = 24.75g Mass of Oil in sample = 3.050g
 Perforation Diameter = 0.5mm Mass of Dry Sample = 21.70g

Injection Time	Mass of Flooded Sample	Mass of Saturated Sample	Mass of Oil Produced	Volume of Oil Produced	%OOIP of Oil produced
Min	M2(g)	M1(g)	M3(g)	V3(cc)	%
1	24.41	24.75	0.34	0.366	0.12
2	24.31	24.75	0.44	0.473	0.16
3	24.12	24.75	0.63	0.677	0.22
4	24.12	24.75	0.63	0.677	0.22
5	24.12	24.75	0.63	0.677	0.22
6	24.12	24.75	0.63	0.677	0.22
7	24.07	24.75	0.63	0.677	0.22
8	24.07	24.75	0.63	0.677	0.22
9	24.05	24.75	0.7	0.753	0.25
10	24.00	24.75	0.75	0.806	0.26
11	23.99	24.75	0.76	0.817	0.27
12	23.97	24.75	0.78	0.839	0.27
13	23.92	24.75	0.83	0.892	0.29
14	23.79	24.75	0.96	1.032	0.34
15	23.79	24.75	0.96	1.032	0.34
16	23.74	24.75	1.01	1.086	0.36
17	23.73	24.75	1.02	1.097	0.36
18	23.71	24.75	1.04	1.118	0.37
19	23.71	24.75	1.04	1.118	0.37
20	23.71	24.75	1.04	1.118	0.37
21	23.71	24.75	1.04	1.118	0.37

F2: Data for Core flooding Test 2

Injection Pressure = 2bar Mass of Oil sat. sample = 24.69g Mass of Oil in sample = 2.99g
 Perforation Diameter = 0.5mm Mass of Dry Sample = 21.70g

Injection Time	Mass of Flooded Sample	Mass of Saturated Sample	Mass of Oil Produced	Volume of Oil Produced	%OOIP of Oil produced
Min	M2(g)	M1(g)	M3(g)	V3(cc)	%
1	24.11	24.69	0.58	0.624	0.21
2	23.82	24.69	0.87	0.935	0.31
3	23.8	24.69	0.89	0.957	0.32
4	23.64	24.69	1.05	1.129	0.38
5	23.59	24.69	1.10	1.183	0.40
6	23.56	24.69	1.13	1.215	0.41
7	23.52	24.69	1.17	1.258	0.42
8	23.52	24.69	1.17	1.258	0.42
9	23.52	24.69	1.17	1.258	0.42
10	23.49	24.69	1.20	1.290	0.43
11	23.49	24.69	1.20	1.290	0.43
12	23.44	24.69	1.25	1.344	0.45
13	23.44	24.69	1.25	1.344	0.45
14	23.43	24.69	1.26	1.355	0.45
15	23.42	24.69	1.27	1.366	0.46
16	23.39	24.69	1.30	1.398	0.47
17	23.34	24.69	1.35	1.452	0.49
18	23.34	24.69	1.35	1.452	0.49
19	23.34	24.69	1.35	1.452	0.49
20	23.33	24.69	1.36	1.462	0.49
21	23.33	24.69	1.36	1.462	0.49

F3: Data for Core flooding Test 3

Injection Pressure = 3bar Mass of Oil sat. sample = 24.66g Mass of Oil in sample = 2.96g
 Perforation Diameter = 0.5mm Mass of Dry Sample = 21.70g

Injection Time	Mass of Flooded Sample	Mass of Saturated Sample	Mass of Oil Produced	Volume of Oil Produced	%OOIP of Oil produced
Min	M2(g)	M1(g)	M3(g)	V3(cc)	%
1	23.99	24.66	0.67	0.7204	0.23
2	23.79	24.66	0.87	0.9355	0.29
3	23.70	24.66	0.96	1.0323	0.32
4	23.61	24.66	1.05	1.1290	0.35
5	23.52	24.66	1.14	1.2258	0.39
6	23.49	24.66	1.17	1.2581	0.40
7	23.43	24.66	1.23	1.3226	0.42
8	23.39	24.66	1.27	1.3656	0.43
9	23.39	24.66	1.27	1.3656	0.43
10	23.36	24.66	1.30	1.3978	0.44
11	23.32	24.66	1.34	1.4409	0.45
12	23.30	24.66	1.36	1.4624	0.46
13	23.30	24.66	1.36	1.4624	0.46
14	23.27	24.66	1.39	1.4946	0.47
15	23.26	24.66	1.40	1.5054	0.47
16	23.25	24.66	1.41	1.5161	0.48
17	23.24	24.66	1.42	1.5269	0.48
18	23.24	24.66	1.42	1.5269	0.48
20	23.24	24.66	1.42	1.5269	0.48
21	23.24	24.66	1.42	1.5269	0.48

F4: Data for Core flooding Test 4

Injection Pressure = 4bar Mass of Oil sat. sample = 24.63g Mass of Oil in sample = 2.93g
 Perforation Diameter =0.5mm Mass of Dry Sample = 21.70g

Injection Time	Mass of Flooded Sample	Mass of Saturated Sample	Mass of Oil Produced	Volume of Oil Produced	%OIP of Oil produced
Min	M2(g)	M1(g)	M3(g)	V3(cc)	%
1	23.92	24.63	0.71	0.763	0.24
2	23.72	24.63	0.91	0.978	0.31
3	23.70	24.63	0.93	1.000	0.32
4	23.55	24.63	1.08	1.161	0.37
5	23.51	24.63	1.12	1.204	0.38
6	23.45	24.63	1.18	1.269	0.40
7	23.39	24.63	1.24	1.333	0.42
8	23.35	24.63	1.28	1.376	0.44
9	23.33	24.63	1.30	1.398	0.44
10	23.32	24.63	1.31	1.409	0.45
11	23.31	24.63	1.32	1.419	0.45
12	23.26	24.63	1.37	1.473	0.47
13	23.24	24.63	1.39	1.495	0.47
14	23.23	24.63	1.40	1.505	0.48
15	23.22	24.63	1.41	1.516	0.48
16	23.21	24.63	1.42	1.527	0.48
17	23.20	24.63	1.43	1.538	0.49
18	23.20	24.63	1.43	1.538	0.49
19	23.18	24.63	1.45	1.559	0.49
20	23.16	24.63	1.47	1.581	0.50
21	23.14	24.63	1.49	1.602	0.51

F5: Data for Core flooding Test 5

Injection Pressure = 5bar Mass of Oil sat. sample = 24.60g Mass of Oil in sample = 2.9g
 Perforation Diameter =0.5mm Mass of Dry Sample = 21.70g

Injection Time	Mass of Flooded Sample	Mass of Saturated Sample	Mass of Oil Produced	Volume of Oil Produced	%OOIP of Oil produced
Min	M2(g)	M1(g)	M3(g)	V3(cc)	%
1	23.820	24.60	0.78	0.8387	0.27
2	23.660	24.60	0.94	1.0108	0.32
3	23.560	24.60	1.04	1.1183	0.36
4	23.500	24.60	1.10	1.1828	0.38
5	23.420	24.60	1.18	1.2688	0.41
6	23.390	24.60	1.21	1.3011	0.42
7	23.370	24.60	1.23	1.3226	0.42
8	23.340	24.60	1.26	1.3548	0.43
9	23.310	24.60	1.29	1.3871	0.44
10	23.290	24.60	1.31	1.4086	0.45
11	23.290	24.60	1.31	1.4086	0.45
12	23.270	24.60	1.33	1.4301	0.46
13	23.250	24.60	1.35	1.4516	0.47
14	23.240	24.60	1.36	1.4624	0.47
15	23.230	24.60	1.37	1.4731	0.47
16	23.230	24.60	1.37	1.4731	0.47
17	23.210	24.60	1.39	1.4946	0.48
18	23.190	24.60	1.41	1.5161	0.49
19	23.190	24.60	1.41	1.5161	0.49
20	23.170	24.60	1.43	1.5376	0.49
21	23.170	24.60	1.43	1.5376	0.49
22	23.170	24.60	1.43	1.5376	0.49
23	23.160	24.60	1.44	1.5484	0.50
24	23.160	24.60	1.44	1.5484	0.50

F6: Data for Core flooding Test 6

Perforation Diameter =0.5mm		Mass of Dry Sample = 21.70g	Mass of Oil sat. sample = 24.58g	Mass of Oil in sample = 2.88g	Injection Pressure = 6bar
Injection Time	Mass of Flooded Sample	Mass of Saturated Sample	Mass of Oil Produced	Volume of Oil Produced	%OOIP of Oil produced
Min	M2(g)	M1(g)	M3(g)	V3(cc)	%
1	23.80	24.58	0.78	0.839	0.27
2	23.64	24.58	0.94	1.011	0.33
3	23.57	24.58	1.01	1.086	0.35
4	23.50	24.58	1.08	1.161	0.38
5	23.46	24.58	1.12	1.204	0.39
6	23.43	24.58	1.15	1.237	0.40
7	23.38	24.58	1.20	1.290	0.42
8	23.36	24.58	1.22	1.312	0.42
9	23.33	24.58	1.25	1.344	0.43
10	23.31	24.58	1.27	1.366	0.44
11	23.28	24.58	1.30	1.398	0.45
12	23.26	24.58	1.32	1.419	0.46
13	23.24	24.58	1.34	1.441	0.47
14	23.23	24.58	1.35	1.452	0.47
15	23.21	24.58	1.37	1.473	0.48
16	23.19	24.58	1.39	1.495	0.48
17	23.18	24.58	1.40	1.505	0.49
18	23.17	24.58	1.41	1.516	0.49

19	23.16	24.58	1.42	1.527	0.49
20	23.16	24.58	1.42	1.527	0.49
21	23.15	24.58	1.43	1.538	0.50
22	23.14	24.58	1.44	1.548	0.50
23	23.12	24.58	1.46	1.570	0.51
24	23.12	24.58	1.46	1.570	0.51
25	23.11	24.58	1.47	1.581	0.51
26	23.10	24.58	1.48	1.591	0.51

F7: Data for Core flooding Test 7

Perforation Diameter =1.0mm Mass of Dry Sample = 21.70g Mass of Oil sat. sample = 24.71g Mass of Oil in sample = 3.01g Injection Pressure = 1bar

Injection Time	Mass of Flooded Sample	Mass of Saturated Sample	Mass of Oil Produced	Volume of Oil Produced	%OOIP of Oil produced
Min	M2(g)	M1(g)	M3(g)	V3(cc)	%
1	24.05	24.71	0.66	0.710	0.219
2	23.92	24.71	0.79	0.849	0.262
3	23.82	24.71	0.89	0.957	0.296
4	23.74	24.71	0.97	1.043	0.322
5	23.72	24.71	0.99	1.065	0.329
6	23.66	24.71	1.05	1.129	0.349
7	23.63	24.71	1.08	1.161	0.359
8	23.6	24.71	1.11	1.194	0.369
9	23.58	24.71	1.13	1.215	0.375

10	23.55	24.71	1.16	1.247	0.385
11	23.54	24.71	1.17	1.258	0.389
12	23.53	24.71	1.18	1.269	0.392
13	23.51	24.71	1.20	1.290	0.399
14	23.49	24.71	1.22	1.312	0.405
15	23.48	24.71	1.23	1.323	0.409
16	23.47	24.71	1.24	1.333	0.412
17	23.46	24.71	1.25	1.344	0.415
18	23.46	24.71	1.25	1.344	0.415
19	23.43	24.71	1.28	1.376	0.425
20	23.43	24.71	1.28	1.376	0.425
21	23.41	24.71	1.30	1.398	0.432
22	23.41	24.71	1.30	1.398	0.432
23	23.39	24.71	1.32	1.419	0.439
24	23.39	24.71	1.32	1.419	0.439
25	23.39	24.71	1.32	1.419	0.439
26	23.37	24.71	1.34	1.441	0.445

F8: Data for Core flooding Test 8

Perforation Diameter =1.0mm Mass of Dry Sample = 21.70g Mass of Oil sat. sample = 24.71g Mass of Oil in sample = 3.01g Injection Pressure = 2bar

Injection Time	Mass of Flooded Sample	Mass of Saturated Sample	Mass of Oil Produced	Volume of Oil Produced	%OOIP of Oil produced
Min	M2(g)	M1(g)	M3(g)	V3(cc)	%
1	24.1	24.71	0.61	0.6559	0.203
2	23.85	24.71	0.86	0.9247	0.286

3	23.75	24.71	0.96	1.0323	0.319
4	23.68	24.71	1.03	1.1075	0.342
5	23.65	24.71	1.06	1.1398	0.352
6	23.64	24.71	1.07	1.1505	0.355
7	23.58	24.71	1.13	1.2151	0.375
8	23.57	24.71	1.14	1.2258	0.379
9	23.54	24.71	1.17	1.2581	0.389
10	23.5	24.71	1.21	1.3011	0.402
11	23.47	24.71	1.24	1.3333	0.412
12	23.46	24.71	1.25	1.3441	0.415
13	23.43	24.71	1.28	1.3763	0.425
14	23.43	24.71	1.28	1.3763	0.425
15	23.42	24.71	1.29	1.3871	0.429
16	23.39	24.71	1.32	1.4194	0.439
17	23.39	24.71	1.32	1.4194	0.439
18	23.39	24.71	1.32	1.4194	0.439
19	23.37	24.71	1.34	1.4409	0.445
20	23.36	24.71	1.35	1.4516	0.449
21	23.34	24.71	1.37	1.4731	0.455
22	23.34	24.71	1.37	1.4731	0.455
23	23.33	24.71	1.38	1.4839	0.458
24	23.33	24.71	1.38	1.4839	0.458
25	23.32	24.71	1.39	1.4946	0.462

26	23.32	24.71	1.39	1.4946	0.462
----	-------	-------	------	--------	-------

F9: Data for Core flooding Test 9

Perforation Diameter =1.0mm	Mass of Dry Sample = 21.70g	Mass of Oil sat. sample = 24.71g	Mass of Oil in sample = 3.01g	Injection Pressure = 3bar
-----------------------------	-----------------------------	----------------------------------	-------------------------------	---------------------------

Injection Time	Mass of Flooded Sample	Mass of Saturated Sample	Mass of Oil Produced	Volume of Oil Produced	%OOIP of Oil produced
Min	M2(g)	M1(g)	M3(g)	V3(cc)	%
1	24.07	24.71	0.64	0.688172043	0.213
2	23.94	24.71	0.77	0.827956989	0.256
3	23.77	24.71	0.94	1.010752688	0.312
4	23.68	24.71	1.03	1.107526882	0.342
5	23.62	24.71	1.09	1.172043011	0.362
6	23.56	24.71	1.15	1.23655914	0.382
7	23.54	24.71	1.17	1.258064516	0.389
8	23.5	24.71	1.21	1.301075269	0.402
9	23.48	24.71	1.23	1.322580645	0.409
10	23.46	24.71	1.25	1.344086022	0.415
11	23.44	24.71	1.27	1.365591398	0.422
12	23.42	24.71	1.29	1.387096774	0.429
13	23.4	24.71	1.31	1.408602151	0.435
14	23.39	24.71	1.32	1.419354839	0.439
15	23.38	24.71	1.33	1.430107527	0.442
16	23.37	24.71	1.34	1.440860215	0.445
17	23.36	24.71	1.35	1.451612903	0.449
18	23.34	24.71	1.37	1.47311828	0.455

19	23.33	24.71	1.38	1.483870968	0.458
20	23.32	24.71	1.39	1.494623656	0.462
21	23.32	24.71	1.39	1.494623656	0.462
22	23.31	24.71	1.40	1.505376344	0.465
23	23.3	24.71	1.41	1.516129032	0.468
24	23.29	24.71	1.42	1.52688172	0.472
25	23.28	24.71	1.43	1.537634409	0.475
26	23.28	24.71	1.43	1.537634409	0.475

F10: Data for Core flooding Test 10

Perforation Diameter =1.0mm Mass of Dry Sample = 21.70g Mass of Oil sat. sample = 24.71g Mass of Oil in sample = 3.01g Injection Pressure = 4bar

Injection Time	Mass of Flooded Sample	Mass of Saturated Sample	Mass of Oil Produced	Volume of Oil Produced	%OOIP of Oil produced
Min	M2(g)	M1(g)	M3(g)	V3(cc)	%
1	24.02	24.71	0.69	0.7419	0.229
2	23.84	24.71	0.87	0.9355	0.289
3	23.78	24.71	0.93	1.0000	0.309
4	23.72	24.71	0.99	1.0645	0.329
5	23.65	24.71	1.06	1.1398	0.352
6	23.61	24.71	1.10	1.1828	0.365
7	23.6	24.71	1.11	1.1935	0.369
8	23.56	24.71	1.15	1.2366	0.382
9	23.54	24.71	1.17	1.2581	0.389
10	23.53	24.71	1.18	1.2688	0.392
11	23.51	24.71	1.20	1.2903	0.399

12	23.49	24.71	1.22	1.3118	0.405
13	23.47	24.71	1.24	1.3333	0.412
14	23.46	24.71	1.25	1.3441	0.415
15	23.44	24.71	1.27	1.3656	0.422
16	23.43	24.71	1.28	1.3763	0.425
17	23.42	24.71	1.29	1.3871	0.429
18	23.4	24.71	1.31	1.4086	0.435
19	23.4	24.71	1.31	1.4086	0.435
20	23.38	24.71	1.33	1.4301	0.442
21	23.38	24.71	1.33	1.4301	0.442
22	23.37	24.71	1.34	1.4409	0.445
23	23.36	24.71	1.35	1.4516	0.449
24	23.35	24.71	1.36	1.4624	0.452
25	23.34	24.71	1.37	1.4731	0.455
26	23.34	24.71	1.37	1.4731	0.455

F11: Data for Core flooding Test 11

Perforation Diameter =1.0mm Mass of Dry Sample = 21.70g Mass of Oil sat. sample = 24.60g Mass of Oil in sample = 2.9g Injection Pressure = 5bar

Injection Time	Mass of Flooded Sample	Mass of Saturated Sample	Mass of Oil Produced	Volume of Oil Produced	%OOIP of Oil produced
Min	M2(g)	M1(g)	M3(g)	V3(cc)	%
1	23.92	24.6	0.68	0.7312	0.226
2	23.77	24.6	0.83	0.8925	0.276
3	23.68	24.6	0.92	0.9892	0.306
4	23.62	24.6	0.98	1.0538	0.326

5	23.57	24.6	1.03	1.1075	0.342
6	23.53	24.6	1.07	1.1505	0.355
7	23.5	24.6	1.10	1.1828	0.365
8	23.48	24.6	1.12	1.2043	0.372
9	23.44	24.6	1.16	1.2473	0.385
10	23.41	24.6	1.19	1.2796	0.395
11	23.4	24.6	1.20	1.2903	0.399
12	23.37	24.6	1.23	1.3226	0.409
13	23.36	24.6	1.24	1.3333	0.412
14	23.34	24.6	1.26	1.3548	0.419
15	23.33	24.6	1.27	1.3656	0.422
16	23.32	24.6	1.28	1.3763	0.425
17	23.32	24.6	1.28	1.3763	0.425
18	23.3	24.6	1.30	1.3978	0.432
19	23.29	24.6	1.31	1.4086	0.435
20	23.28	24.6	1.32	1.4194	0.439
21	23.28	24.6	1.32	1.4194	0.439
22	23.27	24.6	1.33	1.4301	0.442
23	23.26	24.6	1.34	1.4409	0.445
24	23.25	24.6	1.35	1.4516	0.449
25	23.24	24.6	1.36	1.4624	0.452
26	23.24	24.6	1.36	1.4624	0.452

F12: Data for Core flooding Test 12

Perforation Diameter =1.0mm Mass of Dry Sample = 21.70g Mass of Oil sat. sample = 24.73g Mass of Oil in sample = 3.03g Injection Pressure = 6bar

Injection Time	Mass of Flooded Sample	Mass of Saturated Sample	Mass of Oil Produced	Volume of Oil Produced	%OOIP of Oil produced
Min	M2(g)	M1(g)	M3(g)	V3(cc)	%
1	23.9	24.73	0.83	0.8925	0.276
2	23.75	24.73	0.98	1.0538	0.326
3	23.68	24.73	1.05	1.1290	0.349
4	23.61	24.73	1.12	1.2043	0.372
5	23.56	24.73	1.17	1.2581	0.389
6	23.52	24.73	1.21	1.3011	0.402
7	23.49	24.73	1.24	1.3333	0.412
8	23.46	24.73	1.27	1.3656	0.422
9	23.44	24.73	1.29	1.3871	0.429
10	23.42	24.73	1.31	1.4086	0.435
11	23.4	24.73	1.33	1.4301	0.442
12	23.38	24.73	1.35	1.4516	0.449
13	23.36	24.73	1.37	1.4731	0.455
14	23.35	24.73	1.38	1.4839	0.458
15	23.34	24.73	1.39	1.4946	0.462
16	23.32	24.73	1.41	1.5161	0.468
17	23.32	24.73	1.41	1.5161	0.468
18	23.31	24.73	1.42	1.5269	0.472

19	23.3	24.73	1.43	1.5376	0.475
20	23.28	24.73	1.45	1.5591	0.482
21	23.27	24.73	1.46	1.5699	0.485
22	23.27	24.73	1.46	1.5699	0.485
23	23.26	24.73	1.47	1.5806	0.488
24	23.25	24.73	1.48	1.5914	0.492
25	23.24	24.73	1.49	1.6022	0.495
26	23.24	24.73	1.49	1.6022	0.495

F13: Data for Core flooding 13 Test

Perforation Diameter =1.5mm Mass of Oil sat. sample = 24.70g Mass of Dry Sample = 21.70g Mass of Oil in sample = 3.0g Injection Pressure = 1bar

Injection Time	Mass of Flooded Sample	Mass of Saturated Sample M1	Mass of Oil Produced	Volume of Oil Produced	%OOIP of Oil produced
Min	M2(g)	M1(g)	M3(g)	V3(cc)	%
1	24.11	24.7	0.59	0.6344	0.20
2	23.89	24.7	0.81	0.8710	0.27
3	23.8	24.7	0.90	0.9677	0.30
4	23.72	24.7	0.98	1.0538	0.33
5	23.67	24.7	1.03	1.1075	0.34
6	23.62	24.7	1.08	1.1613	0.36
7	23.61	24.7	1.09	1.1720	0.36
8	23.57	24.7	1.13	1.2151	0.38
9	23.56	24.7	1.14	1.2258	0.38
10	23.55	24.7	1.15	1.2366	0.38
11	23.52	24.7	1.18	1.2688	0.39

12	23.51	24.7	1.19	1.2796	0.40
13	23.49	24.7	1.21	1.3011	0.40
14	23.49	24.7	1.21	1.3011	0.40
15	23.46	24.7	1.24	1.3333	0.41
16	23.46	24.7	1.24	1.3333	0.41
17	23.44	24.7	1.26	1.3548	0.42
18	23.44	24.7	1.26	1.3548	0.42
19	23.43	24.7	1.27	1.3656	0.42
20	23.4	24.7	1.30	1.3978	0.43
21	23.4	24.7	1.30	1.3978	0.43
22	23.38	24.7	1.32	1.4194	0.44
23	23.38	24.7	1.32	1.4194	0.44
24	23.37	24.7	1.33	1.4301	0.44
25	23.37	24.7	1.33	1.4301	0.44
26	23.37	24.7	1.33	1.4301	0.44

F14: Data for Core flooding 14 Test

Perforation Diameter =1.5mm

Mass of Oil sat. sample = 24.84g

Mass of Dry Sample = 21.70g

Mass of Oil in sample = 3.14g

Injection Pressure = 2bar

Injection Time	Mass of Flooded Sample	Mass of Saturated Sample M1	Mass of Oil Produced	Volume of Oil Produced	%OOIP of Oil produced
Min	M2(g)	M1(g)	M3(g)	V3(cc)	%
1	24.19	24.84	0.65	0.6989	0.21
2	23.79	24.84	1.05	1.1290	0.33
3	23.69	24.84	1.15	1.2366	0.37
4	23.62	24.84	1.22	1.3118	0.39

5	23.55	24.84	1.29	1.3871	0.41
6	23.51	24.84	1.33	1.4301	0.42
7	23.47	24.84	1.37	1.4731	0.44
8	23.45	24.84	1.39	1.4946	0.44
9	23.42	24.84	1.42	1.5269	0.45
10	23.39	24.84	1.45	1.5591	0.46
11	23.37	24.84	1.47	1.5806	0.47
12	23.35	24.84	1.49	1.6022	0.47
13	23.35	24.84	1.49	1.6022	0.47
14	23.35	24.84	1.49	1.6022	0.47
15	23.33	24.84	1.51	1.6237	0.48
16	23.32	24.84	1.52	1.6344	0.48
17	23.3	24.84	1.54	1.6559	0.49
18	23.28	24.84	1.56	1.6774	0.50
19	23.28	24.84	1.56	1.6774	0.50
20	23.26	24.84	1.58	1.6989	0.50
21	23.26	24.84	1.58	1.6989	0.50
22	23.25	24.84	1.59	1.7097	0.51
23	23.24	24.84	1.60	1.7204	0.51
24	23.22	24.84	1.62	1.7419	0.52
25	23.2	24.84	1.64	1.7634	0.52
26	23.2	24.84	1.64	1.7634	0.52

F15: Data for Core flooding 15 Test

Perforation Diameter =1.5mm

Mass of Oil sat. sample = 24.65g

Mass of Dry Sample = 21.70g

Mass of Oil in sample = 2.95g

Injection Pressure = 3bar

Injection Time	Mass of Flooded Sample	Mass of Saturated Sample M1	Mass of Oil Produced	Volume of Oil Produced	%OOIP of Oil produced
Min	M2(g)	M1(g)	M3(g)	V3(cc)	%
1	23.87	24.65	0.78	0.8387	0.26
2	23.70	24.65	0.95	1.0215	0.32
3	23.65	24.65	1.00	1.0753	0.34
4	23.60	24.65	1.05	1.1290	0.36
5	23.55	24.65	1.10	1.1828	0.37
6	23.50	24.65	1.15	1.2366	0.39
7	23.46	24.65	1.19	1.2796	0.40
8	23.44	24.65	1.21	1.3011	0.41
9	23.42	24.65	1.23	1.3226	0.42
10	23.41	24.65	1.24	1.3333	0.42
11	23.39	24.65	1.26	1.3548	0.43
12	23.37	24.65	1.28	1.3763	0.43
13	23.37	24.65	1.28	1.3763	0.43
14	23.34	24.65	1.31	1.4086	0.44
15	23.33	24.65	1.32	1.4194	0.45
16	23.32	24.65	1.33	1.4301	0.45
17	23.30	24.65	1.35	1.4516	0.46
18	23.29	24.65	1.36	1.4624	0.46

19	23.29	24.65	1.36	1.4624	0.46
20	23.27	24.65	1.38	1.4839	0.47
21	23.27	24.65	1.38	1.4839	0.47
22	23.25	24.65	1.40	1.5054	0.47
23	23.25	24.65	1.40	1.5054	0.47
24	23.24	24.65	1.41	1.5161	0.48
25	23.24	24.65	1.41	1.5161	0.48
26	23.24	24.65	1.41	1.5161	0.48

F16: Data for Core flooding 16 Test

Perforation Diameter =1.5mm Mass of Oil sat. sample = 24.66g Mass of Dry Sample = 21.70g Mass of Oil in sample = 2.96g Injection Pressure = 4bar

Injection Time	Mass of Flooded Sample	Mass of Saturated Sample M1	Mass of Oil Produced	Volume of Oil Produced	%OOIP of Oil produced
Min	M2(g)	M1(g)	M3(g)	V3(cc)	%
1	23.85	24.66	0.81	0.8710	0.27
2	23.70	24.66	0.96	1.0323	0.32
3	23.63	24.66	1.03	1.1075	0.35
4	23.57	24.66	1.09	1.1720	0.37
5	23.54	24.66	1.12	1.2043	0.38
6	23.50	24.66	1.16	1.2473	0.39
7	23.48	24.66	1.18	1.2688	0.40
8	23.45	24.66	1.21	1.3011	0.41
9	23.44	24.66	1.22	1.3118	0.41
10	23.43	24.66	1.23	1.3226	0.42
11	23.41	24.66	1.25	1.3441	0.42

12	23.40	24.66	1.26	1.3548	0.43
13	23.38	24.66	1.28	1.3763	0.43
14	23.34	24.66	1.32	1.4194	0.45
15	23.33	24.66	1.33	1.4301	0.45
16	23.32	24.66	1.34	1.4409	0.45
17	23.31	24.66	1.35	1.4516	0.46
18	23.30	24.66	1.36	1.4624	0.46
19	23.30	24.66	1.36	1.4624	0.46
20	23.28	24.66	1.38	1.4839	0.47
21	23.27	24.66	1.39	1.4946	0.47
22	23.26	24.66	1.40	1.5054	0.47
23	23.26	24.66	1.40	1.5054	0.47
24	23.25	24.66	1.41	1.5161	0.48
25	23.25	24.66	1.41	1.5161	0.48
26	23.24	24.66	1.42	1.5269	0.48

F17: Data for Core flooding 17 Test

Perforation Diameter =1.5mm		Mass of Oil sat. sample = 24.74g	Mass of Dry Sample = 21.70g	Mass of Oil in sample = 3.04g	Injection Pressure = 5bar
Injection Time	Mass of Flooded Sample	Mass of Saturated Sample M1	Mass of Oil Produced	Volume of Oil Produced	%OOIP of Oil produced
Min	M2(g)	M1(g)	M3(g)	V3(cc)	%
1	23.84	24.74	0.90	0.9677	0.30
2	23.70	24.74	1.04	1.1183	0.34
3	23.62	24.74	1.12	1.2043	0.37
4	23.58	24.74	1.16	1.2473	0.38

5	23.54	24.74	1.20	1.2903	0.39
6	23.49	24.74	1.25	1.3441	0.41
7	23.47	24.74	1.27	1.3656	0.42
8	23.45	24.74	1.29	1.3871	0.42
9	23.42	24.74	1.32	1.4194	0.43
10	23.40	24.74	1.34	1.4409	0.44
11	23.38	24.74	1.36	1.4624	0.45
12	23.37	24.74	1.37	1.4731	0.45
13	23.36	24.74	1.38	1.4839	0.45
14	23.35	24.74	1.39	1.4946	0.46
15	23.34	24.74	1.40	1.5054	0.46
16	23.32	24.74	1.42	1.5269	0.47
17	23.31	24.74	1.43	1.5376	0.47
18	23.29	24.74	1.45	1.5591	0.48
19	23.29	24.74	1.45	1.5591	0.48
20	23.27	24.74	1.47	1.5806	0.48
21	23.26	24.74	1.48	1.5914	0.49
22	23.26	24.74	1.48	1.5914	0.49
23	23.24	24.74	1.50	1.6129	0.49
24	23.24	24.74	1.50	1.6129	0.49
25	23.23	24.74	1.51	1.6237	0.50
26	23.23	24.74	1.51	1.6237	0.50

F18: Data for Core flooding 18 Test

Perforation Diameter =1.5mm

Mass of Oil sat. sample = 24.75g

Mass of Dry Sample = 21.70g

Mass of Oil in sample = 3.05g

Injection Pressure = 6bar

Injection Time	Mass of Flooded Sample	Mass of Saturated Sample M1	Mass of Oil Produced	Volume of Oil Produced	%OOIP of Oil produced
Min	M2(g)	M1(g)	M3(g)	V3(cc)	%
1	23.79	24.75	0.96	1.0323	0.31
2	23.64	24.75	1.11	1.1935	0.36
3	23.57	24.75	1.18	1.2688	0.39
4	23.51	24.75	1.24	1.3333	0.41
5	23.46	24.75	1.29	1.3871	0.42
6	23.44	24.75	1.31	1.4086	0.43
7	23.41	24.75	1.34	1.4409	0.44
8	23.40	24.75	1.35	1.4516	0.44
9	23.37	24.75	1.38	1.4839	0.45
10	23.34	24.75	1.41	1.5161	0.46
11	23.32	24.75	1.43	1.5376	0.47
12	23.30	24.75	1.45	1.5591	0.48
13	23.29	24.75	1.46	1.5699	0.48
14	23.29	24.75	1.46	1.5699	0.48
15	23.26	24.75	1.49	1.6022	0.49
16	23.25	24.75	1.50	1.6129	0.49
17	23.24	24.75	1.51	1.6237	0.50
18	23.23	24.75	1.52	1.6344	0.50

19	23.22	24.75	1.53	1.6452	0.50
20	23.21	24.75	1.54	1.6559	0.50
21	23.20	24.75	1.55	1.6667	0.51
22	23.20	24.75	1.55	1.6667	0.51
23	23.19	24.75	1.56	1.6774	0.51
24	23.18	24.75	1.57	1.6882	0.51
25	23.17	24.75	1.58	1.6989	0.52
26	23.17	24.75	1.58	1.6989	0.52

F19: Data for Core flooding 19 Test

Perforation Diameter =2.0mm Mass of Oil sat. sample = 24.65g Mass of Dry Sample = 21.90g Mass of Oil in sample = 2.75g Injection Pressure = 1bar

Injection Time	Mass of Flooded Sample	Mass of Saturated Sample M1	Mass of Oil Produced	Volume of Oil Produced	%OOIP of Oil produced
Min	M2(g)	M1(g)	M3(g)	V3(cc)	%
1	23.99	24.65	0.66	0.7097	0.24
2	23.79	24.65	0.86	0.9247	0.31
3	23.65	24.65	1.00	1.0753	0.36
4	23.57	24.65	1.08	1.1613	0.39
5	23.55	24.65	1.10	1.1828	0.40
6	23.51	24.65	1.14	1.2258	0.41
7	23.46	24.65	1.19	1.2796	0.43
8	23.43	24.65	1.22	1.3118	0.44
9	23.4	24.65	1.25	1.3441	0.45
10	23.37	24.65	1.28	1.3763	0.47
11	23.36	24.65	1.29	1.3871	0.47

12	23.33	24.65	1.32	1.4194	0.48
13	23.31	24.65	1.34	1.4409	0.49
14	23.29	24.65	1.36	1.4624	0.49
15	23.28	24.65	1.37	1.4731	0.50
16	23.27	24.65	1.38	1.4839	0.50
17	23.26	24.65	1.39	1.4946	0.51
18	23.24	24.65	1.41	1.5161	0.51
19	23.23	24.65	1.42	1.5269	0.52
20	23.22	24.65	1.43	1.5376	0.52
21	23.21	24.65	1.44	1.5484	0.52
22	23.2	24.65	1.45	1.5591	0.53
23	23.19	24.65	1.46	1.5699	0.53
24	23.19	24.65	1.46	1.5699	0.53
25	23.17	24.65	1.48	1.5914	0.54
26	23.16	24.65	1.49	1.6022	0.54

F20: Data for Core flooding 20 Test

Perforation Diameter =2.0mm	Mass of Oil sat. sample = 24.71g	Mass of Dry Sample = 21.90g	Mass of Oil in sample =2.81 g	Injection Pressure = 2bar	
Injection Time	Mass of Flooded Sample	Mass of Saturated Sample M1	Mass of Oil Produced	Volume of Oil Produced	%OOIP of Oil produced
Min	M2(g)	M1(g)	M3(g)	V3(cc)	%
1	23.68	24.71	1.03	1.1075	0.37
2	23.62	24.71	1.09	1.1720	0.39
3	23.6	24.71	1.11	1.1935	0.40
4	23.54	24.71	1.17	1.2581	0.42

5	23.52	24.71	1.19	1.2796	0.42
6	23.49	24.71	1.22	1.3118	0.43
7	23.47	24.71	1.24	1.3333	0.44
8	23.44	24.71	1.27	1.3656	0.45
9	23.38	24.71	1.33	1.4301	0.47
10	23.36	24.71	1.35	1.4516	0.48
11	23.33	24.71	1.38	1.4839	0.49
12	23.31	24.71	1.40	1.5054	0.50
13	23.31	24.71	1.40	1.5054	0.50
14	23.31	24.71	1.40	1.5054	0.50
15	23.27	24.71	1.44	1.5484	0.51
16	23.25	24.71	1.46	1.5699	0.52
17	23.23	24.71	1.48	1.5914	0.53
18	23.2	24.71	1.51	1.6237	0.54
19	23.19	24.71	1.52	1.6344	0.54
20	23.17	24.71	1.54	1.6559	0.55
21	23.17	24.71	1.54	1.6559	0.55
22	23.16	24.71	1.55	1.6667	0.55
23	23.16	24.71	1.55	1.6667	0.55
24	23.15	24.71	1.56	1.6774	0.56
25	23.15	24.71	1.56	1.6774	0.56
26	23.15	24.71	1.56	1.6774	0.56

F21: Data for Core flooding 21 Test

Perforation Diameter =2.0mm Mass of Oil sat. sample = 24.77g Mass of Dry Sample = 21.90g Mass of Oil in sample =2.81 g Injection Pressure = 3bar

Injection Time	Mass of Flooded Sample	Mass of Saturated Sample M1	Mass of Oil Produced	Volume of Oil Produced	%OOIP of Oil produced	
Min	M2(g)	M1(g)	M3(g)	V3(cc)	%	
1	1	23.72	24.77	1.05	1.1290	0.37
2	2	23.58	24.77	1.19	1.2796	0.42
3	3	23.51	24.77	1.26	1.3548	0.44
4	4	23.42	24.77	1.35	1.4516	0.47
5	5	23.38	24.77	1.39	1.4946	0.49
6	6	23.32	24.77	1.45	1.5591	0.51
7	7	23.30	24.77	1.47	1.5806	0.51
8	8	23.18	24.77	1.59	1.7097	0.56
9	9	23.17	24.77	1.60	1.7204	0.56
10	10	23.14	24.77	1.63	1.7527	0.57
11	11	23.10	24.77	1.67	1.7957	0.58
12	12	23.10	24.77	1.67	1.7957	0.58
13	13	23.08	24.77	1.69	1.8172	0.59
14	14	23.08	24.77	1.69	1.8172	0.59
15	15	23.07	24.77	1.70	1.8280	0.59
16	16	23.05	24.77	1.72	1.8495	0.60
17	17	23.03	24.77	1.74	1.8710	0.61
18	18	23.01	24.77	1.76	1.8925	0.61

19	19	23.00	24.77	1.77	1.9032	0.62
20	20	22.99	24.77	1.78	1.9140	0.62
21	21	22.97	24.77	1.80	1.9355	0.63
22	22	22.97	24.77	1.80	1.9355	0.63
23	23	22.95	24.77	1.82	1.9570	0.64
24	24	22.94	24.77	1.83	1.9677	0.64
25	25	22.94	24.77	1.83	1.9677	0.64
26	26	22.93	24.77	1.84	1.9785	0.64

F22: Data for Core flooding 22 Test

Perforation Diameter =2.0mm

Mass of Oil sat. sample = 24.79g

Mass of Dry Sample = 21.90g

Mass of Oil in sample =2.89 g

Injection Pressure = 4bar

Injection Time	Mass of Flooded Sample	Mass of Saturated Sample M1	Mass of Oil Produced	Volume of Oil Produced	%OOIP of Oil produced
Min	M2(g)	M1(g)	M3(g)	V3(cc)	%
1	23.69	24.79	1.10	1.1828	0.38
2	23.53	24.79	1.26	1.3548	0.44
3	23.47	24.79	1.32	1.4194	0.46
4	23.36	24.79	1.43	1.5376	0.49
5	23.30	24.79	1.49	1.6022	0.52
6	23.24	24.79	1.55	1.6667	0.54
7	23.21	24.79	1.58	1.6989	0.55
8	23.18	24.79	1.61	1.7312	0.56
9	23.17	24.79	1.62	1.7419	0.56

10	23.14	24.79	1.65	1.7742	0.57
11	23.10	24.79	1.69	1.8172	0.58
12	23.10	24.79	1.69	1.8172	0.58
13	23.08	24.79	1.71	1.8387	0.59
14	23.08	24.79	1.71	1.8387	0.59
15	23.07	24.79	1.72	1.8495	0.60
16	23.05	24.79	1.74	1.8710	0.60
17	23.03	24.79	1.76	1.8925	0.61
18	23.01	24.79	1.78	1.9140	0.62
19	23.00	24.79	1.79	1.9247	0.62
20	22.99	24.79	1.80	1.9355	0.62
21	22.97	24.79	1.82	1.9570	0.63
22	22.97	24.79	1.82	1.9570	0.63
23	22.95	24.79	1.84	1.9785	0.64
24	22.94	24.79	1.85	1.9892	0.64
25	22.94	24.79	1.85	1.9892	0.64
26	22.93	24.79	1.86	2.0000	0.64

F23: Data for Core flooding 23 Test

Perforation Diameter =2.0mm

Mass of Oil sat. sample = 24.66g

Mass of Dry Sample = 21.90g

Mass of Oil in sample =2.66 g

Injection Pressure = 5bar

Injection Time

Mass of Flooded Sample

Mass of Saturated Sample M1

Mass of Oil Produced

Volume of Oil Produced

%OOIP of Oil produced

Min

M2(g)

M1(g)

M3(g)

V3(cc)

%

1	23.58	24.66	1.08	1.1613	0.39
2	23.37	24.66	1.29	1.3871	0.47
3	23.3	24.66	1.36	1.4624	0.49
4	23.23	24.66	1.43	1.5376	0.52
5	23.17	24.66	1.49	1.6022	0.54
6	23.13	24.66	1.53	1.6452	0.55
7	23.11	24.66	1.55	1.6667	0.56
8	23.08	24.66	1.58	1.6989	0.57
9	23.07	24.66	1.59	1.7097	0.58
10	23.06	24.66	1.60	1.7204	0.58
11	23.04	24.66	1.62	1.7419	0.59
12	23.01	24.66	1.65	1.7742	0.60
13	22.99	24.66	1.67	1.7957	0.61
14	22.99	24.66	1.67	1.7957	0.61
15	22.98	24.66	1.68	1.8065	0.61
16	22.98	24.66	1.68	1.8065	0.61
17	22.97	24.66	1.69	1.8172	0.61
18	22.95	24.66	1.71	1.8387	0.62
19	22.94	24.66	1.72	1.8495	0.62
20	22.94	24.66	1.72	1.8495	0.62
21	22.93	24.66	1.73	1.8602	0.63
22	22.92	24.66	1.74	1.8710	0.63
23	22.91	24.66	1.75	1.8817	0.63

24	22.9	24.66	1.76	1.8925	0.64
25	22.88	24.66	1.78	1.9140	0.64
26	22.87	24.66	1.79	1.9247	0.65

F24: Data for Core flooding 24 Test

Perforation Diameter =2.0mm Mass of Oil sat. sample = 24.75g Mass of Dry Sample = 21.90g Mass of Oil in sample =2.85 g Injection Pressure = 6bar

Injection Time	Mass of Flooded Sample	Mass of Saturated Sample M1	Mass of Oil Produced	Volume of Oil Produced	%OOIP of Oil produced
Min	M2(g)	M1(g)	M3(g)	V3(cc)	%
1	23.53	24.75	1.22	1.3118	0.43
2	23.35	24.75	1.40	1.5054	0.49
3	23.25	24.75	1.50	1.6129	0.53
4	23.21	24.75	1.54	1.6559	0.54
5	23.18	24.75	1.57	1.6882	0.55
6	23.14	24.75	1.61	1.7312	0.56
7	23.1	24.75	1.65	1.7742	0.58
8	23.08	24.75	1.67	1.7957	0.59
9	23.05	24.75	1.70	1.8280	0.60
10	23.03	24.75	1.72	1.8495	0.60
11	23.01	24.75	1.74	1.8710	0.61
12	22.99	24.75	1.76	1.8925	0.62
13	22.98	24.75	1.77	1.9032	0.62
14	22.96	24.75	1.79	1.9247	0.63
15	22.95	24.75	1.80	1.9355	0.63
16	22.94	24.75	1.81	1.9462	0.64

17	22.93	24.75	1.82	1.9570	0.64
18	22.91	24.75	1.84	1.9785	0.65
19	22.91	24.75	1.84	1.9785	0.65
20	22.9	24.75	1.85	1.9892	0.65
21	22.88	24.75	1.87	2.0108	0.66
22	22.87	24.75	1.88	2.0215	0.66
23	22.87	24.75	1.88	2.0215	0.66
24	22.86	24.75	1.89	2.0323	0.66
25	22.86	24.75	1.89	2.0323	0.66
26	22.84	24.75	1.91	2.0538	0.67

F25: Data for Core flooding 25 Test

Perforation Diameter =2.5mm

Mass of Oil sat. sample = 24.63g

Mass of Dry Sample = 21.62g

Mass of Oil in sample =3.01 g

Injection Pressure = 1bar

Injection Time	Mass of Flooded Sample	Mass of Saturated Sample M1	Mass of Oil Produced	Volume of Oil Produced	%OOIP of Oil produced
Min	M2(g)	M1(g)	M3(g)	V3(cc)	%
1	24.37	24.63	0.26	0.2796	0.09
2	24.34	24.63	0.29	0.3118	0.10
3	24.30	24.63	0.33	0.3548	0.11
4	24.28	24.63	0.35	0.3763	0.12
5	24.25	24.63	0.38	0.4086	0.13
6	24.24	24.63	0.39	0.4194	0.13
7	24.21	24.63	0.42	0.4516	0.14

8	24.17	24.63	0.46	0.4946	0.15
9	24.16	24.63	0.47	0.5054	0.16
10	24.15	24.63	0.48	0.5161	0.16
11	24.12	24.63	0.51	0.5484	0.17
12	24.13	24.63	0.50	0.5376	0.17
13	24.11	24.63	0.52	0.5591	0.17
14	24.09	24.63	0.54	0.5806	0.18
15	24.07	24.63	0.56	0.6022	0.19
16	24.06	24.63	0.57	0.6129	0.19
17	24.05	24.63	0.58	0.6237	0.19
18	24.03	24.63	0.60	0.6452	0.20
19	24.02	24.63	0.61	0.6559	0.20
20	24.01	24.63	0.62	0.6667	0.21
21	24.00	24.63	0.63	0.6774	0.21
22	23.99	24.63	0.64	0.6882	0.21
23	23.98	24.63	0.65	0.6989	0.22
24	23.97	24.63	0.66	0.7097	0.22
25	23.96	24.63	0.67	0.7204	0.22
26	23.95	24.63	0.68	0.7312	0.23

F26: Data for Core flooding 26 Test

Perforation Diameter =2.5mm

Mass of Oil sat. sample = 24.69g

Mass of Dry Sample = 21.62g

Mass of Oil in sample =3.07 g

Injection Pressure = 2bar

Injection Time

Mass of Flooded Sample

Mass of Saturated Sample M1

Mass of Oil Produced

Volume of Oil Produced

%OOIP of Oil produced

Min

M2(g)

M1(g)

M3(g)

V3(cc)

%

1	24.37	24.69	0.32	0.3441	0.10
2	24.34	24.69	0.35	0.3763	0.11
3	24.30	24.69	0.39	0.4194	0.13
4	24.28	24.69	0.41	0.4409	0.13
5	24.25	24.69	0.44	0.4731	0.14
6	24.24	24.69	0.45	0.4839	0.15
7	24.21	24.69	0.48	0.5161	0.16
8	24.17	24.69	0.52	0.5591	0.17
9	24.16	24.69	0.53	0.5699	0.17
10	24.15	24.69	0.54	0.5806	0.18
11	24.12	24.69	0.57	0.6129	0.19
12	24.13	24.69	0.56	0.6022	0.18
13	24.11	24.69	0.58	0.6237	0.19
14	24.09	24.69	0.60	0.6452	0.20
15	24.07	24.69	0.62	0.6667	0.20
16	24.06	24.69	0.63	0.6774	0.21
17	24.05	24.69	0.64	0.6882	0.21
18	24.03	24.69	0.66	0.7097	0.21
19	24.02	24.69	0.67	0.7204	0.22
20	24.01	24.69	0.68	0.7312	0.22
21	24.00	24.69	0.69	0.7419	0.22
22	23.99	24.69	0.70	0.7527	0.23
23	23.98	24.69	0.71	0.7634	0.23

24	23.97	24.69	0.72	0.7742	0.23
25	23.96	24.69	0.73	0.7849	0.24
26	23.95	24.69	0.74	0.7957	0.24

F27: Data for Core flooding 27 Test

Perforation Diameter =2.5mm Mass of Oil sat. sample = 24.67g Mass of Dry Sample = 21.62g Mass of Oil in sample =3.05 g Injection Pressure = 3bar

Injection Time	Mass of Flooded Sample	Mass of Saturated Sample M1	Mass of Oil Produced	Volume of Oil Produced	%OOIP of Oil produced
Min	M2(g)	M1(g)	M3(g)	V3(cc)	%
1	24.33	24.67	0.34	0.3656	0.11
2	24.31	24.67	0.36	0.3871	0.12
3	24.30	24.67	0.37	0.3978	0.12
4	24.28	24.67	0.39	0.4194	0.13
5	24.25	24.67	0.42	0.4516	0.14
6	24.22	24.67	0.45	0.4839	0.15
7	24.19	24.67	0.48	0.5161	0.16
8	24.17	24.67	0.50	0.5376	0.16
9	24.15	24.67	0.52	0.5591	0.17
10	24.11	24.67	0.56	0.6022	0.18
11	24.10	24.67	0.57	0.6129	0.19
12	24.09	24.67	0.58	0.6237	0.19
13	24.06	24.67	0.61	0.6559	0.20
14	24.03	24.67	0.64	0.6882	0.21
15	24.02	24.67	0.65	0.6989	0.21

16	24.00	24.67	0.67	0.7204	0.22
17	23.88	24.67	0.79	0.8495	0.26
18	23.77	24.67	0.90	0.9677	0.30
19	23.75	24.67	0.92	0.9892	0.30
20	23.74	24.67	0.93	1.0000	0.30
21	23.73	24.67	0.94	1.0108	0.31
22	23.73	24.67	0.94	1.0108	0.31
23	23.72	24.67	0.95	1.0215	0.31
24	23.71	24.67	0.96	1.0323	0.31
25	23.69	24.67	0.98	1.0538	0.32
26	23.69	24.67	0.98	1.0538	0.32

F28: Data for Core flooding 28 Test

Perforation Diameter =2.5mm

Mass of Oil sat. sample = 24.67g

Mass of Dry Sample = 21.62g

Mass of Oil in sample =3.05 g

Injection Pressure = 4bar

Injection Time	Mass of Flooded Sample	Mass of Saturated Sample M1	Mass of Oil Produced	Volume of Oil Produced	%OOIP of Oil produced
Min	M2(g)	M1(g)	M3(g)	V3(cc)	%
1	24.17	24.67	0.50	0.5376	0.16
2	24.13	24.67	0.54	0.5806	0.18
3	24.11	24.67	0.56	0.6022	0.18
4	24.07	24.67	0.60	0.6452	0.20
5	24.04	24.67	0.63	0.6774	0.21
6	24.00	24.67	0.67	0.7204	0.22

7	23.95	24.67	0.72	0.7742	0.24
8	23.91	24.67	0.76	0.8172	0.25
9	23.88	24.67	0.79	0.8495	0.26
10	23.84	24.67	0.83	0.8925	0.27
11	23.82	24.67	0.85	0.9140	0.28
12	23.81	24.67	0.86	0.9247	0.28
13	23.77	24.67	0.90	0.9677	0.30
14	23.74	24.67	0.93	1.0000	0.30
15	23.72	24.67	0.95	1.0215	0.31
16	23.71	24.67	0.96	1.0323	0.31
17	23.70	24.67	0.97	1.0430	0.32
18	23.68	24.67	0.99	1.0645	0.32
19	23.67	24.67	1.00	1.0753	0.33
20	23.67	24.67	1.00	1.0753	0.33
21	23.64	24.67	1.03	1.1075	0.34
22	23.64	24.67	1.03	1.1075	0.34
23	23.63	24.67	1.04	1.1183	0.34
24	23.63	24.67	1.04	1.1183	0.34
25	23.62	24.67	1.05	1.1290	0.34
26	23.61	24.67	1.06	1.1398	0.35

F29: Data for Core flooding 29 Test

Perforation Diameter =2.5mm

Mass of Oil sat. sample = 24.71g

Mass of Dry Sample = 21.62g

Mass of Oil in sample =3.09 g

Injection Pressure = 5bar

Injection Time	Mass of Flooded Sample	Mass of Saturated Sample M1	Mass of Oil Produced	Volume of Oil Produced	%OOIP of Oil produced
Min	M2(g)	M1(g)	M3(g)	V3(cc)	%
1	23.96	24.71	0.75	0.8065	0.24
2	23.92	24.71	0.79	0.8495	0.26
3	23.86	24.71	0.85	0.9140	0.28
4	23.83	24.71	0.88	0.9462	0.28
5	23.79	24.71	0.92	0.9892	0.30
6	23.77	24.71	0.94	1.0108	0.30
7	23.75	24.71	0.96	1.0323	0.31
8	23.71	24.71	1.00	1.0753	0.32
9	23.68	24.71	1.03	1.1075	0.33
10	23.66	24.71	1.05	1.1290	0.34
11	23.62	24.71	1.09	1.1720	0.35
12	23.61	24.71	1.10	1.1828	0.36
13	23.50	24.71	1.21	1.3011	0.39
14	23.47	24.71	1.24	1.3333	0.40
15	23.38	24.71	1.33	1.4301	0.43
16	23.36	24.71	1.35	1.4516	0.44
17	23.31	24.71	1.40	1.5054	0.45
18	23.29	24.71	1.42	1.5269	0.46
19	23.28	24.71	1.43	1.5376	0.46

20	23.27	24.71	1.44	1.5484	0.47
21	23.27	24.71	1.44	1.5484	0.47
22	23.26	24.71	1.45	1.5591	0.47
23	23.26	24.71	1.45	1.5591	0.47
24	23.25	24.71	1.46	1.5699	0.47
25	23.24	24.71	1.47	1.5806	0.48
26	23.23	24.71	1.48	1.5914	0.48

F30: Data for Core flooding 30 Test

Perforation Diameter =2.5mm Mass of Oil sat. sample = 24.65g Mass of Dry Sample = 21.62g Mass of Oil in sample =3.093g Injection Pressure = 6bar

Injection Time	Mass of Flooded Sample	Mass of Saturated Sample M1	Mass of Oil Produced	Volume of Oil Produced	%OOIP of Oil produced
Min	M2(g)	M1(g)	M3(g)	V3(cc)	%
1	24.23	24.65	0.42	0.4516	0.14
2	23.78	24.65	0.87	0.9355	0.29
3	23.75	24.65	0.90	0.9677	0.30
4	23.71	24.65	0.94	1.0108	0.31
5	23.70	24.65	0.95	1.0215	0.31
6	23.63	24.65	1.02	1.0968	0.34
7	23.60	24.65	1.05	1.1290	0.35
8	23.54	24.65	1.11	1.1935	0.37
9	23.52	24.65	1.13	1.2151	0.37
10	23.39	24.65	1.26	1.3548	0.42
11	23.24	24.65	1.41	1.5161	0.47
12	23.12	24.65	1.53	1.6452	0.50

13	23.11	24.65	1.54	1.6559	0.51
14	23.10	24.65	1.55	1.6667	0.51
15	23.10	24.65	1.55	1.6667	0.51
16	23.09	24.65	1.56	1.6774	0.51
17	23.08	24.65	1.57	1.6882	0.52
18	23.08	24.65	1.57	1.6882	0.52
19	23.04	24.65	1.61	1.7312	0.53
20	23.04	24.65	1.61	1.7312	0.53
21	23.03	24.65	1.62	1.7419	0.53
22	23.02	24.65	1.63	1.7527	0.54
23	23.00	24.65	1.65	1.7742	0.54
24	23.00	24.65	1.65	1.7742	0.54
25	23.00	24.65	1.65	1.7742	0.54
26	22.99	24.65	1.66	1.7849	0.55

F31: Data for Core flooding 31 Test

Perforation Diameter =3.0mm		Mass of Oil sat. sample = 24.66g		Mass of Dry Sample = 21.81g		Mass of Oil in sample =2.85g		Injection Pressure = 1bar			
Injection Time		Mass of Flooded Sample		Mass of Saturated Sample M1		Mass of Oil Produced		Volume of Oil Produced		%OOIP of Oil produced	
Min		M2(g)		M1(g)		M3(g)		V3(cc)		%	
1		24.42		24.66		0.24		0.2581		0.08	
2		24.38		24.66		0.28		0.3011		0.10	
3		24.35		24.66		0.31		0.3333		0.11	

4	24.32	24.66	0.34	0.3656	0.12
5	24.30	24.66	0.36	0.3871	0.13
6	24.26	24.66	0.40	0.4301	0.14
7	24.22	24.66	0.44	0.4731	0.15
8	24.16	24.66	0.50	0.5376	0.18
9	24.10	24.66	0.56	0.6022	0.20
10	24.06	24.66	0.60	0.6452	0.21
11	24.02	24.66	0.64	0.6882	0.22
12	23.99	24.66	0.67	0.7204	0.24
13	23.96	24.66	0.70	0.7527	0.25
14	23.94	24.66	0.72	0.7742	0.25
15	23.91	24.66	0.75	0.8065	0.26
16	23.90	24.66	0.76	0.8172	0.27
17	23.90	24.66	0.76	0.8172	0.27
18	23.88	24.66	0.78	0.8387	0.27
19	23.86	24.66	0.80	0.8602	0.28
20	23.85	24.66	0.81	0.8710	0.28
21	23.85	24.66	0.81	0.8710	0.28
22	23.84	24.66	0.82	0.8817	0.29
23	23.84	24.66	0.82	0.8817	0.29
24	23.83	24.66	0.83	0.8925	0.29
25	23.83	24.66	0.83	0.8925	0.29
26	23.82	24.66	0.84	0.9032	0.29

F32: Data for Core flooding 32 Test

Perforation Diameter =3.0mm

Mass of Oil sat. sample = 24.65g

Mass of Dry Sample = 21.81g

Mass of Oil in sample =2.84g

Injection Pressure = 2bar

Injection Time	Mass of Flooded Sample	Mass of Saturated Sample M1	Mass of Oil Produced	Volume of Oil Produced	%OIP of Oil produced
Min	M2(g)	M1(g)	M3(g)	V3(cc)	%
1	24.22	24.65	0.43	0.4624	0.15
2	24.18	24.65	0.47	0.5054	0.17
3	24.12	24.65	0.53	0.5699	0.19
4	24.08	24.65	0.57	0.6129	0.20
5	24.04	24.65	0.61	0.6559	0.21
6	24.02	24.65	0.63	0.6774	0.22
7	23.99	24.65	0.66	0.7097	0.23
8	23.95	24.65	0.70	0.7527	0.25
9	23.92	24.65	0.73	0.7849	0.26
10	23.89	24.65	0.76	0.8172	0.27
11	23.87	24.65	0.78	0.8387	0.27
12	23.86	24.65	0.79	0.8495	0.28
13	23.83	24.65	0.82	0.8817	0.29
14	23.81	24.65	0.84	0.9032	0.30
15	23.81	24.65	0.84	0.9032	0.30
16	23.80	24.65	0.85	0.9140	0.30
17	23.79	24.65	0.86	0.9247	0.30
18	23.78	24.65	0.87	0.9355	0.31

19	23.77	24.65	0.88	0.9462	0.31
20	23.76	24.65	0.89	0.9570	0.31
21	23.75	24.65	0.90	0.9677	0.32
22	23.75	24.65	0.90	0.9677	0.32
23	23.75	24.65	0.90	0.9677	0.32
24	23.75	24.65	0.90	0.9677	0.32
25	23.74	24.65	0.91	0.9785	0.32
26	23.74	24.65	0.91	0.9785	0.32

F33: Data for Core flooding 33 Test

Perforation Diameter =3.0mm

Mass of Oil sat. sample = 24.72g

Mass of Dry Sample = 21.81g

Mass of Oil in sample =2.91g

Injection Pressure = 3bar

Injection Time	Mass of Flooded Sample	Mass of Saturated Sample M1	Mass of Oil Produced	Volume of Oil Produced	%OIP of Oil produced
Min	M2(g)	M1(g)	M3(g)	V3(cc)	%
1	24.20	24.72	0.52	0.5591	0.18
2	24.00	24.72	0.72	0.7742	0.25
3	23.97	24.72	0.75	0.8065	0.26
4	23.92	24.72	0.80	0.8602	0.27
5	23.89	24.72	0.83	0.8925	0.29
6	23.86	24.72	0.86	0.9247	0.30
7	23.84	24.72	0.88	0.9462	0.30
8	23.82	24.72	0.90	0.9677	0.31
9	23.80	24.72	0.92	0.9892	0.32
10	23.78	24.72	0.94	1.0108	0.32
11	23.76	24.72	0.96	1.0323	0.33

12	23.74	24.72	0.98	1.0538	0.34
13	23.72	24.72	1.00	1.0753	0.34
14	23.70	24.72	1.02	1.0968	0.35
15	23.68	24.72	1.04	1.1183	0.36
16	23.67	24.72	1.05	1.1290	0.36
17	23.67	24.72	1.05	1.1290	0.36
18	23.65	24.72	1.07	1.1505	0.37
19	23.65	24.72	1.07	1.1505	0.37
20	23.64	24.72	1.08	1.1613	0.37
21	23.64	24.72	1.08	1.1613	0.37
22	23.64	24.72	1.08	1.1613	0.37
23	23.63	24.72	1.09	1.1720	0.37
24	23.63	24.72	1.09	1.1720	0.37
25	23.63	24.72	1.09	1.1720	0.37
26	23.63	24.72	1.09	1.1720	0.37

F34: Data for Core flooding 34 Test

Perforation Diameter =3.0mm		Mass of Oil sat. sample = 24.67g		Mass of Dry Sample = 21.81g		Mass of Oil in sample =2.86g		Injection Pressure = 4bar			
Injection Time		Mass of Flooded Sample		Mass of Saturated Sample M1		Mass of Oil Produced		Volume of Oil Produced		%OOIP of Oil produced	
Min		M2(g)		M1(g)		M3(g)		V3(cc)		%	
1		24.15		24.67		0.52		0.5591		0.18	
2		24.12		24.67		0.55		0.5914		0.19	

3	24.10	24.67	0.57	0.6129	0.20
4	23.90	24.67	0.77	0.8280	0.27
5	23.90	24.67	0.77	0.8280	0.27
6	23.83	24.67	0.84	0.9032	0.29
7	23.80	24.67	0.87	0.9355	0.30
8	23.77	24.67	0.90	0.9677	0.31
9	23.74	24.67	0.93	1.0000	0.33
10	23.72	24.67	0.95	1.0215	0.33
11	23.70	24.67	0.97	1.0430	0.34
12	23.66	24.67	1.01	1.0860	0.35
13	23.62	24.67	1.05	1.1290	0.37
14	23.60	24.67	1.07	1.1505	0.37
15	23.59	24.67	1.08	1.1613	0.38
16	23.59	24.67	1.08	1.1613	0.38
17	23.59	24.67	1.08	1.1613	0.38
18	23.57	24.67	1.10	1.1828	0.38
19	23.56	24.67	1.11	1.1935	0.39
20	23.54	24.67	1.13	1.2151	0.40
21	23.54	24.67	1.13	1.2151	0.40
22	23.53	24.67	1.14	1.2258	0.40
23	23.53	24.67	1.14	1.2258	0.40
24	23.52	24.67	1.15	1.2366	0.40
25	23.52	24.67	1.15	1.2366	0.40

26

23.51

24.67

1.16

1.2473

0.41

F35: Data for Core flooding 35 Test

Perforation Diameter =3.0mm

Mass of Oil sat. sample = 24.68g

Mass of Dry Sample = 21.81g

Mass of Oil in sample =2.87g

Injection Pressure = 5bar

Injection Time	Mass of Flooded Sample	Mass of Saturated Sample M1	Mass of Oil Produced	Volume of Oil Produced	%OIP of Oil produced
Min	M2(g)	M1(g)	M3(g)	V3(cc)	%
1	23.71	24.68	0.97	1.0430	0.34
2	23.56	24.68	1.12	1.2043	0.39
3	23.49	24.68	1.19	1.2796	0.41
4	23.47	24.68	1.21	1.3011	0.42
5	23.38	24.68	1.30	1.3978	0.45
6	23.32	24.68	1.36	1.4624	0.47
7	23.31	24.68	1.37	1.4731	0.48
8	23.27	24.68	1.41	1.5161	0.49
9	23.25	24.68	1.43	1.5376	0.50
10	23.22	24.68	1.46	1.5699	0.51
11	23.20	24.68	1.48	1.5914	0.52
12	23.18	24.68	1.50	1.6129	0.52
13	23.16	24.68	1.52	1.6344	0.53
14	23.16	24.68	1.52	1.6344	0.53
15	23.16	24.68	1.52	1.6344	0.53
16	23.15	24.68	1.53	1.6452	0.53

17	23.14	24.68	1.54	1.6559	0.54
18	23.13	24.68	1.55	1.6667	0.54
19	23.13	24.68	1.55	1.6667	0.54
20	23.10	24.68	1.58	1.6989	0.55
21	23.09	24.68	1.59	1.7097	0.55
22	23.08	24.68	1.60	1.7204	0.56
23	23.08	24.68	1.60	1.7204	0.56
24	23.07	24.68	1.61	1.7312	0.56
25	23.07	24.68	1.61	1.7312	0.56
26	23.06	24.68	1.62	1.7419	0.56

F36: Data for Core flooding 36 Test

Perforation Diameter =3.0mm

Mass of Oil sat. sample = 24.69g

Mass of Dry Sample = 21.81g

Mass of Oil in sample =2.88g

Injection Pressure = 6bar

Injection Time	Mass of Flooded Sample	Mass of Saturated Sample M1	Mass of Oil Produced	Volume of Oil Produced	%OOIP of Oil produced
Min	M2(g)	M1(g)	M3(g)	V3(cc)	%
1	23.71	24.69	0.98	1.0538	0.34
2	23.58	24.69	1.11	1.1935	0.39
3	23.49	24.69	1.20	1.2903	0.42
4	23.47	24.69	1.22	1.3118	0.43
5	23.45	24.69	1.24	1.3333	0.43
6	23.41	24.69	1.28	1.3763	0.45
7	23.38	24.69	1.31	1.4086	0.46
8	23.32	24.69	1.37	1.4731	0.48
9	23.25	24.69	1.44	1.5484	0.50

10	23.22	24.69	1.47	1.5806	0.51
11	23.20	24.69	1.49	1.6022	0.52
12	23.18	24.69	1.51	1.6237	0.53
13	23.16	24.69	1.53	1.6452	0.53
14	23.16	24.69	1.53	1.6452	0.53
15	23.16	24.69	1.53	1.6452	0.53
16	23.15	24.69	1.54	1.6559	0.54
17	23.13	24.69	1.56	1.6774	0.55
18	23.13	24.69	1.56	1.6774	0.55
19	23.13	24.69	1.56	1.6774	0.55
20	23.10	24.69	1.59	1.7097	0.56
21	23.09	24.69	1.60	1.7204	0.56
22	23.08	24.69	1.61	1.7312	0.56
23	23.07	24.69	1.62	1.7419	0.57
24	23.07	24.69	1.62	1.7419	0.57
25	23.07	24.69	1.62	1.7419	0.57
26	23.06	24.69	1.63	1.7527	0.57

Appendix G: Core Flooding Test-Homogeneous Model

G1: Data for Core flooding Test 1

Perforation Diameter =0.5mm

Mass of Oil sat. sample = 25.83g

Mass of Dry Sample = 23.03g

Mass of Oil in sample =2.8g

Injection Pressure = 1bar

Injection Time	Mass of Flooded Sample	Mass of Saturated Sample M1	Mass of Oil Produced	Volume of Oil Produced	%OOIP of Oil produced
Min	M2(g)	M1(g)	M3(g)	V3(cc)	%
1	25.63	25.83	0.20	0.2151	0.071
2	25.33	25.83	0.50	0.5376	0.179
3	25.13	25.83	0.70	0.7527	0.250
4	25.03	25.83	0.80	0.8602	0.286
5	24.95	25.83	0.88	0.9462	0.314
6	24.91	25.83	0.92	0.9892	0.329
7	24.87	25.83	0.96	1.0323	0.343
8	24.84	25.83	0.99	1.0645	0.354
9	24.80	25.83	1.03	1.1075	0.368
10	24.77	25.83	1.06	1.1398	0.379
11	24.74	25.83	1.09	1.1720	0.389
12	24.71	25.83	1.12	1.2043	0.400
13	24.69	25.83	1.14	1.2258	0.407
14	24.68	25.83	1.15	1.2366	0.411
15	24.66	25.83	1.17	1.2581	0.418
16	24.65	25.83	1.18	1.2688	0.421
17	24.65	25.83	1.18	1.2688	0.421

18	24.64	25.83	1.19	1.2796	0.425
19	24.64	25.83	1.19	1.2796	0.425
20	24.64	25.83	1.19	1.2796	0.425
21	24.64	25.83	1.19	1.2796	0.425
22	24.64	25.83	1.19	1.2796	0.425
23	24.64	25.83	1.19	1.2796	0.425
24	24.64	25.83	1.19	1.2796	0.425
25	24.64	25.83	1.19	1.2796	0.425
26	24.64	25.83	1.19	1.2796	0.425

G2: Data for Core flooding Test 2

Perforation Diameter =0.5mm

Mass of Oil sat. sample = 25.83g

Mass of Dry Sample = 23.03g

Mass of Oil in sample =2.8g

Injection Pressure = 2bar

Injection Time	Mass of Flooded Sample	Mass of Saturated Sample M1	Mass of Oil Produced	Volume of Oil Produced	%OOIP of Oil produced
Min	M2(g)	M1(g)	M3(g)	V3(cc)	%
1	25.55	25.83	0.28	0.301	0.100
2	25.25	25.83	0.58	0.624	0.207
3	24.95	25.83	0.88	0.946	0.314
4	24.75	25.83	1.08	1.161	0.386
5	24.67	25.83	1.16	1.247	0.414
6	24.63	25.83	1.20	1.290	0.429
7	24.59	25.83	1.24	1.333	0.443
8	24.56	25.83	1.27	1.366	0.454
9	24.52	25.83	1.31	1.409	0.468
10	24.49	25.83	1.34	1.441	0.479

11	24.46	25.83	1.37	1.473	0.489
12	24.43	25.83	1.40	1.505	0.500
13	24.41	25.83	1.42	1.527	0.507
14	24.39	25.83	1.44	1.548	0.514
15	24.37	25.83	1.46	1.570	0.521
16	24.36	25.83	1.47	1.581	0.525
17	24.35	25.83	1.48	1.591	0.529
18	24.34	25.83	1.49	1.602	0.532
19	24.34	25.83	1.49	1.602	0.532
20	24.34	25.83	1.49	1.602	0.532
21	24.34	25.83	1.49	1.602	0.532
22	24.34	25.83	1.49	1.602	0.532
23	24.34	25.83	1.49	1.602	0.532
24	24.34	25.83	1.49	1.602	0.532
25	24.34	25.83	1.49	1.602	0.532
26	24.34	25.83	1.49	1.602	0.532

G3: Data for Core flooding Test 3

Perforation Diameter =0.5mm

Mass of Oil sat. sample = 25.82g

Mass of Dry Sample = 23.03g

Mass of Oil in sample =2.7g

Injection Pressure = 3bar

Injection Time	Mass of Flooded Sample	Mass of Saturated Sample M1	Mass of Oil Produced	Volume of Oil Produced	%OOIP of Oil produced
Min	M2(g)	M1(g)	M3(g)	V3(cc)	%
1	25.43	25.82	0.39	0.4194	0.140
2	25.13	25.82	0.69	0.7419	0.247
3	24.83	25.82	0.99	1.0645	0.355

4	24.63	25.82	1.19	1.2796	0.427
5	24.55	25.82	1.27	1.3656	0.455
6	24.51	25.82	1.31	1.4086	0.470
7	24.47	25.82	1.35	1.4516	0.484
8	24.44	25.82	1.38	1.4839	0.495
9	24.4	25.82	1.42	1.5269	0.509
10	24.37	25.82	1.45	1.5591	0.520
11	24.34	25.82	1.48	1.5914	0.530
12	24.31	25.82	1.51	1.6237	0.541
13	24.29	25.82	1.53	1.6452	0.548
14	24.27	25.82	1.55	1.6667	0.556
15	24.25	25.82	1.57	1.6882	0.563
16	24.24	25.82	1.58	1.6989	0.566
17	24.23	25.82	1.59	1.7097	0.570
18	24.22	25.82	1.60	1.7204	0.573
19	24.22	25.82	1.60	1.7204	0.573
20	24.22	25.82	1.60	1.7204	0.573
21	24.22	25.82	1.60	1.7204	0.573
22	24.22	25.82	1.60	1.7204	0.573
23	24.22	25.82	1.60	1.7204	0.573
24	24.22	25.82	1.60	1.7204	0.573
25	24.22	25.82	1.60	1.7204	0.573
26	24.22	25.82	1.60	1.7204	0.573

G4: Data for Core flooding Test 4

Perforation Diameter =0.5mm

Mass of Oil sat. sample = 25.83g

Mass of Dry Sample = 23.03g

Mass of Oil in sample =2.8g

Injection Pressure = 4bar

Injection Time	Mass of Flooded Sample	Mass of Saturated Sample M1	Mass of Oil Produced	Volume of Oil Produced	%OOIP of Oil produced
Min	M2(g)	M1(g)	M3(g)	V3(cc)	%
1	25.26	25.83	0.57	0.6129	0.204
2	24.96	25.83	0.87	0.9355	0.311
3	24.66	25.83	1.17	1.2581	0.418
4	24.46	25.83	1.37	1.4731	0.489
5	24.38	25.83	1.45	1.5591	0.518
6	24.34	25.83	1.49	1.6022	0.532
7	24.3	25.83	1.53	1.6452	0.546
8	24.27	25.83	1.56	1.6774	0.557
9	24.23	25.83	1.60	1.7204	0.571
10	24.2	25.83	1.63	1.7527	0.582
11	24.17	25.83	1.66	1.7849	0.593
12	24.14	25.83	1.69	1.8172	0.604
13	24.12	25.83	1.71	1.8387	0.611
14	24.1	25.83	1.73	1.8602	0.618
15	24.08	25.83	1.75	1.8817	0.625
16	24.07	25.83	1.76	1.8925	0.629
17	24.06	25.83	1.77	1.9032	0.632
18	24.05	25.83	1.78	1.9140	0.636
19	24.05	25.83	1.78	1.9140	0.636

20	24.05	25.83	1.78	1.9140	0.636
21	24.05	25.83	1.78	1.9140	0.636
22	24.05	25.83	1.78	1.9140	0.636
23	24.05	25.83	1.78	1.9140	0.636
24	24.05	25.83	1.78	1.9140	0.636
25	24.05	25.83	1.78	1.9140	0.636
26	24.05	25.83	1.78	1.9140	0.636

G5: Data for Core flooding Test 5

Perforation Diameter =0.5mm

Mass of Oil sat. sample = 25.83g

Mass of Dry Sample = 23.03g

Mass of Oil in sample =2.8g

Injection Pressure = 5bar

Injection Time	Mass of Flooded Sample	Mass of Saturated Sample M1	Mass of Oil Produced	Volume of Oil Produced	%OOIP of Oil produced
Min	M2(g)	M1(g)	M3(g)	V3(cc)	%
1	25.02	25.81	0.79	0.8495	0.284
2	24.72	25.81	1.09	1.1720	0.392
3	24.52	25.81	1.29	1.3871	0.464
4	24.42	25.81	1.39	1.4946	0.500
5	24.34	25.81	1.47	1.5806	0.529
6	24.3	25.81	1.51	1.6237	0.543
7	24.26	25.81	1.55	1.6667	0.558
8	24.23	25.81	1.58	1.6989	0.568
9	24.19	25.81	1.62	1.7419	0.583
10	24.16	25.81	1.65	1.7742	0.594
11	24.13	25.81	1.68	1.8065	0.604
12	24.1	25.81	1.71	1.8387	0.615

13	24.08	25.81	1.73	1.8602	0.622
14	24.06	25.81	1.75	1.8817	0.629
15	24.04	25.81	1.77	1.9032	0.637
16	24.03	25.81	1.78	1.9140	0.640
17	24.02	25.81	1.79	1.9247	0.644
18	24.01	25.81	1.80	1.9355	0.647
19	24.01	25.81	1.80	1.9355	0.647
20	24.01	25.81	1.80	1.9355	0.647
21	24.01	25.81	1.80	1.9355	0.647
22	24.01	25.81	1.80	1.9355	0.647
23	24.01	25.81	1.80	1.9355	0.647
24	24.01	25.81	1.80	1.9355	0.647
25	24.01	25.81	1.80	1.9355	0.647
26	24.01	25.81	1.80	1.9355	0.647

G6: Data for Core flooding Test 6

Perforation Diameter =0.5mm

Mass of Oil sat. sample = 25.83g

Mass of Dry Sample = 23.03g

Mass of Oil in sample =2.8g

Injection Pressure = 6bar

Injection Time	Mass of Flooded Sample	Mass of Saturated Sample M1	Mass of Oil Produced	Volume of Oil Produced	%OOIP of Oil produced
Min	M2(g)	M1(g)	M3(g)	V3(cc)	%
1	24.83	25.83	1.00	1.0753	0.357
2	24.53	25.83	1.30	1.3978	0.464
3	24.33	25.83	1.50	1.6129	0.536
4	24.23	25.83	1.60	1.7204	0.571
5	24.15	25.83	1.68	1.8065	0.600

6	24.11	25.83	1.72	1.8495	0.614
7	24.07	25.83	1.76	1.8925	0.629
8	24.04	25.83	1.79	1.9247	0.639
9	24	25.83	1.83	1.9677	0.654
10	23.97	25.83	1.86	2.0000	0.664
11	23.94	25.83	1.89	2.0323	0.675
12	23.91	25.83	1.92	2.0645	0.686
13	23.89	25.83	1.94	2.0860	0.693
14	23.87	25.83	1.96	2.1075	0.700
15	23.85	25.83	1.98	2.1290	0.707
16	23.84	25.83	1.99	2.1398	0.711
17	23.83	25.83	2.00	2.1505	0.714
18	23.82	25.83	2.01	2.1613	0.718
19	23.82	25.83	2.01	2.1613	0.718
20	23.82	25.83	2.01	2.1613	0.718
21	23.82	25.83	2.01	2.1613	0.718
22	23.82	25.83	2.01	2.1613	0.718
23	23.82	25.83	2.01	2.1613	0.718
24	23.82	25.83	2.01	2.1613	0.718
25	23.82	25.83	2.01	2.1613	0.718
26	23.82	25.83	2.01	2.1613	0.718

G7: Data for Core flooding Test 7

Perforation Diameter =1.0mm

Mass of Oil sat. sample = 25.81g

Mass of Dry Sample = 23.02g

Mass of Oil in sample =2.79g

Injection Pressure = 1bar

Injection Time	Mass of Flooded Sample	Mass of Saturated Sample M1	Mass of Oil Produced	Volume of Oil Produced	%OOIP of Oil produced
Min	M2(g)	M1(g)	M3(g)	V3(cc)	%
1	25.69	25.81	0.12	0.1290	0.043
2	25.39	25.81	0.42	0.4516	0.151
3	25.19	25.81	0.62	0.6667	0.222
4	25.09	25.81	0.72	0.7742	0.258
5	25.01	25.81	0.80	0.8602	0.287
6	24.97	25.81	0.84	0.9032	0.301
7	24.93	25.81	0.88	0.9462	0.315
8	24.90	25.81	0.91	0.9785	0.326
9	24.86	25.81	0.95	1.0215	0.341
10	24.83	25.81	0.98	1.0538	0.351
11	24.80	25.81	1.01	1.0860	0.362
12	24.77	25.81	1.04	1.1183	0.373
13	24.75	25.81	1.06	1.1398	0.380
14	24.74	25.81	1.07	1.1505	0.384
15	24.72	25.81	1.09	1.1720	0.391
16	24.71	25.81	1.10	1.1828	0.394
17	24.71	25.81	1.10	1.1828	0.394
18	24.70	25.81	1.11	1.1935	0.398
19	24.70	25.81	1.11	1.1935	0.398

20	24.70	25.81	1.11	1.1935	0.398
21	24.70	25.81	1.11	1.1935	0.398
22	24.70	25.81	1.11	1.1935	0.398
23	24.70	25.81	1.11	1.1935	0.398
24	24.70	25.81	1.11	1.1935	0.398
25	24.70	25.81	1.11	1.1935	0.398
26	24.70	25.81	1.11	1.1935	0.398

G8: Data for Core flooding Test 8

Perforation Diameter =1.0mm Mass of Oil sat. sample = 25.83g Mass of Dry Sample = 23.02g Mass of Oil in sample =2.81g Injection Pressure = 2bar

Injection Time	Mass of Flooded Sample	Mass of Saturated Sample M1	Mass of Oil Produced	Volume of Oil Produced	%OOIP of Oil produced
Min	M2(g)	M1(g)	M3(g)	V3(cc)	%
1	25.6	25.83	0.23	0.2473	0.082
2	25.3	25.83	0.53	0.5699	0.189
3	25	25.83	0.83	0.8925	0.295
4	24.8	25.83	1.03	1.1075	0.367
5	24.72	25.83	1.11	1.1935	0.395
6	24.68	25.83	1.15	1.2366	0.409
7	24.64	25.83	1.19	1.2796	0.423
8	24.61	25.83	1.22	1.3118	0.434
9	24.57	25.83	1.26	1.3548	0.448
10	24.54	25.83	1.29	1.3871	0.459
11	24.51	25.83	1.32	1.4194	0.470
12	24.48	25.83	1.35	1.4516	0.480

13	24.46	25.83	1.37	1.4731	0.488
14	24.44	25.83	1.39	1.4946	0.495
15	24.42	25.83	1.41	1.5161	0.502
16	24.41	25.83	1.42	1.5269	0.505
17	24.41	25.83	1.42	1.5269	0.505
18	24.4	25.83	1.43	1.5376	0.509
19	24.4	25.83	1.43	1.5376	0.509
20	24.4	25.83	1.43	1.5376	0.509
21	24.4	25.83	1.43	1.5376	0.509
22	24.4	25.83	1.43	1.5376	0.509
23	24.4	25.83	1.43	1.5376	0.509
24	24.39	25.83	1.44	1.5484	0.512
25	24.39	25.83	1.44	1.5484	0.512
26	24.39	25.83	1.44	1.5484	0.512

G9: Data for Core flooding Test 9

Perforation Diameter =1.0mm

Mass of Oil sat. sample = 25.82g

Mass of Dry Sample = 23.02g

Mass of Oil in sample =2.8g

Injection Pressure = 3bar

Injection Time	Mass of Flooded Sample	Mass of Saturated Sample M1	Mass of Oil Produced	Volume of Oil Produced	%OOIP of Oil produced
Min	M2(g)	M1(g)	M3(g)	V3(cc)	%
1	25.5	25.82	0.32	0.3441	0.114
2	25.2	25.82	0.62	0.6667	0.221
3	24.9	25.82	0.92	0.9892	0.329
4	24.7	25.82	1.12	1.2043	0.400
5	24.62	25.82	1.20	1.2903	0.429

6	24.58	25.82	1.24	1.3333	0.443
7	24.54	25.82	1.28	1.3763	0.457
8	24.51	25.82	1.31	1.4086	0.468
9	24.47	25.82	1.35	1.4516	0.482
10	24.44	25.82	1.38	1.4839	0.493
11	24.41	25.82	1.41	1.5161	0.504
12	24.38	25.82	1.44	1.5484	0.514
13	24.36	25.82	1.46	1.5699	0.521
14	24.34	25.82	1.48	1.5914	0.529
15	24.32	25.82	1.50	1.6129	0.536
16	24.31	25.82	1.51	1.6237	0.539
17	24.3	25.82	1.52	1.6344	0.543
18	24.29	25.82	1.53	1.6452	0.546
19	24.29	25.82	1.53	1.6452	0.546
20	24.29	25.82	1.53	1.6452	0.546
21	24.29	25.82	1.53	1.6452	0.546
22	24.29	25.82	1.53	1.6452	0.546
23	24.29	25.82	1.53	1.6452	0.546
24	24.29	25.82	1.53	1.6452	0.546
25	24.29	25.82	1.53	1.6452	0.546
26	24.29	25.82	1.53	1.6452	0.546

G10: Data for Core flooding Test 10

Perforation Diameter =1.0mm Mass of Oil sat. sample = 25.83g Mass of Dry Sample = 23.02g Mass of Oil in sample =2.81g Injection Pressure = 4bar

Injection Time	Mass of Flooded Sample	Mass of Saturated Sample M1	Mass of Oil Produced	Volume of Oil Produced	%OOIP of Oil produced
Min	M2(g)	M1(g)	M3(g)	V3(cc)	%
1	25.33	25.83	0.50	0.5376	0.178
2	25.03	25.83	0.80	0.8602	0.285
3	24.73	25.83	1.10	1.1828	0.391
4	24.53	25.83	1.30	1.3978	0.463
5	24.45	25.83	1.38	1.4839	0.491
6	24.41	25.83	1.42	1.5269	0.505
7	24.37	25.83	1.46	1.5699	0.520
8	24.34	25.83	1.49	1.6022	0.530
9	24.3	25.83	1.53	1.6452	0.544
10	24.27	25.83	1.56	1.6774	0.555
11	24.24	25.83	1.59	1.7097	0.566
12	24.21	25.83	1.62	1.7419	0.577
13	24.19	25.83	1.64	1.7634	0.584
14	24.17	25.83	1.66	1.7849	0.591
15	24.15	25.83	1.68	1.8065	0.598
16	24.14	25.83	1.69	1.8172	0.601
17	24.13	25.83	1.70	1.8280	0.605
18	24.12	25.83	1.71	1.8387	0.609
19	24.12	25.83	1.71	1.8387	0.609

20	24.12	25.83	1.71	1.8387	0.609
21	24.12	25.83	1.71	1.8387	0.609
22	24.11	25.83	1.72	1.8495	0.612
23	24.11	25.83	1.72	1.8495	0.612
24	24.11	25.83	1.72	1.8495	0.612
25	24.11	25.83	1.72	1.8495	0.612
26	24.11	25.83	1.72	1.8495	0.612

G11: Data for Core flooding Test 11

Perforation Diameter =1.0mm Mass of Oil sat. sample = 25.81g Mass of Dry Sample = 23.02g Mass of Oil in sample =2.79g Injection Pressure = 5bar

Injection Time	Mass of Flooded Sample	Mass of Saturated Sample M1	Mass of Oil Produced	Volume of Oil Produced	%OOIP of Oil produced
Min	M2(g)	M1(g)	M3(g)	V3(cc)	%
1	25.02	25.81	0.79	0.8495	0.284
2	24.72	25.81	1.09	1.1720	0.392
3	24.52	25.81	1.29	1.3871	0.464
4	24.42	25.81	1.39	1.4946	0.500
5	24.34	25.81	1.47	1.5806	0.529
6	24.3	25.81	1.51	1.6237	0.543
7	24.26	25.81	1.55	1.6667	0.558
8	24.23	25.81	1.58	1.6989	0.568
9	24.19	25.81	1.62	1.7419	0.583
10	24.16	25.81	1.65	1.7742	0.594

11	24.13	25.81	1.68	1.8065	0.604
12	24.1	25.81	1.71	1.8387	0.615
13	24.08	25.81	1.73	1.8602	0.622
14	24.06	25.81	1.75	1.8817	0.629
15	24.04	25.81	1.77	1.9032	0.637
16	24.03	25.81	1.78	1.9140	0.640
17	24.02	25.81	1.79	1.9247	0.644
18	24.01	25.81	1.80	1.9355	0.647
19	24.01	25.81	1.80	1.9355	0.647
20	24.01	25.81	1.80	1.9355	0.647
21	24.01	25.81	1.80	1.9355	0.647
22	24.01	25.81	1.80	1.9355	0.647
23	24.01	25.81	1.80	1.9355	0.647
24	24	25.81	1.81	1.9462	0.651
25	24	25.81	1.81	1.9462	0.651
26	24	25.81	1.81	1.9462	0.651

G12: Data for Core flooding Test 12

Perforation Diameter =1.0mm Mass of Oil sat. sample = 25.83g Mass of Dry Sample = 23.02g Mass of Oil in sample =2.81g Injection Pressure = 6bar

Injection Time	Mass of Flooded Sample	Mass of Saturated Sample M1	Mass of Oil Produced	Volume of Oil Produced	%OOIP of Oil produced
Min	M2(g)	M1(g)	M3(g)	V3(cc)	%
1	24.94	25.83	0.89	0.9570	0.317
2	24.64	25.83	1.19	1.2796	0.423
3	24.44	25.83	1.39	1.4946	0.495
4	24.34	25.83	1.49	1.6022	0.530
5	24.26	25.83	1.57	1.6882	0.559
6	24.22	25.83	1.61	1.7312	0.573
7	24.18	25.83	1.65	1.7742	0.587
8	24.15	25.83	1.68	1.8065	0.598
9	24.11	25.83	1.72	1.8495	0.612
10	24.08	25.83	1.75	1.8817	0.623
11	24.05	25.83	1.78	1.9140	0.633
12	24.02	25.83	1.81	1.9462	0.644
13	24.00	25.83	1.83	1.9677	0.651
14	23.98	25.83	1.85	1.9892	0.658
15	23.96	25.83	1.87	2.0108	0.665
16	23.95	25.83	1.88	2.0215	0.669
17	23.94	25.83	1.89	2.0323	0.673
18	23.93	25.83	1.90	2.0430	0.676
19	23.93	25.83	1.90	2.0430	0.676

20	23.93	25.83	1.90	2.0430	0.676
21	23.92	25.83	1.91	2.0538	0.680
22	23.92	25.83	1.91	2.0538	0.680
23	23.91	25.83	1.92	2.0645	0.683
24	23.91	25.83	1.92	2.0645	0.683
25	23.91	25.83	1.92	2.0645	0.683
26	23.91	25.83	1.92	2.0645	0.683

G13: Data for Core flooding Test 13

Perforation Diameter =1.5mm

Mass of Oil sat. sample = 25.83g

Mass of Dry Sample = 23.03g

Mass of Oil in sample =2.8g

Injection Pressure = 1bar

Injection Time	Mass of Flooded Sample	Mass of Saturated Sample M1	Mass of Oil Produced	Volume of Oil Produced	%OOIP of Oil produced
Min	M2(g)	M1(g)	M3(g)	V3(cc)	%
1	25.73	25.83	0.10	0.1075	0.036
2	25.43	25.83	0.40	0.4301	0.143
3	25.23	25.83	0.60	0.6452	0.214
4	25.13	25.83	0.70	0.7527	0.250
5	25.05	25.83	0.78	0.8387	0.279
6	25.01	25.83	0.82	0.8817	0.293
7	24.97	25.83	0.86	0.9247	0.307
8	24.94	25.83	0.89	0.9570	0.318
9	24.90	25.83	0.93	1.0000	0.332
10	24.87	25.83	0.96	1.0323	0.343
11	24.84	25.83	0.99	1.0645	0.354
12	24.81	25.83	1.02	1.0968	0.364

13	24.79	25.83	1.04	1.1183	0.371
14	24.78	25.83	1.05	1.1290	0.375
15	24.76	25.83	1.07	1.1505	0.382
16	24.75	25.83	1.08	1.1613	0.386
17	24.75	25.83	1.08	1.1613	0.386
18	24.74	25.83	1.09	1.1720	0.389
19	24.74	25.83	1.09	1.1720	0.389
20	24.74	25.83	1.09	1.1720	0.389
21	24.74	25.83	1.09	1.1720	0.389
22	24.74	25.83	1.09	1.1720	0.389
23	24.73	25.83	1.10	1.1828	0.393
24	24.73	25.83	1.10	1.1828	0.393
25	24.73	25.83	1.10	1.1828	0.393
26	24.73	25.83	1.10	1.1828	0.393

G14: Data for Core flooding Test 14

Perforation Diameter =1.5mm

Mass of Oil sat. sample = 25.83g

Mass of Dry Sample = 23.03g

Mass of Oil in sample =2.8g

Injection Pressure = 2bar

Injection Time	Mass of Flooded Sample	Mass of Saturated Sample M1	Mass of Oil Produced	Volume of Oil Produced	%OOIP of Oil produced
Min	M2(g)	M1(g)	M3(g)	V3(cc)	%
1	25.67	25.83	0.16	0.1720	0.057
2	25.37	25.83	0.46	0.4946	0.164
3	25.17	25.83	0.66	0.7097	0.236
4	25.07	25.83	0.76	0.8172	0.271
5	24.99	25.83	0.84	0.9032	0.300

6	24.95	25.83	0.88	0.9462	0.314
7	24.91	25.83	0.92	0.9892	0.329
8	24.88	25.83	0.95	1.0215	0.339
9	24.84	25.83	0.99	1.0645	0.354
10	24.81	25.83	1.02	1.0968	0.364
11	24.78	25.83	1.05	1.1290	0.375
12	24.75	25.83	1.08	1.1613	0.386
13	24.73	25.83	1.10	1.1828	0.393
14	24.71	25.83	1.12	1.2043	0.400
15	24.69	25.83	1.14	1.2258	0.407
16	24.68	25.83	1.15	1.2366	0.411
17	24.67	25.83	1.16	1.2473	0.414
18	24.66	25.83	1.17	1.2581	0.418
19	24.66	25.83	1.17	1.2581	0.418
20	24.66	25.83	1.17	1.2581	0.418
21	24.66	25.83	1.17	1.2581	0.418
22	24.66	25.83	1.17	1.2581	0.418
23	24.66	25.83	1.17	1.2581	0.418
24	24.66	25.83	1.17	1.2581	0.418
25	24.66	25.83	1.17	1.2581	0.418
26	24.66	25.83	1.17	1.2581	0.418

G15: Data for Core flooding Test 15

Perforation Diameter =1.5mm

Mass of Oil sat. sample = 25.83g

Mass of Dry Sample = 23.03g

Mass of Oil in sample =2.8g

Injection Pressure = 3bar

Injection Time	Mass of Flooded Sample	Mass of Saturated Sample M1	Mass of Oil Produced	Volume of Oil Produced	%OOIP of Oil produced
Min	M2(g)	M1(g)	M3(g)	V3(cc)	%
1	25.58	25.83	0.25	0.2688	0.089
2	25.28	25.83	0.55	0.5914	0.196
3	24.98	25.83	0.85	0.9140	0.304
4	24.78	25.83	1.05	1.1290	0.375
5	24.7	25.83	1.13	1.2151	0.404
6	24.66	25.83	1.17	1.2581	0.418
7	24.62	25.83	1.21	1.3011	0.432
8	24.59	25.83	1.24	1.3333	0.443
9	24.55	25.83	1.28	1.3763	0.457
10	24.52	25.83	1.31	1.4086	0.468
11	24.49	25.83	1.34	1.4409	0.479
12	24.46	25.83	1.37	1.4731	0.489
13	24.44	25.83	1.39	1.4946	0.496
14	24.42	25.83	1.41	1.5161	0.504
15	24.4	25.83	1.43	1.5376	0.511
16	24.39	25.83	1.44	1.5484	0.514
17	24.38	25.83	1.45	1.5591	0.518
18	24.37	25.83	1.46	1.5699	0.521
19	24.37	25.83	1.46	1.5699	0.521

20	24.37	25.83	1.46	1.5699	0.521
21	24.37	25.83	1.46	1.5699	0.521
22	24.37	25.83	1.46	1.5699	0.521
23	24.37	25.83	1.46	1.5699	0.521
24	24.37	25.83	1.46	1.5699	0.521
25	24.37	25.83	1.46	1.5699	0.521
26	24.37	25.83	1.46	1.5699	0.521

G16: Data for Core flooding Test 16

Perforation Diameter =1.5mm

Mass of Oil sat. sample = 25.83g

Mass of Dry Sample = 23.03g

Mass of Oil in sample =2.8g

Injection Pressure = 4bar

Injection Time	Mass of Flooded Sample	Mass of Saturated Sample M1	Mass of Oil Produced	Volume of Oil Produced	%OOIP of Oil produced
Min	M2(g)	M1(g)	M3(g)	V3(cc)	%
1	25.41	25.83	0.42	0.4516	0.150
2	25.11	25.83	0.72	0.7742	0.257
3	24.81	25.83	1.02	1.0968	0.364
4	24.61	25.83	1.22	1.3118	0.436
5	24.53	25.83	1.30	1.3978	0.464
6	24.49	25.83	1.34	1.4409	0.479
7	24.45	25.83	1.38	1.4839	0.493
8	24.42	25.83	1.41	1.5161	0.504
9	24.38	25.83	1.45	1.5591	0.518
10	24.35	25.83	1.48	1.5914	0.529
11	24.32	25.83	1.51	1.6237	0.539
12	24.29	25.83	1.54	1.6559	0.550

13	24.27	25.83	1.56	1.6774	0.557
14	24.25	25.83	1.58	1.6989	0.564
15	24.23	25.83	1.60	1.7204	0.571
16	24.23	25.83	1.60	1.7204	0.571
17	24.23	25.83	1.60	1.7204	0.571
18	24.23	25.83	1.60	1.7204	0.571
19	24.23	25.83	1.60	1.7204	0.571
20	24.23	25.83	1.60	1.7204	0.571
21	24.22	25.83	1.61	1.7312	0.575
22	24.22	25.83	1.61	1.7312	0.575
23	24.21	25.83	1.62	1.7419	0.579
24	24.21	25.83	1.62	1.7419	0.579
25	24.21	25.83	1.62	1.7419	0.579
26	24.21	25.83	1.62	1.7419	0.579

G17: Data for Core flooding Test 17

Perforation Diameter =1.5mm

Mass of Oil sat. sample = 25.83g

Mass of Dry Sample = 23.03g

Mass of Oil in sample =2.8g

Injection Pressure = 5bar

Injection Time	Mass of Flooded Sample	Mass of Saturated Sample M1	Mass of Oil Produced	Volume of Oil Produced	%OOIP of Oil produced
Min	M2(g)	M1(g)	M3(g)	V3(cc)	%
1	25.22	25.83	0.61	0.6559	0.218
2	24.92	25.83	0.91	0.9785	0.325
3	24.72	25.83	1.11	1.1935	0.396
4	24.62	25.83	1.21	1.3011	0.432
5	24.54	25.83	1.29	1.3871	0.461

6	24.5	25.83	1.33	1.4301	0.475
7	24.46	25.83	1.37	1.4731	0.489
8	24.43	25.83	1.40	1.5054	0.500
9	24.39	25.83	1.44	1.5484	0.514
10	24.36	25.83	1.47	1.5806	0.525
11	24.33	25.83	1.50	1.6129	0.536
12	24.3	25.83	1.53	1.6452	0.546
13	24.28	25.83	1.55	1.6667	0.554
14	24.26	25.83	1.57	1.6882	0.561
15	24.24	25.83	1.59	1.7097	0.568
16	24.23	25.83	1.60	1.7204	0.571
17	24.22	25.83	1.61	1.7312	0.575
18	24.22	25.83	1.61	1.7312	0.575
19	24.22	25.83	1.61	1.7312	0.575
20	24.21	25.83	1.62	1.7419	0.579
21	24.21	25.83	1.62	1.7419	0.579
22	24.21	25.83	1.62	1.7419	0.579
23	24.2	25.83	1.63	1.7527	0.582
24	24.2	25.83	1.63	1.7527	0.582
25	24.2	25.83	1.63	1.7527	0.582
26	24.2	25.83	1.63	1.7527	0.582

G18: Data for Core flooding Test 18

Perforation Diameter =1.5mm

Mass of Oil sat. sample = 25.83g

Mass of Dry Sample = 23.03g

Mass of Oil in sample =2.8g

Injection Pressure = 6bar

Injection Time	Mass of Flooded Sample	Mass of Saturated Sample M1	Mass of Oil Produced	Volume of Oil Produced	%OOIP of Oil produced
Min	M2(g)	M1(g)	M3(g)	V3(cc)	%
1	25.13	25.83	0.70	0.7527	0.250
2	24.83	25.83	1.00	1.0753	0.357
3	24.63	25.83	1.20	1.2903	0.429
4	24.53	25.83	1.30	1.3978	0.464
5	24.45	25.83	1.38	1.4839	0.493
6	24.41	25.83	1.42	1.5269	0.507
7	24.37	25.83	1.46	1.5699	0.521
8	24.34	25.83	1.49	1.6022	0.532
9	24.3	25.83	1.53	1.6452	0.546
10	24.27	25.83	1.56	1.6774	0.557
11	24.24	25.83	1.59	1.7097	0.568
12	24.21	25.83	1.62	1.7419	0.579
13	24.19	25.83	1.64	1.7634	0.586
14	24.17	25.83	1.66	1.7849	0.593
15	24.15	25.83	1.68	1.8065	0.600
16	24.14	25.83	1.69	1.8172	0.604
17	24.13	25.83	1.70	1.8280	0.607
18	24.12	25.83	1.71	1.8387	0.611
19	24.12	25.83	1.71	1.8387	0.611

20	24.12	25.83	1.71	1.8387	0.611
21	24.12	25.83	1.71	1.8387	0.611
22	24.12	25.83	1.71	1.8387	0.611
23	24.12	25.83	1.71	1.8387	0.611
24	24.12	25.83	1.71	1.8387	0.611
25	24.12	25.83	1.71	1.8387	0.611
26	24.12	25.83	1.71	1.8387	0.611

G19: Data for Core flooding Test 19

Perforation Diameter =2.0mm Mass of Oil sat. sample = 25.81g Mass of Dry Sample = 23.02g Mass of Oil in sample =2.79g Injection Pressure = 1bar

Injection Time	Mass of Flooded Sample	Mass of Saturated Sample M1	Mass of Oil Produced	Volume of Oil Produced	%OOIP of Oil produced
Min	M2(g)	M1(g)	M3(g)	V3(cc)	%
1	25.74	25.81	0.07	0.0753	0.025
2	25.44	25.81	0.37	0.3978	0.132
3	25.24	25.81	0.57	0.6129	0.203
4	25.14	25.81	0.67	0.7204	0.238
5	25.06	25.81	0.75	0.8065	0.267
6	25.02	25.81	0.79	0.8495	0.281
7	24.98	25.81	0.83	0.8925	0.295
8	24.95	25.81	0.86	0.9247	0.306
9	24.91	25.81	0.90	0.9677	0.320
10	24.88	25.81	0.93	1.0000	0.331
11	24.85	25.81	0.96	1.0323	0.342
12	24.82	25.81	0.99	1.0645	0.352

13	24.80	25.81	1.01	1.0860	0.359
14	24.79	25.81	1.02	1.0968	0.363
15	24.77	25.81	1.04	1.1183	0.370
16	24.76	25.81	1.05	1.1290	0.374
17	24.76	25.81	1.05	1.1290	0.374
18	24.75	25.81	1.06	1.1398	0.377
19	24.75	25.81	1.06	1.1398	0.377
20	24.75	25.81	1.06	1.1398	0.377
21	24.75	25.81	1.06	1.1398	0.377
22	24.75	25.81	1.06	1.1398	0.377
23	24.75	25.81	1.06	1.1398	0.377
24	24.75	25.81	1.06	1.1398	0.377
25	24.75	25.81	1.06	1.1398	0.377
26	24.75	25.81	1.06	1.1398	0.377

G20: Data for Core flooding Test 20

Perforation Diameter =2.0mm Mass of Oil sat. sample = 25.81g Mass of Dry Sample = 23.02g Mass of Oil in sample =2.79g Injection Pressure = 2bar

Injection Time	Mass of Flooded Sample	Mass of Saturated Sample M1	Mass of Oil Produced	Volume of Oil Produced	%OOIP of Oil produced
Min	M2(g)	M1(g)	M3(g)	V3(cc)	%
1	25.67	25.81	0.14	0.1505	0.050
2	25.37	25.81	0.44	0.4731	0.157
3	25.17	25.81	0.64	0.6882	0.228
4	25.07	25.81	0.74	0.7957	0.263
5	24.99	25.81	0.82	0.8817	0.292

6	24.95	25.81	0.86	0.9247	0.306
7	24.91	25.81	0.90	0.9677	0.320
8	24.88	25.81	0.93	1.0000	0.331
9	24.84	25.81	0.97	1.0430	0.345
10	24.81	25.81	1.00	1.0753	0.356
11	24.78	25.81	1.03	1.1075	0.367
12	24.75	25.81	1.06	1.1398	0.377
13	24.73	25.81	1.08	1.1613	0.384
14	24.71	25.81	1.10	1.1828	0.391
15	24.69	25.81	1.12	1.2043	0.399
16	24.68	25.81	1.13	1.2151	0.402
17	24.67	25.81	1.14	1.2258	0.406
18	24.66	25.81	1.15	1.2366	0.409
19	24.66	25.81	1.15	1.2366	0.409
20	24.66	25.81	1.15	1.2366	0.409
21	24.66	25.81	1.15	1.2366	0.409
22	24.66	25.81	1.15	1.2366	0.409
23	24.66	25.81	1.15	1.2366	0.409
24	24.66	25.81	1.15	1.2366	0.409
25	24.66	25.81	1.15	1.2366	0.409
26	24.66	25.81	1.15	1.2366	0.409

G21: Data for Core flooding Test 21

Perforation Diameter =2.0mm Mass of Oil sat. sample = 25.81g Mass of Dry Sample = 23.02g Mass of Oil in sample =2.79g Injection Pressure = 3bar

Injection Time	Mass of Flooded Sample	Mass of Saturated Sample M1	Mass of Oil Produced	Volume of Oil Produced	%OOIP of Oil produced
Min	M2(g)	M1(g)	M3(g)	V3(cc)	%
1	25.59	25.81	0.22	0.2366	0.079
2	25.29	25.81	0.52	0.5591	0.186
3	25.09	25.81	0.72	0.7742	0.258
4	24.99	25.81	0.82	0.8817	0.294
5	24.91	25.81	0.90	0.9677	0.323
6	24.87	25.81	0.94	1.0108	0.337
7	24.83	25.81	0.98	1.0538	0.351
8	24.8	25.81	1.01	1.0860	0.362
9	24.76	25.81	1.05	1.1290	0.376
10	24.73	25.81	1.08	1.1613	0.387
11	24.7	25.81	1.11	1.1935	0.398
12	24.67	25.81	1.14	1.2258	0.409
13	24.65	25.81	1.16	1.2473	0.416
14	24.63	25.81	1.18	1.2688	0.423
15	24.61	25.81	1.20	1.2903	0.430
16	24.6	25.81	1.21	1.3011	0.434
17	24.59	25.81	1.22	1.3118	0.437
18	24.58	25.81	1.23	1.3226	0.441
19	24.58	25.81	1.23	1.3226	0.441

20	24.58	25.81	1.23	1.3226	0.441
21	24.58	25.81	1.23	1.3226	0.441
22	24.58	25.81	1.23	1.3226	0.441
23	24.58	25.81	1.23	1.3226	0.441
24	24.58	25.81	1.23	1.3226	0.441
25	24.58	25.81	1.23	1.3226	0.441
26	24.58	25.81	1.23	1.3226	0.441

G22: Data for Core flooding Test 22

Perforation Diameter =2.0mm Mass of Oil sat. sample = 25.81g Mass of Dry Sample = 23.02g Mass of Oil in sample =2.79g Injection Pressure = 4bar

Injection Time	Mass of Flooded Sample	Mass of Saturated Sample M1	Mass of Oil Produced	Volume of Oil Produced	%OOIP of Oil produced
Min	M2(g)	M1(g)	M3(g)	V3(cc)	%
1	25.51	25.81	0.30	0.3226	0.108
2	25.21	25.81	0.60	0.6452	0.215
3	25.01	25.81	0.80	0.8602	0.287
4	24.91	25.81	0.90	0.9677	0.323
5	24.83	25.81	0.98	1.0538	0.351
6	24.79	25.81	1.02	1.0968	0.366
7	24.75	25.81	1.06	1.1398	0.380
8	24.72	25.81	1.09	1.1720	0.391
9	24.68	25.81	1.13	1.2151	0.405
10	24.65	25.81	1.16	1.2473	0.416
11	24.62	25.81	1.19	1.2796	0.427
12	24.59	25.81	1.22	1.3118	0.437

13	24.57	25.81	1.24	1.3333	0.444
14	24.55	25.81	1.26	1.3548	0.452
15	24.53	25.81	1.28	1.3763	0.459
16	24.52	25.81	1.29	1.3871	0.462
17	24.51	25.81	1.30	1.3978	0.466
18	24.51	25.81	1.30	1.3978	0.466
19	24.51	25.81	1.30	1.3978	0.466
20	24.51	25.81	1.30	1.3978	0.466
21	24.51	25.81	1.30	1.3978	0.466
22	24.51	25.81	1.30	1.3978	0.466
23	24.51	25.81	1.30	1.3978	0.466
24	24.51	25.81	1.30	1.3978	0.466
25	24.51	25.81	1.30	1.3978	0.466
26	24.51	25.81	1.30	1.3978	0.466

G23: Data for Core flooding Test 23

Perforation Diameter =2.0mm

Mass of Oil sat. sample = 25.81g

Mass of Dry Sample = 23.02g

Mass of Oil in sample =2.79g

Injection Pressure = 5bar

Injection Time	Mass of Flooded Sample	Mass of Saturated Sample M1	Mass of Oil Produced	Volume of Oil Produced	%OOIP of Oil produced
Min	M2(g)	M1(g)	M3(g)	V3(cc)	%
1	25.39	25.81	0.42	0.4516	0.151
2	25.09	25.81	0.72	0.7742	0.258
3	24.89	25.81	0.92	0.9892	0.330
4	24.79	25.81	1.02	1.0968	0.366
5	24.71	25.81	1.10	1.1828	0.394

6	24.67	25.81	1.14	1.2258	0.409
7	24.63	25.81	1.18	1.2688	0.423
8	24.6	25.81	1.21	1.3011	0.434
9	24.56	25.81	1.25	1.3441	0.448
10	24.53	25.81	1.28	1.3763	0.459
11	24.5	25.81	1.31	1.4086	0.470
12	24.47	25.81	1.34	1.4409	0.480
13	24.45	25.81	1.36	1.4624	0.487
14	24.43	25.81	1.38	1.4839	0.495
15	24.41	25.81	1.40	1.5054	0.502
16	24.4	25.81	1.41	1.5161	0.505
17	24.39	25.81	1.42	1.5269	0.509
18	24.38	25.81	1.43	1.5376	0.513
19	24.38	25.81	1.43	1.5376	0.513
20	24.38	25.81	1.43	1.5376	0.513
21	24.38	25.81	1.43	1.5376	0.513
22	24.38	25.81	1.43	1.5376	0.513
23	24.38	25.81	1.43	1.5376	0.513
24	24.38	25.81	1.43	1.5376	0.513
25	24.38	25.81	1.43	1.5376	0.513
26	24.38	25.81	1.43	1.5376	0.513

G24: Data for Core flooding Test 24

Perforation Diameter =2.0mm Mass of Oil sat. sample = 25.81g Mass of Dry Sample = 23.02g Mass of Oil in sample =2.79g Injection Pressure = 6bar

Injection Time	Mass of Flooded Sample	Mass of Saturated Sample M1	Mass of Oil Produced	Volume of Oil Produced	%OOIP of Oil produced
Min	M2(g)	M1(g)	M3(g)	V3(cc)	%
1	25.27	25.81	0.54	0.5806	0.194
2	24.97	25.81	0.84	0.9032	0.301
3	24.77	25.81	1.04	1.1183	0.373
4	24.67	25.81	1.14	1.2258	0.409
5	24.59	25.81	1.22	1.3118	0.437
6	24.55	25.81	1.26	1.3548	0.452
7	24.51	25.81	1.30	1.3978	0.466
8	24.48	25.81	1.33	1.4301	0.477
9	24.44	25.81	1.37	1.4731	0.491
10	24.41	25.81	1.40	1.5054	0.502
11	24.38	25.81	1.43	1.5376	0.513
12	24.35	25.81	1.46	1.5699	0.523
13	24.33	25.81	1.48	1.5914	0.530
14	24.31	25.81	1.50	1.6129	0.538
15	24.29	25.81	1.52	1.6344	0.545
16	24.28	25.81	1.53	1.6452	0.548
17	24.27	25.81	1.54	1.6559	0.552
18	24.26	25.81	1.55	1.6667	0.556
19	24.26	25.81	1.55	1.6667	0.556

20	24.26	25.81	1.55	1.6667	0.556
21	24.26	25.81	1.55	1.6667	0.556
22	24.26	25.81	1.55	1.6667	0.556
23	24.26	25.81	1.55	1.6667	0.556
24	24.26	25.81	1.55	1.6667	0.556
25	24.26	25.81	1.55	1.6667	0.556
26	24.26	25.81	1.55	1.6667	0.556

G25: Data for Core flooding Test 25

Perforation Diameter =2.5mm

Mass of Oil sat. sample = 25.83g

Mass of Dry Sample = 23.05g

Mass of Oil in sample =2.78g

Injection Pressure = 1bar

Injection Time	Mass of Flooded Sample	Mass of Saturated Sample M1	Mass of Oil Produced	Volume of Oil Produced	%OOIP of Oil produced
Min	M2(g)	M1(g)	M3(g)	V3(cc)	%
1	25.78	25.83	0.05	0.0538	0.018
2	25.48	25.83	0.35	0.3763	0.126
3	25.28	25.83	0.55	0.5914	0.198
4	25.18	25.83	0.65	0.6989	0.234
5	25.10	25.83	0.73	0.7849	0.263
6	25.06	25.83	0.77	0.8280	0.277
7	25.02	25.83	0.81	0.8710	0.291
8	24.99	25.83	0.84	0.9032	0.302
9	24.95	25.83	0.88	0.9462	0.317
10	24.92	25.83	0.91	0.9785	0.327
11	24.89	25.83	0.94	1.0108	0.338
12	24.86	25.83	0.97	1.0430	0.349

13	24.84	25.83	0.99	1.0645	0.356
14	24.83	25.83	1.00	1.0753	0.360
15	24.81	25.83	1.02	1.0968	0.367
16	24.80	25.83	1.03	1.1075	0.371
17	24.80	25.83	1.03	1.1075	0.371
18	24.79	25.83	1.04	1.1183	0.374
19	24.79	25.83	1.04	1.1183	0.374
20	24.79	25.83	1.04	1.1183	0.374
21	24.79	25.83	1.04	1.1183	0.374
22	24.79	25.83	1.04	1.1183	0.374
23	24.79	25.83	1.04	1.1183	0.374
24	24.79	25.83	1.04	1.1183	0.374
25	24.79	25.83	1.04	1.1183	0.374
26	24.79	25.83	1.04	1.1183	0.374

G26: Data for Core flooding Test 26

Perforation Diameter =2.5mm

Mass of Oil sat. sample = 25.83g

Mass of Dry Sample = 23.05g

Mass of Oil in sample =2.78g

Injection Pressure = 2bar

Injection Time	Mass of Flooded Sample	Mass of Saturated Sample M1	Mass of Oil Produced	Volume of Oil Produced	%OOIP of Oil produced
Min	M2(g)	M1(g)	M3(g)	V3(cc)	%
1	25.73	25.83	0.10	0.1075	0.036
2	25.43	25.83	0.40	0.4301	0.144
3	25.23	25.83	0.60	0.6452	0.216
4	25.13	25.83	0.70	0.7527	0.252
5	25.05	25.83	0.78	0.8387	0.281

6	25.01	25.83	0.82	0.8817	0.296
7	24.97	25.83	0.86	0.9247	0.310
8	24.94	25.83	0.89	0.9570	0.321
9	24.9	25.83	0.93	1.0000	0.335
10	24.87	25.83	0.96	1.0323	0.346
11	24.84	25.83	0.99	1.0645	0.357
12	24.81	25.83	1.02	1.0968	0.368
13	24.79	25.83	1.04	1.1183	0.375
14	24.77	25.83	1.06	1.1398	0.382
15	24.75	25.83	1.08	1.1613	0.389
16	24.74	25.83	1.09	1.1720	0.393
17	24.74	25.83	1.09	1.1720	0.393
18	24.73	25.83	1.10	1.1828	0.397
19	24.73	25.83	1.10	1.1828	0.397
20	24.73	25.83	1.10	1.1828	0.397
21	24.73	25.83	1.10	1.1828	0.397
22	24.73	25.83	1.10	1.1828	0.397
23	24.73	25.83	1.10	1.1828	0.397
24	24.73	25.83	1.10	1.1828	0.397
25	24.73	25.83	1.10	1.1828	0.397
26	24.73	25.83	1.10	1.1828	0.397

G27: Data for Core flooding Test 27

Perforation Diameter =2.5mm Mass of Oil sat. sample = 25.83g Mass of Dry Sample = 23.05g Mass of Oil in sample =2.78g Injection Pressure = 3bar

Injection Time	Mass of Flooded Sample	Mass of Saturated Sample M1	Mass of Oil Produced	Volume of Oil Produced	%OOIP of Oil produced
Min	M2(g)	M1(g)	M3(g)	V3(cc)	%
1	25.64	25.83	0.19	0.2043	0.068
2	25.34	25.83	0.49	0.5269	0.176
3	25.14	25.83	0.69	0.7419	0.248
4	25.04	25.83	0.79	0.8495	0.284
5	24.96	25.83	0.87	0.9355	0.313
6	24.92	25.83	0.91	0.9785	0.327
7	24.88	25.83	0.95	1.0215	0.342
8	24.85	25.83	0.98	1.0538	0.353
9	24.81	25.83	1.02	1.0968	0.367
10	24.78	25.83	1.05	1.1290	0.378
11	24.75	25.83	1.08	1.1613	0.388
12	24.72	25.83	1.11	1.1935	0.399
13	24.7	25.83	1.13	1.2151	0.406
14	24.68	25.83	1.15	1.2366	0.414
15	24.66	25.83	1.17	1.2581	0.421
16	24.65	25.83	1.18	1.2688	0.424
17	24.65	25.83	1.18	1.2688	0.424
18	24.64	25.83	1.19	1.2796	0.428
19	24.64	25.83	1.19	1.2796	0.428

20	24.64	25.83	1.19	1.2796	0.428
21	24.64	25.83	1.19	1.2796	0.428
22	24.64	25.83	1.19	1.2796	0.428
23	24.64	25.83	1.19	1.2796	0.428
24	24.64	25.83	1.19	1.2796	0.428
25	24.64	25.83	1.19	1.2796	0.428
26	24.64	25.83	1.19	1.2796	0.428

G28: Data for Core flooding Test 28

Perforation Diameter =2.5mm Mass of Oil sat. sample = 25.83g Mass of Dry Sample = 23.05g Mass of Oil in sample =2.78g Injection Pressure = 4bar

Injection Time	Mass of Flooded Sample	Mass of Saturated Sample M1	Mass of Oil Produced	Volume of Oil Produced	%OOIP of Oil produced
Min	M2(g)	M1(g)	M3(g)	V3(cc)	%
1	25.57	25.83	0.26	0.2796	0.094
2	25.27	25.83	0.56	0.6022	0.201
3	25.07	25.83	0.76	0.8172	0.273
4	24.97	25.83	0.86	0.9247	0.309
5	24.89	25.83	0.94	1.0108	0.338
6	24.85	25.83	0.98	1.0538	0.353
7	24.81	25.83	1.02	1.0968	0.367
8	24.78	25.83	1.05	1.1290	0.378
9	24.74	25.83	1.09	1.1720	0.392
10	24.71	25.83	1.12	1.2043	0.403
11	24.68	25.83	1.15	1.2366	0.414
12	24.65	25.83	1.18	1.2688	0.424

13	24.63	25.83	1.20	1.2903	0.432
14	24.61	25.83	1.22	1.3118	0.439
15	24.59	25.83	1.24	1.3333	0.446
16	24.58	25.83	1.25	1.3441	0.450
17	24.58	25.83	1.25	1.3441	0.450
18	24.57	25.83	1.26	1.3548	0.453
19	24.57	25.83	1.26	1.3548	0.453
20	24.57	25.83	1.26	1.3548	0.453
21	24.57	25.83	1.26	1.3548	0.453
22	24.57	25.83	1.26	1.3548	0.453
23	24.57	25.83	1.26	1.3548	0.453
24	24.57	25.83	1.26	1.3548	0.453
25	24.57	25.83	1.26	1.3548	0.453
26	24.57	25.83	1.26	1.3548	0.453

G29: Data for Core flooding Test 29

Perforation Diameter =2.5mm

Mass of Oil sat. sample = 25.83g

Mass of Dry Sample = 23.05g

Mass of Oil in sample =2.78g

Injection Pressure = 5bar

Injection Time	Mass of Flooded Sample	Mass of Saturated Sample M1	Mass of Oil Produced	Volume of Oil Produced	%OOIP of Oil produced
Min	M2(g)	M1(g)	M3(g)	V3(cc)	%
1	25.49	25.83	0.34	0.3656	0.122
2	25.19	25.83	0.64	0.6882	0.230
3	24.99	25.83	0.84	0.9032	0.302
4	24.89	25.83	0.94	1.0108	0.338
5	24.81	25.83	1.02	1.0968	0.367

6	24.77	25.83	1.06	1.1398	0.381
7	24.73	25.83	1.10	1.1828	0.396
8	24.70	25.83	1.13	1.2151	0.406
9	24.66	25.83	1.17	1.2581	0.421
10	24.63	25.83	1.20	1.2903	0.432
11	24.60	25.83	1.23	1.3226	0.442
12	24.57	25.83	1.26	1.3548	0.453
13	24.55	25.83	1.28	1.3763	0.460
14	24.53	25.83	1.30	1.3978	0.468
15	24.51	25.83	1.32	1.4194	0.475
16	24.51	25.83	1.32	1.4194	0.475
17	24.51	25.83	1.32	1.4194	0.475
18	24.50	25.83	1.33	1.4301	0.478
19	24.50	25.83	1.33	1.4301	0.478
20	24.50	25.83	1.33	1.4301	0.478
21	24.50	25.83	1.33	1.4301	0.478
22	24.50	25.83	1.33	1.4301	0.478
23	24.50	25.83	1.33	1.4301	0.478
24	24.50	25.83	1.33	1.4301	0.478
25	24.50	25.83	1.33	1.4301	0.478
26	24.50	25.83	1.33	1.4301	0.478

G30: Data for Core flooding Test 30

Perforation Diameter =2.5mm Mass of Oil sat. sample = 25.83g Mass of Dry Sample = 23.05g Mass of Oil in sample =2.78g Injection Pressure = 6bar

Injection Time	Mass of Flooded Sample	Mass of Saturated Sample M1	Mass of Oil Produced	Volume of Oil Produced	%OOIP of Oil produced
Min	M2(g)	M1(g)	M3(g)	V3(cc)	%
1	25.4	25.83	0.43	0.4624	0.155
2	25.1	25.83	0.73	0.7849	0.263
3	24.9	25.83	0.93	1.0000	0.335
4	24.8	25.83	1.03	1.1075	0.371
5	24.72	25.83	1.11	1.1935	0.399
6	24.68	25.83	1.15	1.2366	0.414
7	24.64	25.83	1.19	1.2796	0.428
8	24.61	25.83	1.22	1.3118	0.439
9	24.57	25.83	1.26	1.3548	0.453
10	24.54	25.83	1.29	1.3871	0.464
11	24.51	25.83	1.32	1.4194	0.475
12	24.48	25.83	1.35	1.4516	0.486
13	24.46	25.83	1.37	1.4731	0.493
14	24.44	25.83	1.39	1.4946	0.500
15	24.42	25.83	1.41	1.5161	0.507
16	24.41	25.83	1.42	1.5269	0.511
17	24.41	25.83	1.42	1.5269	0.511
18	24.41	25.83	1.42	1.5269	0.511
19	24.41	25.83	1.42	1.5269	0.511

20	24.41	25.83	1.42	1.5269	0.511
21	24.41	25.83	1.42	1.5269	0.511
22	24.41	25.83	1.42	1.5269	0.511
23	24.41	25.83	1.42	1.5269	0.511
24	24.41	25.83	1.42	1.5269	0.511
25	24.41	25.83	1.42	1.5269	0.511
26	24.41	25.83	1.42	1.5269	0.511

G31: Data for Core flooding Test 31

Perforation Diameter =3.0mm

Mass of Oil sat. sample = 25.82g

Mass of Dry Sample = 23.03g

Mass of Oil in sample =2.79g

Injection Pressure = 1bar

Injection Time	Mass of Flooded Sample	Mass of Saturated Sample M1	Mass of Oil Produced	Volume of Oil Produced	%OOIP of Oil produced
Min	M2(g)	M1(g)	M3(g)	V3(cc)	%
1	25.80	25.82	0.02	0.0215	0.007
2	25.50	25.82	0.32	0.3441	0.115
3	25.30	25.82	0.52	0.5591	0.186
4	25.20	25.82	0.62	0.6667	0.222
5	25.12	25.82	0.70	0.7527	0.251
6	25.08	25.82	0.74	0.7957	0.265
7	25.04	25.82	0.78	0.8387	0.280
8	25.01	25.82	0.81	0.8710	0.290
9	24.97	25.82	0.85	0.9140	0.305
10	24.94	25.82	0.88	0.9462	0.315
11	24.91	25.82	0.91	0.9785	0.326
12	24.88	25.82	0.94	1.0108	0.337

13	24.86	25.82	0.96	1.0323	0.344
14	24.85	25.82	0.97	1.0430	0.348
15	24.83	25.82	0.99	1.0645	0.355
16	24.82	25.82	1.00	1.0753	0.358
17	24.82	25.82	1.00	1.0753	0.358
18	24.81	25.82	1.01	1.0860	0.362
19	24.81	25.82	1.01	1.0860	0.362
20	24.81	25.82	1.01	1.0860	0.362
21	24.81	25.82	1.01	1.0860	0.362
22	24.81	25.82	1.01	1.0860	0.362
23	24.81	25.82	1.01	1.0860	0.362
24	24.81	25.82	1.01	1.0860	0.362
25	24.81	25.82	1.01	1.0860	0.362
26	24.81	25.82	1.01	1.0860	0.362

G32: Data for Core flooding Test 32

Perforation Diameter =3.0mm

Mass of Oil sat. sample = 25.82g

Mass of Dry Sample = 23.03g

Mass of Oil in sample =2.79g

Injection Pressure = 2bar

Injection Time	Mass of Flooded Sample	Mass of Saturated Sample M1	Mass of Oil Produced	Volume of Oil Produced	%OOIP of Oil produced
Min	M2(g)	M1(g)	M3(g)	V3(cc)	%
1	25.76	25.82	0.06	0.0645	0.022
2	25.46	25.82	0.36	0.3871	0.129
3	25.26	25.82	0.56	0.6022	0.201
4	25.16	25.82	0.66	0.7097	0.237
5	25.08	25.82	0.74	0.7957	0.265

6	25.04	25.82	0.78	0.8387	0.280
7	25.00	25.82	0.82	0.8817	0.294
8	24.97	25.82	0.85	0.9140	0.305
9	24.93	25.82	0.89	0.9570	0.319
10	24.9	25.82	0.92	0.9892	0.330
11	24.87	25.82	0.95	1.0215	0.341
12	24.84	25.82	0.98	1.0538	0.351
13	24.82	25.82	1.00	1.0753	0.358
14	24.8	25.82	1.02	1.0968	0.366
15	24.78	25.82	1.04	1.1183	0.373
16	24.77	25.82	1.05	1.1290	0.376
17	24.76	25.82	1.06	1.1398	0.380
18	24.75	25.82	1.07	1.1505	0.384
19	24.75	25.82	1.07	1.1505	0.384
20	24.75	25.82	1.07	1.1505	0.384
21	24.75	25.82	1.07	1.1505	0.384
22	24.75	25.82	1.07	1.1505	0.384
23	24.75	25.82	1.07	1.1505	0.384
24	24.75	25.82	1.07	1.1505	0.384
25	24.75	25.82	1.07	1.1505	0.384
26	24.75	25.82	1.07	1.1505	0.384

G33: Data for Core flooding Test 33

Perforation Diameter =3.0mm Mass of Oil sat. sample = 25.82g Mass of Dry Sample = 23.03g Mass of Oil in sample =2.79g Injection Pressure = 3bar

Injection Time	Mass of Flooded Sample	Mass of Saturated Sample M1	Mass of Oil Produced	Volume of Oil Produced	%OOIP of Oil produced
Min	M2(g)	M1(g)	M3(g)	V3(cc)	%
1	25.71	25.82	0.11	0.1183	0.039
2	25.41	25.82	0.41	0.4409	0.147
3	25.21	25.82	0.61	0.6559	0.219
4	25.11	25.82	0.71	0.7634	0.254
5	25.03	25.82	0.79	0.8495	0.283
6	24.99	25.82	0.83	0.8925	0.297
7	24.95	25.82	0.87	0.9355	0.312
8	24.92	25.82	0.90	0.9677	0.323
9	24.88	25.82	0.94	1.0108	0.337
10	24.85	25.82	0.97	1.0430	0.348
11	24.82	25.82	1.00	1.0753	0.358
12	24.79	25.82	1.03	1.1075	0.369
13	24.77	25.82	1.05	1.1290	0.376
14	24.75	25.82	1.07	1.1505	0.384
15	24.73	25.82	1.09	1.1720	0.391
16	24.72	25.82	1.10	1.1828	0.394
17	24.71	25.82	1.11	1.1935	0.398
18	24.7	25.82	1.12	1.2043	0.401
19	24.7	25.82	1.12	1.2043	0.401

20	24.7	25.82	1.12	1.2043	0.401
21	24.7	25.82	1.12	1.2043	0.401
22	24.7	25.82	1.12	1.2043	0.401
23	24.7	25.82	1.12	1.2043	0.401
24	24.7	25.82	1.12	1.2043	0.401
25	24.7	25.82	1.12	1.2043	0.401
26	24.7	25.82	1.12	1.2043	0.401

G34: Data for Core flooding Test 34

Perforation Diameter =3.0mm Mass of Oil sat. sample = 25.82g Mass of Dry Sample = 23.03g Mass of Oil in sample =2.79g Injection Pressure = 4bar

Injection Time	Mass of Flooded Sample	Mass of Saturated Sample M1	Mass of Oil Produced	Volume of Oil Produced	%OOIP of Oil produced
Min	M2(g)	M1(g)	M3(g)	V3(cc)	%
1	25.65	25.82	0.17	0.1828	0.061
2	25.35	25.82	0.47	0.5054	0.168
3	25.15	25.82	0.67	0.7204	0.240
4	25.05	25.82	0.77	0.8280	0.276
5	24.97	25.82	0.85	0.9140	0.305
6	24.93	25.82	0.89	0.9570	0.319
7	24.89	25.82	0.93	1.0000	0.333
8	24.86	25.82	0.96	1.0323	0.344
9	24.82	25.82	1.00	1.0753	0.358
10	24.79	25.82	1.03	1.1075	0.369
11	24.76	25.82	1.06	1.1398	0.380
12	24.73	25.82	1.09	1.1720	0.391

13	24.71	25.82	1.11	1.1935	0.398
14	24.69	25.82	1.13	1.2151	0.405
15	24.67	25.82	1.15	1.2366	0.412
16	24.66	25.82	1.16	1.2473	0.416
17	24.65	25.82	1.17	1.2581	0.419
18	24.64	25.82	1.18	1.2688	0.423
19	24.64	25.82	1.18	1.2688	0.423
20	24.64	25.82	1.18	1.2688	0.423
21	24.64	25.82	1.18	1.2688	0.423
22	24.64	25.82	1.18	1.2688	0.423
23	24.64	25.82	1.18	1.2688	0.423
24	24.64	25.82	1.18	1.2688	0.423
25	24.64	25.82	1.18	1.2688	0.423
26	24.64	25.82	1.18	1.2688	0.423

G35: Data for Core flooding Test 35

Perforation Diameter =3.0mm

Mass of Oil sat. sample = 25.82g

Mass of Dry Sample = 23.03g

Mass of Oil in sample =2.79g

Injection Pressure = 5bar

Injection Time	Mass of Flooded Sample	Mass of Saturated Sample M1	Mass of Oil Produced	Volume of Oil Produced	%OOIP of Oil produced
Min	M2(g)	M1(g)	M3(g)	V3(cc)	%
1	25.58	25.82	0.24	0.2581	0.086
2	25.28	25.82	0.54	0.5806	0.194
3	25.08	25.82	0.74	0.7957	0.265
4	24.98	25.82	0.84	0.9032	0.301
5	24.9	25.82	0.92	0.9892	0.330

6	24.86	25.82	0.96	1.0323	0.344
7	24.82	25.82	1.00	1.0753	0.358
8	24.79	25.82	1.03	1.1075	0.369
9	24.75	25.82	1.07	1.1505	0.384
10	24.72	25.82	1.10	1.1828	0.394
11	24.69	25.82	1.13	1.2151	0.405
12	24.66	25.82	1.16	1.2473	0.416
13	24.64	25.82	1.18	1.2688	0.423
14	24.62	25.82	1.20	1.2903	0.430
15	24.6	25.82	1.22	1.3118	0.437
16	24.59	25.82	1.23	1.3226	0.441
17	24.58	25.82	1.24	1.3333	0.444
18	24.57	25.82	1.25	1.3441	0.448
19	24.57	25.82	1.25	1.3441	0.448
20	24.57	25.82	1.25	1.3441	0.448
21	24.57	25.82	1.25	1.3441	0.448
22	24.57	25.82	1.25	1.3441	0.448
23	24.57	25.82	1.25	1.3441	0.448
24	24.57	25.82	1.25	1.3441	0.448
25	24.57	25.82	1.25	1.3441	0.448
26	24.57	25.82	1.25	1.3441	0.448

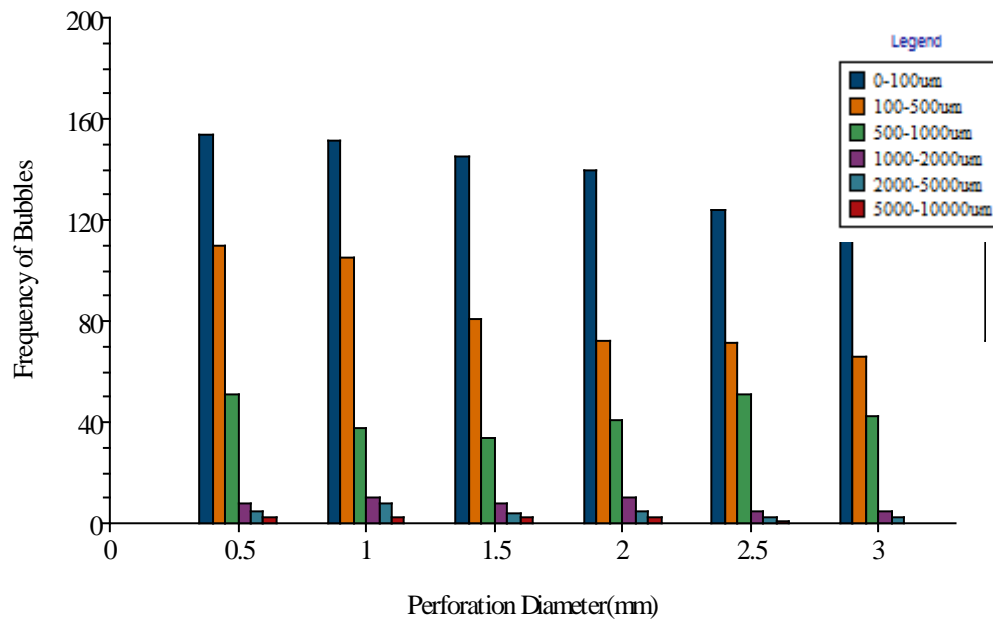
G36: Data for Core flooding Test 36

Perforation Diameter =3.0mm Mass of Oil sat. sample = 25.82g Mass of Dry Sample = 23.03g Mass of Oil in sample =2.79g Injection Pressure = 6bar

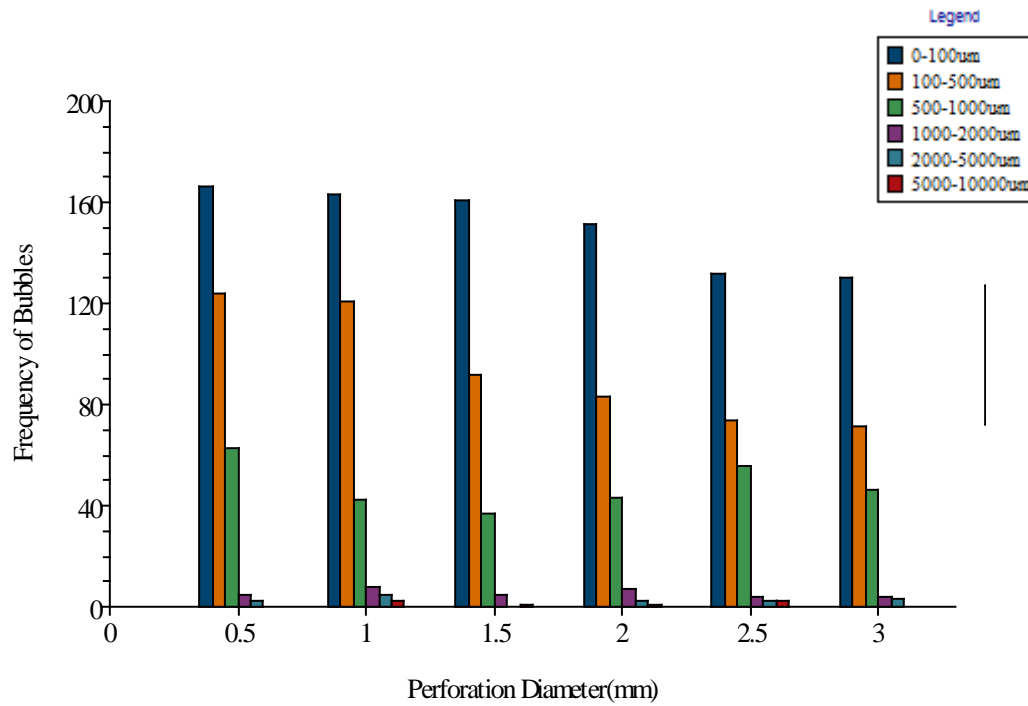
Injection Time	Mass of Flooded Sample	Mass of Saturated Sample M1	Mass of Oil Produced	Volume of Oil Produced	%OOIP of Oil produced
Min	M2(g)	M1(g)	M3(g)	V3(cc)	%
1	25.51	25.82	0.31	0.3333	0.111
2	25.21	25.82	0.61	0.6559	0.219
3	25.01	25.82	0.81	0.8710	0.290
4	24.91	25.82	0.91	0.9785	0.326
5	24.83	25.82	0.99	1.0645	0.355
6	24.79	25.82	1.03	1.1075	0.369
7	24.75	25.82	1.07	1.1505	0.384
8	24.72	25.82	1.10	1.1828	0.394
9	24.68	25.82	1.14	1.2258	0.409
10	24.65	25.82	1.17	1.2581	0.419
11	24.62	25.82	1.20	1.2903	0.430
12	24.59	25.82	1.23	1.3226	0.441
13	24.57	25.82	1.25	1.3441	0.448
14	24.55	25.82	1.27	1.3656	0.455
15	24.53	25.82	1.29	1.3871	0.462
16	24.52	25.82	1.30	1.3978	0.466
17	24.51	25.82	1.31	1.4086	0.470
18	24.5	25.82	1.32	1.4194	0.473
19	24.5	25.82	1.32	1.4194	0.473

20	24.5	25.82	1.32	1.4194	0.473
21	24.5	25.82	1.32	1.4194	0.473
22	24.5	25.82	1.32	1.4194	0.473
23	24.5	25.82	1.32	1.4194	0.473
24	24.5	25.82	1.32	1.4194	0.473
25	24.5	25.82	1.32	1.4194	0.473
26	24.5	25.82	1.32	1.4194	0.473

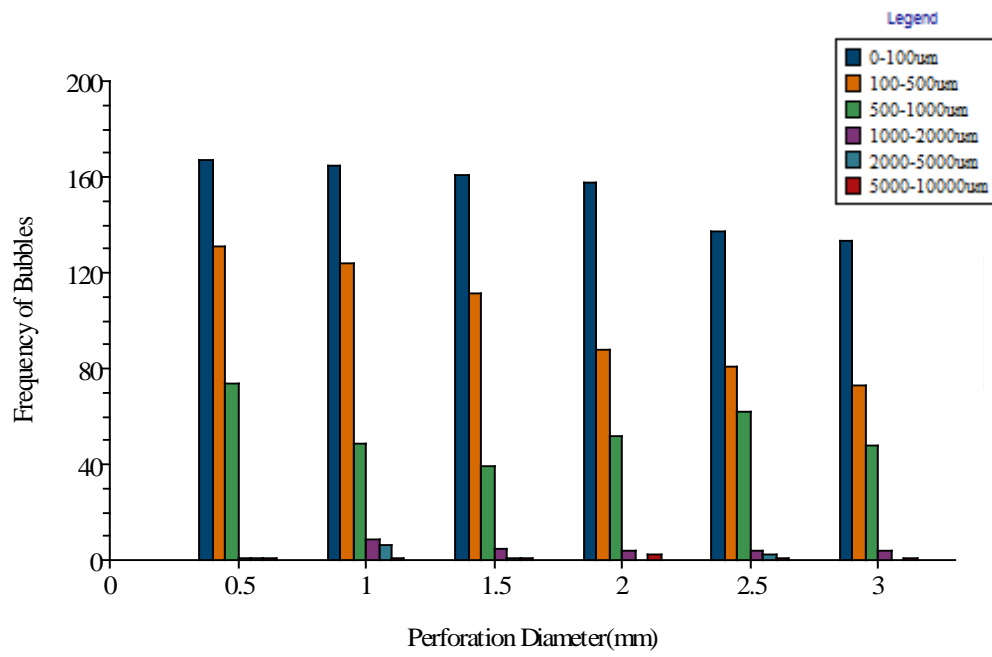
Appendix H: Figure 4.4 (b) –(f)



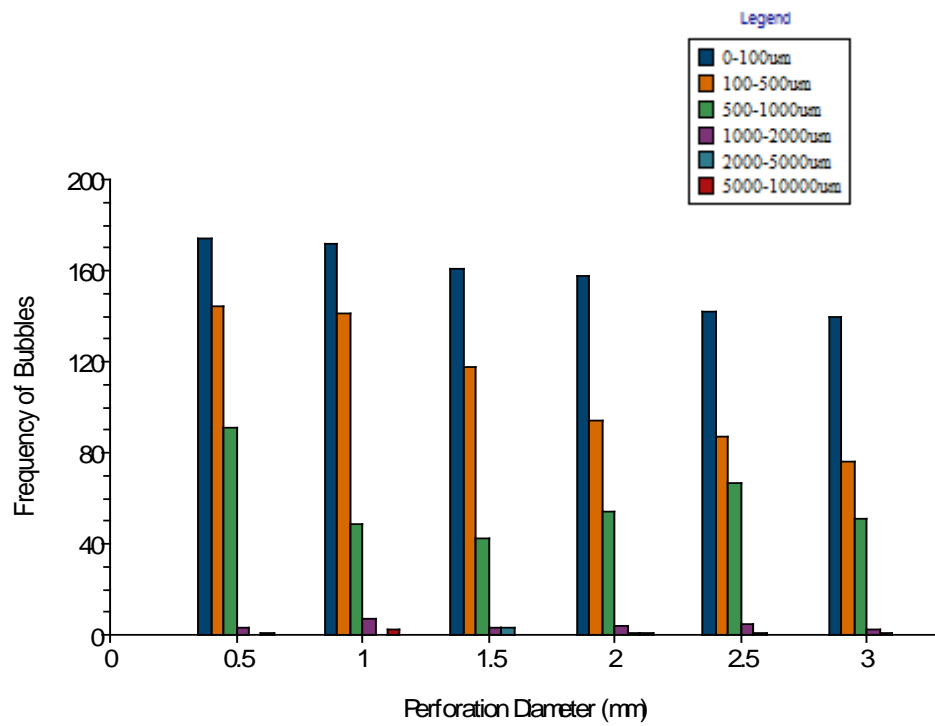
(b) Variation of CO₂ bubbles size with perforation diameter at 1.4bar



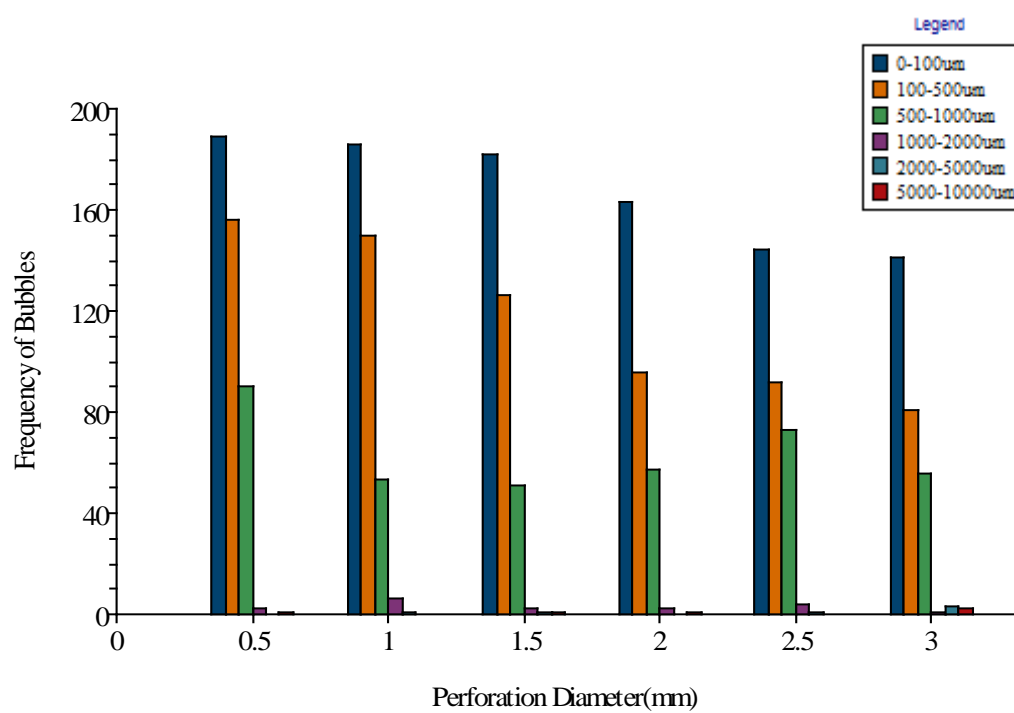
(c) Variation of CO₂ bubbles size with perforation diameter at 1.6bar



(d) Variation of CO₂ bubbles size with perforation diameter at 1.8bar

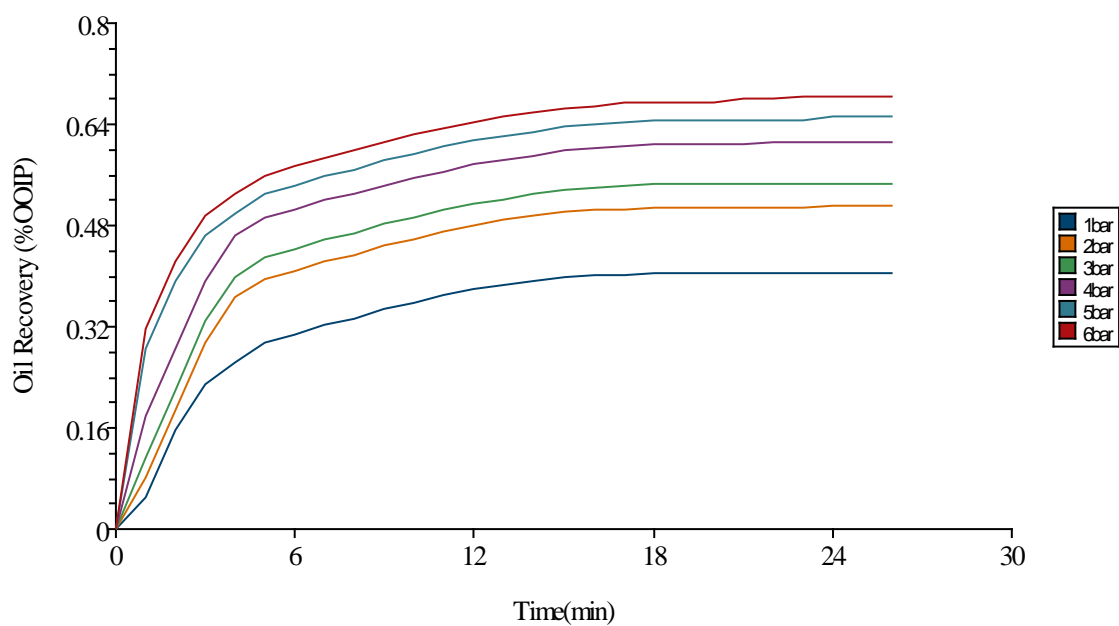


(e) Variation of CO₂ bubbles size with perforation diameter at 2.0bar

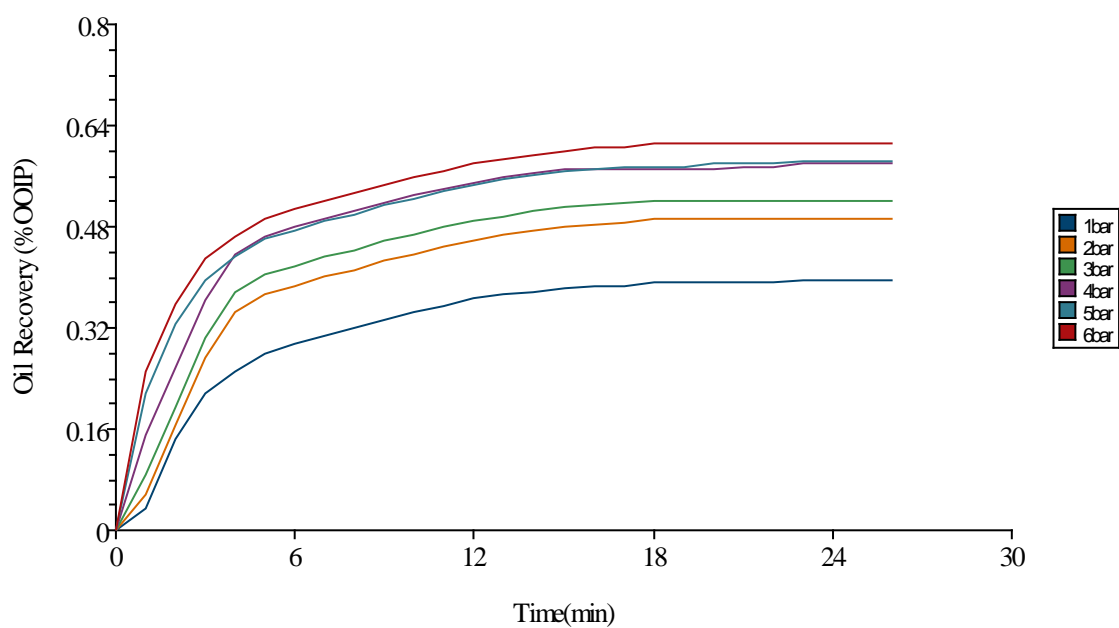


(f) Variation of CO₂ bubbles size with perforation diameter at 2.2bar

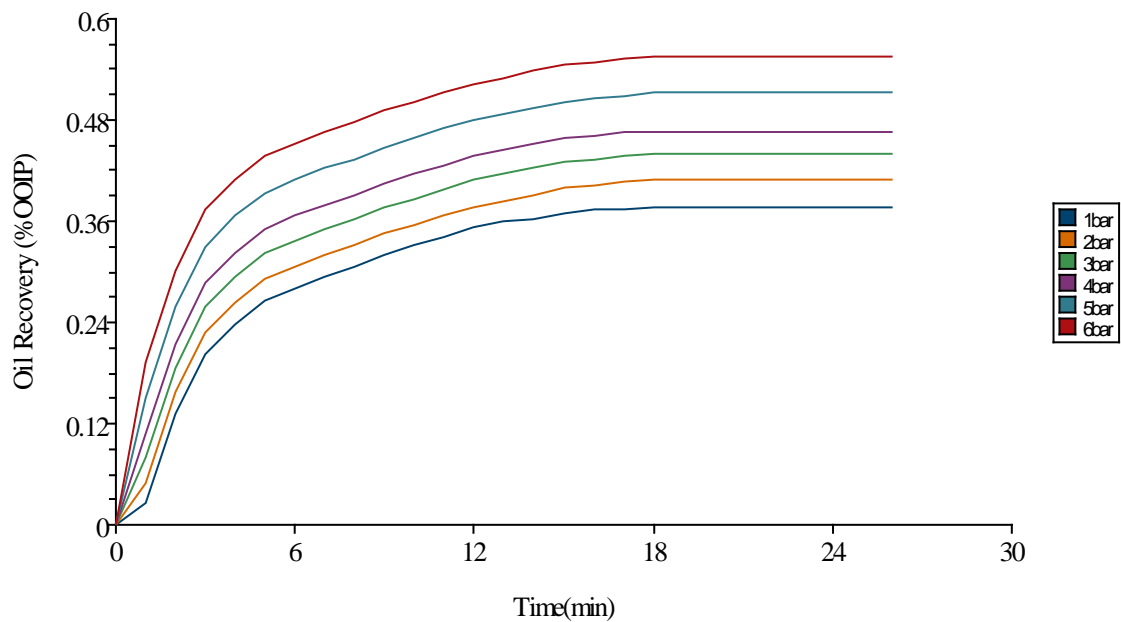
Appendix I: Figure 4.10 (b)-(f)



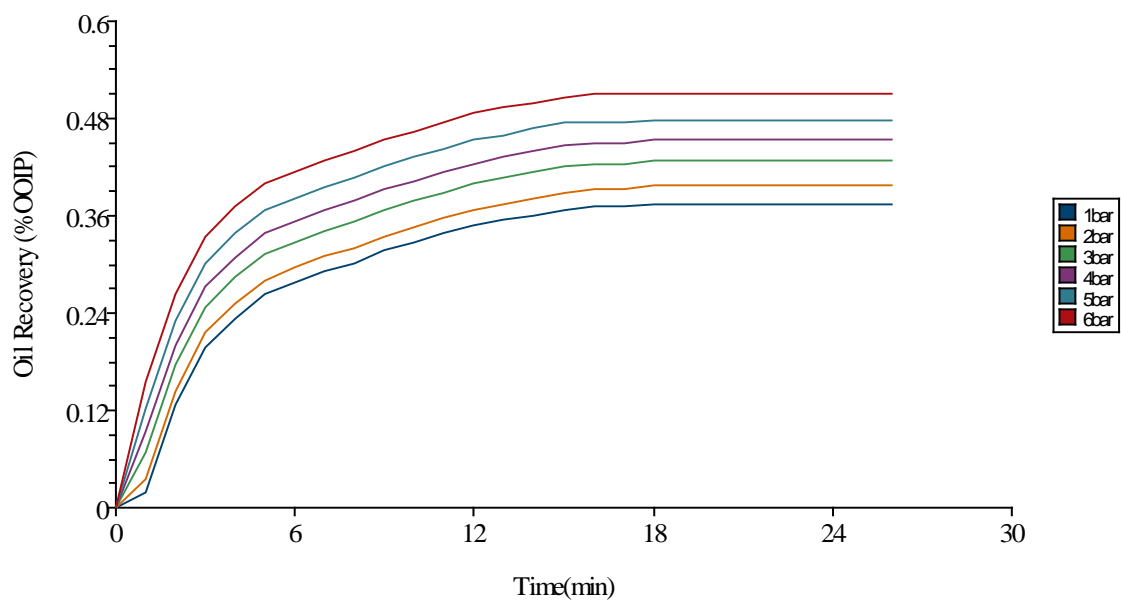
(b) Oil recovery versus time at 1.0mm perforation diameter



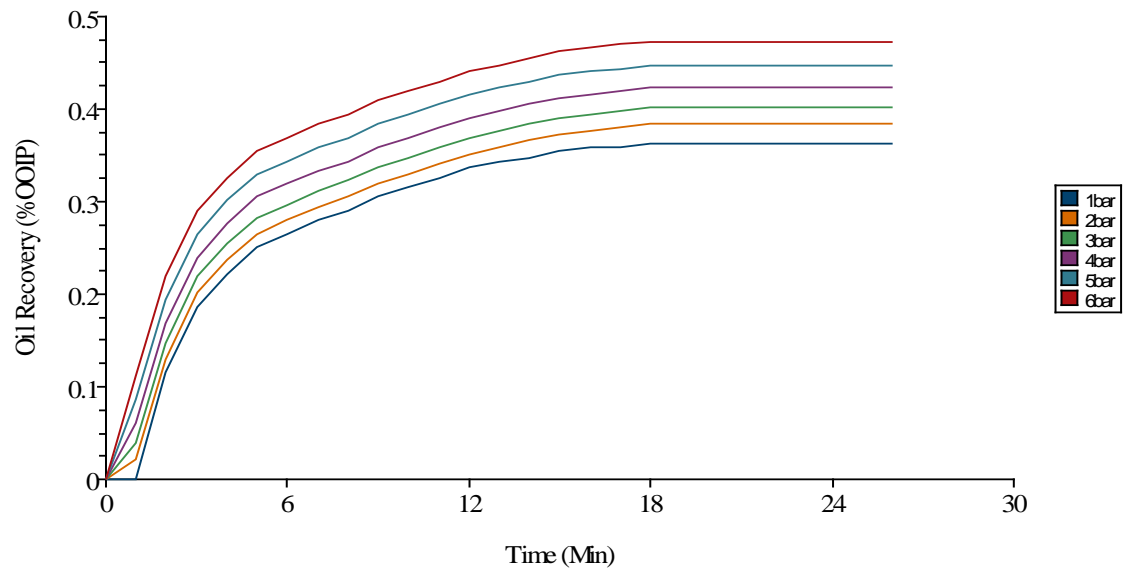
(c) Oil recovery versus time at 1.5mm perforation diameter



(d) Oil recovery versus time at 2.0mm perforation diameter

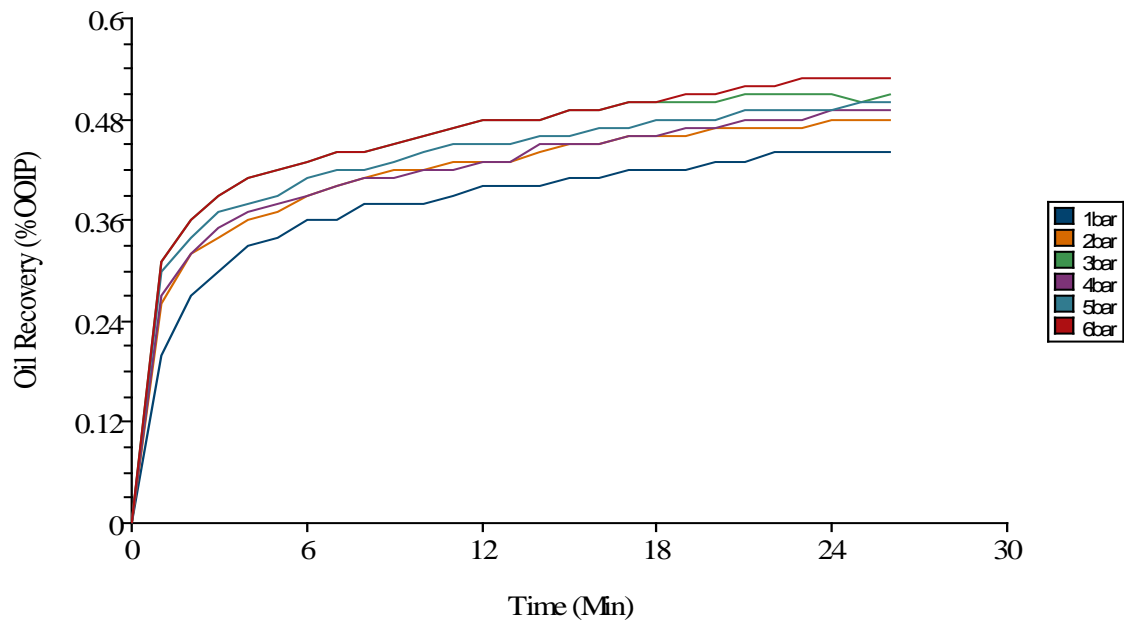


(e) Oil recovery versus time at 2.5mm perforation diameter

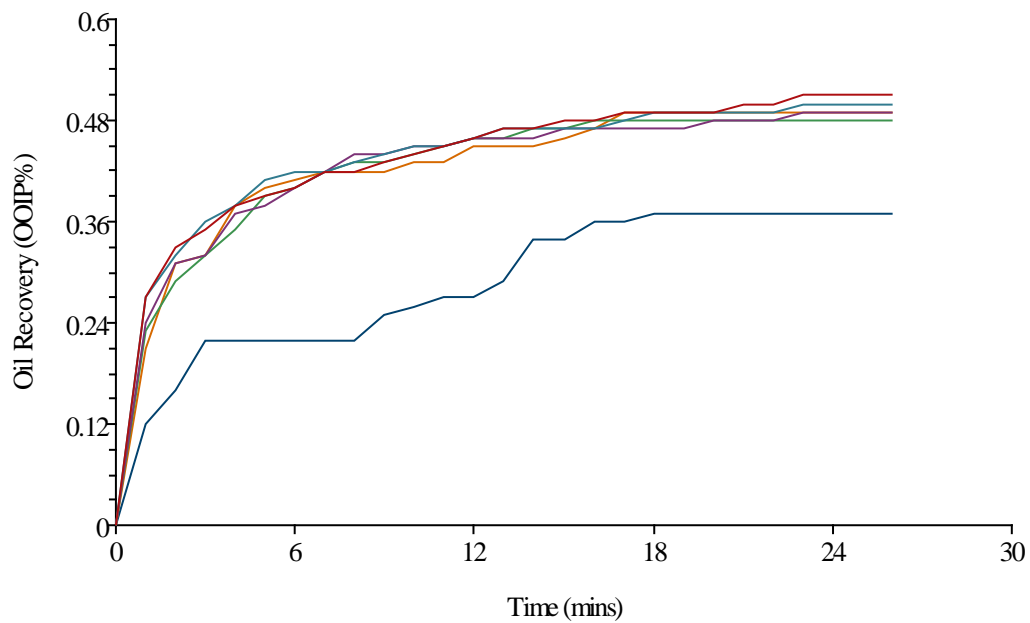


(f) Oil recovery versus time at 3.0mm perforation diameter

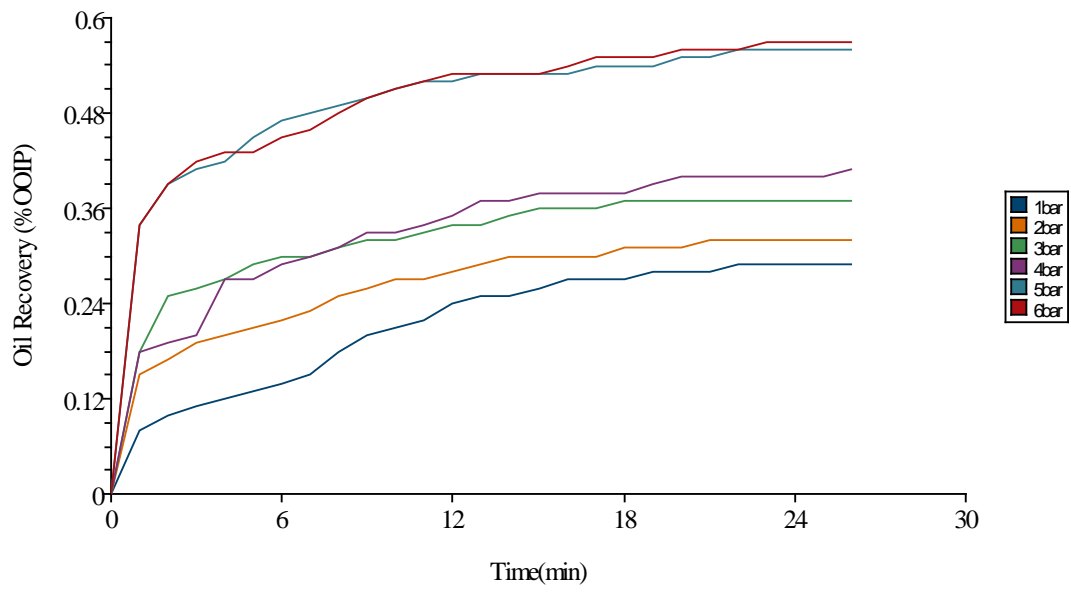
Appendix J : Figure 4.12 (b) –(f)



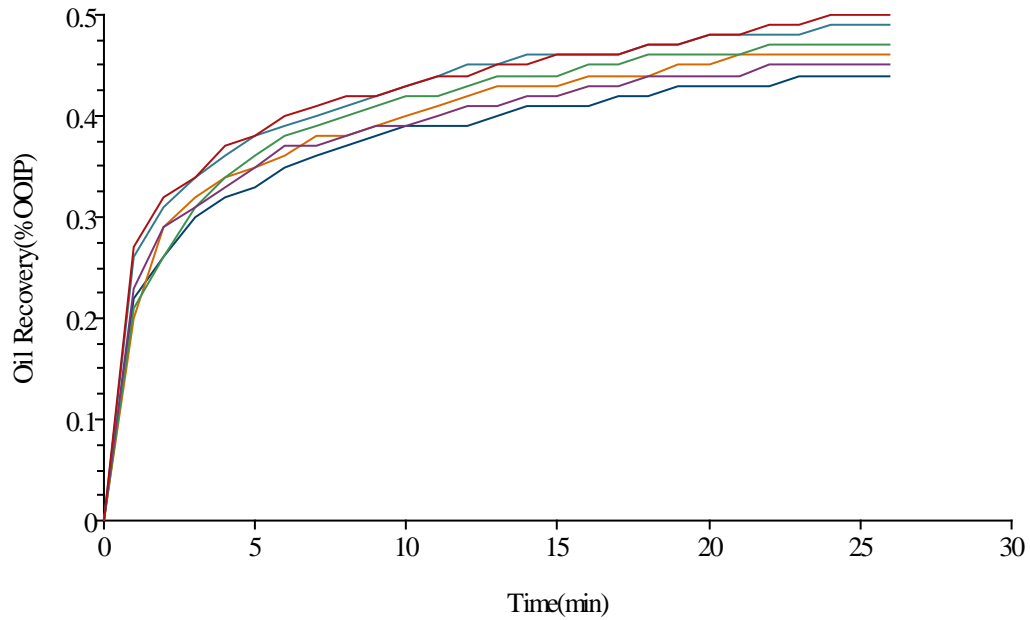
(b) Oil recovery versus time at 1.0mm perforation diameter



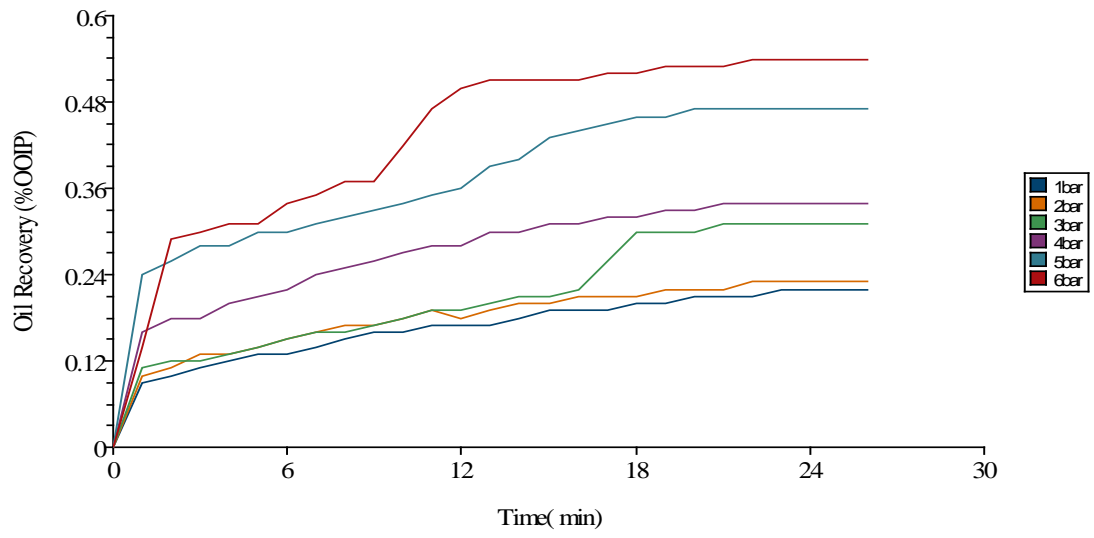
(c) Oil recovery versus time at 1.5mm perforation diameter



(d) Oil recovery versus time at 2.0mm perforation diameter



(e) Oil recovery versus time at 2.5mm perforation diameter



(f) Oil recovery versus time at 3.0mm perforation diameter